UNIVERSITÄT ZÜRICH
MATHEMATISCH-NATURWISSENSCHAFTLICHEN FAKULTÄT
Institut für Computational Science

Professor Jaiyul Yoo

General Relativistic Effects in the Large Scale Structure of the Universe

DISSERTATION

zur
Erlangung der naturwissenschaftlichen Doktorwürde
(Dr. sc. nat.)
vorgelegt der
Mathematisch-naturwissenschaftlichen Fakultät
der
Universität Zürich

von

Fulvio Scaccabarozzi

aus
Milano (Italien)

Abstract

This thesis studies the impact of general relativistic effects in galaxy clustering. A comprehensive description of this topic is of great importance at this particular moment in time. Indeed, in the near future, planned redshift surveys will measure the large-scale galaxy distribution with unprecedented precision. The aim of these experiments is to gain a better understanding of the properties of dark matter and dark energy as well as the behavior of gravity on large scales, where modifications to general relativity may occur. In order to interpret correctly the physical information in the data, we need accurate theoretical predictions for the observables that will be measured. The purpose of this thesis is to provide theoretical predictions for large scale structure observables accounting for all relativistic effects that alter the light propagation with the ultimate goal of testing general relativity on large scales. In particular, we focus on two key observables in cosmology: the galaxy two-point correlation function and the galaxy power spectrum. Using the gauge-invariant relativistic description of galaxy clustering we demonstrate that the complete theoretical expressions for both these observables are devoid of any long-mode contributions from the perturbations and do not have infrared divergences in agreement with the equivalence principle. We numerically compute the two quantities and study the contributions of various relativistic terms in the conformal Newtonian gauge. Our theoretical and numerical studies provide a complete understanding of the relativistic effects in the galaxy two-point correlation function and the galaxy power spectrum. The results of this thesis may then contribute to formulating new tests of general relativity with future large-scale data.

Contents

Acknowledgements

I would like to express my gratitude to Jaiyul Yoo for *everything* he taught me. His mentoring, his support and his passion have always been precious during the years of my doctorate.

I am very grateful to my collaborators Jaiyul Yoo, Ermis Mitsou, Sang Gyu Biern, Giuseppe Fanizza, Ruth Durrer and Vittorio Tansella for the work we did together.

A special thanks to my colleagues and friends Sang Gyu Biern, Ermis Mitsou, Giuseppe Fanizza, Yves Dirian, Nastassia Grim, Sandra Baumgartner, Jennifer Pollack, Vittorio Tansella, Maria Han Veiga, François Ged and many others.

Jury Members

- Prof. Ruth Durrer
  Département de Physique Théorique & Center for Astroparticle Physics,
  Université de Genève, 24 quai E. Ansermet, CH-1211 Genève 4, Switzerland
- Prof. Lucio Mayer
  Center for Theoretical Astrophysics and Cosmology,
  Institute for Computational Science, University of Zürich,
  Winterthurerstrasse 190, CH-8057, Zürich, Switzerland
- Prof. Romain Teyssier
  Center for Theoretical Astrophysics and Cosmology,
  Institute for Computational Science, University of Zürich,
  Winterthurerstrasse 190, CH-8057, Zürich, Switzerland
- Prof. Jaiyul Yoo
  Center for Theoretical Astrophysics and Cosmology,
  Institute for Computational Science, University of Zürich,
  Winterthurerstrasse 190, CH-8057, Zürich, Switzerland
  Physics Institute, University of Zürich,
  Winterthurerstrasse 190, CH-8057, Zürich, Switzerland

I would like to thank them all for having accepted to be part of the Jury for my Thesis defense.

List of Publications

The following works have been considered as part of this thesis:

[1] F. Scaccabarozzi and J. Yoo,
" *Light-Cone Observables and Gauge-Invariance in the Geodesic Light-Cone Formalism*",
JCAP 1706 (2017) no.06, 007, [arXiv:1703.08552].

[2] F. Scaccabarozzi, J. Yoo and S. G. Biern,
"*Galaxy Two-Point Correlation Function in General Relativity*",
JCAP 1810 (2018) no.10, 024, [arXiv:1807.09796].

[3] F. Scaccabarozzi, J. Yoo, S. G. Biern and J. O. Gong "*Galaxy Power Spectrum in General Relativity*"
in preparation

Additional publications related to this work:

[4] J. Yoo and F. Scaccabarozzi
"*Unified Treatment of the Luminosity Distance in Cosmology*",
JCAP 1609 (2016) no.09, 046, [arXiv:1606.08453].

[5] E. Mitsou, F. Scaccabarozzi and G. Fanizza,
"*Observed Angles and Geodesic Light-Cone Coordinates*"
Class.Quant.Grav. 35 (2018) no.10, 107002, [arXiv:1712.05675].

[6] E. Mitsou, J. Yoo, R. Durrer, F. Scaccabarozzi, V. Tansella.
"*Angular N-point spectra and cosmic variance on the light-cone*"
in publication [arXiv:1905.01293].

CHAPTER 1

Introduction

Since the beginning of time, mankind has always wondered about the world's origin and, in the corse of history, many cultures have looked for the answer in the night sky. Today, in 2019, the question about the origin of the universe and how it evolved to its current status is still a matter of efforts and the answer is still believed to be in the sky. We now use the scientific method and we call cosmology the science that deals with the origin, the evolution and the structure of the universe.

Our modern picture of the universe started to develop with Einstein's formulation of General Relativity (GR) in 1915. GR is a theory of gravity that relates the energy density with the curvature of space-time. If applied to the universe as a whole, GR predicts that the universe is expanding or contracting, depending on its total energy content. Einstein was the first to find such solution to his field equations, to which he added a term - the cosmological constant Λ - to make the universe static, in agreement with the common belief of that time. However, a few years later the idea of a static universe was questioned again by Friedmann and Lemaître [7, 8] who found a solution to the Einstein's equations that implies the expansion of space. Indeed, Robertson and Walker [9, 10, 11, 12] showed that this was the only viable solution if the cosmological principle is assumed to hold. The latter simply states that the properties of the universe are the same for all observers (at any location) when viewed on sufficiently large scales. In 1929, by measuring the recession velocities of galaxies, Hubble [13] discovered that galaxies further away from us move faster away from us. This observation was the first experimental evidence supporting the idea of an expanding universe and contributed to the development of the prevailing cosmological model: the Big Bang model. The model describes how the universe expanded from a very high-density and high-temperature state to its current structure displayed by the distribution of galaxies.

Despite the fact that the Big Bang model offered a comprehensive explanation of Hubble's observation and it is based on GR, which was experimentally confirmed by several tests, the scientific community was still divided between supporters of the Big Bang theory and supporters of the steady state theory. The latter is an alternative to the Big Bang model, in which the density of matter in the expanding universe remains unchanged due to a continuous creation of matter, thus complying with the cosmological principle. The crucial evidence in favor of the Big Bang model arrived in 1964, when the cosmic microwave background (CMB) radiation was discovered by Penzias and Wilson [14]. It was also the confirmation that the known laws of physics could be used to predict in detail the characteristics of the universe back in time.

Since the discovery of the CMB, we have built several astronomical instruments and formulated different theories to explain all the details and to provide all the missing pieces in the description of our universe. Indeed, there have been some experimental observations that the Big Bang model alone could not explain. These efforts resulted in the formulation of the Lambda cold dark matter (ΛCDM) model, a parametrization of the Big Bang model in which the universe contains three major components: first, dark energy, an unknown form of energy acting like the cosmological constant and denoted by Λ (precisely as the term introduced by Einstein in his field equations); second, dark matter, an unknown form of matter that interacts only gravitationally; and third, ordinary matter, or baryonic particles. The reasons for introducing dark energy and dark matter are both from experimental evidences.

Let us first focus on dark energy. In 1998, measurements of the redshifts of type Ia supernovae by Riess, Schmidt and Perlmutter [15, 16, 17] indicated that the expansion of the universe is accelerating, i.e. the velocity at which a distant object is receding from the observer is continuously increasing with time. Since type Ia supernovae have almost the same intrinsic brightness (they are indeed called standard candles), one can use the observed brightness of such sources to measure their distance. The distance can then be compared to the redshift, which measures how much the universe has expanded since the supernova occurred. Additional confirmatory evidences have been found later in baryon acoustic oscillations (BAO) – by comparing the size of the sound horizon at decoupling (using the CMB) and today (using the galaxy correlation function) – and in analyses of the clustering of galaxies – by comparing the number density of galaxy clusters above a certain mass at high and low redshifts with that predicted by different models. These probes also enabled to quantify the amount of dark energy needed to produce the observed acceleration, that is 68.6% of the total energy density. Despite its existence is evidenced by various observations, dark energy is still seen as problem in cosmology. The reason is that in its simplest form, in which it is described as a cosmological constant, dark energy is unjustified from a theoretical point of view. Indeed, in GR there is no formally no need for a cosmological constant, meaning that it can be set to zero or any other value. Even if we assume a non-vanishing cosmological

constant we have a fine tuning problem: the measured value of the dark energy density differs from the vacuum expectation value predicted by quantum field theories by 120 orders of magnitude. In other words, in order to obtain an energy density as small as the one we observe we need the contributions arising from quantum field theories to cancel to better than a part in 10^{120}. Possible solutions to this problem are i) modifying the matter content in the universe, ii) modifying the physics describing the behavior of gravity or iii) back-reaction. Point i) and ii) are somehow similar. Consider, for example, an additional scalar field coupled to the matter sector, as in massive gravity theories. It is not clear whether in this case we are modifying the gravity sector or the matter sector. The same problem affects the definition of the cosmological constant, as it is unclear whether it is a modification of gravity or an additional matter field with constant energy-density and equation of state. The solution is to some degree arbitrary and some authors define as modified gravity theories only those in which the additional degrees of freedom are non-minimally coupled to the Einstein-Hilbert term in the action. A unified treatment of some classes of dark energy and modified gravity models is given by the effective field theory of dark energy. The idea of modifying the theory of gravity to match the outcome of observations has generated an active field of research in modern cosmology. Observables that are sensitive to the behavior of dark energy are of crucial importance because they allow to discriminate between possible deviations from a cosmological constant. The third possible solution to the dark energy problem is back-reaction, i.e. the idea that inhomogeneities in the universe have an impact on the large-scale evolution. By relating the late-time acceleration of the universe expansion with the growth of structures, the back-reaction approach solves the coincidence problem: why are the density of matter and that of dark energy comparable right now? This topic is still debated in the cosmology community, even though it has been demonstrated that back-reaction alone cannot account for the accelerated expansion.

The second most abundant and most mysterious component in the universe is dark matter, which accounts for 26.5% of the total energy density and approximately 85% of the matter content. The primary evidence for dark matter comes from galaxy rotation curves: since the luminous mass density of a spiral galaxy decreases as one goes from the center to the outskirts, from Kepler's second law it is expected that the rotation velocity of stars around the galactic center decreases with distance from the center. Instead, the galaxy rotation curve remains flat, implying that there is a lot of non-luminous matter (dark matter) in the outskirts of the galaxy. Other lines of evidence include measurements of the velocity dispersion of galaxies in a cluster, observations of gravitational lensing, BAO in galaxy clustering and the photon acoustic oscillations in the CMB. Let us first discuss the evidences provided by gravitational lensing. Since matter bends and distorts light trajectories passing near it, we can infer the amount and distribution of matter that caused a deformation of some background object's

image. Gravitational lensing is usually distinguished in two regimes: strong and weak lensing. On the one hand strong lensing occurs when the object acting as the lens is very massive, the source is not too far away and both are roughly aligned with the line of sight. In this situation strongly distorted multiple images of the source are produced and one can reconstruct the mass distribution in the lens plane. As this is a purely gravitational effect, it is sensitive to both baryonic matter and dark matter. On the other hand in the weak lensing regime we do not obtain multiple images but instead the resulting image is magnified (convergence) or deformed (shear). The idea is that one can link the lensing effect with the distribution of dark matter between the source and us. Because we only the average properties of the un-lensed galaxies, weak lensing is treated with a statistical approach. Weak lensing allowed for the reconstruction of the dark matter distribution in the Bullet cluster, which represents one of the main evidences for dark matter. The Bullet cluster formed from the collision of two clusters of galaxies in which the different behaviors of baryonic matter and dark matter behave are clearly visible. On cosmological scales the dark matter density can be measured from the BAO in galaxy clustering and the photon acoustic oscillations in the CMB. In the galaxy correlation function, for example, one can link the position of the BAO peak with the speed of sound at photon decoupling which, in turn, is related to the baryon-to-photon density ratio. In the CMB we observe a similar pattern as photons are more energetic in over-dense regions and less energetic in under-dense regions. Since we usually look at the CMB spectrum in angular space we see a number of succeeding peaks. The position (in angular space) and the relative amplitudes of these peaks can be used to extract information about the baryon density and the dark matter density. Thanks to these observations, we now believe that most of the dark matter is gravitationally clustered into halos and filaments connecting them. Since baryonic matter falls into the gravitational potential wells generated by halos, forming structures, dark matter halos can be considered as the building blocks of the universe. Finally, we should point out that beside the indirect observational evidences we have listed, the debate on the nature of dark matter amongst particle physicist is still ongoing and dark matter still escapes direct (non-gravitational) detection.

One fundamental extension to the ΛCDM model is inflation, a period of exponential expansion that occurred in the very early universe, about 10^{-36} seconds after the Big Bang singularity. Inflation was first proposed by Alan Guth [18] in 1979 while studying the problem of why no magnetic monopoles are found today, but it was quickly realized that it would have resolved several problems in the Big Bang scenario that came to surface in the 1970s. These problems arise from the ascertainment that, in order to be as we observe it today, the universe should have started from very finely tuned initial conditions. Inflation resolves these problems by providing a mechanism that brings the universe to this special state. Here we only discuss briefly the horizon problem, because the notion of horizon will be important throughout this thesis. The horizon

problem arises due to the difficulty in explaining the observed homogeneity of causally disconnected regions of space in the absence of a mechanism that sets the same initial conditions everywhere. In the big bang model without inflation two widely separated regions of the observable universe cannot have thermally equilibrated because they move apart from each other faster than the speed of light and thus have never come into causal contact. In the early Universe, it was not possible to send a light signal between the two regions. Because they have had no interaction, it is difficult to explain why they have the same temperature, as we observe in the CMB. In order to explain how inflation resolves the problem, it is convenient to define the Hubble horizon (often simply called horizon): it defines the distance beyond which objects move away from the observer faster than the light (they are not causally connected) because of the expansion of space (it corresponds to the causal horizon in a static universe). We can now reformulate the horizon problem as follows: why do we observe isotropic CMB in patches of the sky separated by a distance bigger than the causal horizon at the time of photon decoupling (when the radiation that we observe today as CMB was formed)? Since inflation consists of a period of exponential expansion, the causal horizon also grows exponentially while the Hubble horizon is constant. Therefore, if inflation lasts long enough, at the end the causal horizon is larger than the Hubble horizon and the problem is solved. Finally, it is important to mention that inflation also explains the origin of the large scale structure (LSS) of the universe, as quantum fluctuations in the matter and radiation fields in the early universe were stretched by inflation to macroscopic scales, becoming the seeds for the growth of galaxies.

While, on the one hand, inflation provides a solution to various conceptual problems in cosmology and is necessary to explain several observations, on the other hand the detailed particle physics mechanism responsible for inflation is unknown. In the basic inflationary paradigm, called single field slow-roll inflation, inflation is driven by a scalar field – the inflaton – rolling down a slowly decreasing potential energy until falling into a minimum. When the field rolls very slowly compared to the expansion of the universe, inflation occurs, and when it reaches the minimum it stops and reheating can occur. Despite the fact that this simple model is accepted by most physicists, as a number of predictions have been confirmed by observation, more complicated models involving more fields or more complicated potential shapes are an active field of study. Distinguishing the correct model among these variants requires very precise observations as the differences in the predictions can be tiny. However, a large class of inflationary models has been already ruled out by observations. For instance the models predicting more power on small scales rather than on large scales in the primordial spectrum of density perturbations (leading to a so-called blue tilted primordial spectrum, with spectral index larger than unity) are already excluded by measurements of the CMB. Achieving an accurate description of inflation is of crucial importance because inflation sets the initial conditions for the growth of perturbations that results

in the structure of galaxies we observe today. With the increase of experimental precision, the tiny differences in the predictions of different inflationary models will matter more and more in our understanding of the universe evolution.

Having discussed some of the most challenging topics in modern cosmology, we can now attempt to cover the remaining parts by following the history of the universe in a chronological order and describe the relevant physical processes that have happened and are responsible for the complicated structures in the universe that we observe today.

According to our understanding, the universe originated 13.8 billion years ago from the Big Bang singularity, a state of infinite density and temperature. During the very first moments, the energies and conditions were so extreme that our knowledge of physics can only suggest possibilities and different stages of the early universe are understood to different extents. The rapid expansion of space induced by inflation (about 10^{-36} seconds after the Big Bang) enabled the cooling of the still immensely hot universe from about 10^{27} down to 10^{22} Kelvins. Tiny fluctuations in the universe at this stage are believed to be the basis of large-scale structures that formed much later.

After inflation ends, the universe is filled with a hot quark-gluon plasma, the relics of the huge potential energy that triggered the expansion. From this point onwards the physics of the early universe is much better understood, and the energies involved in the quark epoch (between 10^{-12} seconds and 10^{-6} seconds after the Big Bang) are directly accessible in particle physics experiments. The quark epoch is the period in the evolution of the early universe immediately after electroweak symmetry breaking, when the fundamental interactions – gravity, electromagnetism, the strong interaction and the weak interaction – had taken their present forms, but the temperature of the universe was still too high to allow quarks to bind together to form hadrons. During the quark epoch the universe was filled with a dense, hot quark-gluon plasma, containing quarks, leptons and their antiparticles. Collisions between particles were too energetic to allow quarks to combine into mesons or baryons. The quark epoch ended when the energy of particle interactions (related to the temperature of the universe, which decreases with the expansion of space) had fallen below the binding energy of hadrons. Then, between 10^{-6} seconds and 1 second after the Big Bang, the quark-gluon plasma that composes the universe cools until hadrons form, including baryons such as protons and neutrons. After this point, it would be expected that both baryons and anti-baryons formed in equal numbers. Instead, the universe was left with a lot more baryons than anti-baryons and, in fact, almost no anti-baryons are observed in nature. Theory also predicts that about 1 neutron for every 7 protons remained. We have good reasons to believe this to be correct because later all neutrons and some of the protons fused, producing hydrogen, deuterium, helium and other elements, whose abundance can be measured. A 1 to 7 ratio of neutrons to protons at the end of this

epoch would indeed produce the observed element ratios in the current universe.

At about one second, when the temperature of the universe was approximately 10 billion Kelvins (or 1 MeV), the universe expansion rate becomes comparable to the rate of weak interactions, so that neutrinos decouple from baryonic matter and begin to travel freely through space, generating the so-called cosmic neutrino background (CNB). As neutrinos rarely interact with matter, these neutrinos still exist today, but they cannot be detected because of their very low energy. However, the Big Bang model makes many predictions about the CNB, and there is very strong indirect evidence that it exists, both from Big Bang nucleosynthesis predictions of the helium abundance, and from anisotropies in the CMB. Indeed, the decoupled neutrinos should have had a very slight effect on the phase of the various CMB fluctuations. Such shifts have been detected in the CMB. Moreover, the fluctuations corresponded to neutrinos of almost exactly the temperature predicted by theory (1.96 ± 0.02 Kelvins compared to a prediction of 1.95 Kelvins), and exactly three types of neutrino, as the number of neutrino flavors predicted by the Standard Model of particle physics.

Between 1 second and 10 seconds after the Big Bang, the energy content of the universe is dominated by leptons (such as the electrons and muons), left by the annihilation of hadrons and anti-hadrons. As the temperature of the universe falls, leptons are no longer created and most remaining leptons and anti-leptons quickly annihilate each other into high energy photons. Now the energy of the universe and its overall behavior is dominated by radiation, i.e. photons and other relativistic particles. The photons continue to interact frequently with charged particles such as electrons and protons for the next 377'000 years, in which the universe remains an opaque plasma.

During this time, however, many other important events occur which we shall briefly discuss. Between 2 and 20 minutes after the Big Bang, the temperature and pressure of the universe allow nuclear fusion to happen, producing nuclei of a few light elements beyond hydrogen. Such event is known as Big Bang nucleosynthesis. About 25% of the protons, and all the neutrons fuse to form deuterium, which in turn quickly fuses to form helium-4. Above a certain temperature, energetic photons easily break apart atomic nuclei, according to their binding energy. From about 2 minutes, the temperature decrease allows deuterium to be stable, and starting from about 3 minutes, helium and other elements formed by the fusion of deuterium also no longer unbind. Only small amounts of nuclei beyond helium are created, because nucleosynthesis of heavier elements requires thousands of years even in stars. The amounts of each light element in the early universe can be estimated by looking at old galaxies, providing a very strong evidence for the Big Bang model. For example, about 1 neutron for every 7 protons should be produced, so that 25% of the protons and all the neutrons fuse into helium-4, in the exact amount we find today. By 20 minutes, the universe is no longer hot enough for fusion, but still too hot for neutral atoms to exist or for photons to travel far. The universe remains therefore an opaque plasma

for quite a long time.

At around 47'000 years, as the space expands and the temperature falls down, the universe's large scale dynamics and behavior begin to be dominated by matter rather than radiation. This allows small structures to form, as gravity starts to overcome the pressure and the density inhomogeneities left by inflation can grow in amplitude, instead of being swept away by radiation. The presence of dark matter further accelerates the formation of structures in the universe. Indeed, dark matter gradually cluster in huge filaments and halos under the effects of gravity, collapsing faster than baryonic matter due to the absence of radiation pressure. Because of the presence of these concentrations of dark matter, baryonic matter eventually gathers together in a shorter amount of time.

At about 377'000 years, the universe finally becomes cold enough for the ionized particles to combine and form the first neutral atoms, a process known as recombination. During recombination, free electrons became bound to protons to form neutral hydrogen atoms. These hydrogen atoms generally form with the electrons in a high energy state, but they quickly reach their ground state by emitting photons. Because the free electron density suddenly dropped, those photons were able, for the first time in the history of the universe, to travel long distances. The photons that had their last interaction back then can still be detected today as the CMB, which is indeed the oldest observation we have of the universe.

Recombination not only caused the photon decoupling but also it stopped the propagation of pressure waves within the electron-baryon plasma - the BAO - created by the competition of gravity and pressure in overdense regions of the primordial plasma. As these overdense region contains dark matter, baryons and photons, the pressure results in spherical sound waves of both baryons and photons moving outwards from the overdensity. The dark matter interacts only gravitationally, and so it stays at the center of the sound wave, the origin of the overdensity. After recombination the photons were no longer interacting with the baryonic matter and they spread away. That removed the pressure on the system, leaving behind shells of baryonic matter. Therefore, under the only effect of gravity, the baryons and dark matter formed overdensities both at the original site of the perturbation and in the shell at the sound horizon. As a result, one would expect to see a greater number of galaxies separated by the sound horizon than at other length scales. Indeed, the BAO became imprinted in the distribution of matter, giving rise to a preference in the distribution of large-scale objects. In the same way that supernovae provide a standard candle for astronomical observations, the BAO provide a standard ruler for length scales in cosmology. The length of this standard ruler is given by the maximum distance the acoustic waves could travel in the primordial plasma before recombination, and can be measured by looking at the large scale structure of matter.

After recombination, even though the universe became transparent to light, there

were no light sources such as stars and galaxies, so that the only photons existing were those released by decoupling (observed today as the CMB) and those occasionally released by hydrogen atoms, known as the 21 cm spin line of neutral hydrogen. The clouds of hydrogen that form where dark matter is denser only collapsed very slowly to form stars and galaxies. Indeed, the first generation of stars formed within a few hundred million years after the Big Bang, when the temperature dropped from 4000 Kelvins (at recombination) to 60 Kelvins. These stars were the first source of visible light in the universe after recombination. Structures may have begun to emerge from around 150 million years, and early galaxies from around 380 to 700 million years. Where numerous galaxies have formed, galaxy clusters and superclusters eventually arise. Because this process was gradual, this period, known as the dark ages, lasted until 1 billion years after the Big Bang, when the universe took its present appearance.

As the first stars and galaxies gradually form, the intense radiation they emit reionizes much of the surrounding universe, splitting the neutral hydrogen atoms back into a plasma of free electrons and protons for the first time since recombination and decoupling. Reionization is evidenced from observations of quasars, active galaxies that represent the most luminous objects observed in the universe. Since neutral hydrogen has specific energy levels, called the Lyman series, the light emitted by a quasar and traveling through ionized hydrogen and neutral hydrogen shows different absorption lines. Furthermore, the light travels for billions of years before reaching our detectors, so that any absorption line is redshifted by a specific amount, indicating when it happened. In this way it possible to study the state of ionization at different times in the past. It is evinced that reionization began as bubbles of ionized hydrogen, forming around the newly emerged light sources, which became larger over time. It is also concluded that the absorption occurred in the intergalactic medium and not due to the fact that the light passed through dense regions or galaxies.

From 1 billion years, and for about 12.8 billions of years, the universe has looked much as it does today. The only remarkable event is the transition from the matter dominated era to the dark energy dominated era, at about 9.8 billion years, when the expansion of space gradually begins to accelerate under the influence of dark energy. In the mean time, the disk of our galaxy (the milky way) began to form. About 4.6 billion years ago our solar system also formed, with the earliest traces of life on Earth emerging by 3.5 billion years ago.

The present-day universe is understood quite well. Thanks to the interplay between theory and observations we achieved a good comprehension of the large scale structure of the universe. Nevertheless, questions about the nature of dark energy and the fundamental properties of gravity can be answered by looking precisely at the large scale structure of the universe. With the huge amount of data coming from future galaxy surveys, such as [19, 20, 21, 22, 23, 24], we hope to answer these questions. Because of the unprecedented precision achieved by the observational advances, we need accurate

theoretical predictions to interpret these data correctly and extract physical information from them. The goal of this work is to contribute to this matter, by providing a general relativistic description of the observables that will be measured.

This thesis is organized as follows. The remainder of this introduction is dedicated to the main subjects of this thesis: the large scale structure of the universe and the general relativistic effects in its observations. In chapter 2 we introduce the basics of cosmological perturbation theory and the equations governing the evolution of the perturbations responsible for the general relativistic effects. In chapter 3 we study the geodesic light-cone approach to the large scale structure observables, showing that the resulting expressions are gauge invariant. In chapter 4 we introduce the galaxy number density and we compute the galaxy two-point correlation function accounting for the relativistic effects to linear order in perturbation theory. In chapter 5 we perform a similar study for the galaxy power spectrum. Finally, in chapter 6 we summarize our results and present our conclusions. One last remark: In this thesis we use units in which the speed of light, the Planck constant and the Boltzmann constant are all equal to one

$$c = \hbar = k_B = 1\,.$$

1.1 The Large Scale Structure of the Universe

Several remarkable space-based missions (COBE, WMAP, Planck), have detected very slight variations in the density and temperature of the CMB. These variations are subtle, and the CMB appears nearly the same in every direction. However, the small temperature fluctuations of order of a few parts in 100'000 are of enormous importance, as they are essentially early seeds from which all complex structures in the universe ultimately developed. In this section we provide a more detailed introduction to galaxy clustering: the study of how primordial fluctuations coming from inflation and imprinted in the CMB are amplified through gravitational instability to form the large scale structure of the universe.

What seems like a simple task is however extremely complicated. Firstly, we need to deal with physics governing a very wide range of scales: from the size of the Hubble horizon $H_0^{-1} \sim 4000$ Mpc to the typical size of galaxies ~ 10 kpc and secondly one in principle needs to solve the coupled Boltzmann-Liouville equations for each species in the universe. The ΛCDM model is successful at predicting the observed distribution of galaxies, as the large-scale evolution of the universe can be understood through linear cosmological perturbation theory, in which all structures are described as small deviations from a perfectly homogeneous universe. However, on the scale of individual galaxies there are many complications due to highly non-linear processes involving baryonic physics, gas heating and cooling, star formation and feedbacks. As a result, galaxy formation cannot be fully described by perturbation theory and different tech-

niques, such as N-body simulations, need to be used to understand the small-scale dynamics.

In order to describe the processes of structure formation, we have to start from the early universe, when the fluctuations that provide the seeds for the growth of galaxies originate. The very early universe was dominated by radiation. In this case, density fluctuations larger than the horizon grow with the universe expansion, while fluctuations smaller than the horizon remained essentially frozen because the radiation prevented their growth. After matter-radiation equality, all dark matter overdensities grow freely through gravitational clustering, forming potential wells into which the baryons could fall later. As the Hubble radius grows in the expanding universe, it encompasses larger and larger perturbations. For this reason, the shorter-wavelength perturbations that are inside the horizon during radiation domination have their growth retarded until matter domination.

The physics of structure formation in this epoch is particularly simple, since perturbations are small and we can treat them in the regime of linear perturbation theory, where different Fourier modes evolve independently. Indeed, at early times, the perturbations have Fourier coefficients with Gaussian probability distribution, because they come from quantum fluctuations produced during inflation. Each coefficient is uncorrelated with the other, so that also the real space fluctuations are Gaussian. Furthermore the variance is independent of the direction of the wave-vector $\boldsymbol{k}$: for the primordial curvature perturbation the power spectrum scales as $P_\zeta \sim k^{n_s-1}$, where the spectral index n_s measures the deviation from a scale-invariant spectrum. The value of n_s measured by WMAP [25] is very close to what predicted by the simplest and most robust models of inflation indicating that there is more power on small scales rather than on large scales in the primordial spectrum of density perturbations. Another important property of the primordial perturbations, that they are adiabatic fluctuations (perturbations in different components have equal fractional over/underdensities) instead of isocurvature fluctuations (fluctuations in the form of the local equation of state of the system, with the total density of the system remaining homogeneous), is also predicted by inflation and has been favored by CMB observations. The adiabatic perturbations are also known as curvature perturbations, as they induce inhomogeneities in the spatial curvature.

The way in which curvature perturbations convert into late-time perturbations is usually encoded in the transfer function: for the matter density fluctuation we could for example write $\delta_{\boldsymbol{k}}(t) = T(k,t)\zeta_{\boldsymbol{k}}$ where $\zeta_{\boldsymbol{k}}$ is the value of the curvature perturbation at horizon exit during inflation. The same equation can be written, with a different transfer function, for every perturbation in the universe. For a pressure-less and collision-less fluid, such as cold dark matter, the transfer function is obtained by solving the continuity and Euler equations, together with the Poisson equation. On the other hand, when considering baryons and photons the Boltzmann hierarchy is not

closed and to compute the transfer function one needs to use numerical codes such as `CLASS` [26] and `CAMB` [27] or rely on analytical approximations, which we will discuss briefly in a few paragraphs.

After recombination, structure formation in the ΛCDM model proceeds hierarchically, due to gravitational collapse, with smaller structures forming before larger ones. Because of photon decoupling, the baryons are no longer subject to pressure and we can describe them as a pressure-less fluid, together with cold dark matter. The evolution of such fluid can be derived in perturbation theory by following mainly two approaches: Eulerian and Lagrangian. In Eulerian perturbation theory, often called standard perturbation theory (SPT) [28, 29, 30], the fluid motion is described by the evolution of the density and velocity fields in fixed comoving coordinates. In Lagrangian perturbation theory (LPT) [28, 29, 31, 32, 33] the fluid motion is described by following the trajectories of individual fluid elements in space and time. The main predictions of linear perturbation theory are the growth of the matter density fluctuations with time, given by the growth function $D_1(t)$ relating the matter density fluctuation at time t to its initial value at inflation, and the linear matter power spectrum $P_m(k)$, which describes the matter density fluctuations as a function of scale. The latter, as a tool for cosmology, it is of comparable importance to the cosmic microwave background. Galaxy surveys, such as the Sloan Digital Sky Survey, and surveys of the Lyman-alpha forest have measured the power spectrum. Since these studies observe radiation emitted from galaxies and quasars, they do not directly measure the dark matter, but the large-scale distribution of galaxies (and of absorption lines in the Lyman-alpha forest) is expected to mirror the distribution of dark matter closely.

Linear perturbation theory is able to describe a significant range of scales and most of the history of the universe but it eventually breaks down, as gravity is non-linear and with time it feeds this property into the primordial perturbations. Since there is no exact solution for the perturbation variables in the non-linear regime, one must rely on expansion schemes, taking into account that different Fourier modes no longer evolve independently and the perturbations loose their Gaussian properties. Furthermore the convergence properties of some schemes are in question when higher order contributions get bigger than the lower order ones and do not improve agreement with N-body simulations. Recently developed perturbative approaches such as higher order SPT [34, 35, 36] and LPT [33, 37, 38] and Effective field theory [39, 40, 41] are able to describe the growth of structure on scales as small as 0.1 Mpc^{-1} (at $z = 0$) but eventually we enter the non-linear scales where a perturbation theory description is not at all suited. On smaller scales, simplified models such as the Spherical Collapse Model, Secondary Infall Models [30, 42, 43] and the Zeldovich Approximation [44] can be used to understand the non-linear processes that lead to the formation of a virialized structure. In the Spherical Collapse Model the universe is assumed to be in the matter-dominated phase and to be homogeneous, except for a single spherical perturbation.

Furthermore, the only fluid in the universe is supposed to be collisionless dark matter. The model considers an overdensity as consisting of many individual thin mass shells and study the evolution of a single mass shell of collisionless dark matter. Because of its collisionless nature, the shell crosses itself and starts to oscillate. What happens is that the shell expands until it reaches a maximum radius and then collapses back and form a virialized structure. Secondary Infall Models follow a similar description but with more realistic initial density profile, while the Zeldovich Approximation completely gives up on the assumption of spherical symmetry. The main result of these models is that a region in which the density field extrapolated by linear theory is bigger than the critical value

$$\delta(x,t) > \delta_c = 1.686$$

will have collapsed to form a structure (dark matter halo) by time t. It is natural to wonder which is the probability that the Gaussian density field is bigger that δ_c or, a closely related question, which is the number of dark matter halos per comoving volume with a certain mass: the halo mass function. Theoretical understanding of this issue comes from the Press-Schechter formalism [45] or, in a more recent formulation, the Excursion Set Formalism [46].

Despite the insight offered by simplified analytical models of structure formation, N-body simulations represent the only reliable tool to study the clustering of objects on scales smaller than 0.1 Mpc^{-1} (with the disadvantage that they are very slow when the number of particles is large). An N-body simulation is a simulation of a dynamical system of particles under the influence of physical forces, such as gravity. The particles treated by the simulation may or may not correspond to physical objects. For example, an N-body simulation of a star cluster might have a particle per star, so each particle has some physical significance but it is not possible to resolve scales smaller than the size of a star. Many simulations simulate only cold dark matter, and thus include only the gravitational force. Incorporating baryons, leptons and photons into the simulations dramatically increases their complexity and often radical simplifications of the underlying physics must be made. However, this is an extremely important area and many modern simulations are now trying to understand processes that occur during galaxy formation. The result of N-body simulations suggests that the universe is composed largely of voids with very low density, while the dark matter condenses in large filaments and haloes with an intricate web-like structure. Galaxies form inside the dark matter halos and, therefore, they are supposed to mirror the matter distribution in the universe (it is often said that galaxies are tracers of the density field). However, because galaxies are collapsed, non-linear structures, the way in which their statistic is related to that of the matter field is non-trivial. This relationship between the spatial distribution of galaxies and the underlying dark matter density field is called galaxy bias. Due to the fact that we do not observe the matter filed but only the galaxies, understanding this relation is crucial if we want to compare theory and observations,

and the galaxy bias is indeed an active field of research (see [47]). In its simplest formulation the bias is linear and scale-independent: it can be defined as the ratio of the correlation function of the tracers with respect to the correlation function of matter. At large scales this is a good approximation (and we will stick to it for the purposes of this thesis), however at smaller scales (or if we want to profit from more precise surveys) a full bias expansion is required: a finite number of bias parameters is then needed to relate the galaxy density to the properties of the large-scale environment.

1.2 General Relativistic Effects

The large scale structure of the universe is a powerful probe to understand the universe's origin and evolution, investigate the properties of dark matter and dark energy and unveil the details of inflation. Being the final result of complicated processes starting from inflation and involving all the universe's components, it enables us to test our understanding by comparing theory and observation. Indeed, by observing the spatial distribution of galaxies in the sky it is possible to compute statistics, such as correlation functions, and compare them with the predictions of theoretical models. In this way we can, first of all, see which models correctly describe the data and, secondly, constrain the parameters of such models. When a model is favored by different observations and the parameter constraints from different experiments are in agreement, then we have strong reasons to believe that we are going towards the right direction to develop a complete theory able to describe the universe. This is the case of the ΛCDM model. It is able to explain various probes, including the CMB and the LSS, with six independent parameters: the baryon density parameter, the dark matter density parameter, the age of the universe, the scalar spectral index, the curvature perturbation amplitude at the scale $k_0 = 0.002$ Mpc^{-1} and the reionization optical depth, respectively given by

$$
\begin{aligned}
&\Omega_b h^2 = 0.02230 \pm 0.00014\,, \\
&\Omega_c h^2 = 0.1188 \pm 0.0010\,, \\
&t_0 = 13.799 \pm 0.021 \times 10^9 \text{ years}\,, \\
&n_s = 0.9667 \pm 0.0040\,, \\
&A_s = 2.441^{+0.088}_{-0.092} \times 10^{-9}\,, \\
&\tau = 0.066 \pm 0.012\,.
\end{aligned}
$$

Future galaxy surveys [19, 20, 21, 22, 23, 24] will challenge further the ΛCDM model with high precision data taken on large scales at high redshift. This will enable us not only to reduce the uncertainties associated with the model's parameters but also to test our theory of gravity. Indeed, given the unprecedented precision achieved by the experimental advances, the effects of gravity on the light propagation that were considered negligible so far will become important in the data analysis. It is precisely

on large scales that the general relativistic effects play an important role and if we do not take them into account in our theoretical predictions we might misunderstand the physical information in the coming data.

In this section we aim at describing the physics of such effects and explain how they impact the observations of the LSS. As one of the goals of this thesis is to provide accurate theoretical predictions for LSS observables in GR, an introduction on the general relativistic effects is of great importance at this point. However, we should mention that GR is not the only theory that we have at hand, and various modified gravity models have been proposed, with small differences in their tangible predictions. Discriminating which one is the correct theory of gravity is the ultimate ambition that the coming data may help us to achieve.

The general relativistic effects altering the light propagation are the result of the inhomogeneities along the light path from the source to the observer. The inhomogeneities curve the space-time through which the light travel, causing deflections of the light trajectory as well as change in the photons energy. As a result, when we observe the galaxies distribution by measuring the position of individual galaxies through their redshift z and their angular position $\hat{\boldsymbol{n}}$ on the sky, our statistics are altered by the fact that, because of the relativistic effects, the apparent galaxies positions are different than the real ones. In other words, both the redshift and the angular position are affected by the relativistic effects. When observing a single source, we cannot simply trace back the light trajectory as a straight line up to the distance inferred from the redshift assuming a homogeneous universe. In this case, even if we accept that the light propagation is altered by the relativistic effects, we cannot derive the real source position, because we do not have access to the inhomogeneities distribution along the light path from the source to the observer. On the other hand, when we are interested in statistics of the galaxies distribution and we measure the positions of large samples of galaxies, it is possible to predict the impact of the general relativistic effects on the statistical quantities extracted from the data. The reason is that, while we do not know the exact distribution of matter between a single source and the observer, we know the variance of its probability distribution function: the power spectrum, essentially the ensemble average of the product of two density fluctuation Fourier modes. Therefore, by taking the ensemble average of the expression for a given observable, one obtains a theoretical prediction that can be compared with the observation. While in theory we can perform ensemble averages over infinite realizations of the universe, in observations we are limited to measurements from our location and time, without the possibility of making repeatable experiments. Despite the fact that observationally we only have access to a limited region of one single universe, the ergodic theorem allows us to compare the theoretical ensemble averages with spatial averages over different patches in the sky. Therefore, what we can do when observing a fluctuation on a given scale λ is to average over many distinct regions of size $\sim \lambda$. Nevertheless, observations

of the universe at extreme distances will always be limited by the cosmic variance, i.e. the statistical uncertainty due to the fact that we can only observe one realization of all the possible observable universes. For example, we can only observe one CMB, so the measured positions of the peaks in the CMB spectrum, integrated over the visible sky, are limited by the fact that only one spectrum is observable from Earth. The observable universe viewed from another galaxy will have the peaks in slightly different places, while remaining consistent with the same physical laws. Furthermore, measurements are affected by cosmic large-scale structure, so a measurement of any region of sky (viewed from Earth) may differ from a measurement of a different region of sky (also viewed from Earth) by an amount that may be much greater than the sample variance. Additional limitations are due to sample variance: the difference between different finite samples of the same parent population, following a Poissonian distribution.

We now want to describe the effects due to the inhomogeneities in our universe that alter the light propagation and, in turn, our measurements of the sources' redshift z and angular position $\hat{\boldsymbol{n}} = (\theta, \phi)$. Since any light-cone observable is a function of these two quantity, the general relativistic effects have an impact on the measured value for the observable. Indeed, the redshift z and the angular position $\hat{\boldsymbol{n}}$ parametrize the past light-cone on which our observations are performed. Due to the inhomogeneities in our universe, the geometry of the light-cone is modified with respect to that of Minkowski space-time, and one has to solve the perturbed null geodesic equation to follow the light propagation. As a result, the redshift and the angular position of sources located on the light-cone receive corrections δz, $\delta\hat{\boldsymbol{n}} = (\delta\theta, \delta\phi)$, which, if not accounted for, would lead to misinterpretations of our measurements. Indeed, the general relativistic effects, responsible for the corrections δz and $\delta\hat{\boldsymbol{n}}$, obviously modify the shape of the observed areas and volumes containing the sources, the radial distance to them and in some measurements the number of sources.

In order to understand how the relativistic effects enter in the measurements of LSS observables, we provide the reader with a description of the following ones: redshift-space distortion, local potentials, integrated Sachs-Wolfe effect, gravitational lensing and Shapiro time delay. The redshift-space distortion, introduced by Kaiser in 1987 [48], is the effect that causes the spatial distribution of galaxies to appear squashed and distorted when their positions are plotted as a function of their redshift rather than as a function of their distance. The idea is that the mapping from real space to redshift space is not only derived by considering the Hubble flow, as the peculiar velocities of the galaxies generate a Doppler shift on top of the redshift due to the universe expansion. Redshift-space distortions manifest in two ways. The Fingers of God effect is what causes the galaxy distribution to appear elongated in redshift space along the direction of observation. It is due to a Doppler shift associated with the random peculiar velocities of galaxies bound in structures such as clusters. The

fact that we observe the galaxies from a particular direction breaks the symmetry of the system and generates finger-like structures pointing toward the observer in the redshift-space map of the galaxy distribution, as the Doppler shift is only due to the component of the peculiar velocities aligned with the direction of observation. Because of this effect, the deviation from the Hubble's law relationship between distance and redshift is altered, and, if not accounted for, this would lead to inaccurate distance measurements. The other way in which redshift-space distortions manifest in the measurements of the galaxy distribution is the so-called Kaiser effect. In this case the distortion is caused by the coherent motions of galaxies as they fall inwards towards the cluster center, and it appears as a flattening of the structure (sometimes referred to as Pancake of God). It is a much smaller effect than the Fingers of God but it is more important to us as it occurs on larger scales, where the general relativistic effect manifest themselves. For this reason, in this thesis we refer to the Kaiser effect when we talk about redshift-space distortions. While the previous effects are a consequence of special relativity, there are additional effects that arise from general relativity. One is the effect of local potentials, which originates from the redshift, or blueshift, that is acquired when the photons climb out of the gravitational potential well of the distant source galaxy and then falls into the potential well of the Milky Way galaxy. This effect will make galaxies at a higher gravitational potential than Earth appear closer, and galaxies at lower potential will appear farther away.

The other effects of general relativity on clustering statistics are observed when the light from a background galaxy passes near, or through, a closer galaxy or cluster. These effects are the integrated Sachs-Wolfe effect, gravitational lensing and Shapiro time delay. The integrated Sachs-Wolfe effect is the gravitational redshift that occurs when light travels through a time evolving potential. For example, when the light from a distant galaxy travels into a large overdense region, such as a supercluster, it gains potential energy. When the light leaves the supercluster, it must loose that energy to climb the gravitational potential up. However, dark energy stretches and flattens the potential in the meantime, and allows the light to keep some of the energy it gained. Similarly, light leaving large underdense regions, such as supervoids, looses some of its initial energy. Gravitational lensing, unlike all of the previous effects, distorts the apparent position and number of background galaxies. There are two regimes of gravitational lensing, called strong and weak gravitational lensing, depending on the amplitude of the deflection angle in the photon path. While the presence of any mass bends the trajectory of light passing near it, this effect rarely produces the giant arcs and multiple images associated with strong gravitational lensing. Most lines of sight in the universe are in the weak lensing regime, in which the deflection is impossible to detect in a single background source. Weak gravitational lensing is indeed an intrinsically statistical effect describing how small deflection angles all along the photon paths alter the galaxy distribution. The main effect of gravitational lensing in LSS measure-

ments is the magnification and distortions of observed areas in the sky. Because of multiple small deflections of the photon path due to the inhomogeneities between the sources and the observer, the physical area containing the sources and subtended by a solid angle at the observer is different from the apparent one. Another important and consequent effect of gravitational lensing is flux magnification. A galaxy survey can only detect galaxies whose flux is greater than the detector sensitivity. By magnifying (or demagnifying) the area containing the galaxies, the gravitational lensing effect decreases (increases) the observed flux and thus we detect a lower (higher) number of sources. Finally, the Shapiro time delay is the change in the radial distance to the source galaxy due to the gravitational potentials that the photons encounter from the source to the observer. The gravitational potentials of the inhomogeneities cause a time delay in the arrival of photons, which increases the path length. In this thesis we deal with the luminosity distance, the galaxy number density, the galaxy two-point correlation function and the galaxy power spectrum, but the relativistic effects enter in many other LSS observables such as, for example, the Lyman-alpha forest, 21-cm intensity mapping and the Hubble diagram.

CHAPTER 2

Cosmological Perturbation Theory

In this chapter we review the basic equations and concepts of the universe evolution in perturbation theory. In this approach, the inhomogeneities responsible for the general relativistic effects in the light propagation are treated as small perturbations from a fictitious perfectly homogeneous and isotropic background. We will first introduce the geometry (described by the metric tensor) and the energy-momentum tensor of the background universe in sec. 2.1, presenting the equations governing the evolution of both the universe expansion and the energy density of its components. Then, in sec. 2.2, we will consider the inhomogeneities in the real universe, describing them as small variations of the geometry and of the energy-momentum tensor. This allows us to solve for their evolution in perturbation theory. After discussing the issues associated with the gauge freedom of general relativity, we will therefore present the evolution equations for the perturbations and their initial conditions.

2.1 The homogenous and isotropic universe

In general relativity the geometry and the causal structure of the space-time is described by the metric tensor $g_{\mu\nu}$. The metric of the homogenous and isotropic background universe is the Friedmann Lemaître Robertson Walker (FLRW) metric:

$$ds^2 = g_{\mu\nu}dx^\mu dx^\nu = -dt^2 + a^2(t)\, q_{ij}\, dx^i dx^j = a^2(\eta)\big(- d\eta^2 + q_{ij}\, dx^i dx^j \big)\,, \tag{2.1}$$

where x^μ is a generic space-time coordinate ($\mu = 0, \dots, 3$), t is cosmic time, $a(t)$ is the scale factor, q_{ij} is the spatial metric tensor, x^i is a generic spatial coordinate ($i = 1, 2, 3$) and η is conformal time. Cosmic time represents the proper time of an

observer who sees a spatially homogeneous and isotropic universe. It is the choice of time coordinate x^0 that foliates the four-dimensional space-time manifold into three-dimensional spatial slices of constant curvature. Conformal time is related to cosmic time via $d\eta = dt/a$ and its definition allows one to write the FLRW metric conformally to the Minkowski metric. The scale factor parametrizes the relative expansion of the universe with values ranging from zero at the big bang to one at the present time. It is linked to the cosmological redshift as $1 + z = 1/a$, and to the temperature of the universe as $T = T_0/a$, where T_0 is the temperature today. The spatial metric can be written in spherical coordinates as

$$q_{ij}\, dx^i dx^j = dr^2 + S_K^2(r) d\Omega^2 = dr^2 + S_K^2(r)\left(d\theta^2 + \sin^2\theta d\phi^2\right), \tag{2.2}$$

where K is the curvature parameter and the analytical function $S_K(r)$ of both r and K is given by

$$S_K(r) \equiv \begin{cases} 1/\sqrt{K}\,\sin(\sqrt{K}r) & K > 0\,, \\ r & K = 0\,, \\ 1/\sqrt{K}\,\sinh(\sqrt{K}r) & K < 0\,. \end{cases} \tag{2.3}$$

The coordinates (r, θ, ϕ) are called comoving coordinates and for a particle moving on a background geodesic they remain constant as the universe expands.

While the metric tensor describes the geometry of space-time, the density and flux of energy and momentum in space-time are described by the energy-momentum tensor. In a homogeneous and isotropic universe, the energy-momentum tensor is that of a perfect fluid and can be written in terms of the energy density ρ and pressure p of the fluid as

$$T_{\mu\nu} = \begin{pmatrix} -\rho\, g_{00} & 0 \\ 0 & p\, g_{ij} \end{pmatrix}, \tag{2.4}$$

where the scale factor enters through the components of the metric. Note that, written in this way, the energy-momentum tensor is independent on our choice of coordinates.

2.1.1 Friedmann and energy conservation equations

We now have all ingredients to introduce the Einstein equations, which govern the evolution of the scale factor, and the energy conservation equations, which govern the evolution of the energy density for different components. We first write down the Einstein equations for a generic space-time:

$$R_{\mu\nu} - \frac{1}{2} R\, g_{\mu\nu} + \Lambda\, g_{\mu\nu} = 8\pi G\, T_{\mu\nu}\,, \tag{2.5}$$

where $R_{\mu\nu}$ is the Riemann tensor and R is the Ricci scalar. In a homogeneous and isotropic universe the Einstein equations reduce to the Friedmann equations:

$$H^2 + \frac{K}{a^2} - \frac{\Lambda}{3} = \frac{8\pi G}{3}\rho\,, \qquad 2\frac{\ddot{a}}{a} + H^2 + \frac{K}{a^2} - \Lambda = -8\pi G\, p\,, \tag{2.6}$$

where a dot denotes derivative with respect to cosmic time and $H = \dot{a}/a$ is the Hubble parameter describing the universe expansion rate. It is common to define also a conformal Hubble parameter $\mathcal{H} = a'/a = aH$, where a prime denotes derivative with respect to conformal time. Since one usually sets $a_0 = 1$, we have $\mathcal{H}(\eta_0) \equiv \mathcal{H}_0 = H(t_0) \equiv H_0 \equiv h \cdot 100\,\mathrm{km/s/Mpc}$, with $h \simeq 0.7$.

We now consider the energy conservation equations: $\nabla_\mu T^{\mu\nu} = 0$, where ∇_μ is the covariant derivative. By taking the $\nu = 0$ component we obtain the conservation law in an expanding universe:

$$\rho' = -3\mathcal{H}(\rho + p)\,. \tag{2.7}$$

The conservation law can be applied immediately to glean information about the scaling of different components with the expansion. Indeed, by specifying the equation of state for a given component as $p = w\rho$, where $w =$ constant, one obtains

$$\rho = \rho_0\, a^{-3(1+w)}\,, \tag{2.8}$$

from which the evolution of the energy density for that component is inferred. For instance, in the case of matter we have $w = 0$ and therefore $\rho_m \propto a^{-3}$, for radiation and relativistic particles we have $w = 1/3$ and therefore $\rho_r \propto a^{-4}$, while for the cosmological constant we have $w = -1$ and therefore $\rho_\Lambda =$ contant.

From the first Friedmann equation without dark energy ($\Lambda = 0$) one can derive the value of the energy density for which the spatial geometry is flat, i.e. $K = 0$. This value is called the critical density and it is given by

$$\rho_c = \frac{3H^2}{8\pi G}\,. \tag{2.9}$$

With this one can define the density parameter $\Omega = \rho/\rho_c$ for every component. In this thesis we will deal with the matter density parameter, the radiation density parameter, the baryon density parameter and the dark energy density parameter, respectively defined as

$$\Omega_m = \rho_m(t_0)/\rho_c(t_0)\,, \tag{2.10}$$
$$\Omega_r = \rho_r(t_0)/\rho_c(t_0)\,, \tag{2.11}$$
$$\Omega_b = \rho_b(t_0)/\rho_c(t_0)\,, \tag{2.12}$$
$$\Omega_\Lambda = \rho_\Lambda(t_0)/\rho_c(t_0)\,. \tag{2.13}$$

Note that the first Friedmann equation implies $1 = \sum_i \Omega_i$, which is usually used to fix the dark energy content of a flat universe as $\Omega_\Lambda = 1 - \sum_{i \neq \Lambda} \Omega_i$. Finally, we can write down the first Friedmann equation in terms of the evolution of the Hubble parameter as a function of redshift:

$$H(z) = H_0 \sqrt{\Omega_r (1+z)^4 + \Omega_m (1+z)^3 + \Omega_K (1+z)^2 + \Omega_\Lambda + \dots}\,, \tag{2.14}$$

where $\Omega_K = -K/H_0^2$ is the curvature density parameter and the dots stand for any additional components in the universe such as baryons or neutrinos. In conclusion, the Ω parameters fix the background evolution of the universe given by $a(t)$. However, the differential equation for $a(t)$ has no general analytic solution.

2.1.2 Distances in cosmology

We conclude this section by discussing the notions of distances and horizons in cosmology. First of all, the comoving distance to a source emitting photons at time t_z (corresponding to the redshift z) that are detected at the present time t_0 (corresponding to redshift zero) is given by

$$r_z = \eta_0 - \eta_z = \int_{t_z}^{t_0} \frac{dt'}{a(t')} = \int_0^z \frac{dz'}{H(z)}\,. \tag{2.15}$$

Note that the comoving distance does not change in time if the source moves only with the expansion. At this point it is also important to stress that the only way we have to infer the time of photon emission is by measuring the redshift. This fact should be kept in mind as it is essential for understanding the description of light-cone observables later on in this thesis. From the above definition of the comoving distance we realize that conformal time corresponds to the maximum distance that the light could have travelled at time t since $t = 0$

$$\eta = \int_0^t \frac{dt'}{a(t')}\,, \tag{2.16}$$

also called the comoving horizon, as no signal can propagate further. We can now define the particle horizon as the corresponding proper distance

$$R_H(t) = a(t) \int_0^t \frac{dt'}{a(t')}\,. \tag{2.17}$$

The particle horizon should not be confused with the Hubble radius defined as H^{-1}. Indeed, events separated by a distance greater that R_H were never in causal contact while events separated by a distance greater than $H(t)^{-1}$ are not in causal contact at time t.

A common way to determine distances in cosmology is to measure the angle θ subtended by an object of known physical size l. The distance to that object, called the angular diameter distance, is then given by

$$\mathcal{D}_A = \frac{l}{\theta}\,, \tag{2.18}$$

assuming that θ is small. In a spatially flat expanding universe its derivation yields

$$\mathcal{D}_A(z) = \frac{r_z}{1+z}\,. \tag{2.19}$$

Another way to infer distances in comsology is to measure the flux F from an object of known luminosity L. The distance to that object, called the luminosity distance, is then given by

$$\mathcal{D}_L = \sqrt{\frac{L}{4\pi F}}\,, \tag{2.20}$$

which is also valid in an expanding universe as long as we define

$$\mathcal{D}_L(z) = r_z(1+z)\,. \tag{2.21}$$

The Etherington relation links $\mathcal{D}_A$ to $\mathcal{D}_L$ through

$$\mathcal{D}_L(z) = (1+z)^2\mathcal{D}_A(z)\,, \tag{2.22}$$

where one factor of $(1+z)$ comes from the arrival time delay of photons and the other is due to the redshift of individual photons.

2.2 The inhomogenous universe

We now leave the comfortable (back)ground of a homogenous and isotropic universe to discuss the properties of our real inhomogeneous universe. The way we introduce inhomogeneities in perturbation theory is through small perturbations to the metric tensor and the energy-momentum tensor of the background. We can write the metric $g_{\mu\nu}$ of the inhomogeneous universe as $g_{\mu\nu} = \bar{g}_{\mu\nu} + \delta g_{\mu\nu}$, where $\bar{g}_{\mu\nu}$ is the background metric and $\delta g_{\mu\nu}$ is a small perturbation around it. Analogously, the energy-momentum tensor can be written as $T_{\mu\nu} = \bar{T}_{\mu\nu} + \delta T_{\mu\nu}$. From now on we will use a bar to denote quantities in the background, which we assume to be flat ($K = 0$), and we will implicitly use Cartesian spatial coordinates ($q_{ij} = \delta_{ij}$).

2.2.1 Perturbed metric and energy-momentum tensors

The perturbations to the background FLRW metric are represented by

$$\delta g_{\mu\nu} dx^\mu dx^\nu = -2a^2 \mathcal{A}\, d\eta^2 - 2a^2 \mathcal{B}_i\, d\eta dx^i + 2a^2 \mathcal{C}_{ij}\, dx^i dx^j \,. \tag{2.23}$$

Since the metric tensor is symmetric, it has ten independent components and therefore 10 degrees of freedom. Using the scalar-vector-tensor decomposition, the perturbation variables can be expressed in terms of 4 scalar, 4 vector and 2 tensor degrees of freedom (readily distinguishable by their spatial indices) as

$$\begin{aligned} \mathcal{A} &\equiv \alpha \,, \\ \mathcal{B}_i &\equiv \partial_i \beta + B_i \,, \\ \mathcal{C}_{ij} &\equiv \varphi\, q_{ij} + \partial_i \partial_j \gamma + \frac{1}{2}\big(\partial_i C_j + \partial_j C_i\big) + C_{ij} \,, \end{aligned} \tag{2.24}$$

where B_i and C_i are divergenceless vectors ($\partial_i B^i = \partial_i C^i = 0$) and C_{ij} is a symmetric, traceless tensor ($\partial_i C^{ij} = C^i_i = 0$). In this way we have have exactly 10 degrees of freedom: one from each scalar (α, β, φ, γ), two from each vector field (B_i, C_i) and two from the tensor field (C_{ij}), with the advantage that the scalar, vector and tensor evolution equations are decoupled in linear theory. For the energy-momentum tensor we have

$$T_{\mu\nu} = p g_{\mu\nu} + (\rho + p) u_\mu u_\nu + q_\mu u_\nu + q_\nu u_\mu + \pi_{\mu\nu} \,, \tag{2.25}$$

where $\rho = T^{\mu\nu} u_\mu u_\nu$ represents the energy density, $p = \frac{1}{3} T^{\mu\nu}(g_{\mu\nu} + u_\mu u_\nu)$ is the isotropic and entropic pressure, q_μ is the energy flux and $\pi_{\mu\nu}$ is the anisotropic pressure of the fluid, all measured by an observer with four-velocity u_μ such that $u_\mu u^\mu = -1$. Note that the time component of the four-velocity is fixed by the normalization

$$\begin{aligned} u_0 &= -a\,(1 + \alpha) \,, \\ u^0 &= \frac{1}{a}(1 - \alpha) \,, \end{aligned} \tag{2.26}$$

while for the spatial components we set

$$\begin{aligned} u^i &= \frac{1}{a} v^i \,, \\ u_i &= a(v_i - \mathcal{B}_i) \,. \end{aligned} \tag{2.27}$$

The spatial part v^i can be further decomposed into its scalar and vector components as $v^i = -\partial^i v + V^i$, where $\partial_i V^i = 0$. We now write the linear order perturbations to the energy density and the pressure as

$$\begin{aligned} \rho &= \bar{\rho}\,(1 + \delta) \,, \\ p &= \bar{p} + \delta p \,. \end{aligned} \tag{2.28}$$

With these definitions the perturbed part of the energy-momentum tensor is given by

$$\begin{aligned}\delta T_{00} &= a^2\bar{\rho}\,(\delta + 2\mathcal{A})\,,\\ \delta T_{0i} &= a^2\big[-(\bar{\rho}+\bar{p})v_i - \bar{p}\,\mathcal{B}_i - q_i\big]\,,\\ \delta T_{ij} &= a^2\big[q_{ij}\delta p + 2\bar{p}\,\mathcal{C}_{ij}\big] + \pi_{ij}\,.\end{aligned} \tag{2.29}$$

Finally, we decompose the anisotropic stress into its scalar, vector and tensor part as

$$\pi_{ij} = \left(\partial_i\partial_j - \frac{1}{3}q_{ij}\Delta\right)\Pi + \frac{1}{2}\big(\partial_i\Pi_j + \partial_j\Pi_i\big) + \Pi_{ij}\,. \tag{2.30}$$

2.2.2 Gauge invariance

At this point, before writing down the perturbed Einstein equations and energy-momentum conservation equations, it is rightful to discuss the issues associated with the gauge freedom of general relativity. The problem is that, since the theory is invariant under coordinate transformation, the perturbations are not uniquely defined, but depend on our gauge choice. Indeed, when we introduce perturbations, we are dealing with two different space-times: the physical space-time $g_{\mu\nu}$ and the fictitious background $\bar{g}_{\mu\nu}$ with respect to which the perturbations are defined. For a given coordinate system in the background there is no unique choice of coordinates in the perturbed space-time. Different coordinate systems are related by a gauge transformation and fixing them corresponds to a gauge choice. To clarify this, let us consider a generic coordinate transformation

$$x^\mu \longrightarrow \tilde{x}^\mu = x^\mu + \xi^\mu(x)\,, \tag{2.31}$$

where $\xi^\mu = (T, \mathcal{L}^i)$ and we further decompose the spatial component into scalar and vector part as $\mathcal{L}^i = \partial^i L + L^i$, where $\partial_i L^i = 0$. Note that T, L and L^i are all functions of the coordinate x^μ. The gauge transformation for a tensor G is given in terms of the Lie derivative along the field ξ^μ

$$\tilde{G}(x) = G(x) - \pounds_\xi G(x)\,, \tag{2.32}$$

so that for the metric tensor we have

$$\tilde{g}_{\mu\nu} = g_{\mu\nu} - \xi^\rho\partial_\rho g_{\mu\nu} - \partial_\mu\xi^\rho g_{\rho\nu} - \partial_\nu\xi^\rho g_{\mu\rho}\,. \tag{2.33}$$

For the metric perturbations $\delta g_{\mu\nu}$ this implies

$$\begin{aligned}
\tilde{\alpha} &= \alpha - T' - \mathcal{H}T\,, && (2.34)\\
\tilde{\beta} &= \beta - T + L'\,, && (2.35)\\
\tilde{\gamma} &= \gamma - L\,, && (2.36)\\
\tilde{\varphi} &= \varphi - \mathcal{H}T\,, && (2.37)\\
\tilde{B}_i &= B_i + L_i' && (2.38)\\
\tilde{C}_i &= C_i - L_i\,, && (2.39)\\
\tilde{C}_{ij} &= C_{ij}\,. && (2.40)
\end{aligned}$$

On other hand, for the energy momentum tensor $T_{\mu\nu}$ one obtains

$$\begin{aligned}
\tilde{\delta} &= \delta - \frac{\bar{\rho}'}{\bar{\rho}}T\,, && (2.41)\\
\tilde{\delta p} &= \delta p - \bar{p}'T\,, && (2.42)\\
\tilde{v} &= v - T\,, && (2.43)\\
\tilde{V}_i &= V_i + L_i'\,, && (2.44)\\
\tilde{\pi}_{ij} &= \pi_{ij}\,. && (2.45)
\end{aligned}$$

We now see that, if we start in a gauge where, for instance, g_{00} is unperturbed ($\alpha = 0$), a gauge transformation can introduce a perturbation $\tilde{\alpha} = -T' - \mathcal{H}T$. In general, with a gauge transformation we can introduce spurious degrees of freedom in the metric perturbations which are unphysical but still satisfy the Einstein equations. The problem is now to distinguish physical perturbations and spurious gauge modes. Since the perturbation $\delta g_{\mu\nu}$ is a symmetric tensor, it has 10 degrees of freedom: 4 scalar, 4 vector and 2 tensor degrees of freedom. With a coordinate transformation one can eliminate 2 scalar and 2 vector degrees of freedom, obtaining the 6 physical degrees of freedom of the theory. Finally, we are left with 2 scalars, 1 transverse vector and 1 transverse, traceless tensor. A gauge choice fixes how these 6 physical d.o.f. are combined in $\delta g_{\mu\nu}$, as one can remove perturbations from the metric with an appropriate gauge transformation. Different choices of gauge are

- Poisson gauge: In this gauge the metric has the following form:

$$ds^2 = a^2(\eta)\Big\{-(1+2\alpha)d\eta^2 - 2B_i\,d\eta dx^i + \Big[(1+2\varphi)q_{ij} + 2C_{ij}\Big]dx^i dx^j\Big\}\,. \qquad (2.46)$$

  This means that the gauge conditions are given by

$$\begin{aligned}
&\tilde{\gamma} = \gamma = 0 \;\rightarrow\; L = 0\,,\\
&\tilde{\beta} = \beta = 0 \;\rightarrow\; T = 0\,, && (2.47)\\
&\tilde{C}_i = C_i = 0 \;\rightarrow\; L_i = 0\,.
\end{aligned}$$

- Conformal Newtonian gauge: The conformal Newtonian gauge is a restricted version of the Poisson gauge with scalar perturbations only. The scalar perturbation variables commonly used are

$$\psi = \alpha - \mathcal{H}(\beta + \gamma') - (\beta' + \gamma'')\,, \tag{2.48}$$
$$\phi = \varphi - \mathcal{H}(\beta + \gamma')\,. \tag{2.49}$$

  In this case, the metric becomes

$$ds^2 = a^2(\eta)\Big\{-(1+2\psi)d\eta^2 + (1+2\phi)q_{ij}dx^i dx^j\Big\}\,. \tag{2.50}$$

- Synchronous-comoving gauge: In this gauge, the time-time component and the space-time component of the metric tensor are unperturbed

$$ds^2 = a^2(\eta)\Big\{-d\eta^2 + (q_{ij} + 2\mathcal{C}_{ij})dx^i dx^j\Big\}\,. \tag{2.51}$$

  This means that the gauge conditions are given by

$$\tilde{\alpha} = \alpha = 0 \;\rightarrow\; (aT)' = 0\,, \tag{2.52}$$
$$\tilde{\beta} = \beta = 0 \;\rightarrow\; T = L'\,, \tag{2.53}$$
$$\tilde{B}_i = B_i = 0 \;\rightarrow\; L_i' = 0\,, \tag{2.54}$$

  which do not fix the gauge freedom completely.

One important point to stress is the following: observables are gauge-invariant, i.e. they do not transform under gauge-transformation, as the result of a measurement cannot depend on our choice of coordinates. As a consequence, the gauge-invariance of general relativity offers a powerful way to check the validity of theoretical predictions derived in perturbation theory. However, If we fix the gauge before starting the computations we cannot check the gauge-invariance of any expression. The solution is to introduce gauge-invariant variables, i.e. combinations of metric perturbation which do not transform under a gauge transformation, and which therefore represents physical degrees of freedom. For the metric the most important gauge-invariant variables are given by the Bardeen potentials defined above as ψ and ϕ, while for the energy-momentum tensor the comoving gauge ($v = 0$) density perturbation is gauge-invariant: $\delta_v = \delta - (\bar{\rho}'/\bar{\rho})v$. We will come back to the gauge problem in chapter 3, where we will demonstrate the importance of following a gauge-invariant formalism even for a non-perturbative approach to the LSS observables.

2.2.3 Einstein and energy-momentum conservation equations

We can finally write down the perturbed Einstein equations. At linear order, the scalar, vector and tensor perturbations do not mix and can therefore be considered

separately. By switching to Fourier space and choosing the Poisson gauge, where the metric perturbations α and φ correspond to the Bardeen potentials ψ and $-\phi$ respectively, the linearized Einstein equations read

- '00' equation

$$k^2\phi + 3\mathcal{H}(\phi' + \mathcal{H}\psi) = -4\pi G a^2 \bar{\rho}\delta\,, \tag{2.55}$$

- '$0i$' equations

$$k_i(\phi' + \mathcal{H}\psi) = (\mathcal{H}^2 - \mathcal{H}')k_i v\,, \tag{2.56}$$

$$k^2 B_i = 4(\mathcal{H}^2 - \mathcal{H}')(V_i - B_i)\,, \tag{2.57}$$

- 'ij' equations

$$(\partial_\eta + 2\mathcal{H})k^2 B_i = 8\pi G a^2 k^2 \Pi_i\,, \tag{2.58}$$

$$\left(\frac{1}{3}q_{ij}k^2 - k_i k_j\right)(\phi - \psi) = 8\pi G a^2\left(\frac{1}{3}q_{ij}k^2 - k_i k_j\right)\Pi\,, \tag{2.59}$$

$$\phi'' + 3\mathcal{H}\phi' + (2\mathcal{H}' + \mathcal{H}^2)\phi = 4\pi G a^2 \delta p\,, \tag{2.60}$$

$$(\partial_\eta^2 + 2\mathcal{H}\partial_\eta + k^2)C_{ij} = 8\pi G a^2 \Pi_{ij}\,. \tag{2.61}$$

By combining eqs. (2.55) and (2.56) with the definition of the matter density perturbation in the comoving gauge, $\delta_v = \delta + 3\mathcal{H}v$, and the background Friedmann equations, we also obtain the Poisson equation

$$-k^2\phi = 4\pi G a^2 \bar{\rho}\,\delta_v\,. \tag{2.62}$$

The equations governing the evolution of the fluid quantities are derived from the energy-momentum conservation $\nabla_\mu T^{\mu\nu} = 0$. For $\nu = 0$ we obtain the continuity equation

$$\delta' + (1+w)(-k^2 v - 3\phi') + 3\mathcal{H}\left(\frac{\delta p}{\delta\bar{\rho}} - w\right)\delta = 0\,. \tag{2.63}$$

For $\nu = i$ we obtain the Euler equation

$$V' + \mathcal{H}V - 3\mathcal{H}wV - k\psi = \frac{\delta p}{(1+w)\bar{\rho}}\,, \tag{2.64}$$

where we defined $V = kv$. Note that, if one considers more components in the universe, the continuity and Euler equations hold if the energy-momentum of the different components is separately conserved. In this case one can specify the continuity and Euler equations for a given component. On the other hand the Einstein equations determine the metric induced by the full perturbations, i.e., one has to consider the sum over all components in the fluid quantities.

2.2.4 Initial conditions and linear growth

In order to solve for the evolution of the perturbations until the formation of the large scale structure in which we are interested, we also need to know the initial conditions. Any mode which is relevant today was outside the horizon back in the past, during the inflationary epoch, when the perturbations originated. The initial conditions are therefore set by inflation, which predicts the configurations of these super-horizon modes. In particular, inflation predicts the power spectrum of the comoving curvature perturbation $\zeta = \varphi - \mathcal{H}v$. The advantage of considering this quantity is that it is constant on super-horizon scales ($k \ll \mathcal{H}$). Indeed, by using the Einstein equations, one can show that

$$\frac{d\ln\zeta}{d\ln a} \sim \left(\frac{k}{\mathcal{H}}\right)^2 . \tag{2.65}$$

This means that, for each mode $\boldsymbol{k}$, the value of $\zeta_{\boldsymbol{k}}$ at horizon exit during inflation remains unchanged until horizon entry. Therefore, one can relate the super-horizon values of the perturbations ($\psi_{\boldsymbol{k}}$, $\phi_{\boldsymbol{k}}$, $\delta_{\boldsymbol{k}}$, $v_{\boldsymbol{k}}$ etc.) to the constant value $\zeta_{\boldsymbol{k}}$ until horizon entry, and then study their evolution through radiation domination and/or matter domination, depending on the time of horizon crossing. In matter domination, since cold dark matter produces no pressure, all modes grow uniformly independently of the wavevector $\boldsymbol{k}$. As we mentioned in the introduction, the evolution of perturbations is described by the transfer function. If we consider, for instance, the matter density fluctuation, we can write

$$\delta_{\boldsymbol{k}}(\eta) = T_\delta(k,\eta)\zeta_{\boldsymbol{k}} . \tag{2.66}$$

In general, the transfer function $T(k,\eta)$ can be factorized as $\mathcal{T}(k)D(\eta)$, where $\mathcal{T}(k)$ describes the evolution between horizon exit and entry, while the growth function $D(\eta)$ describes the wavelength-independent evolution at late times. To obtain the exact expressions of the transfer functions for different perturbations, codes such as `CAMB` and `CLASS` solve the hierarchy of Boltzmann equations and Einstein equations. The latter also provide relations between the transfer functions of different perturbations at late times. For instance, the Poisson equation for matter

$$-k^2\phi = \frac{3H_0^2\Omega_m}{2a}\delta , \tag{2.67}$$

where we substituted $\bar{\rho} = \Omega_m\bar{\rho}_c\, a^{-3}$ and $4\pi G\bar{\rho}_c = 3H_0^2/2$ into eq. (2.62), links the transfer function T_ϕ of the gravitational potential to that of the matter perturbation as

$$T_\phi = -\frac{3\Omega_m}{2a}\left(\frac{H_0}{k}\right)^2 T_\delta . \tag{2.68}$$

Therefore, in order to solve for the wavelength-independent evolution of the matter density perturbation during matter domination, we can use eq. (2.60) for cold dark

matter

$$\phi'' + 3\mathcal{H}\phi + (2\dot{\mathcal{H}} + \mathcal{H}^2)\phi = 0\,. \tag{2.69}$$

Indeed, since $\phi \propto \delta/a$, we obtain

$$\delta'' + \mathcal{H}\delta' + (\mathcal{H}' - \mathcal{H}^2)\delta = 0\,. \tag{2.70}$$

By defining $\delta(\eta) = \delta(\eta_{\rm in})D_1(\eta)/D_1(\eta_{\rm in})$, where $\eta_{\rm in}$ is the time of horizon entry (or any later time), the above equation can be written as

$$\frac{d^2D_1}{da^2} + (2 - \Omega_m(a))\frac{3}{2a}\frac{dD_1}{da} - \frac{3}{2a^2}D_1 = 0\,. \tag{2.71}$$

The analytic solution is well-known:

$$D_1(a) = a\,{}_2F_1\left[\frac{1}{3}, 1, \frac{11}{6}, -\frac{a^3}{\Omega_m(a)}(1 - \Omega_m(a))\right], \tag{2.72}$$

where ${}_2F_1$ is the hypergeometric function and $\Omega_m(a) = \rho_m(a)/\rho_c(a)$. This result represents one of the main achievements of linear perturbation theory. Similar predictions can be obtained for the other perturbation variables, as their growth functions are linked to D_1 through the Einstein equations (see appendix 4.A of chapter 4).

We have described how inhomogeneities in the early universe evolve from the initial conditions set by inflation to form the large scale structure we observe today. Knowledge of the perturbations' growth at any time is essential for the purpose of this thesis, that is: providing accurate theoretical prediction for LSS observables. Indeed, the perturbations are responsible for the relativistic effects in the measurements of these observables, as they alter the photon propagation. In a redshift survey, galaxy positions are identified by measuring the redshift z and the angular direction $\hat{\boldsymbol{n}} = (\theta, \phi)$ of incoming photons. The photons emitted by distant galaxies travel along the past light-cone of the observer, who measures their redshift and angular direction in his rest frame. Because of the perturbations between the sources and the observer, in order to relate the values z, θ, ϕ measured in the observer rest frame to the real source positions, one has to solve the perturbed null geodesic equation. For a complete description of how the geodesic equation can be used to trace the photon path backward from the observer and solve for the real source positions we refer to [72]. In the following chapters we will use the geometric approach presented in [72] to compute the distortions in the source positions and derive expressions for LSS observables in general relativity. In particular, we will consider the luminosity distance, the galaxy number density, the galaxy two-point correlation function and the galaxy power spectrum.

CHAPTER 3

Observables and Gauge-Invariance in the Geodesic Light-Cone Formalism

Preface

In this chapter, which is thoroughly based on the work presented in [1], we introduce some of the key light-cone observables used in modern cosmology and topic of this thesis. These are the observed redshift, the luminosity distance and the physical area and volume of the observed source field. The other main light-cone observables – the galaxy number density, the galaxy correlation function and the galaxy power spectrum – will be studied in the following chapters to provide a comprehensive description of galaxy clustering and large scale structure observations. The focus of this chapter is on the use of gauge invariance as a validity check for theoretical predictions in general relativity. Indeed, as discussed in chapter 2, the expressions for physical observables must be independent on our gauge choice. We use this crucial property to test the validity of the expressions for the above mentioned light-cone observables when these are derived using Geodesic Light-Cone (GLC) coordinates. The GLC coordinates are interesting because they allow analytic expressions for light-cone observables, providing a non-perturbative way for calculating the effects of inhomogeneities in our universe. In order to show explicitly the gauge invariance of these expression and the validity of the GLC approach we develop a dictionary between the latter and the usual perturbative approach described in chapter 2. This dictionary allows to derive the gauge transformation properties of the GLC quantities directly from those of the usual perturbation variables. By comparing the results obtained in the GLC approach with those of perturbation theory we also demonstrate the full consistency of the two meth-

ods. This chapter provides the complete theoretical framework and all technical tools necessary to achieve the results presented in following chapters. Despite the fact that we will only use perturbation theory to investigate the effect of inhomogeneities on the galaxy number density, the galaxy correlation function and the galaxy power spectrum, the study of light propagation in GLC coordinates offers a powerful insight on the theoretical description of large scale structure observations.

Based on:

[1] F. Scaccabarozzi and J. Yoo,
"*Light-Cone Observables and Gauge-Invariance in the Geodesic Light-Cone Formalism*",
JCAP 1706 (2017) no.06, 007, [arXiv:1703.08552].

Abstract. The remarkable properties of the geodesic light-cone (GLC) coordinates allow analytic expressions for the light-cone observables, providing a new non-perturbative way for calculating the effects of inhomogeneities in our Universe. However, the gauge-invariance of these expressions in the GLC formalism has not been shown explicitly. Here we provide this missing part of the GLC formalism by proving the gauge-invariance of the GLC expressions for the light-cone observables, such as the observed redshift, the luminosity distance, and the physical area and volume of the observed sources. Our study provides a new insight on the properties of the GLC coordinates and it complements the previous work by the GLC collaboration, leading to a comprehensive description of light propagation in the GLC representation.

3.1 Introduction

The next generation of galaxy surveys will probe the Universe with high precision at very large scales [49, 50, 51]. Due to the precision achieved by observations, the theoretical representation of what is observed can no longer rely on the assumption that our Universe is homogeneous and isotropic. Indeed, the light we measure in galaxy surveys is affected by the local inhomogeneities distributed along its path. To attain the level of accuracy set by the precision of observations, theoretical predictions must take into account the relativistic effects generated by the inhomogeneities, which play a key role at the large scales explored (see for instance [52]). Only in this way we can avoid misinterpretation of surveys' measurements and extract the maximum physical information underlying the data (see [53, 54]).

Many studies have been devoted to developing a relativistic description of the observables containing the information carried by the light. In most works, the descrip-

tion of the inhomogeneities in our Universe is obtained by adding perturbations to a homogeneous and isotropic FRW metric (see e.g. [55]). In this case, the application of perturbation theory and general relativity enables the derivation of theoretical expressions for physical observables, accounting for the effects of the inhomogeneities to a certain perturbative level. Furthermore, it is often the case that specific gauge conditions are imposed to the metric perturbations before the calculations are performed.

In order to simplify the task of making theoretical predictions in the context of general relativity, the geodesic light-cone (GLC) coordinates were introduced in [56]. The GLC coordinates belong to a larger class of adapted coordinates that goes back to the pioneering works [57, 58, 59, 60]. Contrary to the perturbative approach, the GLC coordinate system defines an exact (non-perturbative) metric representation of our Universe accounting for inhomogeneities. This representation is greatly helpful for problems associated with the observation of light sources lying on the past light-cone of a given observer, allowing fully non-linear and simple expressions of light-cone observables: the observed redshift, the luminosity distance, and the physical area and volume occupied by sources. Once the expression of a given observable is obtained analytically in the GLC representation, it can be expressed perturbatively in any choice of gauge conditions by connecting the GLC metric to the chosen gauge with a coordinate transformation valid at the desired order in the perturbative theory.

In [61, 62, 63] the GLC metric was expressed in the conformal Newtonian gauge (or Poisson gauge when the calculations are extended to second order), computing the observed redshift and the luminosity distance in the presence of inhomogeneities. In these works, the GLC angular coordinate was intended to describe the observed angle of the source. However, the subtle difference between the observed angle in the observer rest frame and that in a global coordinate was neglected. Furthermore, the presence of additional degrees of freedom in the GLC variables was not taken into account. This was considered later in [64, 65], but without describing explicitly how to make use of the residual gauge freedom associated to the GLC representation.

In [64] the normalization condition for the GLC angular coordinate was fixed, bringing the expression of the luminosity distance derived with the GLC approach fully consistent with other approaches. Indeed, as we showed in [66], the geometric approach, the Sachs approach, the Jacobi mapping approach and the GLC approach reproduce the same correct prediction in the conformal Newtonian gauge.

After the correction suggested in [64], the GLC approach has been successfully used to calculate the expressions of the light-cone observables up to second order in perturbation theory in the Poisson gauge (see [64, 67, 68, 69]). However, an explicit proof of gauge-invariance for these expressions is missing in the literature. According to the general covariance of general relativity, any coordinate can be used, but the expressions of observables must be the same in any choice of gauge conditions [55]. The purpose of this chapter is to provide this missing part of the GLC formalism.

Despite the consistency of the previous results [61, 62, 63, 64, 67, 69, 68], we believe that it is important to prove the gauge-invariance by connecting the GLC metric to the most general perturbed FRW metric without choosing a gauge condition. This proof will ensure that the GLC expressions for the light-cone observables are identical in any gauge conditions beyond the gauge choices studied in previous works. In our derivation we will take into account perturbations to the first order, and we will consider all possible degrees freedom associated to the GLC variables, showing that the final expressions for the light-cone observables are independent from our normalization. Furthermore, we will check the consistency with the approach introduced in [70, 71, 72] to describe the propagation of light in an inhomogeneous universe. This latter successfully reproduces the light-cone observables in a covariant and gauge-invariant way, providing us with a yardstick to compare all results.

The organization of the chapter is as follows. In sec. 3.2.1, we introduce the GLC coordinates, describing their properties and features. In sec. 3.2.2, we express the GLC variables and metric components in terms of the metric perturbations of a general FRW representation. In sec. 3.2.3, we take a gauge transformation of the metric perturbations. Then, we calculate how the GLC quantities change accordingly. Then we derive with the GLC approach the expressions of the observed redshift in sec. 3.3.1, the luminosity distance in sec. 3.3.2, and of the source volume in sec. 3.3.3, showing the gauge-invariance. We conclude with a discussion in sec. 3.4.

Throughout the chapter, we set the speed of light $c \equiv 1$, we use the Greek indices μ, ν, ρ, σ for the spacetime components, the Greek indices $\alpha, \beta, \gamma, \delta$ for the spatial components and the Latin indices a, b, c, d for the angular components.

3.2 GLC Representation

Adopting the GLC representation one can write down exact (non-perturbative) expressions for light-cone observables. For this reason, it has been successfully used to derive the expressions for the observed redshift, the luminosity distance of faraway galaxies and the observed galaxy number density. However, in order to compute these expressions, one always has to convert the final expressions of these observables into those in the FRW metric with a particular choice of gauge conditions. Since physical quantities should be independent of our choice of gauge conditions for computation, this procedure should not cause any ambiguity, provided that the GLC approach is valid in any of these gauge choices. In this section, after presenting the GLC coordinates in detail, we perform a coordinate transformation from the GLC representation to the most general FRW metric representation at first order in perturbations. Then we take a gauge transformation and study how the GLC quantities transform.

3.2.1 GLC coordinates and their main properties

The GLC coordinates, first introduced in [56], constitute a special coordinate system, which is particularly suitable when the purpose is to extract physical information from the light emitted by distant sources. The GLC coordinates $x^\mu_{\rm GLC} = (w, \tau, \tilde\theta^a)$ are defined by the line element[1]

$$ds^2_{\rm GLC} = \Upsilon^2 dw^2 - 2\,\Upsilon\, dw\, d\tau + \gamma_{ab}\,(d\tilde\theta^a - U^a dw)(d\tilde\theta^b - U^b dw)\,, \tag{3.1}$$

which specifies the metric tensor in the GLC representation:

$$g^{\rm GLC}_{\mu\nu} = \begin{bmatrix} \Upsilon^2 + U^2 & -\Upsilon & -U_b \\ -\Upsilon & 0 & \vec 0 \\ -U_a & \vec 0 & \gamma_{ab} \end{bmatrix}, \qquad g^{\mu\nu}_{\rm GLC} = \begin{bmatrix} 0 & -1/\Upsilon & \vec 0 \\ -1/\Upsilon & -1 & -U^b/\Upsilon \\ \vec 0 & -U^a/\Upsilon & \gamma^{ab} \end{bmatrix}, \tag{3.2}$$

$$\sqrt{-g} = \Upsilon\sqrt{|\gamma|}\,, \qquad g = \det g_{\mu\nu}\,, \qquad \gamma = \det \gamma_{ab}\,, \qquad \mu,\nu = w,\tau,\tilde\theta,\tilde\phi, \qquad a,b = \tilde\theta,\tilde\phi\,.$$

In such coordinates, a generic space-time point is identified by a past light-cone hypersurface w, a proper-time hypersurface τ, and the angular position $\tilde\theta^a$ measured by the observer at the tip of the light-cone. In accordance with this definition, w generates the photon wavevector $k_\mu = \partial_\mu w$ and is therefore a null coordinate ($\partial^\mu w\, \partial_\mu w = 0$), τ generates the observer four-velocity $u_\mu = -\partial_\mu \tau$, which follows a geodesic flow ($u^\nu \nabla_\nu u^\mu = 0$) and satisfies $k^\mu u_\mu = \Upsilon^{-1}$, while $\tilde\theta^a$ parametrizes a two-sphere orthogonal to the photon wavevector and is constant along the null geodesics ($k^\mu \partial_\mu \tilde\theta^a = \vec 0$). As we shall see, the metric components can be interpreted as follows: Υ describes the expansion of the universe, γ_{ab} is the induced metric on the two-sphere of constant time, U^a represents a measure of the space-time anisotropy [62].

The physical meaning of the GLC variables and metric components becomes evident when we consider a homogeneous universe. For a spatially homogeneous and isotropic FRW metric

$$ds^2 = a^2(\eta)(-d\eta^2 + dr^2 + r^2 d\theta^2 + r^2 \sin^2\theta d\phi^2)\,, \tag{3.3}$$

the transformations from a GLC coordinate $x^\mu_{\rm GLC} = (w, \tau, \tilde\theta, \tilde\phi\,)$ and metric components $g^{\mu\nu}_{\rm GLC}$ to a FRW coordinate $y^\mu_{\rm FRW} = (\eta, r, \theta, \phi)$ are given by

$$\begin{aligned} &w = \eta + r\,, && \tau = t\,, && \tilde\theta^a = \theta^a = (\theta, \phi)\,, \\ &\Upsilon = a\,, && U^a = 0\,, && \gamma_{ab} = a^2\,\bar g_{ab}\,, \end{aligned} \tag{3.4}$$

where $a(\eta)$ is the expansion scale factor, η is the conformal time, t is the proper-time (such that $dt = a\, d\eta$), $\bar g_{ab} = {\rm diag}(r^2, r^2\sin^2\theta)$, which lowers the two-dimensional indices,

[1] See [65] for the construction of the GLC line element through the coordinate basis vectors $\vec\partial_w, \vec\partial_\tau, \vec\partial_a$.

and the FRW metric is written in spherical coordinates. Mind the difference of the GLC angles $(\tilde{\theta}, \tilde{\phi})$ and the FRW coordinates (θ, ϕ). For future use, we also define the two-dimensional (angular) tensor $\hat{\bar{g}}_{ab} = \mathrm{diag}(1, \sin^2\theta)$, so that $\bar{g}_{ab} = r^2\, \hat{\bar{g}}_{ab}$.

When inhomogeneities in our Universe are taken into account, the light-cone hypersurface w and its intersection with the proper-time hypersurface τ are no longer a cone and a two-sphere, as inhomogeneities generate geometric distortions. However, when no caustics form on the past light-cone, these inhomogeneous surfaces are still *topologically equivalent* to a cone and a uniform two-sphere.[2] Consequently, in the GLC representation, photons travel along the straight line connecting the source point on the topological two-sphere and the tip of the topological cone. This straightforward geometry represents the great advantage of the GLC representation, leading to the simple expressions of light-cone observables.

3.2.2 Coordinate transformation from GLC to perturbed FRW

Physical observables must be the same in any choice of gauge conditions, regardless of the method adopted for the derivation. Our goal is to establish the gauge-invariance of light-cone observables derived in the GLC approach. So far light-cone observables in the GLC representation have been expressed in the conformal Newtonian gauge and in the synchronous gauge. Despite the consistency of the previous results [56, 61, 62, 63, 64, 65, 67, 68, 69, 73, 74, 75], we believe that it is important to prove the gauge-invariance by adopting the most general metric without choosing a gauge condition. This proof will ensure that the GLC expressions for the light-cone observables are identical in any gauge conditions beyond the two gauge choices studied in previous works.

First of all, we need to take a coordinate transformation from the GLC to the fully general perturbed FRW representation accounting for inhomogeneities. In this representation the description of the physical universe is obtained by adding perturbations to a homogeneous and isotropic FRW metric. Considering perturbations only to first order, the most general perturbed FRW metric tensor describing the physical universe is

$$g^{\mathrm{FRW}}_{\mu\nu} = a^2 \begin{bmatrix} -(1+2\mathcal{A}) & -\mathcal{B}_\alpha \\ -\mathcal{B}_\alpha & (\,\bar{g}_{\alpha\beta} + 2\mathcal{C}_{\alpha\beta}) \end{bmatrix}, \quad g^{\mu\nu}_{\mathrm{FRW}} = \frac{1}{a^2} \begin{bmatrix} -(1-2\mathcal{A}) & -\mathcal{B}^\alpha \\ -\mathcal{B}^\alpha & (\,\bar{g}^{\alpha\beta} - 2\mathcal{C}^{\alpha\beta}\,) \end{bmatrix}, \tag{3.5}$$

[2] Geometric distortions of the light-cone hypersurface may lead to the intersection of light rays, at points called caustics. In this situation the GLC formalism fails, as the topological equivalence with a cone and a uniform sphere obviously breaks down. This issue becomes important for instance at small scales where strong lensing is involved.

where $\alpha, \beta = r, \theta, \phi$, and the small perturbations from the background metric are represented by[3,4]

$$\begin{aligned} \delta g_{00} &\equiv -2\,a^2\mathcal{A} \equiv -2\,a^2\alpha\,, \qquad \delta g_{0\alpha} \equiv -a^2\mathcal{B}_\alpha \equiv -a^2(\beta_{,\alpha} + B_\alpha)\,, \\ \delta g_{\alpha\beta} &\equiv 2\,a^2\mathcal{C}_{\alpha\beta} \equiv 2a^2(\varphi\,\bar{g}_{\alpha\beta} + \gamma_{,\alpha|\beta} + C_{(\alpha|\beta)} + C_{\alpha\beta})\,. \end{aligned} \tag{3.6}$$

We decomposed the metric perturbations into scalars $(\alpha, \beta, \varphi, \gamma)$, vectors (B_α, C_α) and tensors $(C_{\alpha\beta})$, where the vector perturbations are divergenceless and the tensor perturbations are both divergenceless and traceless:

$$B^\alpha{}_{|\alpha} = 0\,, \qquad C^\alpha{}_{|\alpha} = 0\,, \qquad C^{\alpha\beta}{}_{|\alpha} = 0\,, \qquad C^\alpha_\alpha = 0\,. \tag{3.7}$$

Here the perturbations depend on the space-time point, the comma is the ordinary derivative and the vertical bar is the covariant derivative with respect to the three-spatial metric $\bar{g}_{\alpha\beta}$, which lowers the three-dimensional indices (the affine connections are given in appendix 3.A). In a global coordinate $y^\mu_{\rm FRW} = (\eta, r, \theta, \phi)$, the three-spatial metric is $\bar{g}_{\alpha\beta} = \mathrm{diag}(1, r^2, r^2\sin^2\theta)$ and a space-time point is identified by a conformal time and spherical coordinates with origin at the position of an observer moving with time-like four-velocity $u^\mu \equiv a^{-1}(1-\alpha\,, V^\alpha)$.

The GLC metric tensor in eq. (3.2) is related to the FRW metric tensor in eq. (3.5) through a coordinate transformation from $x^\mu_{\rm GLC} = (w, \tau, \tilde{\theta}^a)$ to $y^\mu_{\rm FRW} = (\eta, r, \theta^a)$:

$$g^{\mu\nu}_{\rm GLC}(x) = \frac{\partial x^\mu}{\partial y^\rho}\frac{\partial x^\nu}{\partial y^\sigma} g^{\rho\sigma}_{\rm FRW}(y)\,. \tag{3.8}$$

By solving these differential equations, we obtain the perturbative form of the GLC quantities. As a result, the coordinates w, τ, $\tilde{\theta}^a$ and the functions Υ, U^a, γ^{ab} will be expressed in terms of the coordinates η, r, θ^a and the metric perturbations $\mathcal{A}$, $\mathcal{B}_\alpha$, $\mathcal{C}_{\alpha\beta}$. In order to solve the differential equations, we first split the GLC variables into the background and perturbation quantities: $w = \bar{w} + \delta w$, $\tau = \bar{\tau} + \delta\tau$, $\tilde{\theta}^a = \bar{\tilde{\theta}}^a + \delta\tilde{\theta}^a$. In this way we can simplify the calculations by making use of the background relations in eq. (3.4). Furthermore, we parametrize the background path $\bar{x}^\mu(\bar{r}) = (\bar{\eta}_o - \bar{r}, \bar{r}, \theta^a)$ of a photon traveling from a source to the observer with an affine parameter $\bar{r}$ representing the comoving distance

$$\bar{r} = \bar{\eta}_o - \eta = \int_0^{\bar{z}(\eta)} \frac{dz}{H(z)}\,, \qquad 1 + \bar{z}(\eta) \equiv \frac{a(\bar{\eta}_o)}{a(\eta)}\,. \tag{3.9}$$

[3]The notation $C_{(\alpha|\beta)}$ means symmetrization of the indices. Analogously $C_{[\alpha|\beta]}$ means antisymmetrization.

[4]By constructing the line element from the metric tensor in eq. (3.5), the dimensions of the perturbations are $[\alpha] = [\varphi] = 1$, $[\beta] = L$, $[\gamma] = L^2$, $[B_r] = 1$, $[B_a] = L$, $[C_r] = L$, $[C_a] = L^2$, $[C_{rr}] = 1$, $[C_{ra}] = L$, $[C_{ab}] = L^2$, where L is the dimension of a length.

Here $\bar{\eta}_o$ is the conformal time of the observer today in a homogeneous universe, $H(z)$ is the Hubble parameter, and $1+\bar{z}(\eta)$ is the redshift parameter of a time coordinate η.[5] The tangent vector to the unperturbed photon geodesic $\bar{x}^\mu(\bar{r})$ is the background photon wavevector $\bar{k}^\mu$ and the variation of a given function f along $\bar{x}^\mu(\bar{r})$ is given by

$$\frac{df}{d\bar{r}} = \frac{d\bar{x}^\mu}{d\bar{r}}\frac{\partial f}{\partial \bar{x}^\mu} = \bar{k}^\mu \partial_\mu f = -\frac{\partial f}{\partial \eta} + \frac{\partial f}{\partial r}\,, \qquad \bar{k}^\mu = \frac{d\bar{x}^\mu}{d\bar{r}}\,. \tag{3.10}$$

In [61] the light-cone variables $\eta_\pm \equiv \eta \pm r$ and the corresponding partial derivatives $\partial_\pm = (\partial_\eta \pm \partial_r)/2$, were introduced to simplify the coordinate transformation in eq. (3.8). The conversion between the light-cone variables and our (background) affine parameter $\bar{r}$ is given by

$$\partial_- = -\frac{1}{2}\frac{d}{d\bar{r}}\,, \qquad \partial_+ = \frac{\partial}{\partial\eta} + \frac{1}{2}\frac{d}{d\bar{r}}\,, \qquad \int_{\eta_+}^{\eta_-} d\eta'_- = -2\int_0^{\bar{r}} d\bar{r}'\,. \tag{3.11}$$

Moreover, given a generic function $f(\bar{r})$ integrated along the background photon path from the observer to a source, we can extract boundary terms in the following way:

$$\int_0^{\bar{r}_s} d\bar{r}\,\partial_r f = \int_0^{\bar{r}_s} d\bar{r}\, f' + f\Big|_o^s\,, \tag{3.12}$$

where a prime means the derivative with respect to conformal time, and $\bar{r}_s$ represents the value of the affine parameter $\bar{r}$ corresponding to the source point along the unperturbed photon geodesic. The integration over the comoving distance $\bar{r}$ can be directly translated into an integral over conformal time η, justifying the change of derivation for the integrands. The letters "s" and "o" are used to represent that the quantities are evaluated at the source and observer positions, respectively.

Let us now put everything together to express the GLC coordinates in terms of the metric perturbations. First, to obtain w we consider the component ww of eq. (3.8):

$$\bar{w} = \eta + r\,, \qquad \frac{d}{d\bar{r}}\delta w = -\mathcal{A} + \mathcal{B}^r + \mathcal{C}^{rr}\,. \tag{3.13}$$

[5] In cosmology, the observed redshift z provides the unique physically meaningful way to express the time coordinate of a source. In the presence of inhomogeneities, the observed redshift z is split into the background expansion contribution $\bar{z}$ and a perturbation δz, such that $1+z \equiv (1+\bar{z})(1+\delta z)$. The observed redshift is used to infer the source coordinate time $\bar{\eta}_z$ using the distance-redshift relation in a homogeneous universe

$$\bar{\eta}_o - \bar{\eta}_z = \int_0^z \frac{dz}{H(z)}\,,$$

and the coordinate time $\bar{\eta}_z$ associated with the observed redshift is different from the source coordinate time η associated with the redshift parameter $\bar{z}$ (see eq. (3.45)). Note that the conformal time today in a homogeneous universe is uniquely determined (given a set of cosmological parameters) as $\bar{\eta}_o = \int_0^\infty dz/H(z)$, and the scale factor a is usually set to unity at $\bar{\eta}_o$.

The solution of the differential equation can be written as

$$\delta w_s - \delta w_o = -\int_0^{\bar{r}_s} d\bar{r}\big[\mathcal{A} - \mathcal{B}^r - \mathcal{C}^{rr}\big]\,, \tag{3.14}$$

where the integrand is a function of the position along the photon path $\bar{r}$. By using eq. (3.12) we extract the boundary terms and derive

$$\begin{aligned} w_s = \eta_s + r_s + \delta w_o - \int_0^{\bar{r}_s} d\bar{r}\,\big[\alpha - (\varphi + \beta' + \gamma'' + B^r + C^{r\prime} + C^{rr})\big] \\ + \big[\beta + \gamma' + \gamma^{\cdot r} + C^r\big]_o^s\,. \end{aligned} \tag{3.15}$$

In the literature the integration constant δw_o is often set to zero. At this point we do not specify the value of this quantity, which is related to the perturbations to the photon propagation at observation through the exact relation $k_\mu = \partial_\mu w$ (see below and appendix 3.B).[6] For a proper-time τ we consider the component $\tau\tau$ of eq. (3.8):

$$\bar{\tau} = t\,, \qquad \frac{\partial}{\partial\eta}\delta\tau = a\,\alpha\,; \qquad \tau_s = \int_0^{\eta_s} d\eta\, a\,[1+\alpha]\,. \tag{3.16}$$

For the GLC angles $\tilde{\theta}^a$ we consider the component wa of eq. (3.8):

$$\begin{aligned} \bar{\tilde{\theta}}^a &= \theta^a\,, & \frac{d}{d\bar{r}}\delta\tilde{\theta}^a &= \mathcal{B}^a + 2\mathcal{C}^{ra} - \bar{g}^{ac}\partial_c\,\delta w\,, \\ \tilde{\theta}^a_s &= \theta^a_s + \delta\tilde{\theta}^a_o + \int_0^{\bar{r}_s} d\bar{r}\,\big[\mathcal{B}^a + 2\mathcal{C}^{ra} - \bar{g}^{ac}\partial_c\,\delta w\big]\,. \end{aligned} \tag{3.17}$$

We make use of eq. (3.12) to simplify the integration as

$$\begin{aligned} \tilde{\theta}^a_s = \theta^a_s + \delta\tilde{\theta}^a_o - \bar{r}_s\,\delta w_o^{,a} + \bar{r}_s\big[(\beta+\gamma')^{,a} + (\gamma^{\cdot r} + C^r)^{,a}\big]_o \\ + \int_0^{\bar{r}_s} d\bar{r}\left(\frac{\bar{r}_s - \bar{r}}{\bar{r}_s\bar{r}}\right)\hat{\bar{g}}^{ac}\partial_c[\alpha - (\varphi + \beta' + \gamma'' + B^r + C^{r\prime} + C^{rr})] \\ + \int_0^{\bar{r}_s} d\bar{r}\,\big[B^a + C^{a\prime} + 2\,C^{ra}\big] + \big[\gamma^{\cdot a} + C^a\big]_o^s\,. \end{aligned} \tag{3.18}$$

The quantities $\delta\tilde{\theta}^a_o$ and δw_o represent initial conditions, related to our choice of normalization at the observer point. These degrees of freedom are related to the residual gauge freedom of the GLC representation pointed out in [64, 65]. Indeed, as described in [65], the definition of the GLC coordinates in sec. 3.2.1 does not fully specify the choice of light-cone and its observed angles. Consequently, it is always possible to find coordinate transformations that redefine w and $\tilde{\theta}^a$, but leave the GLC metric unchanged. These degrees of freedom should be set according to physical constraints,

[6] It is worth noting that eq. (3.15) can also be obtained from the null condition $k^\mu k_\mu = g^{\mu\nu}\partial_\mu w\,\partial_\nu w = 0$.

considering the observer peculiar velocity, the gravitational potential at the observer position and the orientation of directions in the observer rest frame with respect to the global coordinates. In appendix 3.B we show how to properly fix such freedom in order to match the GLC angles with the angles measured by the observer in the rest frame (the observed angles). However, any different choice can be made (for instance, one can set $\delta\tilde{\theta}^a_o = \delta w^a_o = 0$) with the GLC angles corresponding to the observed angles plus a constant at the observer. Naturally, the final expression of physical observables should not depend on our parametrization, as we show in sec. 3.3.2, where we derive the luminosity distance without choosing any particular normalization for $\delta\tilde{\theta}^a_o$ and δw^a_o.

Now, starting again from eq. (3.8), we derive the remaining components of the GLC variables in terms of the metric perturbations. First, for the expansion factor Υ we simply consider the component $w\tau$ of eq. (3.8):

$$\Upsilon = a(\eta)\big[1 + \alpha - V^r - \delta w'\big] \equiv a\,[1 + \delta\Upsilon]\,, \tag{3.19}$$

where we defined the fractional perturbation $\delta\Upsilon$. The induced metric γ^{ab} is obtained by considering the component ab of eq. (3.8):

$$\gamma^{ab} = \frac{1}{a^2}\Big\{(1-2\,\varphi)\bar{g}^{ab} + \big[\bar{g}^{ac}\partial_c\,\delta\tilde{\theta}^b - (\gamma^{,a|b} + C^{a|b} + C^{ab}) + a \leftrightarrow b\big]\Big\} \equiv \frac{1}{a^2}[\,\bar{g}^{ab} + \delta\gamma^{ab}\,]\,, \tag{3.20}$$

where we also defined the fractional fluctuation $\delta\gamma^{ab}$. Finally, to derive the solution for U^a we need to consider the component τa of (3.8):

$$U^a = V^a + \delta\tilde{\theta}^{a\prime}\,. \tag{3.21}$$

Since $U^a = 0$ in the homogeneous background, there is no reason to define δU^a. Note that the components of the peculiar velocity appearing in eqs. (3.19) and (3.21) are given by

$$V^\alpha = \mathcal{B}^\alpha - \frac{1}{a}\,\delta\tau^{,\alpha}\,, \tag{3.22}$$

which is obtained from considering the relation $u_\mu = -\partial_\mu\tau$, where $u_\mu = g_{\mu\nu}u^\nu = -a\,(1 + \alpha\,, \mathcal{B}_\alpha - V_\alpha)$.

3.2.3 Gauge transformation of GLC variables

In the previous section we expressed the GLC quantities in terms of the perturbations of a general metric representation. Using the gauge transformation of the metric perturbations we derive the gauge transformation of the GLC variables.

We consider the most general coordinate transformation: $\hat{x}^\mu = x^\mu + \xi^\mu$, where $\xi^\mu = (T, \mathcal{L}^\alpha)$ and $\mathcal{L}^\alpha \equiv L^{,\alpha} + L^\alpha$. The transformations of the metric perturbations are well-known

$$\begin{aligned} &\hat{\alpha} = \alpha - T' - \mathcal{H}T\,, \qquad \hat{\beta} = \beta - T + L'\,, \qquad \hat{\varphi} = \varphi - \mathcal{H}T\,, \qquad \hat{\gamma} = \gamma - L\,, \\ &\hat{B}^\alpha = B^\alpha + L^{\alpha\prime}\,, \qquad \hat{C}^\alpha = C^\alpha - L^\alpha\,, \qquad \hat{V}^\alpha = V^\alpha + \mathcal{L}^{\alpha\prime}\,, \qquad \hat{C}^{\alpha\beta} = C^{\alpha\beta}\,, \end{aligned} \tag{3.23}$$

where $\mathcal{H} = a'/a = aH$ is the conformal Hubble parameter. Based on these gauge transformation properties we can define gauge-invariant quantities at linear level:

$$\alpha_\chi = \alpha - \frac{1}{a}\chi', \quad \varphi_\chi = \varphi - H\chi, \quad \Psi^\alpha = B^\alpha + C^{\alpha\prime}, \quad \mathcal{V}^\alpha = V^\alpha + \mathcal{G}^{\alpha\prime}, \tag{3.24}$$

where $\chi = a(\beta + \gamma')$ is the scalar shear of the normal observer, transforming as $\hat{\chi} = \chi - aT$. The notation for scalar gauge-invariant variables is set up such that α_χ and φ_χ correspond to the gravitational potentials α and φ in the conformal Newtonian gauge (where $\chi = 0$) [72]. In the same spirit, we defined $\mathcal{G}^\alpha = \gamma^{,\alpha} + C^\alpha$, which conversely is a pure gauge term transforming as $\hat{\mathcal{G}}^\alpha = \mathcal{G}^\alpha - \mathcal{L}^\alpha$. With these definitions we can rewrite the GLC quantities as

$$w_s = \eta_s + r_s + \delta w_o - \int_0^{\bar{r}_s} d\bar{r}\left[\alpha_\chi - \varphi_\chi - \Psi^r - C^{rr}\right] + \left[\frac{\chi}{a} + \mathcal{G}^r\right]_o^s, \tag{3.25}$$

$$\tau_s = \int_0^{\eta_s} d\eta\left[a(1+\alpha_\chi) + \chi'\right], \tag{3.26}$$

$$\tilde{\theta}_s^a = \theta_s^a + \delta\tilde{\theta}_o^a - \bar{r}_s\,\delta w_o^{;a} + \bar{r}_s\left[\frac{\chi}{a}^{,a} + \mathcal{G}^{r,a}\right]_o + \mathcal{G}^a\Big|_o^s + \int_0^{\bar{r}_s} d\bar{r}\left[\Psi^a + 2\,C^{ra} + \left(\frac{\bar{r}_s - \bar{r}}{\bar{r}_s\bar{r}}\right)\hat{\bar{g}}^{ac}\partial_c(\alpha_\chi - \varphi_\chi - \Psi^r - C^{rr})\right], \tag{3.27}$$

$$\Upsilon = a(\eta)\left[1 + \alpha_\chi - \mathcal{V}^r + H\chi + \int_0^{\bar{r}_s} d\bar{r}\left[\alpha_\chi - \varphi_\chi - \Psi^r - C^{rr}\right]'\right], \tag{3.28}$$

$$\gamma^{ab} = \frac{1}{a^2}\left\{(1 - 2\,\varphi_\chi - 2\,H\chi)\,\bar{g}^{ab} + \left[\bar{g}^{ac}\partial_c\,\delta\tilde{\theta}^b - (\mathcal{G}^{a|b} + C^{ab}) + a \leftrightarrow b\right]\right\}, \tag{3.29}$$

$$U^a = \mathcal{V}^a - \mathcal{G}^{\alpha\prime} + \delta\tilde{\theta}^{a\prime}. \tag{3.30}$$

Thanks to the relations in eq. (3.23) we can derive how the GLC variables change under the gauge transformation:

$$\delta\hat{w}_s = \delta w_s + (\delta\hat{w}_o - \delta w_o) - \left[T + \mathcal{L}^r\right]_o^s, \tag{3.31}$$

$$\delta\hat{\tau}_s = \delta\tau_s - a(\eta_s)\,T_s, \tag{3.32}$$

$$\delta\hat{\tilde{\theta}}_s^a = \delta\tilde{\theta}_s^a + (\delta\hat{\tilde{\theta}}_o^a - \delta\tilde{\theta}_o^a) - \bar{r}_s\,(\delta\hat{w}_o^{;a} - \delta w_o^{;a}) - \bar{r}_s\left[T^{,a} + \mathcal{L}^{r,a}\right]_o - \mathcal{L}^a\Big|_o^s, \tag{3.33}$$

$$\delta\hat{\Upsilon} = \delta\Upsilon - \mathcal{H}\,T, \tag{3.34}$$

$$\delta\hat{\gamma}^{ab} = \delta\gamma^{ab} + 2\,\mathcal{H}T\,\bar{g}^{ab} + \left[(\delta\hat{\tilde{\theta}}^a - \delta\tilde{\theta}^a)^{,b} + \mathcal{L}^{a|b} + a \leftrightarrow b\right], \tag{3.35}$$

$$\hat{U}^a = U^a. \tag{3.36}$$

Clearly, the proper-time τ is a gauge-invariant physical observable. However, according to the way we split it, both the background part $\bar{\tau}$ and the perturbation $\delta\tau$ are gauge-dependent quantities, and the gauge modes associated with the two parts cancel each other. The same argument applies to the GLC angles $\tilde{\theta}^a$ when the degrees of freedom in $\delta\tilde{\theta}^a_o$ and δw^a_o are set to match the observed angles in the rest frame of the observer (see appendix 3.B), which are gauge-invariant physical observables.

3.3 Gauge-Invariance of the Light-Cone Observables in GLC

The position of a source galaxy is identified by the observed redshift z_s and the observed angles $\theta^a_{\rm obs} = (\theta_{\rm obs}, \phi_{\rm obs})$, measured in the observer rest frame. Based on these quantities, the observer infers the source position $\bar{x}^\alpha$ by using the distance - redshift relation in a homogeneous universe. However, the real position x^α_s of the source is different from the inferred one $\bar{x}^\alpha_s$, because the inhomogeneities affect the photon propagation. To account for the effect of the inhomogeneities on the real source position with respect to the inferred position we define the distortion δz in the observed redshift (related to the time distortion $\Delta\eta$) and the geometric distortions $(\delta r, \delta\theta, \delta\phi)$ of the source position. These can be computed by tracing the photon path backward from the observer to the source and solving for the real position, as described in [72]. On the other hand, the advantage of the GLC approach is that the distortions due to inhomogeneities are already incorporated in the coordinate system. As a consequence, the expressions of the light-cone observables in the GLC approach can be derived analytically. In this section we derive the light-cone observables in the GLC approach and show that their final expressions are gauge-invariant.

3.3.1 Observed redshift

In GLC coordinates, the null geodesic connecting source and observer is characterized by the tangent vector $k^\mu = \delta^\mu_\tau\,\Upsilon^{-1}$, so that the coordinates w and $\tilde{\theta}^a$ are constant along the photon propagation. Consider photons emitted by a geodesic source at the two-sphere identified by the past light-cone w of the geodesic observer and the proper-time of emission τ_s, and received by the observer at τ_o. The observed redshift z_s of these photons is then given by the exact relation [56]

$$1 + z_s = \frac{(k^\mu u_\mu)_s}{(k^\nu u_\nu)_o} = \frac{(\partial^\mu w\,\partial_\mu\tau)_s}{(\partial^\nu w\,\partial_\nu\tau)_o} = \frac{\Upsilon_o}{\Upsilon_s}\,. \tag{3.37}$$

As a consequence, by using eq. (3.19) and considering that the source is located on the observer past light-cone (given by $w = \eta_o$) at distance $r_s = \eta_o - \eta_s$, we obtain

$$\begin{aligned} 1 + z_s &= \frac{a(\eta_o)}{a(\eta_s)}\big[1 + \delta\Upsilon_o - \delta\Upsilon_s\big]\,, \\ \delta\Upsilon_o &= \alpha_{\chi o} - \mathcal{V}^r_o + H_o\chi_o\,, \\ \delta\Upsilon_s &= \alpha_{\chi s} - \mathcal{V}^r_s + H_s\chi_s + \int_0^{\bar{r}_s} d\bar{r}\,\big[\alpha_\chi - \varphi_\chi - \Psi^r - C^{rr}\big]'\,. \end{aligned} \tag{3.38}$$

In agreement with eq. (3.34), these first order quantities gauge-transform as $\delta\hat{\Upsilon}_o = \delta\Upsilon_o - \mathcal{H}_o T_o$ and $\delta\hat{\Upsilon}_s = \delta\Upsilon_s - \mathcal{H}_s T_s$.

Before we proceed we need to consider a coordinate lapse, often ignored in literature (see [66]): the observer time coordinate in an inhomogeneous universe deviates from its background value $\bar{\eta}_o$ by

$$\delta\eta_o = -\frac{1}{a(\bar{\eta}_o)}\int_0^{\bar{\eta}_o} d\bar{\eta}\,a\,\alpha = -\frac{1}{a(\bar{\eta}_o)}\delta\tau_o\,. \tag{3.39}$$

This quantity represents the lapse between the coordinate time η_o at the observer and the observer's proper-time τ_o.[7] Therefore, by noting the conformal time at the observer $\eta_o = \bar{\eta}_o + \delta\eta_o$, we have that $a(\eta_o) = a(\bar{\eta}_o)[1 + \mathcal{H}_o\delta\eta_o]$, and then

$$1 + z_s = \frac{a(\bar{\eta}_o)}{a(\eta_s)}\big[1 + \mathcal{H}_o\delta\eta_o + \delta\Upsilon_o - \delta\Upsilon_s\big]\,. \tag{3.40}$$

Furthermore, since the observed redshift z_s is used to identify the time at the source in a homogeneous universe, we note the conformal time at the source as $\eta_s \equiv \bar{\eta}_z + \Delta\eta$, where the time $\bar{\eta}_z$ is defined as the time coordinate at the observed redshift z_s and $\Delta\eta$ is the residual distortion caused by inhomogeneities. With this definition, the comoving distance to the source is

$$\bar{r}_z \equiv \bar{r}(z_s) = \bar{\eta}_o - \bar{\eta}_z = \int_0^{z_s}\frac{dz}{H(z)}\,, \tag{3.41}$$

which corresponds to the value of the affine parameter $\bar{r}$ at the time identified by the observed redshift z_s, according to the relation in eq. (3.9). Having introduced the time

[7] By considering the time component of the observer four-velocity $u^\mu = dx^\mu/d\tau$ we get the relation between the proper-time τ and the coordinate time t. Then, the time lapse is obtained by expanding the coordinate time as $t = \bar{t} + \delta t$ and taking into account that the proper-time would correspond to the time measured by the observer in a homogeneous universe, i.e., $\tau = \bar{t}$ at the exact non-perturbative level. In formulae,

$$\tau(t,\mathbf{x}) = t + \int_0^{\bar{t}} dt'\alpha(t',\mathbf{x}) \quad \to \quad \delta t = t - \bar{t} = t - \tau = -\int_0^{\bar{t}} dt'\alpha(t',\mathbf{x})\,,$$

and similarly for conformal time we obtain eq. (3.39).

distortion $\Delta\eta$ at the source, we define the redshift distortion δz by writing the observed redshift as

$$\begin{aligned} 1+z_s &= \frac{a(\bar\eta_o)}{a(\bar\eta_z)} \equiv (1+\bar z)(1+\delta z)\,, \qquad\qquad 1+\bar z = \frac{a(\bar\eta_o)}{a(\eta_s)}\,, \\ 1+\delta z &= 1+\mathcal{H}_o\delta\eta_o + \delta\Upsilon_o - \delta\Upsilon_s \\ &= 1+\mathcal{H}_o\delta\eta_o + \left[\mathcal{V}^r - \alpha_\chi - H\chi\right]_o^s - \int_0^{\bar r_z} d\bar r\left[\alpha_\chi - \varphi_\chi - \Psi^r - C^{rr}\right]', \end{aligned} \tag{3.42}$$

where $1+\bar z$ corresponds to the background expansion, while the redshift distortion δz (related to the time distortion $\Delta\eta$) represents the effect of inhomogeneities. Given a coordinate transformation, the scale factor is related as

$$\hat\eta_s = \eta_s + T_s\,, \qquad a(\hat\eta_s) = a(\eta_s)\left[1+\mathcal{H}_sT_s\right], \qquad 1+\hat{\bar z} = (1+\bar z)\,(1-\mathcal{H}_sT_s)\,, \tag{3.43}$$

and the gauge transformation of the redshift distortion is

$$\delta\hat z = \delta z + \mathcal{H}_sT_s\,. \tag{3.44}$$

Naturally, the reciprocal cancellation of these gauge modes proves the gauge-invariance of the observed redshift derived with the GLC approach.

At this point, by expanding the scale factor at the source as $a(\eta_s) = a(\bar\eta_z)[1+\mathcal{H}_s\Delta\eta]$, from eq. (3.40) we obtain

$$1+z_s = \frac{a(\bar\eta_o)}{a(\bar\eta_z)}\left[1+\delta z - \mathcal{H}_s\Delta\eta\right], \qquad \delta z = \mathcal{H}_s\Delta\eta\,, \tag{3.45}$$

which yields the relation between time and redshift distortions.

We noticed that in the previous works on the GLC approach and its applications, the coordinate time lapse $\delta\eta_o$ was neglected. The primary aim of those works was to obtain the second order fluctuation in the luminosity distance, where terms at the observer are not dominant. However, as we showed above, the time lapse at the observer is essential for ensuring the gauge-invariance of the observed redshift and, as we shall see, of all light-cone observables.

3.3.2 Luminosity distance

As already mentioned, the observed position and the redshift of source galaxies are affected by the matter fluctuations and the gravitational waves between the source galaxies and the observer. The observed flux of the source galaxies is also affected by the same fluctuations and this effect is described by the fluctuation $\delta\mathcal{D}_L$ in the luminosity distance $\mathcal{D}_L = \bar{\mathcal{D}}_L(1+\delta\mathcal{D}_L)$, where $\bar{\mathcal{D}}_L(z_s) = (1+z_s)\,\bar r_z$ is the luminosity distance in a homogeneous universe.

Let us recall that the luminosity distance $\mathcal{D}_L$ of a source at redshift z_s is related to the angular diameter distance $\mathcal{D}_A$ by:

$$\mathcal{D}_L = (1+z_s)^2\,\mathcal{D}_A\,. \tag{3.46}$$

With this exact relation, the perturbation of the angular diameter distance and of the luminosity distance are identical. Therefore, the fluctuation in the luminosity distance can be obtained by computing the angular diameter distance. In the unperturbed background and for a source at redshift z_s the angular diameter distance is simply given by $\bar{\mathcal{D}}_A(z_s) = a(\bar{\eta}_z)\,\bar{r}_z$. When taking inhomogeneities into account this well known result is modified and the angular diameter distance can be obtained by considering a physical area dA perpendicular to the light propagation in the rest frame of the source. This infinitesimal area would appear subtended by a solid angle $d\Omega_{\rm obs} = \sin\theta_{\rm obs}\,d\theta_{\rm obs}\,d\phi_{\rm obs}$ measured by the observer in the rest frame, and it is related to the angular diameter distance as $dA = \mathcal{D}_A^2\,d\Omega_{\rm obs}$.

In GLC coordinates, the area perpendicular to the photon wavevector at the source position is given by

$$dA = \mathcal{D}_A^2\,d\Omega_{\rm obs} = \sqrt{|\gamma|}\,d^2\tilde{\theta}\,. \tag{3.47}$$

This quantity also represents a measure on the two-sphere identified by the redshift z_s and parametrized by $\tilde{\theta}^a$, where γ_{ab} is the induced metric. Such measure can be used to average scalar quantities on the constant redshift two-sphere embedded in the observer past light-cone, according to the prescription introduced in [56]:

$$\langle S\rangle_{w,z_s} \equiv \frac{\int d^2\tilde{\theta}\,\sqrt{|\gamma(w,\tau_s,\tilde{\theta}^a)|}\,S(w,\tau_s,\tilde{\theta}^a)}{\int d^2\tilde{\theta}\,\sqrt{|\gamma(w,\tau_s,\tilde{\theta}^a)|}} = \frac{\int dA\,S}{\int dA}\,, \tag{3.48}$$

where S is a generic scalar. From eq. (3.47), the measure $d^2\tilde{\theta}\sqrt{|\gamma|}$ is expressed in terms of the angular diameter distance and the observed solid angle (both gauge-invariant quantities) yielding a gauge-invariant prescription for the light-cone average. We also note that the physical area element in GLC coordinates ($dA = \sqrt{|\gamma|}\,d^2\tilde{\theta}$) does not depend on how we fix the degrees of freedom in the GLC angles (see sec. (3.2.2) below eq. (3.18)). Indeed, when no condition is imposed, the GLC angles are generally given by the observed angles plus a constant at the observer. As a consequence, the differentiation of the GLC angles is the same whatever value the constant at the observer has, leaving the physical area unaffected by our choice for the GLC angles. Regarding the angular diameter distance, as we show in appendix 3.B, when the GLC angles are matched to the observed angles, $\tilde{\theta}^a = (\theta_{\rm obs}, \phi_{\rm obs})$, eq. (3.47) reduces to the simple formula

$$\mathcal{D}_A^2 = \frac{\sqrt{|\gamma|}}{\sin\tilde{\theta}}\,. \tag{3.49}$$

On the other hand, when no condition is imposed to fix the degrees of freedom in $\tilde{\theta}^a$, the angular diameter distance is generally given by

$$\mathcal{D}_A^2 = \sqrt{|\gamma|}\,\frac{d^2\tilde{\theta}}{d\Omega_{\rm obs}}\,. \tag{3.50}$$

We are now going to calculate the expression of $\mathcal{D}_A$, demonstrating that indeed the final result does not depend on our choice of angles. From eq. (3.20), the determinant $\gamma = \det\gamma_{ab}$ is given by

$$\gamma = a^4 r^4 \sin^2\theta\left[1 + 4\,(\varphi_\chi + H\chi) - 2\,\partial_a\,\delta\tilde{\theta}^a + 2\,\bar{g}_{ab}(\mathcal{G}^{a|b} + C^{ab})\right]. \tag{3.51}$$

Note that to the first order in perturbations the determinant is $\gamma = \gamma_{11}\gamma_{22}$, because the off-diagonal entries contain only first order terms and their product would be of second order. Furthermore, for these diagonal matrix elements the operator ∂_a commutes with $\bar{g}^{ab}$. After substituting the expression of γ in eq. (3.51), we can write the angular diameter distance as

$$\mathcal{D}_A^2 = a_s^2 r_s^2\big[1 + 2\,(\varphi_\chi + H\chi) - \partial_a\delta\tilde{\theta}^a + \bar{g}_{ab}(\mathcal{G}^{a|b} + C^{ab})\big]\frac{\sin\theta_s}{\sin\theta_{\rm obs}}\frac{d\tilde{\theta}d\tilde{\phi}}{d\theta_{\rm obs}\,d\phi_{\rm obs}}\,. \tag{3.52}$$

The last factor (which is unity if the GLC angles are matched to the observed angles) can be conveniently written as

$$\frac{d\tilde{\theta}d\tilde{\phi}}{d\theta_{\rm obs}d\phi_{\rm obs}} = \frac{d\tilde{\theta}d\tilde{\phi}}{d\theta d\phi}\times\frac{d\theta d\phi}{d\theta_{\rm obs}\,d\phi_{\rm obs}}\,, \tag{3.53}$$

and the two Jacobian determinants of the transformations $\theta^a \to \tilde{\theta}^a$ and $\theta^a_{\rm obs} \to \theta^a$ can be calculated according to the relations between the different angles ($\theta^a = \theta^a_{\rm obs} + \delta\theta^a$, $\tilde{\theta}^a = \theta^a + \delta\tilde{\theta}^a$):

$$\begin{aligned}
\frac{d\tilde{\theta}d\tilde{\phi}}{d\theta d\phi} &= \det\left[\frac{\partial\tilde{\theta}^a}{\partial\theta^b}\right] = \det\left[\frac{\partial(\theta^a + \delta\tilde{\theta}^a)}{\partial\theta^b}\right] = 1 + \partial_a\delta\tilde{\theta}^a\,,\\
\frac{d\theta d\phi}{d\theta_{\rm obs}\,d\phi_{\rm obs}} &= \det\left[\frac{\partial\theta^a}{\partial\theta^b_{\rm obs}}\right] = \det\left[\frac{\partial(\theta^a_{\rm obs} + \delta\theta^a)}{\partial\theta^b_{\rm obs}}\right] = 1 + \frac{\partial}{\partial\theta_{\rm obs}}\delta\theta + \frac{\partial}{\partial\phi_{\rm obs}}\delta\phi\,.
\end{aligned} \tag{3.54}$$

Therefore, the angular diameter distance becomes

$$\mathcal{D}_A^2 = a_s^2 r_s^2\big[1+2\,(\varphi_\chi+H\chi)+\bar{g}_{ab}(\mathcal{G}^{a|b}+C^{ab})\big]\frac{\sin(\theta_{\rm obs}+\delta\theta)}{\sin\theta_{\rm obs}}\left[1+\frac{\partial}{\partial\theta_{\rm obs}}\delta\theta+\frac{\partial}{\partial\phi_{\rm obs}}\delta\phi\right], \tag{3.55}$$

where the last two factors are related to the gravitational lensing convergence κ as

$$1 - 2\,\kappa = \frac{\sin(\theta_{\rm obs} + \delta\theta)}{\sin\theta_{\rm obs}}\left[1 + \frac{\partial}{\partial\theta_{\rm obs}}\delta\theta + \frac{\partial}{\partial\phi_{\rm obs}}\delta\phi\right]. \tag{3.56}$$

Since the above expression does not contain GLC variables, it cannot be calculated within the GLC approach here.[8] Instead, we can use the geometric approach described in [72], which gives

$$\begin{aligned}\kappa =&\big[-\mathcal{V}^r+\Psi^r+C^{rr}\big]_o+\frac{1}{2}\hat{\nabla}_a\mathcal{G}^a+\frac{1}{\bar{r}_z}\mathcal{G}^r_o\\&+\frac{1}{2}\int_0^{\bar{r}_z}d\bar{r}\left[\hat{\nabla}_a\big(\Psi^a+2\,C^{ra}\big)+\left(\frac{\bar{r}_z-\bar{r}}{\bar{r}_z\bar{r}}\right)\hat{\nabla}^2(\alpha_\chi-\varphi_\chi-\Psi^r-C^{rr})\right],\end{aligned}\tag{3.57}$$

where $\hat{\nabla}_a\mathcal{G}^a = \partial_a\mathcal{G}^a + \cot\theta\,\mathcal{G}^\theta$. The same result is derived in appendix 3.D, where the GLC angles are matched to the observed angles. This quantity, describing the convergence of light rays due to the effect of inhomogeneities between source and observer, gauge transforms as

$$\hat{\kappa}=\kappa-\frac{1}{2}\hat{\nabla}_a\mathcal{L}^a_s-\frac{1}{\bar{r}_z}\mathcal{L}^r_o\,.\tag{3.58}$$

Then, after taking the square root of eq. (3.55) root we have

$$\mathcal{D}_A(\lambda_s)=a_sr_s\big[1-\kappa+\Xi\big]\,,\qquad\qquad \Xi=\frac{1}{2}(\mathcal{C}^\alpha_\alpha-\mathcal{C}_{\alpha\beta}n^\alpha n^\beta)\,,\tag{3.59}$$

where $n^\alpha = (1,0,0)$ is a unit directional vector representing the light propagation direction in a homogeneous universe. At this point, to complete our derivation, we only need the expression for a_sr_s to first order. As in [61], by applying eq. (3.25) to the observer light-cone $w=\eta_o$ evaluated at the source position, we get

$$w_s=\eta_s+r_s-\bar{r}_z\Psi_{\rm av}=\eta_o\,,\tag{3.60}$$

where we have denoted the average of the perturbations along the unperturbed null geodesic as

$$\Psi_{\rm av}\equiv\frac{1}{\bar{r}_z}\int_0^{\bar{r}_z}d\bar{r}\,[\mathcal{A}-\mathcal{B}^r-\mathcal{C}^{rr}]=\frac{1}{\bar{r}_z}\int_0^{\bar{r}_z}d\bar{r}\,[\alpha_\chi-\varphi_\chi-\Psi^r-C^{rr}]-\frac{1}{\bar{r}_z}\left[\frac{\chi}{a}+\mathcal{G}^r\right]^s_o.\tag{3.61}$$

Now from eqs. (3.45) and (3.60) we can determine the radial coordinate r_s of the source:

$$r_s=\bar{\eta}_o-\bar{\eta}_z+\delta\eta_o-\frac{\delta z}{\mathcal{H}_s}+\bar{r}_z\Psi_{\rm av}=\bar{r}_z\left[1+\frac{\delta\eta_o}{\bar{r}_z}-\frac{\delta z}{\mathcal{H}_s\bar{r}_z}+\Psi_{\rm av}\right]\equiv\bar{r}_z+\delta r\,.\tag{3.62}$$

As a result, we can identify the perturbation δr of the radial coordinate (see also [70, 71, 72, 76]):

$$\frac{\delta r}{\bar{r}_z}=\frac{\delta\eta_o}{\bar{r}_z}-\frac{\delta z}{\mathcal{H}_s\bar{r}_z}+\Psi_{\rm av}\,,\tag{3.63}$$

[8] In [73] the GLC metric was employed to derive exact and non-perturbative expressions of lensing quantities such as shear and optical scalars.

whose gauge transformation is $\delta\hat{r} = \delta r + \mathcal{L}^r|_o^s$. Similarly we can obtain a_s, indeed from eq. (3.45) we have

$$a_s = a(\bar{\eta}_z) + \Delta\eta\, a'(\bar{\eta}_z) = a(\bar{\eta}_z)[1 + \mathcal{H}_z\Delta\eta] = a(\bar{\eta}_z)[1 + \delta z]\,. \tag{3.64}$$

Therefore, we finally get the expression of $a_s r_s$ on the 2-sphere identified by z_s:

$$a_s r_s = a(\bar{\eta}_z)\bar{r}_z\left[1 + \delta z + \frac{\delta r}{\bar{r}_z}\right]. \tag{3.65}$$

Going back to the angular diameter distance we obtain

$$\mathcal{D}_A = \bar{\mathcal{D}}_A\left[1 + \delta z + \frac{\delta r}{\bar{r}_z} - \kappa + \Xi\right], \tag{3.66}$$

and finally, from eq. (3.46),

$$\delta\mathcal{D}_A = \delta\mathcal{D}_L = \delta z + \frac{\delta r}{\bar{r}_z} - \kappa + \Xi\,. \tag{3.67}$$

This covariant expression is fully consistent with the luminosity distance fluctuation derived in [72] with the geometric approach and in a general metric representation. This result also perfectly matches the luminosity distance calculated with other approaches but with specific choice of gauge conditions (see [66]). By taking the gauge transformation of the various terms we obtain

$$\begin{aligned}\delta\hat{\mathcal{D}}_A = \delta\hat{\mathcal{D}}_L &= \delta\hat{z} + \frac{\delta\hat{r}}{\bar{r}_z} - \hat{\kappa} + \frac{1}{2}(\hat{\mathcal{C}}^\alpha_\alpha - \hat{\mathcal{C}}_{\alpha\beta}n^\alpha n^\beta)\\ &= (\delta z + \mathcal{H}_s T_s) + \left(\frac{\delta r}{\bar{r}_z} + \frac{1}{\bar{r}_z}\mathcal{L}^r\Big|_o^s\right) - \left(\kappa - \frac{1}{2}\hat{\nabla}_a\mathcal{L}^a_s - \frac{1}{\bar{r}_z}\mathcal{L}^r_o\right)\\ &\quad + \left(\frac{1}{2}(\mathcal{C}^\alpha_\alpha - \mathcal{C}^\alpha_\beta n^\beta) - \mathcal{H}_s T_s - \frac{1}{\bar{r}_z}\mathcal{L}^r_s - \frac{1}{2}\hat{\nabla}_a\mathcal{L}^a_s\right) = \delta\mathcal{D}_A = \delta\mathcal{D}_L\,.\end{aligned} \tag{3.68}$$

The cancellation of gauge modes among different terms is shown explicitly, demonstrating the gauge-invariance of the angular diameter distance and the luminosity distance in the GLC approach.

The above derivation shows that the expression of the luminosity distance is independent of the normalization of the GLC angles at the observer position. Indeed, the Jacobian of the transformation from the GLC angles to the observed angles cancels the terms related to the GLC angular distortions $\delta\tilde{\theta}^a$. In this way, the nature of the GLC angles becomes irrelevant for the derivation of the luminosity distance. To demonstrate this statement, we derive in appendix 3.B the angular diameter distance after fixing the degrees of freedom in the GLC angles to match the observed angles (measured in the observer rest frame). In this case the angular diameter distance is simply given by eq. (3.49) and the calculation of the gravitational lensing convergence can be performed in the GLC approach, as described in appendix 3.D.

3.3.3 Physical volume

Due to the presence of inhomogeneities the volume $V_{\rm obs}$ inferred from the observed redshift and angle does not correspond to the *physical* volume V occupied by the source galaxies. To account for this effect, we define the volume distortion δV, such that $dV = (1+\delta V)\, dV_{\rm obs}$. The volume distortion is a gauge-invariant quantity, as we demonstrate in this section after deriving its expression with the GLC approach.

In [72] the infinitesimal physical volume occupied by the source is written in terms of the observed redshift z_s and angles $\theta_{\rm obs}$, $\phi_{\rm obs}$:

$$dV = \sqrt{-g}\,\epsilon_{\mu\nu\rho\sigma}\, u_s^\mu\, dx^\nu dx^\rho dx^\sigma = \sqrt{-g}\,\epsilon_{\mu\nu\rho\sigma}\, u_s^\mu \frac{\partial x^\nu}{\partial z_s}\frac{\partial x^\rho}{\partial \theta_{\rm obs}}\frac{\partial x^\sigma}{\partial \phi_{\rm obs}} dz_s d\theta_{\rm obs} d\phi_{\rm obs}\,. \tag{3.69}$$

On the other hand, the inferred volume is given by

$$dV_{\rm obs} = a(\bar\eta_z)^3\, \bar r_z^2\, d\bar r_z\, d\Omega_{\rm obs} = \frac{\bar r_z^2\, dz_s\, d\Omega_{\rm obs}}{H_s (1+z_s)^3}\,, \tag{3.70}$$

where we set $a(\bar\eta_o) \equiv 1$, so that $a(\bar\eta_z) = 1/(1+z_s)$.

In GLC coordinates, the physical volume element occupied by the source is simply given by

$$dV = dA\, d\tau = \sqrt{|\gamma|}\, d^2\tilde\theta\, d\tau\,. \tag{3.71}$$

To compare our result with that found in [72], we can change the GLC coordinates into the observed variables $\theta_{\rm obs}$,$\phi_{\rm obs}$ and z_s. As explained in sec. 3.3.2, the differentiation of the GLC angles already corresponds to the differentiation of the observed angles ($d^2\tilde\theta = d\theta_{\rm obs}\, d\phi_{\rm obs}$), therefore, we only need to change variable from the proper-time τ to the observed redshift z_s, obtaining

$$dV = -\sqrt{|\gamma|}\,\frac{\partial \tau}{\partial z_s}\, d^2\tilde\theta\, dz_s\,, \tag{3.72}$$

where the minus sign is due to the fact that when the proper-time increases the redshift decreases and vice versa. Let us now derive the volume distortion by calculating the physical volume element. After substituting the expression of γ in eq. (3.51) and the expansion of the factor $a_s r_s$ in eq. (3.65) we obtain

$$\begin{aligned} dV &= -a(\bar\eta_z)^2 \bar r_z^2 \left[1 + 2\,\delta z + 2\,\frac{\delta r}{\bar r_z} - 2\,\kappa + 2\,\Xi\right]\frac{\partial \tau}{\partial z_s}\, dz_s\, d\Omega_{\rm obs} \\ &= -\left[1 + 2\,\delta z + 2\,\frac{\delta r}{\bar r_z} - 2\,\kappa + 2\,\Xi\right]\frac{\partial \tau}{\partial z_s}\,\frac{\bar r_z^2\, dz_s\, d\Omega_{\rm obs}}{(1+z_s)^2}\,. \end{aligned} \tag{3.73}$$

At this point what we need to compute is the change of the proper-time with respect to the observed redshift, $\partial\tau/\partial z_s$. To simplify the calculation we rewrite this derivative as

$$\frac{\partial \tau}{\partial z_s} = \frac{\partial \tau}{\partial \eta_s}\frac{\partial \eta_s}{\partial z_s} = -\frac{\partial \tau}{\partial \eta_s}\frac{1}{H_s}\,. \tag{3.74}$$

After expanding the emission time as $\eta_s = \bar{\eta}_z + \Delta\eta$, we can express the proper-time at emission as

$$\tau = a(\bar{\eta}_z)\,\frac{\delta z}{\mathcal{H}_s} + \int_0^{\bar{\eta}_z} d\eta\, a(\eta)[1+\alpha]\,, \tag{3.75}$$

obtaining

$$\frac{\partial\tau}{\partial\eta_s} = a(\bar{\eta}_z)\left[1+\alpha+\delta z - \frac{\mathcal{H}_s'}{\mathcal{H}_s^2}\,\delta z + \frac{1}{\mathcal{H}_s}\delta z'\right]. \tag{3.76}$$

Therefore, going back to the volume element, we have

$$dV = \left[1+3\,\delta z + \mathcal{A} + \mathcal{C}^\alpha_\alpha + 2\,\frac{\delta r}{\bar{r}_z} - 2\,\kappa - \frac{\mathcal{H}_s'}{\mathcal{H}_s^2}\,\delta z + \frac{1}{\mathcal{H}_s}\delta z' - \mathcal{C}_{\alpha\beta}n^\alpha n^\beta\right]\frac{\bar{r}_z^2\, dz_s\, d\Omega_{\rm obs}}{H_s(1+z_s)^3}\,. \tag{3.77}$$

The above equation can be further simplified by noting that

$$-\frac{\mathcal{H}_s'}{\mathcal{H}_s^2}\delta z + \frac{1}{\mathcal{H}_s}\delta z' = H_s\frac{\partial}{\partial z_s}\delta r + V_\alpha n^\alpha - \mathcal{A} + \mathcal{C}_{\alpha\beta}n^\alpha n^\beta\,. \tag{3.78}$$

In this way the volume element becomes

$$dV = \left[1+3\,\delta z + \mathcal{C}^\alpha_\alpha + 2\,\frac{\delta r}{\bar{r}_z} - 2\,\kappa + H_s\frac{\partial}{\partial z_s}\delta r + V_\alpha n^\alpha\right]dV_{\rm obs}\,. \tag{3.79}$$

As a result, the final expression for the volume distortion is

$$\delta V = 3\,\delta z + \mathcal{C}^\alpha_\alpha + 2\,\frac{\delta r}{\bar{r}_z} - 2\,\kappa + H_s\frac{\partial}{\partial z_s}\delta r + V_\alpha n^\alpha\,. \tag{3.80}$$

This quantity is covariant and gauge-invariant, besides it coincides with the result found in [72]. If compared with the volume distortion derived in [68] with the GLC approach and in the conformal Newtonian gauge, this result includes perturbations at the observer not considered there, but crucial for the gauge-invariance of the final expression.

3.4 Discussion

In this chapter we showed *explicitly* the gauge-invariance of light-cone observables derived in the GLC approach. We also considered the full general metric to first order in perturbations for the first time within the GLC formalism. Furthermore, by comparing the results with those derived in the approach introduced in [70, 71, 72], we demonstrated the full consistency of the two methods to calculate expressions of light-cone observables in the presence of inhomogeneities in the Universe. Our study provides further understanding of the properties of the GLC representation.

First of all, in sec. 3.2.2 we pointed out the presence of new degrees of freedom in the expression of the GLC angles, given by perturbations evaluated at the observer position. These angular degrees of freedom are also studied in [65], with a discussion about how they can be fixed to describe different physical situations. As we show in appendix 3.B, by fixing the degrees of freedom through a proper normalization, the GLC angles can be identified with the observed angles, measured by the observer in the rest frame. On the other hand, a different normalization at the observer position is possible, leading to a different form of the GLC angles, which would then correspond to the observed angles and a constant at the observer. Naturally, the final expressions of light-cone observables cannot depend on our choice of normalization. To demonstrate this point, in sec. 3.3.2 we derived the gauge-invariant expression of the luminosity distance without fixing the degrees of freedom in the GLC angles. The same result is obtained in appendix 3.B, where a specific normalization is taken instead. Such normalization, according to which the GLC angles match the angles measured by the observer in the rest frame, is probably the most convenient, as it leads to a very simple formula for the angular diameter distance, eq. (3.49). When a different normalization is chosen, the formula of the angular diameter distance contains an additional factor given by the Jacobian of the rotation from the GLC to the observed angles. However, when the GLC angles appear under differentiation, as in the physical area and volume occupied by the source, the difference becomes completely irrelevant since the differentiation of any constant at the observer (representing the difference between GLC angles and observed angles) would vanish.

In [61, 62, 63], the luminosity distance in the presence of inhomogeneities is derived from the angular diameter distance in eq. (3.49). However, the difference between the observed angle in a GLC coordinate and that in the observer rest frame was not considered, as well as the presence of degrees of freedom in GLC angular coordinate at the observer. If the difference between the angle in the observer rest frame and that in a global coordinate is neglected, the degrees of freedom are automatically set to zero and the GLC angular coordinate does not match the angle in the observer rest frame. This results in the absence of some terms in the final expression for the luminosity distance, such as the observer peculiar velocity and the gravitational potential at the observer position. Without these terms the luminosity distance is not gauge-invariant and not consistent with the equivalence principle (see [77]). In [64] the normalization condition for the angular GLC variables was fixed in the expression of the angular diameter distance by a factor evaluated at the observer, which can be interpreted as the Jacobian of the rotation from a generic GLC angular coordinate to the observed angle in the observer rest frame.

In sec. 3.3.1 we derived the observed redshift, stressing the importance of including the time lapse at the observer. This term represents the effect due to the fact that the observer proper-time does not correspond to the coordinate time in the physical

universe. Indeed, the presence of inhomogeneities induces a perturbation in the coordinate time at observation, which is captured by the time lapse. Specifically, the inhomogeneities affect the observer four-velocity, causing a discrepancy between the time measured and the coordinate time. As we showed in sec. 3.3.1, only if the time lapse at the observer is included the expression of the redshift is gauge-invariant. This argument is later extended to any light-cone observable, as the time lapse appears not only in the redshift distortion but also in the distortion of the radial distance between source and observer.

In sec. 3.3.2, in order to obtain the angular diameter distance, we made use of the fact that the infinitesimal area dA occupied by the source is equal to the measure $\sqrt{\gamma}\, d^2\tilde{\theta}$ on the fixed-time two-sphere embedded in the light-cone. This equality results directly in the gauge-invariance of the light-cone average prescription introduced in [56]. Given the gauge-invariance of the light-cone average, this can be applied to compute the mean of observables in the presence of inhomogeneities, as it has been done in [63, 74] (and partially in [61]). Indeed, deriving the full relativistic expression of a given observable is not enough to interpret the outcome of a survey. Consider for instance the relation between the luminosity distance $\mathcal{D}_L$ and the observed redshift z_s of a given source. As described in [78], the observational strategy consists in collecting many data points $(z_s, \mathcal{D}_L)$, and the value of $\mathcal{D}_L$ at a given redshift z_s is obtained by averaging over the data in the redshift bin containing z_s. Consequently, also the theoretical expression of the luminosity distance as a function of the observed redshift needs to be averaged. To this purpose, second-order calculations are needed (see [63, 74, 79]). The study of the GLC formalism in this chapter can also be used to go beyond the linear order, providing the correct starting point for the derivation and a concrete way to use the observed angles in the GLC angular coordinate, being this the most physically meaningful choice.

Finally, in sec. 3.3.3 we derived the expression of physical volume occupied by sources, obtaining the volume distortion due to relativistic effects. The importance of a precise theoretical derivation of the volume distortion relies on the fact that this latter is used to predict the number density of galaxies, which is a key observable to test different cosmological models. The observed galaxy number density is obtained by counting the number of galaxies in the observed redshift range and within the observed solid angle. Whereas the observed volume occupied by the source galaxies is different from the physical volume, the number of galaxies within the volume is not affected by the inhomogeneities. As a consequence, by calculating the volume distortion we can relate the observed galaxy number density to the predicted physical one.

The GLC approach, if exercised properly, results in the correct and consistent expressions of light-cone observables. It offers a covariant and gauge-invariant prescription for averaging scalars on our past light-cone, providing a simple way to estimate the effect of inhomogeneities on observables measured in large-scale-structure surveys.

Appendices

3.A Technical details

In this short appendix, we provide the covariant derivatives of the metric perturbations and useful relations to simplify our calculations in the main text.

First of all, given the background 3-spatial metric tensor $\bar{g}_{\alpha\beta}$ in spherical coordinates, the affine connections are readily derived as

$$\begin{aligned} &\Gamma^r_{rr} = \Gamma^r_{ra} = 0\,, \qquad \Gamma^r_{ab} = -\frac{1}{r}\,\bar{g}_{ab}\,, \qquad \Gamma^a_{rr} = 0\,, \qquad \Gamma^a_{rb} = \frac{1}{r}\,\delta^a_b\,, \\ &\Gamma^\theta_{\theta\theta} = \Gamma^\theta_{\theta\phi} = \Gamma^\phi_{\theta\theta} = \Gamma^\phi_{\phi\phi} = 0\,, \qquad \Gamma^\theta_{\phi\phi} = -\sin\theta\cos\theta\,, \qquad \Gamma^\phi_{\theta\phi} = \cot\theta\,, \end{aligned} \tag{3.81}$$

where δ^a_b is the Kronecker delta. As a result, the covariant derivatives can be expressed in terms of ordinary derivatives as

$$\begin{aligned} &\gamma_{,}{}^{r|r} = \gamma_{,}{}^{rr}\,, \qquad \gamma_{,}{}^{r|a} = \gamma_{,}{}^{a|r} = \gamma_{,}{}^{ra} - \frac{\gamma_{,}{}^{a}}{r}\,, \\ &C^{r|r} = C^{r,r}\,, \qquad C^{r|a} = C^{r,a} - \frac{C^a}{r}\,, \qquad C^{a|r} = C^{a,r} + \frac{C^a}{r}\,, \\ &\bar{g}_{ab}\big(\gamma_{,}{}^{a|b} + C^{a|b}\big) = \partial_a\big[\gamma_{,}{}^{a} + C^a\big] + \cot\theta\,\big[\gamma_{,}{}^{\theta} + C^\theta\big] + \frac{2}{r}\big[\gamma_{,}{}^{r} + C^r\big]\,. \end{aligned} \tag{3.82}$$

It is important to note the distinction

$$\gamma_{,}{}^{ar} = \gamma'_{,}{}^{a} + \frac{d}{d\bar{r}}\gamma_{,}{}^{a}\,, \qquad \gamma_{,}{}^{ra} = \gamma'_{,}{}^{a} + \frac{2}{r}\gamma_{,}{}^{a} + \frac{d}{d\bar{r}}\gamma_{,}{}^{a}\,. \tag{3.83}$$

Indeed, the derivatives ∂^r and ∂^a do not commute and therefore $\gamma_{,}{}^{ra} \neq \gamma_{,}{}^{ar}$, instead $[\partial^a, \partial^r]\gamma = 2\gamma_{,}{}^{a}/r$. Second, in the calculations performed throughout the chapter we

used the following formulas for double integrations:

$$\begin{aligned}\int_0^{\bar{r}_z} d\bar{r} \int_0^{\bar{r}} d\bar{r}'\, f(\bar{r}') &= \int_0^{\bar{r}_z} d\bar{r}\, (\bar{r}_z - \bar{r}) f(\bar{r})\,, \\ \int_0^{\bar{r}_z} d\bar{r}\, \frac{1}{\bar{r}^{\,2}} \int_0^{\bar{r}} d\bar{r}'\, f(\bar{r}') &= \int_0^{\bar{r}_z} d\bar{r} \left(\frac{\bar{r}_z - \bar{r}}{\bar{r}_z \bar{r}} \right) f(\bar{r}) + f(0)\,,\end{aligned} \tag{3.84}$$

where $f(x)$ is a generic function of x.

3.B Matching conditions for the GLC angles

In this appendix we show how to fix the degrees of freedom in the GLC angles to match them with the observed angles (in the observer rest frame). Then, we will derive the angular diameter distance under this condition, showing that we obtain the same result of sec. (3.3.2).

The degrees of freedom which we have at hand are associated with the quantities $\delta\tilde{\theta}^a_o$ and δw^a_o in the expression of the GLC angles $\tilde{\theta}^a$, eq. (3.18). Using the exact relation $k^\mu = g^{\mu\nu}\partial_\nu w$ we relate δw^a_o to the wavevector perturbation δk^a_o as

$$\bar{g}^{ac}\partial_c\, \delta w_o = \left[a^2 \delta k^a\right]_o + \mathcal{B}^a_o + 2\,\mathcal{C}^{ra}_o\,. \tag{3.85}$$

In this case the GLC angles become

$$\begin{aligned}\tilde{\theta}^a_s = \theta^a_s + \delta\tilde{\theta}^a_o - \bar{r}_z \Bigg[a^2 \delta k^a + \frac{d}{d\bar{r}} \mathcal{G}^a + \Psi^a + 2\, C^{ra} \Bigg]_o + \mathcal{G}^a\Big|^s_o \\ + \int_0^{\bar{r}_z} d\bar{r} \Bigg[\Psi^a + 2\, C^{ra} + \left(\frac{\bar{r}_z - \bar{r}}{\bar{r}_z \bar{r}} \right) \hat{\bar{g}}^{ac} \partial_c (\alpha_\chi - \varphi_\chi - \Psi^r - C^{rr}) \Bigg]\,.\end{aligned} \tag{3.86}$$

Both $\delta\tilde{\theta}^a_o$ and δk^a_o represent perturbations to the photon propagation direction at observation, and are the rotational degrees of freedom to set. The observed direction of the photons, described by the observed angles $\theta^a_{\rm obs} = (\theta_{\rm obs}, \phi_{\rm obs})$, is identified in the observer rest frame. Therefore, to fix $\delta\tilde{\theta}^a_o$ and δk^a_o such that $\tilde{\theta}^a = \theta^a_{\rm obs}$, we have to consider the photon wavevector in the observer rest frame and study how it is related to the photon wavevector in the global coordinates $y^\mu_{\rm FRW}$, derived by coordinate transforming the GLC wavevector. First of all, we write the GLC wavevector $k^{\rm GLC}_\mu = (1, 0, \vec{0}\,)$ in the global coordinates $y^\mu_{\rm FRW} = (\eta, r, \theta^a)$ by taking a coordinate transformation from the GLC coordinates $x^\mu_{\rm GLC} = (w, \tau, \tilde{\theta}^a)$:

$$k^{\rm FRW}_\mu = \frac{\partial x^\nu}{\partial y^\mu} k^{\rm GLC}_\nu = \left(1 + \delta w'\,,\, \hat{n}_\alpha + \partial_\alpha \delta w\right), \tag{3.87}$$

$$k^\mu_{\rm FRW} = g^{\mu\nu}_{\rm FRW}\, k^{\rm FRW}_\nu = \frac{1}{a^2}\left(-1 - \delta w' + 2\mathcal{A} - \mathcal{B}_\alpha\, \hat{n}^\alpha\,,\, \hat{n}^\alpha + \bar{g}^{\alpha\beta}\partial_\beta \delta w - \mathcal{B}^\alpha - 2\,\mathcal{C}^\alpha_\beta\, \hat{n}^\beta\right). \tag{3.88}$$

The unit vector $\hat{n}^\alpha$ is defined in the global coordinates, and identifies the photons direction in the absence of perturbations. By making use of the exact relation $k^\mu = g^{\mu\nu}\partial_\nu w$, we can express the wavevector in terms of the perturbations δk^μ which we are interested in:

$$k^\mu_{\rm FRW} = \frac{1}{a^2}(-1 + a^2\delta k^0\,,\, \hat{n}^\alpha + a^2\delta k^\alpha)\,. \tag{3.89}$$

We want to study the relation between this result and that obtained by mapping the photon wavevector $k^m_{\rm L} = \omega_o\,(-1\,, n^i\,)$ in the observer rest frame (local Lorentz frame) into the global coordinates. This procedure, carefully described in appendix 3.C, involves the construction of an orthonormal basis, the tetrads $[e_m]^\mu$, connecting the observer rest frame to the global coordinates at the observer. After deriving the tetrads, the photon wavevector in the global coordinates is given by

$$k^\mu_{\rm FRW} = [e_m]^\mu k^m_{\rm L} = \frac{\omega_o}{a}(-1 + \mathcal{A} + \hat{n}^\alpha V_\alpha - \hat{n}^\alpha\mathcal{B}_\alpha\,,\, n^\alpha - V^\alpha - \hat{n}^\beta\mathcal{C}^\alpha_\beta)\,, \tag{3.90}$$

where ω_o is the observed photon frequency and $n^\alpha \sim (\theta_{\rm obs}, \phi_{\rm obs})$ is the unit directional vector identifying the observed angular position of the source in the rest frame. At this point, we can match the photon wavevector in eq.(3.89) (obtained from the GLC wavevector) evaluated at the observer position and the photon wavevector in eq.(3.90) (obtained from the rest frame wavevector). We are only interested in the spatial components:

$$\hat{n}^\alpha_o + [a^2\delta k^\alpha]_o = (a\omega)_o\,(n^\alpha - V^\alpha_o - \hat{n}^\beta\mathcal{C}^\alpha_{\beta\,o})\,. \tag{3.91}$$

The quantity $(a\omega)$ is not constant in an inhomogeneous universe. Therefore, it is convenient to split it into background and perturbation part as $a\omega = \overline{a\omega}\,(1 + \Delta\nu)$. Considering the observer position this is $(a\omega)_o = \overline{\omega}_o\,(1 + \Delta\nu_o)$, where $a(\bar{\eta}_o) \equiv 1$. Since the real observable we deal with is the redshift of the source, which is determined by the ratio of the photon frequency at the source to the observed frequency ω_o, we never need to consider the value of ω_o in practice and we can normalize its background part as $\overline{\omega}_o \equiv 1$. In this case we have

$$\hat{n}^\alpha_o + \delta k^\alpha_o = (1 + \Delta\nu_o)\,n^\alpha - V^\alpha_o - \hat{n}^\beta\mathcal{C}^\alpha_{\beta\,o}\,, \tag{3.92}$$

where the unit directional vector in the global coordinates is $\hat{n}^\alpha_o \sim (\theta_o, \phi_o) = (\theta_{\rm obs}, \phi_{\rm obs}) + (\delta\theta_o, \delta\phi_o)$ while that in the observer rest frame is $n^\alpha \sim (\theta_{\rm obs}, \phi_{\rm obs})$. Then, the fluctuations of the photon wavevector spatial components have to be

$$\delta k^\alpha_o = \Delta\nu_o\,n^\alpha + (n^\alpha - \hat{n}^\alpha_o) - V^\alpha_o - \hat{n}^\beta\mathcal{C}^\alpha_{\beta\,o}\,, \tag{3.93}$$

where the difference in the unit directional vectors gives the angular corrections at the observer, $(\hat{n}^\alpha_o - n^\alpha) \sim (\delta\theta_o, \delta\phi_o)$. We can now focus on the angular components only, obtaining

$$\delta k^a_o = -\frac{1}{\bar{r}_z}\delta\theta^a_o - V^a_o - \mathcal{C}^{ra}_o\,, \tag{3.94}$$

regardless of the value of the constant $\Delta\nu_o$. At this point we can use the remaining degrees of freedom to compensate for the difference between the two unit directional vectors, in order to align the photons direction in the global coordinates (in a homogeneous universe) to the observed one. To do this, we simply set $\delta\tilde{\theta}^a_o = -\delta\theta^a_o$, and the GLC angular distortions become

$$\begin{aligned}\delta\tilde{\theta}^a_s = &-\bar{r}_z\Big[-\mathcal{V}^a+\Psi^a+C^{[a|r]}+C^{ra}\Big]_o+\mathcal{G}^a\Big|^s_o\\&+\int_0^{\bar{r}_z}d\bar{r}\left[(\Psi^a+2\,C^{ra})+\left(\frac{\bar{r}_z-\bar{r}}{\bar{r}_z\bar{r}}\right)\hat{\tilde{g}}^{ac}\partial_c(\alpha_\chi-\varphi_\chi-\Psi^r-C^{rr})\right].\end{aligned}\tag{3.95}$$

This result perfectly agrees with the angular distortions $\delta\theta^a_s = (\delta\theta_s, \delta\phi_s)$ calculated in [72] with the geometric approach.[9] Specifically, the GLC angular distortions $\delta\tilde{\theta}^a_s$ and the distortions $\delta\theta^a_s$ calculated in [72] are equal but with opposite sign due to definition. Indeed, in [72] the angular position of the source is given by $\theta^a_s = \theta^a_{\rm obs} + \delta\theta^a_s$, where $\theta^a_{\rm obs}$ are the observed angles and $\delta\theta^a$ are geometric distortions due to inhomogeneities. On the other hand, in the GLC approach $\tilde{\theta}^a_s = \theta^a_s + \delta\tilde{\theta}^a_s$, where the angular distortions $\delta\tilde{\theta}^a_s$ cancel the distortions in θ^a_s to give the observed angles, $\tilde{\theta}^a_s = (\theta^a_{\rm obs} + \delta\theta^a_s) + \delta\tilde{\theta}^a_s = (\theta^a_{\rm obs} + \delta\theta^a_s) - \delta\theta^a_s = \theta^a_{\rm obs}$.

The quantity δw_o represents a shift in the photons' phase at the observer position due to perturbations. This constant does not affect the expressions of light-cone observables, reflecting the freedom associated with the definition of phase. By considering the proportionality relation between the GLC phase w (coordinate transformed to FRW) and the FRW phase ϑ (constructed from that in the observer rest frame), the integration constant δw_o is fixed. In a global FRW coordinate the phase is

$$\vartheta = g^{\rm FRW}_{\mu\nu}k^\mu_{\rm FRW}x^\nu_{\rm FRW} = (a\omega)_o\left\{\bar{\eta}_o+\bar{\eta}_o\,(\mathcal{A}-n^iV_i)_o+\delta\eta_o+\delta r_o\right\},\tag{3.96}$$

while in a GLC coordinate the phase is given by

$$w = \bar{\eta}_o+\delta\eta_o+\delta r_o+\delta w_o\,,\tag{3.97}$$

where we evaluated both phases at the observer position. By demanding that both be proportional, i.e. $w_o = C\,\vartheta_o$, we derive the proportionality constant and the integration constant

$$C = 1/(a\omega)_o\,,\qquad\qquad \delta w_o = \bar{\eta}_o\,(\mathcal{A}-n^iV_i)_o\,.\tag{3.98}$$

To conclude this appendix, we derive the angular diameter distance in the GLC approach when the degrees of freedom in $\tilde{\theta}^a$ are fixed as described above, so that

[9] In [72] any quantity is expressed in terms of the observables measured in the observer rest frame, which are the observed redshift z_s and angles $\theta^a_{\rm obs}$.

$\tilde{\theta}^a = \theta^a_{\rm obs}$. From the relation between the physical area occupied by the source and the angular diameter distance, $dA = \sqrt{|\gamma|}\, d^2\tilde{\theta} = \mathcal{D}_A^2\, d\Omega_{\rm obs}$, this latter is given by

$$\mathcal{D}_A^2 = \frac{\sqrt{|\gamma|}}{\sin\theta_{\rm obs}} \frac{d^2\tilde{\theta}}{d^2\theta_{\rm obs}} \,. \tag{3.99}$$

When $\tilde{\theta}^a = \theta^a_{\rm obs}$, the angular diameter distance can be expressed in terms of GLC variables only, as

$$\mathcal{D}_A^2 = \frac{\sqrt{|\gamma|}}{\sin\tilde{\theta}} \,. \tag{3.100}$$

After substituting γ with the expression in eq. (3.51) and taking the square root, we have

$$\mathcal{D}_A = \bar{\mathcal{D}}_A \sqrt{\frac{\sin\theta_s}{\sin\tilde{\theta}}} \left[1 + \delta z + \frac{\delta r}{\bar{r}_z} - \frac{1}{2}\partial_a \delta\tilde{\theta}^a + \Xi \right], \tag{3.101}$$

where we also used eq. (3.65) for the expansion of the factor $a_s r_s$ in the expression of γ. Then, by expanding the source angle as $\theta_s = \theta_{\rm obs} + \delta\theta_s = \tilde{\theta}_s - \delta\tilde{\theta}_s$, we get

$$\mathcal{D}_A = \bar{\mathcal{D}}_A \left[1 + \delta z + \frac{\delta r}{\bar{r}_z} - J_2 + \Xi \right], \tag{3.102}$$

where we defined the quantity

$$J_2 \equiv \frac{1}{2}\partial_a \delta\tilde{\theta}^a + \frac{1}{2}\cot\tilde{\theta}\, \delta\tilde{\theta} = \frac{1}{2}\hat{\nabla}_a \delta\tilde{\theta}^a \,. \tag{3.103}$$

Clearly, J_2 (for which we followed the notation introduced in [61]) corresponds to the gravitational lensing convergence κ introduced in sec. 3.3.2. To compute J_2 we follow the approach described in appendix 3.D, from which we obtain

$$\begin{aligned} J_2 =& \left[-\mathcal{V}^r + \Psi^r + C^{rr}\right]_o + \frac{1}{2}\hat{\nabla}_a \mathcal{G}^a + \frac{1}{\bar{r}_z}\mathcal{G}^r_o \\ &+ \frac{1}{2}\int_0^{\bar{r}_z} d\bar{r} \left[\hat{\nabla}_a\left(\Psi^a + 2\,C^{ra}\right) + \left(\frac{\bar{r}_z - \bar{r}}{\bar{r}_z \bar{r}}\right)\hat{\nabla}^2\left(\alpha_\chi - \varphi_\chi - \Psi^r - C^{rr}\right) \right], \end{aligned} \tag{3.104}$$

where $\hat{\nabla}_a \Psi^a = \partial_a \Psi^a + \cot\theta\, \Psi^\theta$ and $\hat{\nabla}^2 = [\partial_\theta^2 + \cot\theta\, \partial_\theta + (\sin\theta)^{-2}\partial_\phi^2]$. This result perfectly agrees with the gravitational lensing κ obtained in [72], making the result in eq. (3.102) fully consistent with the correct expression of the angular diameter distance in eq. (3.66).

In some previous works δk^a_o and $\delta\tilde{\theta}^a_o$ were set to zero, corresponding to a different choice of the GLC angles. In this case the expression of the angular diameter distance in eq. (3.100) should contain an additional factor given by the Jacobian of the rotation from the GLC angles to the observed ones (see for instance [64]), providing the perturbations at observations, such as the observer peculiar velocity and the gravitational potential, which should appear in the gravitational lensing convergence.

3.C Photon wavevector

In the observer rest frame, where the local metric is Minkowski $g^{\rm L}_{mn} = \eta_{mn}$, the photon wavevector is given by

$$k^m_{\rm L} = \omega\,(-1\,,\,n^i\,)\,, \qquad m = t,x,y,z, \quad i = x,y,z, \tag{3.105}$$

where $\omega = \eta_{mn} u^m_{\rm L} k^n_{\rm L}$ is the photon frequency and $n^i \sim (\theta_{\rm obs}, \phi_{\rm obs})$ is a unit directional vector identifying the observed angular position of the source.

To obtain the photon wavevector in a global coordinate $y^\mu_{\rm FRW}$ we need to construct an orthonormal basis in the observer rest frame, the so-called tetrads $[e_m]^\mu$. First of all, the time-like observer four-velocity u^μ defines the proper-time direction in the observer rest frame

$$[e_t]^\mu \equiv u^\mu\,. \tag{3.106}$$

Spatial hypersurfaces orthogonal to $[e_t]^\mu$ are defined by three space-like vectors $[e_i]^\mu$. To obtain the expression for the space-like tetrads $[e_i]^\mu$, we use the orthonormality condition

$$\eta_{mn} = g_{\mu\nu}[e_m]^\mu[e_n]^\nu\,. \tag{3.107}$$

By taking the metric given in eq. (2.5) as $g_{\mu\nu}$ and considering the spatial components of the above condition, $\delta_{ij} = [e_i]^\mu[e_j]^\nu g_{\mu\nu}$, we obtain

$$[e_i]^\alpha[e_j]^\beta(\bar{g}_{\alpha\beta} + 2\,\mathcal{C}_{\alpha\beta}) = \frac{1}{a^2}\delta_{ij}\,. \tag{3.108}$$

We now make the following ansatz:

$$[e_i]^\alpha \equiv \frac{1}{a}(\delta^\alpha_i + \mathcal{D}^\alpha_i)\,, \tag{3.109}$$

where $\mathcal{D}^\alpha_i$ is a generic tensor perturbation to be determined. This definition (with the Kronecker delta) means that in the absence of perturbations the spatial coordinates in the rest frame are aligned to the spatial global coordinates locally at the observer position. By substituting the ansatz into eq. (3.108) we obtain that $\mathcal{D}_{ij} = -\mathcal{C}_{ij}$ and therefore

$$[e_i]^\alpha = \frac{1}{a}(\delta^\alpha_i - \mathcal{C}^\alpha_i)\,. \tag{3.110}$$

Finally, from the mixed time-space components of the orthonormality condition, $0 = [e_t]^\mu[e_i]^\nu g_{\mu\nu}$, we obtain

$$[e_i]^\eta = \frac{1}{a}(V_i - \mathcal{B}_i)\,. \tag{3.111}$$

Summing up, the tetrads are given by

$$[e_t]^\mu = u^\mu\,, \qquad\qquad [e_i]^\mu = \frac{1}{a}(V_i - \mathcal{B}_i\,,\,\delta^\alpha_i - \mathcal{C}^\alpha_i)\,. \tag{3.112}$$

As a result, the photon wavevector in a global coordinates is given by

$$k^{\mu}_{\rm FRW} = [e_m]^{\mu} k^m_L = \frac{\omega}{a}(-1 + \mathcal{A} + n^i V_i - n^i \mathcal{B}_i \,,\, \delta^{\alpha}_i \, n^i - V^{\alpha} - n^i \mathcal{C}^{\alpha}_i) \,. \tag{3.113}$$

It is noted that the unit directional vector n^i in the observer rest frame is different from the unit directional vector $\hat{n}^{\alpha}$ describing the photons direction in a homogeneous universe and in a global coordinate. The difference becomes subtle at the observer position, as we described in appendix 3.B. However, when these two vectors are contracted with perturbation quantities the result at linear order is identical, as the difference in the two vectors appears at perturbative level. As a consequence, we can write the photon wavevector in a global coordinate as

$$k^{\mu}_{\rm FRW} = \frac{\omega}{a}(-1 + \mathcal{A} + n^{\alpha} V_{\alpha} - n^{\alpha} \mathcal{B}_{\alpha} \,,\, n^{\alpha} - V^{\alpha} - n^{\beta} \mathcal{C}^{\alpha}_{\beta}) \,. \tag{3.114}$$

It should be clear that the above quantity, even though it is expressed in a global coordinate, is physically meaningful only locally at the observer position, where the observer rest frame is defined.

3.D Calculation of the gravitational lensing convergence

In this appendix we calculate the gravitational lensing convergence κ (or J_2 in [61]) when the degrees of freedom in the GLC angles are fixed in such a way that the GLC angles match the observed angles in the observer rest frame (see appendices 3.B and 3.C). The quantity we have to calculate is

$$\kappa \equiv \frac{1}{2}\partial_a \delta\tilde{\theta}^a + \frac{1}{2}\cot\tilde{\theta}\,\delta\tilde{\theta} = \frac{1}{2}\hat{\nabla}_a \,\delta\tilde{\theta}^a \,. \tag{3.115}$$

To simplify this task, we make use of three unit directional vectors: n^{α}, ϑ^{α}, φ^{α}, orthogonal to each other. The observed angular position of the source is represented by the unit vector[10]

$$n^{\alpha} = (\sin\theta\cos\phi, \sin\theta\sin\phi, \cos\theta) \,. \tag{3.116}$$

Based on n^{α}, we define two unit vectors generating the tangent plane to the two-sphere parametrized by (θ, ϕ) at the point where n^{α} is attached:

$$\begin{aligned} \vartheta^{\alpha} &= \partial_{\theta} n^{\alpha} = (\cos\theta\cos\phi, \cos\theta\sin\theta, -\sin\theta) \,, \\ \varphi^{\alpha} &= \frac{1}{\sin\theta}\partial_{\phi} n^{\alpha} = (-\sin\phi, \cos\phi, 0) \,. \end{aligned} \tag{3.117}$$

[10] In this appendix we drop the subscript "obs" to refer to the observed angles.

In spherical coordinates these unit vectors are $n_\alpha = (1,0,0)$, $\vartheta_\alpha = (0,r,0)$, $\varphi_\alpha = (0,0,r\sin\theta)$, and their product with a generic spatial vector A^α gives respectively the radial component and the two angular components:

$$n_\alpha A^\alpha = A^r\,, \qquad \vartheta_\alpha A^\alpha = rA^\theta\,, \qquad \varphi_\alpha A^\alpha = r\sin\theta\, A^\phi\,. \tag{3.118}$$

Consequently, starting from the expression of a given quantity in spherical coordinates, we can rewrite it in a covariant way by using the unit vectors. After that, we can make use of any coordinate system to perform the calculations. Indeed, the calculation of κ greatly simplifies if we first rewrite $\delta\tilde{\theta}^a$ given by eq. (3.95) as

$$\begin{aligned}
\delta\tilde{\theta} &= -\theta_\alpha\Big[-\mathcal{V}^\alpha + \Psi^\alpha + C^{[\alpha|\beta]}n_\beta + C^{\alpha\beta}n_\beta\Big]_o + \frac{\theta_\alpha\mathcal{G}^\alpha}{\bar{r}_z}\bigg|_o^s \\
&+ \int_0^{\bar{r}_z} d\bar{r}\left[\frac{\theta_\alpha(\Psi^\alpha + 2\,C^\alpha_\beta\, n^\beta)}{\bar{r}} + \left(\frac{\bar{r}_z-\bar{r}}{\bar{r}_z\bar{r}}\right)\partial_\theta(\alpha_\chi - \varphi_\chi - \Psi_\beta\, n^\beta - C_{\beta\gamma}\, n^\beta n^\gamma)\right], \\
\delta\tilde{\phi} &= -\frac{1}{\sin\theta}\phi_\alpha\Big[-\mathcal{V}^\alpha + \Psi^\alpha + C^{[\alpha|\beta]}n_\beta + C^{\alpha\beta}n_\beta\Big]_o + \frac{\phi_\alpha\mathcal{G}^\alpha}{\bar{r}_z\sin\theta}\bigg|_o^s \\
&+ \int_0^{\bar{r}_z} d\bar{r}\left[\frac{\phi_\alpha(\Psi^\alpha + 2\,C^\alpha_\beta\, n^\beta)}{\bar{r}\sin\theta} + \left(\frac{\bar{r}_z-\bar{r}}{\bar{r}_z\bar{r}}\right)\frac{1}{\sin^2\theta}\partial_\phi(\alpha_\chi - \varphi_\chi - \Psi_\beta\, n^\beta - C_{\beta\gamma}\, n^\beta n^\gamma)\right],
\end{aligned} \tag{3.119}$$

and we choose cartesian coordinates, so that any covariant derivative with respect to the three-spatial metric $\bar{g}_{\alpha\beta}$ reduces to an ordinary derivative, as $\bar{g}_{\alpha\beta} = \delta_{\alpha\beta}$. After introducing the angular gradient and the angular Laplacian,

$$\hat{\nabla}_\alpha = \theta_\alpha\,\partial_\theta + \frac{1}{\sin\theta}\phi_\alpha\,\partial_\phi\,, \qquad \hat{\nabla}^2 = \partial^2_\theta + \cot\theta\,\partial_\theta + \frac{1}{\sin^2\theta}\partial^2_\phi\,, \tag{3.120}$$

and noting the identity

$$(\cot\theta + \partial_\theta)\,\theta_\alpha + \frac{1}{\sin\theta}\partial_\phi\phi_\alpha = -2n_\alpha\,, \tag{3.121}$$

we derive the gravitational lensing convergence

$$\begin{aligned}
\kappa = n_\alpha\Big[-\mathcal{V}^\alpha + \Psi^\alpha + C^\alpha_\beta n^\beta\Big]_o + \frac{1}{2\bar{r}_z}\hat{\nabla}_\alpha\mathcal{G}^\alpha - \frac{n_\alpha\mathcal{G}^\alpha}{\bar{r}_z}\bigg|_o^s - \int_0^{\bar{r}_z} d\bar{r}\,\frac{n_\alpha(\Psi^\alpha + 2\,C^\alpha_\beta n^\beta)}{\bar{r}} \\
+ \frac{1}{2}\int_0^{\bar{r}_z} d\bar{r}\left[\frac{\hat{\nabla}_\alpha(\Psi^\alpha + 2\,C^\alpha_\beta n^\beta)}{\bar{r}} + \left(\frac{\bar{r}_z-\bar{r}}{\bar{r}_z\bar{r}}\right)\hat{\nabla}^2(\alpha_\chi - \varphi_\chi - \Psi_\alpha n^\alpha - C_{\alpha\beta}n^\alpha n^\beta)\right].
\end{aligned} \tag{3.122}$$

Finally, going back to spherical coordinates, we obtain:

$$\begin{aligned}\kappa =&\left[-\mathcal{V}^r + \Psi^r + C^{rr}\right]_o + \frac{1}{2}\hat{\nabla}_a\mathcal{G}^a + \frac{1}{\bar{r}_z}\mathcal{G}^r_o \\ &+ \frac{1}{2}\int_0^{\bar{r}_z} d\bar{r}\left[\hat{\nabla}_a\left(\Psi^a + 2\,C^{ra}\right) + \left(\frac{\bar{r}_z - \bar{r}}{\bar{r}_z\bar{r}}\right)\hat{\nabla}^2(\alpha_\chi - \varphi_\chi - \Psi^r - C^{rr})\right],\end{aligned} \tag{3.123}$$

where $\hat{\nabla}_a\Psi^a = \partial_a\Psi^a + \cot\theta\,\Psi^\theta$. This result is probably the most complicated to derive but is in agreement with the gravitational lensing convergence calculated in [72] with the geometric approach and with fully general metric representation to first order in perturbations.

CHAPTER 4

Galaxy Two-Point Correlation Function in General Relativity

Preface

In this chapter, which is thoroughly based on the work presented in [2], we introduce the galaxy number density and we study its two-point correlation function taking into account all the relativistic effects that alter the measurements. The first part of the chapter is dedicated to the analysis and solution of theoretical issues in the description of these quantities. In particular, we use the equivalence principle of general relativity to argue that the theoretical predictions must be insensitive to the uniform gravitational field produced by long-mode perturbations. These are the perturbations whose wavelength is larger than the comoving distance between source and observer and, as such, contribute to the uniform gravitational potential and force acting on the system. In agreement with the equivalence principle, these perturbations must have no effect on physical observables. By isolating the contributions of long-mode perturbations to the galaxy number density we show that they cancel when the complete gauge-invariant expression is considered. This is important because it means that when some of the terms in the expression are neglected unphysical uniform gravity mode remain. For this reason some of the predictions for the galaxy two-point correlation function presented in the literature exhibit unphysical infrared divergences. It is indeed common to derive the expression for the galaxy number density in the Newtonian gauge and neglect by hand the perturbations at the observer position arguing that they are not observable. Here we demonstrate that this lead to a gauge-dependent expression that is inconsistent with the equivalence principle and whose variance is infrared-divergent. Indeed, the terms at the observer position in the Newtonian gauge correspond to dif-

ferent kind of terms in another gauge, so that neglecting them is not justified. In the second part of the chapter we present a numerical study to estimate the impact of the relativistic effects on the galaxy correlation function offering a comparison with the standard prediction that is used to analyze data. Our results indicate the need of considering the relativistic effects in future analyses.

Based on:

[2] F. Scaccabarozzi, J. Yoo and S. G. Biern,
"*Galaxy Two-Point Correlation Function in General Relativity*",
JCAP 1810 (2018) no.10, 024, [arXiv:1807.09796].

Abstract. We perform theoretical and numerical studies of the full relativistic two-point galaxy correlation function, considering the linear-order scalar and tensor perturbation contributions and the wide-angle effects. Using the gauge-invariant relativistic description of galaxy clustering and accounting for the contributions at the observer position, we demonstrate that the complete theoretical expression is devoid of any long-mode contributions from scalar or tensor perturbations and it lacks the infrared divergences in agreement with the equivalence principle. Using the full gauge-invariant expression, we numerically compute the galaxy two-point correlation function and study the individual contributions in the conformal Newtonian gauge. We find that several terms at the observer position that are missing in the standard formalism dominate over the other relativistic contributions in the conformal Newtonian gauge. Compared to the standard theoretical predictions, the relativistic effects in galaxy clustering result in a few percent-level systematic errors beyond the scale of the baryonic acoustic oscillation. Our theoretical and numerical studies provide a comprehensive understanding of the relativistic effects in the galaxy two-point correlation function.

4.1 Introduction

Galaxy surveys map the universe by measuring the redshift z and the direction $\hat{\boldsymbol{n}}$ of each galaxy. One simple and direct way to extract physical information from this map is then to compute the galaxy two-point correlation function. In particular, one correlates the number density of galaxies in a redshift bin around z_1 and in a small solid angle around a direction $\hat{\boldsymbol{n}}_1$ with those in a redshift bin around z_2 and in a small solid angle around a direction $\hat{\boldsymbol{n}}_2$. The next generation of galaxy surveys [19, 20, 21, 22, 23, 24] will probe the large scale structure of the universe at high redshift and for wide regions of the sky. Given the unprecedented precision achieved by the recent observational advances, the theoretical predictions of the two-point correlations used to analyze the

data can no longer rely on the flat-sky approximation nor on the assumption that the universe is homogeneous and isotropic. The flat-sky approximation, assuming that the directions $\hat{\boldsymbol{n}}_1$ and $\hat{\boldsymbol{n}}_2$ coincide, is currently used to analyze redshift surveys and constrain cosmological parameters but is not sufficiently accurate to interpret data from future surveys [80]. Furthermore, most expressions used for the analysis only take into account density fluctuations and redshift-space distortions. Clearly, these standard expressions provide an approximation to what we observe, and they are inevitably gauge-dependent. Indeed, a gauge-invariant expression of the two-point correlation function includes all relativistic effects that manifest in galaxy clustering.

Previous works have studied the impact of relativistic effects on the correlation function and the power spectrum (as well as additional subdominant effects such as [81, 82]). In [71, 83, 84], the galaxy power spectrum was derived, including all the relativistic effects, and its detection significance was quantified. However, they adopted the flat-sky approximation, essentially ignoring the relativistic effects at the observer position and along the line-of-sight direction, when computing the detection significance by using the power spectrum. Since the Fourier decomposition is non-local in nature, the standard power spectrum has difficulty in its expression in the all-sky limit (see, however, [85] for the all-sky analysis using the spherical Fourier decomposition). However, the correlation function is subject to no such complications and can be derived directly in terms of observable quantities. Using the standard redshift-space distortion formula, the galaxy two-point correlation function was derived in [86, 87, 88, 89, 90, 91] without assuming the flat-sky approximation. In light of the full relativistic description of galaxy clustering [70, 71, 72], a complete description of the galaxy two-point correlation function was derived [92], while ignoring the gravitational potential contributions, but finding several new corrections from the velocity perturbations.

In recent years, many efforts have been made to compute the galaxy two-point correlation function with all the relativistic effects (see, e.g., [54, 93, 94, 95]). For example, the lensing effect arises from the matter density fluctuations along the line-of-sight direction, and its contribution to the correlation function has been studied in [96, 97, 98, 99]. In particular, the most recent work [100] demonstrated that the relativistic effects and wide-angle effects are of the same order and must be considered together. However, none of these previous studies are complete, when the relativistic effects are concerned. In the presence of the gravitational potential contributions, the computation of the galaxy two-point correlation function diverges in the infrared, a typical sign of theoretical deficiency, and as a consequence one has to introduce an *arbitrary* cut-off scale $k_{\rm IR}$ to the computation to keep the theoretical predictions under control. A similar divergence in the infrared was observed in the variance of the luminosity distance, and it was shown [101, 102] that the such pathology appears due to the use of incorrect relativistic descriptions.

Here we derive the two-point correlation function including all the relativistic effects

in galaxy clustering. The theoretical expression of galaxy clustering used to compute the two-point correlation function must be gauge-invariant, as it represents a physical observable. By adopting a general metric representation with scalar and tensor perturbations we derive the relativistic expression of galaxy clustering ([70, 71, 84, 103, 104]), showing its gauge invariance explicitly. In addition to the gauge invariance, the theoretical expression must be consistent with the equivalence principle of general relativity. Among other consequences, the latter implies that the uniform gravity produced by long-mode perturbations does not affect physical observables. It was shown in [84] that there is no such long-mode scalar contribution to galaxy clustering in the synchronous gauge, and this proof was generalized in [105] for gravitational lensing. Drawing upon these studies, we demonstrate that our relativistic derivation of galaxy clustering is not affected by such long modes either from scalar or tensor perturbations. As described in [101, 106], this also implies that our expression is devoid of infrared divergences. It is known that most relativistic expressions for galaxy clustering in literature have variances that diverge in the infrared [93]. This issue is usually ignored, and an arbitrary infrared cut-off is put in place to eliminate the divergences. Here we show how this issue can be naturally resolved, simply by using the correct theoretical expression.

With the correct theoretical prediction at hand, we numerically study the two-point correlation function. Specifically, we derive the general analytic expressions for each relativistic effect in galaxy clustering: the density fluctuation, the redshift and the radial distortions, the gravitational lensing convergence and redshift-space distortions. This requires, in turn, to write down the correlation functions of the local potentials, the peculiar velocities, the integrated Sachs-Wolf effects and the Shapiro time-delay effects. Our study provides the amplitude of the correlation function for individual contributions, allowing to determine which effect dominates the total observed correlation in a given configuration of the galaxy pair. We perform the numerical investigation of the scalar perturbations in the conformal Newtonian gauge and the primordial gravitational-wave contributions. While the contribution to the observed angular galaxy clustering from gravitational waves has been studied already in [107, 108], we generalize their results to the two-point galaxy correlation function.

The organization of the chapter is as follows. First we study the galaxy number density theoretically in sec. 4.2, showing the gauge invariance in sec. 4.2.2 and the consistency with the equivalence principle in sec. 4.2.3. Then we study the two-point correlation function numerically in sec. 5.4, where we first show that the correlation function does not exhibit infrared divergence. In sec. 4.3.1 we analyze the correlation of individual relativistic effects, indicating the dominant contributions in different configurations. We perform the same analysis for the contribution of primordial gravitational waves in sec. 4.3.2. We conclude with a summary and a discussion in sec. 4.4. In appendix 4.A we provide the solution for the scalar perturbations needed for the numerical results of sec. 4.3.1.

4.2 Galaxy Clustering and Theoretical Investigations

In this section we derive the theoretical expression of the galaxy number density fluctuation to first order in perturbation theory. To prove the correctness of our expression we adopt a general metric representation and explicitly demonstrate the gauge-invariance of the theoretical expression. Then, in the conformal Newtonian gauge, we show that our expression is also consistent with the equivalence principle, further corroborating the sanity of our calculations.

4.2.1 Metric convention and gauge transformations

Here we adopt a flat Friedmann-Robertson-Walker (FRW) metric for our theoretical description of the background universe. In the presence of inhomogeneities, we parametrize the small perturbations to the background FRW metric by

$$\delta g_{00} \equiv -2\,a^2\alpha\,, \qquad \delta g_{0i} \equiv -a^2\beta_{,i}\,, \qquad \delta g_{ij} \equiv 2\,a^2\big[\varphi\,\bar{g}_{ij} + \gamma_{,i|j} + C_{ij}\big]\,, \tag{4.1}$$

where a is the scale factor, $\bar{g}_{ij}$ is the background 3-metric, commas represent the ordinary derivative while vertical bars represent the covariant derivative with $\bar{g}_{ij}$. The tensor perturbations C_{ij} are constructed such that they are traceless ($C_i^{\,i} = 0$) and transverse ($C^{ij}{}_{|j} = 0$), with the longitudinal part being absorbed into the scalar perturbations. The scalar $(\alpha, \beta, \varphi, \gamma)$ and tensor (C_{ij}) perturbations are functions of a space-time point in a global coordinate $x^\mu = (\eta, \boldsymbol{x})$, identified by a conformal time η and spatial coordinates x^i. The metric representation in eq. (4.1) is the most general accounting for scalar and tensor perturbations, and no gauge condition is imposed. In this chapter we do not consider the vector perturbations, as they decay fast in time. The observer motion is described by a time-like four-velocity $u^\mu \equiv a^{-1}\,(1-\alpha\,, \mathcal{U}^i\,)$, where the spatial component is further expressed in terms of a scalar perturbation U as $\mathcal{U}^i \equiv -U^{,i}$. As we shall see in the next paragraph, it is convenient to define a scalar velocity $v \equiv U + \beta$, as it is independent of the spatial gauge transformation.

In order to obtain the gauge transformation properties of the metric perturbations introduced above we consider the coordinate transformation:

$$\tilde{x}^\mu = x^\mu + \xi^\mu\,, \qquad \xi^\mu \equiv (T, L^{,i})\,, \tag{4.2}$$

where the infinitesimal displacement field ξ^μ is decomposed in terms of two scalars T and L. The transformations of the metric perturbations are then given by

$$\begin{aligned} &\tilde{\alpha} = \alpha - \frac{1}{a}(aT)'\,, \qquad &&\tilde{\beta} = \beta - T + L'\,, \qquad &&\tilde{\gamma} = \gamma - L\,, \\ &\tilde{\varphi} = \varphi - \mathcal{H}T\,, \qquad &&\tilde{U} = U - L'\,, \qquad &&\tilde{v} = v - T\,, \end{aligned} \tag{4.3}$$

where a prime indicates the derivative with respect to conformal time and $\mathcal{H} = a'/a = aH$ is the conformal Hubble parameter. Note that there is no gauge ambiguity for tensor perturbations at the linear order, $\tilde{C}_{ij} = C_{ij}$, as evident in eq. (4.2). Based on the gauge transformation properties, we can define gauge-invariant quantities at linear level [72]:

$$\alpha_\chi \equiv \alpha - \frac{1}{a}\chi', \qquad \varphi_\chi \equiv \varphi - H\chi, \qquad v_\chi \equiv v - \frac{1}{a}\chi, \qquad \delta_v \equiv \delta + 3\mathcal{H}v, \tag{4.4}$$

where $\chi \equiv a(\beta + \gamma')$ is the scalar shear of the normal observer, $n_\mu = -a(1+\alpha, 0)$, transforming as $\tilde{\chi} = \chi - aT$, and δ is the matter density fluctuation, transforming as $\tilde{\delta} = \delta + 3\mathcal{H}T$. The notation for scalar gauge-invariant variables is set up such that α_χ, φ_χ and v_χ correspond respectively to the gravitational potentials and the velocity potential in the conformal Newtonian gauge ($\chi = 0$), while δ_v is the matter density fluctuation in the comoving gauge ($v = 0$). For convenience we define a gauge-invariant velocity $V^i \equiv -v_\chi{}^{,i}$ and a pure gauge term $\mathcal{G}^i \equiv \gamma^{,i}$ transforming as $\tilde{\mathcal{G}}^i = \mathcal{G}^i - L^{,i}$.

4.2.2 Gauge-invariant formalism of galaxy clustering

In the past years, a number of groups have worked on the relativistic effects of galaxy clustering using the gauge-invariant formalism ([70, 71, 84, 103, 104], see also [109, 110, 111, 112] for the second-order formalism). The observed galaxy number density is obtained by counting the number of galaxies within the observed volume $dV_{\rm obs}$ that appears to the observer as the volume within the observed redshift interval dz and the observed solid angle $d\Omega$. In the background, the observed volume would be the physical volume occupied by the observed galaxies. However, in the presence of inhomogeneities in the universe, the observed volume $dV_{\rm obs}$ does not correspond to the physical volume $dV \equiv dV_{\rm obs}(1+\delta V)$ and the difference is captured by the dimensionless fluctuation δV. On the other hand, the number of observed galaxies dN_g is unaffected by the inhomogeneities and can be expressed in terms of both the observed and the physical number densities, $n_g^{\rm obs}$ and n_g, which are related by the volume fluctuation as

$$dN_g \equiv n_g^{\rm obs}\, dV_{\rm obs} = n_g dV \quad \longrightarrow \quad n_g^{\rm obs} = n_g(1+\delta V)\,. \tag{4.5}$$

In order to obtain the theoretical expression of the galaxy number density, we need to derive the fluctuation δV in the volume occupied by the source galaxies. This requires the general relativistic relation of the observed redshift and angle to the physical volume along the past light-cone. Here we consider perturbations up to first order and we follow the gauge-invariant formalism developed in [70, 71, 72] to obtain the expressions of the volume fluctuation and then of the observed galaxy number density. Following [72], we will first define the distortions in the position of source galaxies and subsequently use these to obtain the observables of our interest.

The position of a source galaxy is identified by the observed redshift z and the observed angular position $\hat{\boldsymbol{n}} = (\sin\theta\cos\phi, \sin\theta\sin\phi, \cos\theta)$, measured in *the observer rest frame*. Based on these quantities, the observer infers the source position $\bar{x}_s^\mu = (\bar{\eta}_z, \bar{r}_z\hat{\boldsymbol{n}})$ in a FRW coordinate by using the distance - redshift relation in a homogeneous universe,

$$\bar{r}_z = \bar{\eta}_o - \bar{\eta}_z = \int_0^z \frac{dz'}{H(z')}\,, \tag{4.6}$$

where a bar denotes the coordinates at the observer (o) and the source (at redshift z) in the background. The real position of the source is different from the inferred one, because the inhomogeneities affect the photon propagation. To account for the effect of the inhomogeneities on the real source position $x_s^\mu = (\eta_s, r_s, \theta_s, \phi_s)$ with respect to the inferred position $\bar{x}_s^\mu = (\bar{\eta}_z, \bar{r}_z, \theta, \phi)$ we define the time distortion $\Delta\eta \equiv \eta_s - \bar{\eta}_z$ (related to the distortion δz in the observed redshift) and the geometric distortions of the spatial position $\delta r \equiv r_s - \bar{r}_z$, $\delta\theta \equiv \theta_s - \theta$, $\delta\phi \equiv \phi_s - \phi$.

In this approach the redshift distortion and the time distortion are defined with respect to the observed redshift $1+z = 1/a(\bar{\eta}_z) \equiv (1+\delta z)/a(\eta_s)$, which can be calculated as the ratio between the photon energy at the source and at the observer.[1] One obtains the following expression:

$$\delta z = \mathcal{H}\,\Delta\eta = -H\chi + (\mathcal{H}\delta\eta + H\chi)_o + \left[V_i\hat{n}^i - \alpha_\chi\right]_o^z - \int_0^{\bar{r}_z} d\bar{r}\left[\alpha_\chi - \varphi_\chi - C_{ij}\hat{n}^i\hat{n}^j\right]'. \tag{4.7}$$

The quantity $\delta\eta_o$ represents the observer time-lapse, describing the difference between the coordinate time at observation η_o and the observer's proper time τ_o. It is derived from the time component of the four-velocity $u^\mu = dx^\mu/d\tau$ as (see [72, 66, 113, 101])

$$\delta\eta_o = -\frac{1}{a_o}\int_0^{\bar{\eta}_o} d\bar{\eta}\, a\,\alpha\,, \tag{4.8}$$

where $\bar{\eta}_o = \int_0^\infty \frac{dz}{H(z)}$ is uniquely determined and related to the observer proper time as $\tau_o = \int_0^{\bar{\eta}_o} d\eta\, a(\eta)$. By making use of the gauge-invariant variables defined in sec. 4.2.1, the gauge-dependent term $-H\chi$ is isolated in the expression of δz, which transforms in fact as $\widetilde{\delta z} = \delta z + \mathcal{H}T$. We can therefore define a new gauge-invariant variable $\delta z_\chi = \delta z + H\chi$.

The geometric distortions of the source spatial position $\delta x_s^i \equiv x_s^i - \bar{x}_s^i$ can be computed by integrating the photon geodesic equation from the observer position to the source position, as described in [70, 71, 72]. By following that approach we obtain

$$\delta r = \hat{n}_i\, x_s^i - \bar{r}_z = -\hat{n}_i\mathcal{G}^i + \hat{n}_i(\delta x^i + \mathcal{G}^i)_o + (\delta\eta + \chi)_o - \frac{\delta z_\chi}{\mathcal{H}_z} + \int_0^{\bar{r}_z} d\bar{r}\left[\alpha_\chi - \varphi_\chi - C_{ij}\hat{n}^i\hat{n}^j\right], \tag{4.9}$$

[1] The photon energy is given by $E = -g_{\mu\nu}u^\mu k^\nu$, where k^μ is the photon wave-vector.

$$\begin{aligned}\bar{r}_z\delta\theta = \hat{\theta}_i\, x_s^i &= -\hat{\theta}_i\mathcal{G}^i + \hat{\theta}_i(\delta x^i + \mathcal{G}^i)_o + \bar{r}_z\hat{\theta}_i\Big(- V^i + C^i_j\hat{n}^j\Big)_o \\ &\quad - 2\int_0^{\bar{r}_z} d\bar{r}\,\hat{\theta}_i C^i_j\hat{n}^j - \int_0^{\bar{r}_z} d\bar{r}\,(\bar{r}_z-\bar{r})\hat{\theta}_i[(\alpha_\chi-\varphi_\chi)^{,i} - C_{jk}{}^{,i}\hat{n}^j\hat{n}^k]\,,\end{aligned} \tag{4.10}$$

$$\begin{aligned}\bar{r}_z\sin\theta\,\delta\phi = \hat{\phi}_i\, x_s^i &= -\hat{\phi}_i\mathcal{G}^i + \hat{\phi}_i(\delta x^i + \mathcal{G}^i)_o + \bar{r}_z\sin\theta\,\hat{\phi}_i\Big(- V^i + C^i_j\hat{n}^j\Big)_o \\ &\quad - 2\int_0^{\bar{r}_z} d\bar{r}\,\hat{\phi}_i C^i_j\hat{n}^j - \int_0^{\bar{r}_z} d\bar{r}\,(\bar{r}_z-\bar{r})\hat{\phi}_i[(\alpha_\chi-\varphi_\chi)^{,i} - C_{jk}{}^{,i}\hat{n}^j\hat{n}^k]\,,\end{aligned} \tag{4.11}$$

where the unit vectors $\hat{\theta}^i = \partial_\theta\hat{n}^i$ and $\hat{\phi}^i = (1/\sin\theta)\,\partial_\phi\hat{n}^i$ are projectors on the sphere. The quantity δx^i_o represents the spatial shift at the observer position, describing the change caused by the velocity field generated by the inhomogeneities. Exactly in the same way as the observer coordinate lapse $\delta\eta_o$, it is derived from the four-velocity as

$$\delta x^i_o = -\int_0^{\bar{\eta}_o} d\bar{\eta}\; U^{,i}\,. \tag{4.12}$$

This effect has been often neglected in the literature, but, as we shall see, it cancels out in any linear-order expression of the observables.

Given the angular distortions above, one can compute also the change in the solid angle subtended by the source. This effect is known as the gravitational lensing convergence and is given by the ratio between the observed solid angle and the solid angle at the source as

$$\begin{aligned}\kappa &\equiv -\frac{1}{2}\left[\left(\cot\theta + \frac{\partial}{\partial\theta}\right)\delta\theta + \frac{\partial}{\partial\phi}\delta\phi\right] \\ &= -\frac{\hat{n}_i\mathcal{G}^i}{\bar{r}_z} + \frac{1}{2\bar{r}_z}\hat{\nabla}_i\mathcal{G}^i + \frac{\hat{n}_i}{\bar{r}_z}(\mathcal{G}^i+\delta x^i)_o + \hat{n}_i\left(- V^i + \frac{3}{2}C^i_j\hat{n}^j\right)_o \\ &\quad - 2\int_0^{\bar{r}_z} d\bar{r}\,\frac{C_{ij}\hat{n}^i\hat{n}^j}{\bar{r}_z} + \int_0^{\bar{r}_z} d\bar{r}\,\frac{\hat{\nabla}_i(C^i_j\,\hat{n}^j)}{\bar{r}_z} \\ &\quad + \int_0^{\bar{r}_z} d\bar{r}\left(\frac{\bar{r}_z-\bar{r}}{2\,\bar{r}_z\bar{r}}\right)\Big[\hat{\nabla}^2(\alpha_\chi-\varphi_\chi) - \big(\hat{n}^i\hat{n}^j\hat{\nabla}^2 C_{ij} + 2\,\hat{n}^i\hat{\nabla}_j C^j_i\big)\Big]\,,\end{aligned} \tag{4.13}$$

where $\hat{\nabla}_i$ is the angular gradient operator and $\hat{\nabla}^2$ is the angular Laplacian. The gauge transformation properties are transparent:

$$\begin{aligned}&\widetilde{\delta r} = \delta r + \hat{n}_i L^{,i}, \qquad \bar{r}_z\widetilde{\delta\theta} = \bar{r}_z\delta\theta + \hat{\theta}_i L^{,i}\,, \qquad \bar{r}_z\sin\theta\,\widetilde{\delta\phi} = \bar{r}_z\sin\theta\,\delta\phi + \hat{\phi}_i L^{,i}\,, \\ &\tilde{\kappa} = \kappa + \frac{\hat{n}_i L^{,i}}{\bar{r}_z} - \frac{1}{2\,\bar{r}_z}\hat{\nabla}_i L^{,i}\,,\end{aligned} \tag{4.14}$$

and this shows that the real position x^μ_s of the source is a coordinate-dependent quantity. As for the redshift distortion δz_χ, the expressions of δr, $\delta\theta$, $\delta\phi$ and κ can be

arranged in terms of gauge-invariant variables, isolating the gauge-dependent terms (involving $\mathcal{G}^i$), as

$$\delta r_\chi = \delta r + \hat{n}_i \mathcal{G}^i, \qquad \mathcal{K} = \kappa + \frac{\hat{n}_i \mathcal{G}^i}{\bar{r}_z} - \frac{1}{2\,\bar{r}_z} \hat{\nabla}_i \mathcal{G}^i \,. \tag{4.15}$$

Since the effects of the inhomogeneities are conveniently expressed in terms of the geometric distortions that we have introduced, we can write explicitly gauge-invariant expressions of the cosmological observables.

Now we use the gauge-invariant formalism summarized above (see [72] for the extensive description) to derive first the fluctuation in the luminosity distance and then that in the galaxy number density. The fluctuation $\delta\mathcal{D}_L$ in the luminosity distance is defined through $\mathcal{D}_L \equiv \bar{\mathcal{D}}_L(1+\delta\mathcal{D}_L)$, where $\bar{\mathcal{D}}_L = (1+z)\bar{r}_z$. From its exact relation with the angular diameter distance $\mathcal{D}_A = (1+z)^{-2}\mathcal{D}_L$, we can compute $\delta\mathcal{D}_A$ with ease, by using the geometric distortions for a unit area. The angular diameter distance is the distance at which a solid angle $d\Omega = \sin\theta d\theta d\phi$ subtends a physical area dA perpendicular to the photon propagation in the source rest frame,

$$dA \equiv \mathcal{D}_A^2 d\Omega = \sqrt{-g}\,\epsilon_{\mu\nu\rho\sigma} u_s^\mu n_s^\mu \frac{\partial x_s^\rho}{\partial\theta}\frac{\partial x_s^\sigma}{\partial\phi} d\theta d\phi \,, \tag{4.16}$$

where $n^\mu = k^\mu/(k^\nu u_\nu) + u^\mu$ is the observed photon direction for the observer with four-velocity u^μ. From this equation we obtain the fluctuation in the distance as a function of the observed redshift and angles

$$\delta\mathcal{D}_L(z,\hat{\boldsymbol{n}}) = \delta\mathcal{D}_A = \delta z_\chi + \frac{\delta r_\chi}{\bar{r}_z} - \mathcal{K} + \varphi_\chi - \frac{1}{2} C_{ij}\hat{n}^i\hat{n}^j. \tag{4.17}$$

Written in terms of gauge-invariant variables, the gauge-invariance of the luminosity distance fluctuation is manifest (see [72, 101, 113]). Indeed, the luminosity distance is an observable, here expressed in terms of the other observables (redshift and angles), and therefore must be independent from the gauge conditions chosen [55]. Note the cancellation of the observer spatial shift δx_o^i among the radial distortion and the lensing convergence. As anticipated, this occurs for the expression of any observable at linear level.

By extending the previous expression of the infinitesimal area in the source rest frame, the infinitesimal volume occupied by the source galaxies is given by

$$dV = \sqrt{-g}\,\epsilon_{\mu\nu\rho\sigma} u_s^\mu \frac{\partial x_s^\nu}{\partial z}\frac{\partial x_s^\rho}{\partial\theta}\frac{\partial x_s^\sigma}{\partial\phi} dz d\theta d\phi \equiv dV_{\rm obs}(1+\delta V)\,, \qquad dV_{\rm obs} = \frac{\bar{r}_z^2 dz d\Omega}{H(1+z)^3}\,. \tag{4.18}$$

Thus, one obtains the linear-order relativistic correction to the physical volume

$$\delta V = 3\,\delta z_\chi + 3\,\varphi_\chi + 2\,\frac{\delta r_\chi}{\bar{r}_z} - 2\,\mathcal{K} + H\frac{\partial}{\partial z}\delta r_\chi + V_i\hat{n}^i\,, \tag{4.19}$$

which is manifestly gauge-invariant, as required by the fact that the volume itself is an observable. Finally, we have all ingredients to get the galaxy number density and its fluctuation. We can write the observed and physical galaxy number densities respectively as

$$n_g^{\rm obs} \equiv \bar{n}_g(\bar{\eta}_z)(1+\delta_g^{\rm obs})\,, \qquad\qquad n_g \equiv \bar{n}_g(\tau_s)(1+\delta_g^{\rm int})\,, \tag{4.20}$$

where we have defined the fluctuations $\delta_g^{\rm obs}$ and $\delta_g^{\rm int}$. Note that the mean density $\bar{n}_g$ and the intrinsic fluctuation $\delta_g^{\rm int}$ in the physical density are defined over the proper-time hypersurface of the source described by the comoving-synchronous gauge. By denoting the proper-time hypersurface with τ_s, the intrinsic fluctuation can be written as $\delta_g^{\rm int} \equiv b\,\delta_m^{\tau_s} \equiv b\,\delta_v$, where b is the galaxy bias and $\delta_m^{\tau_s} \equiv \delta_v$ is the matter density fluctuation in the comoving-synchronous gauge. Thus, the observed galaxy number density fluctuation is given by

$$\delta_g^{\rm obs}(z,\hat{\boldsymbol{n}}) = b\,\delta_v - e_z\,\delta z_v + \delta V\,, \qquad\qquad e_z \equiv -\frac{1}{\mathcal{H}_z}\frac{\bar{n}_g'(\bar{\eta}_z)}{\bar{n}_g(\bar{\eta}_z)} = \frac{d\ln\bar{n}_g}{d\ln(1+z)}\,. \tag{4.21}$$

Any quantity in the above expression is *gauge-invariant*, indeed δ_v and δz_v are those in the comoving-synchronous gauge and the gauge-invariance of the volume distortion is explicitly verified by expressing it in terms of gauge-invariant variables as in eq. (4.19).

4.2.3 Compatibility check with the equivalence principle

Following the lead by [84, 101, 105], we perform the compatibility check of our theoretical expression with the equivalence principle. The gauge invariance and the equivalence principle of general relativity offer a powerful way to test the validity of our theoretical predictions in sec. 4.2.2. The gauge-invariance reflects the fact that the physics is independent of the way the perturbations are defined with respect to the fictitious background. The equivalence principle asserts the physical equivalence of a gravitational field and its corresponding acceleration of the reference system. It implies that the laws of physics in a reference frame that is in free fall are the same as in the complete absence of gravity, i.e. the laws of physics are those of special relativity. Strictly speaking, however, the equivalence principle is applicable to the limit in which the differential gravity, or the tidal force can be neglected. The tidal effects are, indeed, the leading physical effect of gravity. Applying the equivalence principle to the case of our interest, where the source and the observer are on the past light-cone with the unique scale set by the (comoving) distance $\bar{r}_z$, we will consider any perturbation with wavelength larger than $\bar{r}_z$ as a long-mode perturbation and ignore any tidal effects.

In the previous subsection we showed that our expressions of the luminosity distance and galaxy number density are gauge-invariant. In this subsection we further check the compatibility of these expressions with the equivalence principle. According

to the latter, as discussed above, the uniform gravity generated by long-mode perturbations should have no consequence on the physical observables. We will isolate in the perturbations the contributions to a uniform gravitational field and show that our expressions are devoid of these terms. Besides confirming our derivations, we show that our expressions do not exhibit any infrared divergence on super horizon-scales, as demonstrated in [101, 106].

To focus on the effects of such long-mode perturbations we take the Fourier transformation of the perturbation variables and introduce a cut-off scale $k_{\rm IR}$ set by $k_{\rm IR}\bar{r}_z \ll 1$. To elaborate on this, let us consider a gravitational potential $\Psi(\eta,\boldsymbol{x})$ and its Fourier mode $\Psi(\eta,\boldsymbol{k})$. The gravitational potential can be split into the long-mode and short-mode contributions as

$$\Psi(\eta,\boldsymbol{x}) = \left(\int_0^{k_{\rm IR}} + \int_{k_{\rm IR}}^{\infty}\right)\frac{d^3k}{(2\pi)^3}\,e^{i\boldsymbol{k}\cdot\boldsymbol{x}}\,\Psi(\eta,\boldsymbol{k}) \equiv \Psi^{\ell}(\eta,\boldsymbol{x}) + \Psi^{s}(\eta,\boldsymbol{x})\,. \tag{4.22}$$

By expanding in terms of $k_{\rm IR}\bar{r}_z$, the long-mode potential can be written as

$$\begin{aligned}\Psi^{\ell}(\eta,\boldsymbol{x}) &= \int_0^{k_{\rm IR}}\frac{d^3k}{(2\pi)^3}\left(1 + i\boldsymbol{k}\cdot\boldsymbol{x} - \frac{1}{2}(\boldsymbol{k}\cdot\boldsymbol{x})^2 + \dots\right)\Psi(\eta,\boldsymbol{k}) \\ &= \Psi^{\ell}_o(\eta) + x^i\big[\partial_i\Psi^{\ell}\big]_o(\eta) + \frac{1}{2}x^ix^j\big[\partial_i\partial_j\Psi^{\ell}\big]_o(\eta) + \dots\,,\end{aligned} \tag{4.23}$$

where we defined several functions

$$\Psi^{\ell}_o(\eta) \equiv \int_0^{k_{\rm IR}}\frac{d^3k}{(2\pi)^3}\Psi(\eta,\boldsymbol{k})\,, \qquad \big[\partial_i\cdots\partial_j\Psi^{\ell}\big]_o(\eta) \equiv \int_0^{k_{\rm IR}}\frac{d^3k}{(2\pi)^3}\,(ik_i)\cdots(ik_j)\Psi(\eta,\boldsymbol{k})\,, \tag{4.24}$$

evaluated spatially at the origin $\boldsymbol{x} = 0$. With these definitions, the first term Ψ^{ℓ}_o represents the contribution of the *uniform gravitational potential* to $\Psi(\eta,\boldsymbol{x})$, while the second term $x^i[\partial_i\Psi^{\ell}]_o$ represents the contribution of the *uniform gravitational force*. According to the equivalence principle, both Ψ^{ℓ}_o and $x^i[\partial_i\Psi^{\ell}]_o$ should have no effect on physical observables, as their contributions are indistinguishable from the free-fall. This concept will be generalized to tensor perturbations.

We are now going to show that our theoretical expressions for the luminosity distance and the galaxy number density do not contain the terms discussed above. Since the full expressions in sec. 4.2.2 are gauge-invariant, we choose the conformal Newtonian gauge for simplicity to demonstrate the compatibility with the equivalence principle. As we assume no anisotropic stress and no vector perturbations in the universe, our metric is given by

$$ds^2 = -a^2(1+2\,\Psi)d\eta^2 + a^2\big[(1-2\,\Psi)\bar{g}_{ij} + 2\,C_{ij}\big]dx^idx^j\,, \qquad \mathcal{G}^i = 0\,, \tag{4.25}$$

where we have denoted the gravitational potential as $\alpha_\chi = -\varphi_\chi \equiv \Psi$. Having removed any gauge ambiguity, we will simply drop the subscript χ in the other variables defined in secs. 4.1 and 4.2.2.

Scalar perturbations

We first consider only the scalar perturbations. In the conformal Newtonian gauge with only scalar perturbations the expressions of the luminosity distance, the volume and the galaxy number density fluctuations are

$$\begin{aligned}&\delta\mathcal{D}_L = \delta z + \frac{\delta r}{\bar r_z} - \mathcal{K} - \Psi\,, \qquad \delta V = 3\,\delta z - 3\,\Psi + 2\,\frac{\delta r}{\bar r_z} - 2\,\mathcal{K} + H_z\frac{\partial}{\partial z}\delta r - \hat n^i v_{,i}\,,\\ &\delta_g = \left(b\,\delta_v - e_z\,\delta z_v\right) + \delta V.\end{aligned} \tag{4.26}$$

The geometric distortions are given in terms of the scalar potentials for gravity Ψ and velocity v by

$$\begin{aligned}\delta z &= \mathcal{H}_o\delta\eta_o - \left[\hat n^i v_{,i} + \Psi\right]_o^z - 2\int_0^{\bar r_z} d\bar r\,\Psi'\,,\\ \delta r &= \hat n_i\,\delta x_o^i + \delta\eta_o - \frac{\delta z}{\mathcal{H}_z} + 2\int_0^{\bar r_z} d\bar r\,\Psi\,,\\ \mathcal{K} &= \frac{\hat n_i\,\delta x_o^i}{\bar r_z} + \left(\hat n^i v_{,i}\right)_o + \int_0^{\bar r_z} d\bar r\left(\frac{\bar r_z - \bar r}{\bar r_z \bar r}\right)\hat\nabla^2\Psi\,,\end{aligned} \tag{4.27}$$

where the coordinate lapses at the observer are related to the velocity potential v as

$$\delta\eta_o = -v_o\,, \qquad \delta x_o^i = -\int_0^{\bar\eta_o} d\bar\eta\, v^{,i}. \tag{4.28}$$

As described in appendix 4.A, at linear order we can separate the gravitational potential $\Psi(\eta,\boldsymbol{x})$ in terms of the growth function $D_\Psi(\eta)$ and the curvature perturbation $\zeta(\boldsymbol{x})$ in the comoving gauge: $\Psi(\eta,\boldsymbol{x}) = D_\Psi(\eta)\zeta(\boldsymbol{x})$. The curvature perturbation $\zeta(\boldsymbol{x})$ is constant in time and related to the growing mode $\delta_+(\boldsymbol{x})$ of the density contrast $\delta(\eta,\boldsymbol{x}) \equiv D(\eta)\delta_+(\boldsymbol{x})$. Accordingly, the gravitational potential growth function $D_\Psi(\eta)$ is related to the matter growth function $D(\eta)$, whose solution is given in eq. (5.4). The long-mode gravitational potential is then proportional to the long-mode curvature perturbation and can be expanded as in eq. (4.23),

$$\Psi^\ell(\eta,\bar r\,\hat{\boldsymbol{n}}) = D_\Psi(\eta)\zeta^\ell(\bar r\,\hat{\boldsymbol{n}}) = D_\Psi(\eta)\big[\zeta_o + \bar r\,\zeta_1(\hat{\boldsymbol{n}}) + \dots\big], \tag{4.29}$$

where we have defined

$$\zeta_o \equiv \zeta^\ell\big|_o = \int_0^{k_{\rm IR}}\frac{d^3k}{(2\pi)^3}\zeta(\boldsymbol{k})\,, \qquad \zeta_1(\hat{\boldsymbol{n}}) \equiv \hat n^i\big[\partial_i\zeta^\ell\big]_o = \hat n^i\int_0^{k_{\rm IR}}\frac{d^3k}{(2\pi)^3}\,ik_i\,\zeta(\boldsymbol{k})\,. \tag{4.30}$$

Analogously, the long-mode velocity potential is given by

$$v^\ell(\eta,\bar r\,\hat{\boldsymbol{n}}) = -D_V(\eta)\zeta^\ell(\bar r\,\hat{\boldsymbol{n}}) = -D_V(\eta)\big[\zeta_o + \bar r\,\zeta_1(\hat{\boldsymbol{n}}) + \dots\big]\,, \tag{4.31}$$

where the dimension of v and D_V is $[v] = [D_V] = L$ and D_V is related to D_Ψ through the Einstein equations, as derived in appendix 4.A. In particular, the following relations are essential for our purpose:

$$D_\Psi = \mathcal{H} D_V - 1 = -\frac{1}{2}(D_V' + 1)\,, \qquad \int_0^{\bar{r}_z} d\bar{r}\, D_\Psi = \frac{1}{2}(D_V - D_{Vo} - \bar{r}_z)\,. \tag{4.32}$$

Now we demonstrate that our theoretical expressions for the luminosity distance, the volume and the galaxy number density fluctuations are independent of the uniform gravitational field generated by ζ_o and the uniform acceleration field generated by ζ_1.

In the long-mode limit, where the wavelength of perturbations is much larger than the distance between the observer and the source ($k_{\rm IR}\bar{r}_z \ll 1$), we take the potentials as $\Psi \equiv \Psi^\ell \equiv D_\Psi(\zeta_o + \bar{r}_z\,\zeta_1)$ and $v \equiv v^\ell \equiv -D_V(\zeta_o + \bar{r}_z\,\zeta_1)$. The geometric distortions in terms of ζ_o and ζ_1 are then

$$\begin{aligned}
\delta z(\zeta_o, \zeta_1) &= [D_\Psi + 1](\zeta_o + \bar{r}_z\,\zeta_1)\,,\\
\delta r(\zeta_o, \zeta_1) &= \hat{n}_i\,\delta x_o^i(\zeta_1) - \bar{r}_z\,\zeta_o - \frac{1}{\mathcal{H}_z}[D_\Psi + 1]\bar{r}_z\,\zeta_1 + 2\,\zeta_1 \int_0^{\bar{r}_z} d\bar{r}\,\bar{r}\,D_\Psi\,,\\
\mathcal{K}(\zeta_o, \zeta_1) &= \frac{\hat{n}_i\,\delta x_o^i(\zeta_1)}{\bar{r}_z} - \frac{1}{\mathcal{H}_z}[D_\Psi + 1]\zeta_1 + \bar{r}_z\,\zeta_1 + 2\,\zeta_1 \int_0^{\bar{r}_z} d\bar{r}\,\frac{\bar{r}}{\bar{r}_z} D_\Psi\,,
\end{aligned} \tag{4.33}$$

where we have used eq. (5.5) to express the time dependence only through D_Ψ (and not D_V). Note that the lensing convergence is only affected by $\zeta_1(\hat{\boldsymbol{n}})$ but not ζ_o, while the redshift and the radial distortions contain both terms. This is explained by the fact that $\mathcal{K}$ describes only transverse effects with respect to the line of sight $\hat{\boldsymbol{n}}$ and a constant scalar like ζ_o has no transverse components. On the other hand, the uniform acceleration associated with $\zeta_1(\hat{\boldsymbol{n}})$ generates a velocity that inevitably affects the convergence $\mathcal{K}$, as the observed solid angle changes. By substituting the above contributions into $\delta\mathcal{D}_L$ and δV as in eq. (4.26) we easily verify that the scalar expression of the luminosity distance and the volume are not affected by the uniform gravity generated by long-mode scalar perturbations,

$$\delta\mathcal{D}_L(\zeta_o, \zeta_1) = 0\,, \qquad \delta V(\zeta_o, \zeta_1) = 0\,, \tag{4.34}$$

in agreement with the equivalence principle.

Now, to show that δ_g is likewise not affected by the uniform gravity we only need to prove that $\delta_v(\zeta_o, \zeta_1) = \delta z_v(\zeta_o, \zeta_1) = 0$, as $b \neq e_z$ in general. First of all, the matter density fluctuation δ_v in the comoving gauge is not affected by uniform gravity because the Einstein equation dictates $\delta_v \propto \Delta\Psi$. To prove that also $\delta z_v(\zeta_o, \zeta_1) = 0$ we first need to transform the redshift distortion from the comoving gauge to the conformal Newtonian gauge. By considering the gauge transformations of β and γ in eq. (4.3) we obtain that the displacement field ξ^μ in eq. (4.2), which generates the transformation from the comoving gauge ($\gamma = v = 0$) to the conformal Newtonian gauge ($\beta = \gamma = 0$),

is given by $T = \beta$ and $L = 0$. Then, from the gauge transformations of v and δz we have that $\beta = -v$ and $\delta z_v = \delta z + \mathcal{H} v$. At this point it is straightforward to verify that $\delta z_v(\zeta_o, \zeta_1) = [D_\Psi + 1 - \mathcal{H} D_V](\zeta_o + \bar{r}_z \zeta_1) = 0$, because from eq. (5.5) we have that $\mathcal{H} D_V = D_\Psi + 1$. The fact that the redshift distortion in the comoving-synchronous gauge is devoid of the long-mode contributions can also be readily understood as follows. The redshift z is a gauge-invariant physical observable but the redshift distortion δz is not, as it compensates the difference between the time of photon emission in a homogeneous universe $\bar{\eta}_z$ and the true coordinate time at the source η_s, which changes from one gauge to another. However, in the comoving-synchronous gauge the degrees of freedom in the perturbations are fixed such that at the observer the physical space-time corresponds to the background, i.e. the lapse functions are vanishing. Consequently, a redshift measurement would provide unambiguous information (independent from the potentials at o) about the emission time of the photons. This time measurement cannot be influenced by uniform gravity. In turn, the redshift distortion in the comoving gauge has to be unaffected by uniform gravity, as there is no mode to be compensated. We conclude that the expression of the galaxy number density fluctuation is free from long-mode contributions

$$\delta_g(\zeta_o, \zeta_1) = 0\,. \tag{4.35}$$

Being independent from the presence of a uniform gravitational field, our expression is compatible with the equivalence principle.

Tensor perturbations

We now demonstrate that the luminosity distance and the galaxy number density are not affected by the uniform gravity generated by long-mode tensor perturbations from inflation. The expressions of these observables when only tensor perturbations are taken into account are

$$\delta\mathcal{D}_L = \delta z + \frac{\delta r}{\bar{r}_z} - \kappa - \frac{1}{2} C_{ij}\hat{n}^i\hat{n}^j\,, \qquad \delta_g = (3 - e_z)\delta z + 2\,\frac{\delta r}{\bar{r}_z} - 2\,\kappa + H\frac{\partial}{\partial z}\delta r\,, \tag{4.36}$$

where the geometric distortions are given in terms of the tensor perturbations C_{ij} by

$$\begin{aligned}
&\delta z = \int_0^{\bar{r}_z} d\bar{r}\, C_{ij}{}'\hat{n}^i\hat{n}^j\,, \qquad \delta r = -\frac{\delta z}{\mathcal{H}_z} - \int_0^{\bar{r}_z} d\bar{r}\, C_{ij}\hat{n}^i\hat{n}^j\,, \qquad \delta\eta_o = \delta x^i_o = 0\,,\\
&\kappa = \frac{3}{2} C_{ij}\hat{n}^i\hat{n}^j|_o - \int_0^{\bar{r}_z} \frac{d\bar{r}}{\bar{r}_z}\left\{2C_{ij}\hat{n}^i\hat{n}^j - \hat{\nabla}_i(C^i_j\hat{n}^j) + \frac{\bar{r}_z - \bar{r}}{2\bar{r}}\left[\hat{n}^i\hat{n}^j\hat{\nabla}^2 C_{ij} + 2\hat{n}^i\hat{\nabla}_j C^j_i\right]\right\}.
\end{aligned} \tag{4.37}$$

Tensor perturbations can be decomposed into Fourier modes of two independent polarization states labeled as $s = +, \times$,

$$C_{ij}(\eta, \boldsymbol{k}) = e^+_{ij}(\hat{\boldsymbol{k}})\, C_+(\eta, \boldsymbol{k}) + e^\times_{ij}(\hat{\boldsymbol{k}})\, C_\times(\eta, \boldsymbol{k})\,, \tag{4.38}$$

where the basis tensors $e^s_{ij}(\hat{\boldsymbol{k}})$ are transverse, traceless and normalized through $e^s_{ij}e^{s'ij} \equiv 2\,\delta^{ss'}$. Using the Einstein equation in Fourier space in the absence of anisotropic pressure,

$$C_s''(\eta,\boldsymbol{k}) + 2\,\mathcal{H}\,C_s'(\eta,\boldsymbol{k}) + k^2 C_s(\eta,\boldsymbol{k}) = 0\,, \tag{4.39}$$

we find that, considering long-mode perturbations ($k^2 \approx 0$) and neglecting decaying modes in the solution, each polarization C_s of the tensor perturbations is constant in time, i.e. $C_s^{\ell\prime} = 0$. In real space the long-mode primordial gravitational waves can then be written as

$$\begin{aligned} C^\ell_{ij}(\bar{r}\,\hat{\boldsymbol{n}}) &= \int_0^{k_{\rm IR}} \frac{d^3k}{(2\pi)^3} e^{i\bar{r}\,\hat{\boldsymbol{n}}\cdot\boldsymbol{k}}\, e^s_{ij}(\hat{\boldsymbol{k}})\, C_s(\boldsymbol{k}) \\ &= \int_0^{k_{\rm IR}} \frac{d^3k}{(2\pi)^3} \big[1 + i\bar{r}\,\hat{\boldsymbol{n}}\cdot\boldsymbol{k} + \dots\big]\, e^s_{ij}(\hat{\boldsymbol{k}})\, C_s(\boldsymbol{k}) \\ &= C_{ijo} + \bar{r}\,C_{ij1}(\hat{\boldsymbol{n}}) + \dots\,, \end{aligned} \tag{4.40}$$

where we have defined

$$\begin{aligned} C_{ijo} &\equiv C^\ell_{ij}\big|_o = \int_0^{k_{\rm IR}} \frac{d^3k}{(2\pi)^3} e^s_{ij}(\hat{\boldsymbol{k}}) C_s(\boldsymbol{k})\,, \\ C_{ij1}(\hat{\boldsymbol{n}}) &\equiv \hat{n}^k \big[\partial_k C^\ell_{ij}\big]_o = \hat{n}^k \int_0^{k_{\rm IR}} \frac{d^3k}{(2\pi)^3} i k_k\, e^s_{ij}(\hat{\boldsymbol{k}}) C_s(\boldsymbol{k}). \end{aligned} \tag{4.41}$$

We start again by studying the contributions of the long-modes C_{ijo} and C_{ij1} to the individual components in the luminosity distance and the galaxy number density. In the long-mode limit, where the perturbations wavelength is much larger than the scale of our system ($k_{\rm IR}\bar{r}_z \ll 1$), we take the gravitational waves as $C_{ij} \equiv C^\ell_{ij} \equiv C_{ijo} + \bar{r}_z\,C_{ij1}$. The geometric distortions in terms of C_{ijo} and C_{ij1} are then

$$\begin{aligned} &\delta z(C_{ijo}, C_{ij1}) = 0\,, \qquad\qquad \delta r(C_{ijo}, C_{ij1}) = -\bar{r}_z\,C_{ijo}\hat{n}^i\hat{n}^j - \frac{1}{2}\bar{r}_z^2\,C_{ij1}\hat{n}^i\hat{n}^j\,, \\ &\kappa(C_{ijo}, C_{ij1}) = -\frac{3}{2}C_{ijo}\hat{n}^i\hat{n}^j - \bar{r}_z\,C_{ij1}\hat{n}^i\hat{n}^j\,. \end{aligned} \tag{4.42}$$

By substituting these expressions into eq. (4.36) we verify straightforwardly that the luminosity distance, the volume distortion, and the galaxy number density are not affected by the long-mode primordial gravitational waves,

$$\delta\mathcal{D}_L(C_{ijo}, C_{ij1}) = \delta V(C_{ijo}, C_{ij1}) = \delta_g(C_{ijo}, C_{ij1}) = 0\,. \tag{4.43}$$

As a conclusion, our theoretical expressions for the luminosity distance and the galaxy number density are independent from the presence of a uniform gravitational field and, therefore, consistent with the equivalence principle.

4.3 Numerical Investigation of the Galaxy Two-Point Function

Galaxy clustering is a key observable in cosmology and constitutes the main subject of our study. In particular, the two-point correlation function $\langle n_g(\boldsymbol{x}) n_g(\boldsymbol{x}+\boldsymbol{r})\rangle$ measures the excess of probability of finding a pair of galaxies separated by a vector $\boldsymbol{r}$ relative to the uniform distribution. Of course, the two-point statistics is affected by the same relativistic effects altering the observed galaxy number density. In this section, we compute numerically the two-point correlation functions of the various contributions to the linear-order fluctuation δ_g. These contributions are the matter density contrast δ_v, the redshift and radial distortions δz and δr, the gravitational lensing convergence $\mathcal{K}$ and the term $H_z \frac{\partial}{\partial z}\delta r$, which includes the so-called Kaiser effect (or redshift space distortion), as we shall see.

As in the previous sections, we neglect the vector perturbations and we consider scalar and tensor perturbations separately. Again, we consider the conformal Newtonian gauge with metric given in eq. (4.25). To facilitate the computation of the two-point correlation functions we only consider two specific configurations of two galaxies in our numerical investigations. In one configuration the two galaxies are at the same redshift, i.e. $z_1 \equiv z_2$, and we study how the correlation functions change with the angular separation θ, which is related to the comoving distance r between the galaxies by the simple trigonometric relation $r \equiv \bar{r}_z\sqrt{2(1-\cos\theta)}$, where $\bar{r}_z \equiv \bar{r}_{z_1} \equiv \bar{r}_{z_2}$. In the other configuration the two galaxies lie on the same line of sight, i.e. $\hat{\boldsymbol{n}}_1 \equiv \hat{\boldsymbol{n}}_2$ $(\theta = 0)$, but at different redshifts and we study how the correlation changes with the comoving separation $r = \bar{r}_{z_1} - \bar{r}_{z_2}$. These two configurations represent the two limiting cases of the general configurations of the two-point correlation function.

For numerical calculations we assume a flat ΛCDM universe with matter density $\Omega_m = 0.3038$, baryon density $\Omega_b = 0.0462$, dark energy density $\Omega_\Lambda = 0.65$, scalar amplitude $A_s = 2.1 \times 10^{-9}$ at the pivot scale $k_0 = 0.05\,\mathrm{Mpc}^{-1}$, spectral index $n_s = 0.96$, Hubble parameter $h = 0.70$ and bias factor $b = 2$ unless otherwise stated. Furthermore, we assume no magnification bias and the evolution bias $e_z = 1.5$ at $z = 1$, consistent with dark matter halos of bias $b = 2$ in the Press-Schechter model [45].

4.3.1 Contributions of the scalar perturbations

In this subsection we compute the scalar contributions to the two-point correlation function of the galaxy number density fluctuation $\langle \delta_g(z_1, \hat{\boldsymbol{n}}_1)\delta_g(z_2, \hat{\boldsymbol{n}}_2)\rangle$. In the conformal Newtonian gauge and with only scalar perturbations, the expression of the galaxy number density fluctuation is derived in sec. 4.2.2. We have

$$\delta_g = (b\,\delta_m - e_z\,\delta z_v) + \delta V\,, \tag{4.44}$$

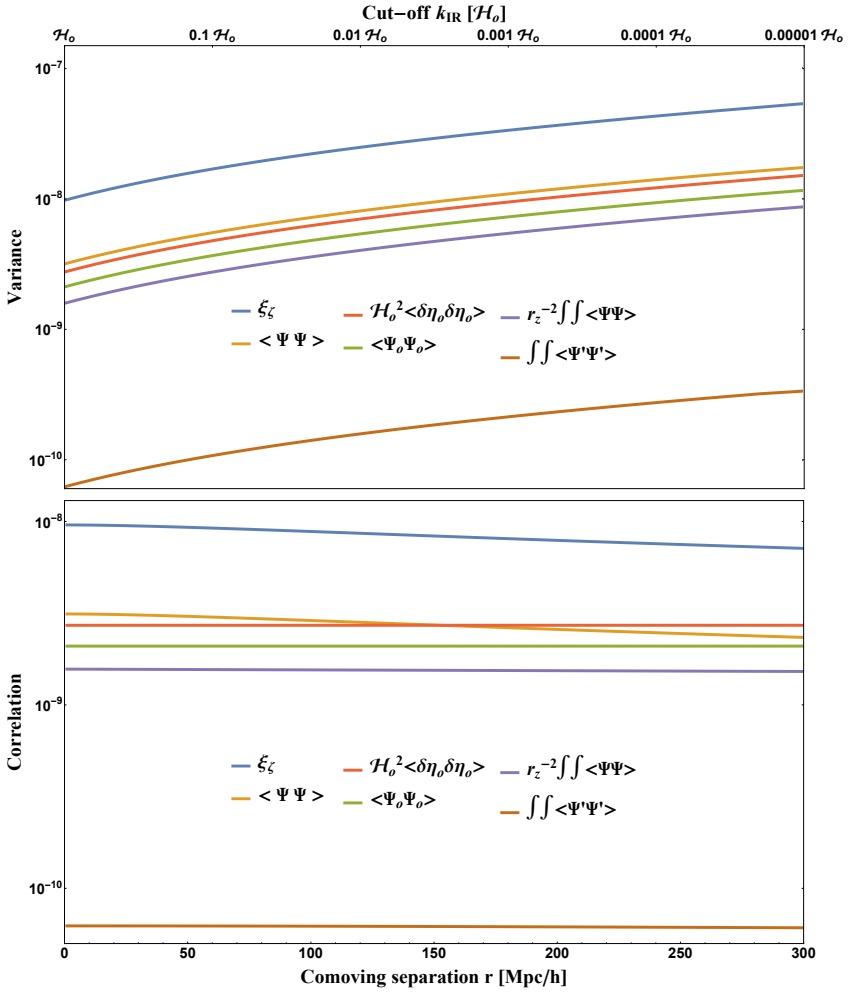

Figure 4.1: *Top panel:* Dependence of the variance on the infrared cut-off for the curvature perturbation (blue), the potential at the source (orange), the time-lapse at the observer (red), the potential at the observer (green), the Shapiro time delay (purple) and the integrated Sachs-Wolf effect (brown). *Bottom panel:* Auto-correlations of the same quantities as a function of the separation, when $k_{\rm IR} = \mathcal{H}_o$. We consider two galaxies at the same redshift $z = 1$, so that the correlations are only functions of the comoving separation.

where $\delta_m \equiv \delta_v$ and $\delta z_v = \delta z + \mathcal{H}\, v$, as explained in the last paragraph of sec. 4.2.3. The scalar contribution to the volume distortion is in turn given by

$$\delta V = 3\,\delta z + 2\,\frac{\delta r}{\bar{r}_z} - 2\,\mathcal{K} + H_z \frac{\partial}{\partial z}\delta r + V_{\parallel} - 3\,\Psi\,, \tag{4.45}$$

where the geometric distortions are expressed in terms of the gravitational potentials Ψ, the line-of-sight component of the peculiar velocities $V_{\parallel} \equiv \hat{n}^i V_i$ and the coordinates

lapses at the observer $\delta\eta_o$ and $\delta r_o \equiv \delta x_{\parallel o} \equiv \hat{n}_i \delta x^i_o$ as

$$\delta z = \mathcal{H}_o \delta\eta_o + \left[V_\parallel - \Psi\right]^z_o - 2\int_0^{\bar{r}_z} d\bar{r}\,\Psi' \,, \tag{4.46}$$

$$\delta r = \delta r_o + \delta\eta_o - \frac{\delta z}{\mathcal{H}_z} + 2\int_0^{\bar{r}_z} d\bar{r}\,\Psi \,, \tag{4.47}$$

$$\mathcal{K} = \frac{\delta r_o}{\bar{r}_z} - V_{\parallel o} + \int_0^{\bar{r}_z} d\bar{r}\left(\frac{\bar{r}_z - \bar{r}}{\bar{r}_z \bar{r}}\right)\hat{\nabla}^2\Psi \,. \tag{4.48}$$

As derived in appendix 4.A, all the variables appearing in the above expressions can be expressed in terms of the (time-independent) curvature perturbation in the comoving gauge $\zeta(\boldsymbol{x})$, which is in turn related to the matter density contrast $\delta_+(\boldsymbol{x})$ at initial epoch. In Fourier space the latter is used to define the matter power spectrum $P_m(k)$ through $\langle\delta_+(\boldsymbol{k}_1)\delta_+(\boldsymbol{k}_2)\rangle \equiv (2\pi)^3\delta_D(\boldsymbol{k}_1 + \boldsymbol{k}_2)P_m(k_1)$, which allows to compute the two-point statistics by taking expectation values of the perturbations in conjunction with the corresponding growth factors.

As we showed in sec. 4.2.3, the monopole and dipole of long-mode perturbations do not affect the galaxy number density fluctuation, in agreement with the equivalence principle. Consequently, the total correlation function (including auto- and cross-correlations of all contributions) does not go to infinity when integrated over all k, because the divergences coming from the monopoles of different contributions cancel each other. Indeed, the correlations of quantities involving the potential Ψ at the source, at the observer or integrated along the line of sight, as well as those involving the time lapse at the observer $\delta\eta_o$, diverge in the infrared, when k is smaller than some value $k_{\rm IR}$ close to zero. Only when these contributions are summed together the correlation function converges, because the effect of long-mode perturbations disappears, as also described in [101]. The divergent behavior of the correlation function in the infrared, claimed in [93], is due to the fact that terms evaluated at the observer position, such as Ψ_o and $\delta\eta_o$, are usually neglected. The top panel of fig. 4.1 shows the dependence on the infrared cut-off for the variances of the terms discussed above, which blow up when $k_{\rm IR}$ approaches zero. The sum of all individually divergent contributions in the correlation is instead finite. As we show, these contributions turn out to be small compared to the density contribution, such that we set a sufficiently large yet arbitrary cut-off $k_{\rm IR} \equiv \mathcal{H}_o$. Indeed, as shown in fig. 4.2, the variance of the sum of the divergent contributions converges for $k_{\rm IR} < \mathcal{H}_o$. In this plot the galaxy number density fluctuation is split as $\delta_g \equiv \delta_{\rm std} + \delta_{\rm vel} + \delta_{\rm len} + \delta_{\rm pot}$, where

$$\delta_{\rm std} = b\,\delta_m - \frac{1}{\mathcal{H}_z}\partial_\parallel V_\parallel \,, \qquad \delta_{\rm vel} = h(z)\left[V_\parallel\right]^z_o + 2V_{\parallel o} \,, \qquad \delta_{\rm len} = -2\int_0^{\bar{r}_z} d\bar{r}\left(\frac{\bar{r}_z - \bar{r}}{\bar{r}_z\bar{r}}\right)\hat{\nabla}^2\Psi \,,$$

$$\delta_{\rm pot} = \left[h(z) - \frac{2}{\mathcal{H}_o\bar{r}_z}\right]\mathcal{H}_o\delta\eta_o + e_z\mathcal{H}_z v - h(z)\left[\Psi\right]^z_o - \Psi + \frac{1}{\mathcal{H}_z}\Psi' + \int_0^{\bar{r}_z} d\bar{r}\left[\frac{4}{\bar{r}_z}\Psi - 2\,h(z)\,\Psi'\right], \tag{4.49}$$

and we have defined the function of redshift $h(z) \equiv 3 - e_z - \mathcal{H}'_z/\mathcal{H}_z^2 - 2/(\bar{r}_z \mathcal{H}_z)$. All the perturbations with divergent individual correlation, or variance (see top panel of fig. 4.1), are contained in $\delta_{\rm pot}$. When we compute the corresponding variance $\sigma^2_{\rm pot} = \langle \delta^2_{\rm pot} \rangle$ these contributions are summed together before taking the ensemble average, leading to a convergent result. This might not be perfectly represented in fig. 4.2, due to numerical residuals in the evaluation of the integrands in the variance expression. Indeed, to compute the variance we split the time and space dependence in the perturbations, using the growth functions defined in appendix 4.A. Therefore, the variance is given by time-dependent factors multiplied by integrals over Fourier modes of the time-independent part of the perturbations. However, as shown in sec. 4.2.3, the time-dependent factor that multiplies the divergent integrations is exactly zero. As a conclusion, the theoretical prediction for the correlation function of the galaxy number density is gauge-invariant and finite, provided that we take into account all terms in the relativistic derivation. In practice, the standard way of computing the variance by using $\delta_{\rm std}$ alone is accurate at the 1% level, and the dominant correction originates from the lensing convergence $\delta_{\rm len}$. For the computation of the gravitational potential contribution $\delta_{\rm pot}$ our numerical calculations demonstrate that one can safely impose an IR cut-off scale, as long as $k_{\rm IR} \lesssim \mathcal{H}_o$.

Matter density fluctuation

We now want to study the two-point correlation functions of the various quantities in eqs. (4.44) and (4.45). Before proceeding it is convenient to split the time and space dependences in the perturbations as in sec. 4.2.3 and appendix 4.A. In this way, the dependence on the redshifts z_1, z_2 in the correlation functions can be factorized through the growth functions D, D_Ψ, D_V of the matter density contrast, the gravitational potential and the peculiar velocity, respectively. The auto-correlation function of the matter density contrast is then given by

$$\langle \delta_m(z_1, \hat{\boldsymbol{n}}_1) \delta_m(z_2, \hat{\boldsymbol{n}}_2) \rangle = D(z_1) D(z_2) \int_{k_{\rm IR}}^{k_{\rm UV}} \frac{dk}{2\pi^2} k^2 P_m(k) j_0(kr) = D(z_1) D(z_2)\, \xi_m(r)\,, \tag{4.50}$$

where r is the length of the spatial separation $\boldsymbol{r} = \bar{r}_{z_1} \hat{\boldsymbol{n}}_1 - \bar{r}_{z_2} \hat{\boldsymbol{n}}_2$ between the two galaxies, $P_m(k)$ is the matter power spectrum computed using `CAMB`, $j_0(x)$ is the spherical Bessel function and in the last equality we have introduced the matter correlation function $\xi_m(r) = \langle \delta_+(\boldsymbol{x}) \delta_+(\boldsymbol{x} + \boldsymbol{r}) \rangle$ at initial epoch. In the numerical evaluation we always set the lower and upper cut-offs in the integration as $k_{\rm IR} \equiv \mathcal{H}_o = 100/c$ km/s h/Mpc $= 3.3 \times 10^{-4}\, h$/Mpc and $k_{\rm UV} \equiv 10\, h$/Mpc, where c is the speed of light and h is the reduced Hubble constant.[2]

[2]The convergence of the correlations in the ultraviolet regime occurs at around $k \approx 1\, h$/Mpc, but choosing a bigger value results in a more accurate numerical evaluation of the integrals.

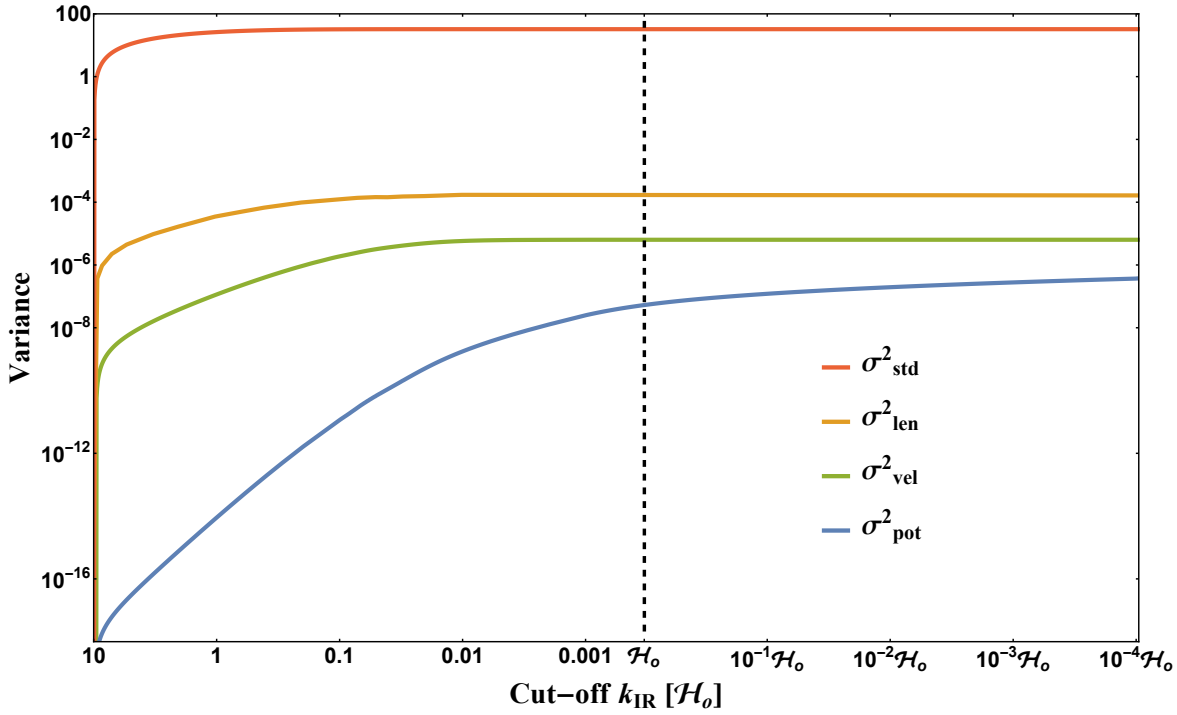

Figure 4.2: Individual contributions to the variance $\sigma^2 = \langle\delta_g^2\rangle$. The galaxy number density fluctuation is split as $\delta_g \equiv \delta_{\rm std} + \delta_{\rm vel} + \delta_{\rm len} + \delta_{\rm pot}$, where the expression of each contribution is given in eq. (4.49). The figure shows the variances $\sigma_i^2 = \langle\delta_i^2\rangle$ of each contribution δ_i as functions of the cut-off $k_{\rm IR}$ for galaxies at redshift $z = 1$. The vertical dashed line marks the horizon scale $k_{\rm IR} = \mathcal{H}_o$. The UV cut-off is $k_{\rm UV} \equiv 10\,h/{\rm Mpc}$, so that the variances are vanishing when $k_{\rm IR} = 10\,h/{\rm Mpc}$.

The behavior of the density auto-correlation given in eq. (4.50) is shown by the blue curve in fig. 4.3 as a function of the comoving separation r between two galaxies at the same redshift $z_1 = z_2 = 1$. The local maximum at around 110 Mpc$/h$ is there a well-known feature of the matter correlation function due to baryon acoustic oscillations (BAO). At around $r = 130$ Mpc$/h$ the correlation is zero, because at this scale there is no deviation from a uniform distribution of galaxies (galaxies do not cluster). At larger scales, the correlation becomes negative, as galaxies tend to avoid each other. Obviously, as the separation increases further the anti-correlation between the density fields at the two end points decreases and reaches zero asymptotically. The other functions in the plot (red and green curves) are the two-point correlations of redshift-space distortions (for two different configurations) and we will discuss them in sec. 4.3.1. The density contrast and the redshift-space distortion are the dominant contributions to the two-point correlation function of the galaxy number density and are devoid of any divergence both at IR and UV scales.

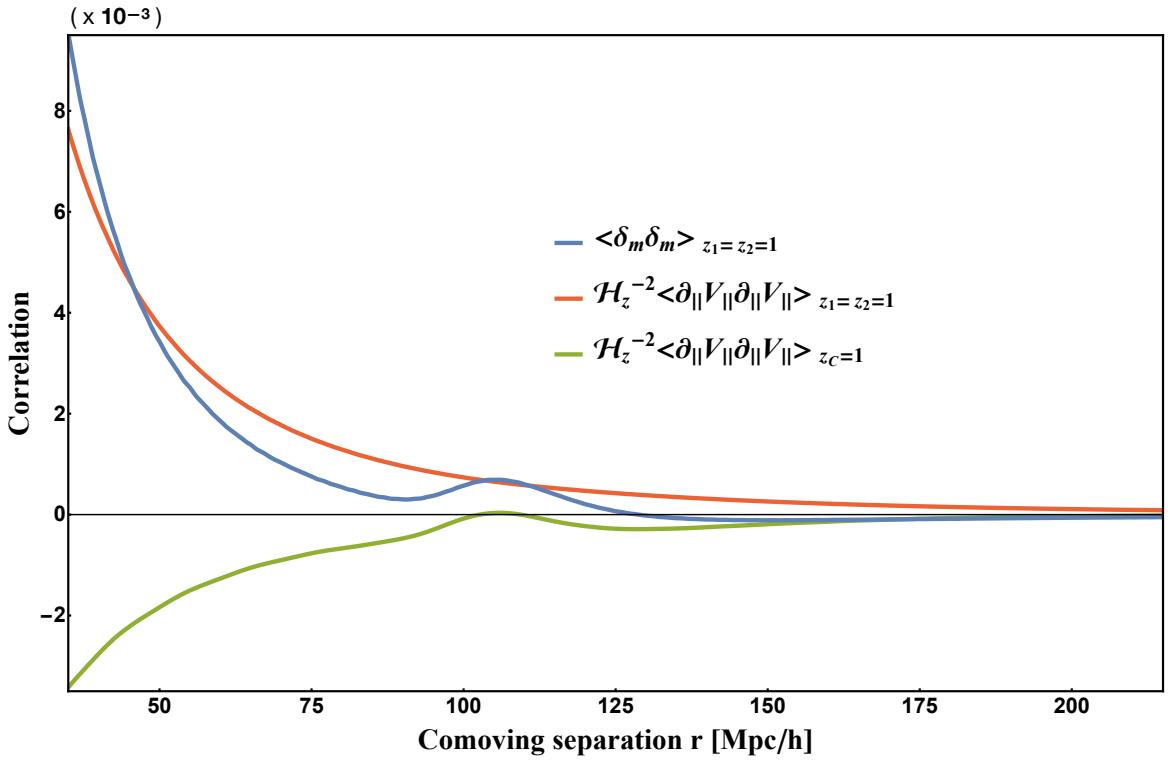

Figure 4.3: The correlation function of the density fluctuations for two galaxies at the same redshift $z_1 = z_2 = 1$ is shown in blue. The correlation function of the Kaiser effects for two galaxies at the same redshift $z_1 = z_2 = 1$ is shown in red, while that of two galaxies lying on the same line-of-sight with middle point at redshift $z_C = 1$ is shown in green.

Redshift and radial distortions

We now want to study the correlation functions of the redshift distortion δz and the radial distortion δr. The analytic expressions are given by the sum of the auto- and cross-correlations of different quantities:

$$\begin{aligned}\langle \delta z(z_1,\hat{\boldsymbol{n}}_1)\delta z(z_2,\hat{\boldsymbol{n}}_2)\rangle &= \mathcal{H}_o^2\langle \delta\eta_o\delta\eta_o\rangle + \langle V_{\parallel 1}V_{\parallel 2}\rangle + \langle V_{\parallel o}(\hat{\boldsymbol{n}}_1)V_{\parallel o}(\hat{\boldsymbol{n}}_2)\rangle + \langle \Psi_1\Psi_2\rangle \\ &+ \langle \Psi_o\Psi_o\rangle + 4\int_0^{\bar{r}_{z_1}} d\bar{r}_1 \int_0^{\bar{r}_{z_2}} d\bar{r}_2 \,\langle \Psi'(\bar{\eta}_o-\bar{r}_1,\bar{r}_1\,\hat{\boldsymbol{n}}_1)\Psi'(\bar{\eta}_o-\bar{r}_2,\bar{r}_2\,\hat{\boldsymbol{n}}_2)\rangle + \text{c-c}\,,\end{aligned} \tag{4.51}$$

where c-c stands for cross correlations and we have introduced the notation $X_1 \equiv X(z_1,\hat{\boldsymbol{n}}_1)$ for any perturbation X,

$$\begin{aligned}\frac{\langle \delta r(z_1,\hat{\boldsymbol{n}}_1)\delta r(z_2,\hat{\boldsymbol{n}}_2)\rangle}{\bar{r}_{z_1}\bar{r}_{z_2}} &= \frac{\langle \delta r_o(\hat{\boldsymbol{n}}_1)\delta r_o(\hat{\boldsymbol{n}}_2)\rangle}{\bar{r}_{z_1}\bar{r}_{z_2}} + \frac{\langle \delta\eta_o\delta\eta_o\rangle}{\bar{r}_{z_1}\bar{r}_{z_2}} + \frac{\langle \delta z_1\delta z_2\rangle}{\bar{r}_{z_1}\mathcal{H}_{z_1}\bar{r}_{z_2}\mathcal{H}_{z_2}} \\ &+ \frac{4}{\bar{r}_{z_1}\bar{r}_{z_2}}\int_0^{\bar{r}_{z_1}} d\bar{r}_1 \int_0^{\bar{r}_{z_2}} d\bar{r}_2\,\langle \Psi_1\Psi_2\rangle + \text{c-c}\,.\end{aligned} \tag{4.52}$$

Therefore, in order to understand which are the leading contributions to the correlations of δz and δr, we have to compute the auto-correlation functions of the time-lapse at the observer $\delta\eta_o$, the peculiar velocities $V_\parallel$, $V_{\parallel o}$, the local potentials Ψ, Ψ_o, the integrated Sachs-Wolfe (ISW) effect $\int d\bar{r}\,\Psi'$, the spatial shift at the observer δr_o and the Shapiro time-delay effect $\int d\bar{r}/\bar{r}_z\,\Psi$.

First of all, the auto-correlations of the potential and the time-lapse at the observer are given by

$$\langle \Psi_o \Psi_o \rangle = C^2 D_{\Psi_o}^2 \int_{k_{\rm IR}}^{k_{\rm UV}} \frac{dk}{2\,\pi^2} \frac{1}{k^2} P_m(k)\,, \tag{4.53}$$

$$\mathcal{H}_o^2 \langle \delta\eta_o \delta\eta_o \rangle = \mathcal{H}_o^2\, C^2 D_{Vo}^2 \int_{k_{\rm IR}}^{k_{\rm UV}} \frac{dk}{2\pi^2} \frac{1}{k^2} P_m(k)\,, \tag{4.54}$$

where $C \equiv -\mathcal{H}^2 D f \Sigma$ is a constant and it becomes $-\frac{5}{2}\mathcal{H}_o^2\Omega_m$ in the matter-dominated universe (see appendix 4.A). Note that, while the growth function D_Ψ is dimensionless, D_V has the same dimension as $\mathcal{H}_o^{-1}$. These correlations are then dimensionless and both independent of separation, adding up to a constant contribution when the IR cut-off is imposed, but they are divergent when the integration is performed from $k = 0$, as shown in fig. 4.1. As explained above, the divergence due to these quantities at the observer cancel the divergence due to the potential at the source and integrated along the line of sight. It is therefore important to consider Ψ_o and $\delta\eta_o$ in the expression of the galaxy number density, also from the numerical point view.

Let us now consider the correlations of the gravitational potential at the source (local) and integrated along the line of sight (non-local). The auto-correlation of the gravitational potential at the source is given by

$$\begin{aligned} \langle \Psi(z_1, \hat{\boldsymbol{n}}_1) \Psi(z_2, \hat{\boldsymbol{n}}_2) \rangle &= C^2 D_\Psi(z_1) D_\Psi(z_2) \int_{k_{\rm IR}}^{k_{\rm UV}} \frac{dk}{2\,\pi^2} \frac{1}{k^2} P_m(k) j_0(kr) \\ &= D_\Psi(z_1) D_\Psi(z_2)\, \xi_\zeta(r)\,, \end{aligned} \tag{4.55}$$

where $\xi_\zeta(r) = \langle \zeta(\boldsymbol{x}) \zeta(\boldsymbol{x}+\boldsymbol{r}) \rangle$ is the correlation function of the curvature perturbation. The non-local terms are the ISW and the Shapiro time-delay. Their auto-correlations are respectively given by

$$\begin{aligned} &\int_0^{\bar{r}_{z_1}} d\bar{r}_1 \int_0^{\bar{r}_{z_2}} d\bar{r}_2\, \langle \Psi'(\bar{\eta}_1, \bar{r}_1\,\hat{\boldsymbol{n}}_1) \Psi'(\bar{\eta}_2, \bar{r}_2\,\hat{\boldsymbol{n}}_2) \rangle \\ &= \int_0^{\bar{r}_{z_1}} d\bar{r}_1 \int_0^{\bar{r}_{z_2}} d\bar{r}_2\, D'_\Psi(\bar{\eta}_o - \bar{r}_1) D'_\Psi(\bar{\eta}_o - \bar{r}_2) \int_{k_{\rm IR}}^{k_{\rm UV}} \frac{dk}{2\pi^2} \frac{P_m(k)}{k^2} j_0(k|\bar{r}_1 \hat{\boldsymbol{n}}_{\boldsymbol{1}} - \bar{r}_2 \hat{\boldsymbol{n}}_{\boldsymbol{2}}|)\,, \end{aligned} \tag{4.56}$$

$$\begin{aligned} &\int_0^{\bar{r}_{z_1}} \frac{d\bar{r}_1}{\bar{r}_{z_1}} \int_0^{\bar{r}_{z_2}} \frac{d\bar{r}_2}{\bar{r}_{z_2}}\, \langle \Psi(\bar{\eta}_1, \bar{r}_1\,\hat{\boldsymbol{n}}_1) \Psi(\bar{\eta}_2, \bar{r}_2\,\hat{\boldsymbol{n}}_2) \rangle \\ &= \int_0^{\bar{r}_{z_1}} \frac{d\bar{r}_1}{\bar{r}_{z_1}} \int_0^{\bar{r}_{z_2}} \frac{d\bar{r}_2}{\bar{r}_{z_2}}\, D_\Psi(\bar{\eta}_o - \bar{r}_1) D_\Psi(\bar{\eta}_o - \bar{r}_2) \xi_\zeta(|\bar{r}_1 \hat{\boldsymbol{n}}_{\boldsymbol{1}} - \bar{r}_2 \hat{\boldsymbol{n}}_{\boldsymbol{2}}|)\,. \end{aligned} \tag{4.57}$$

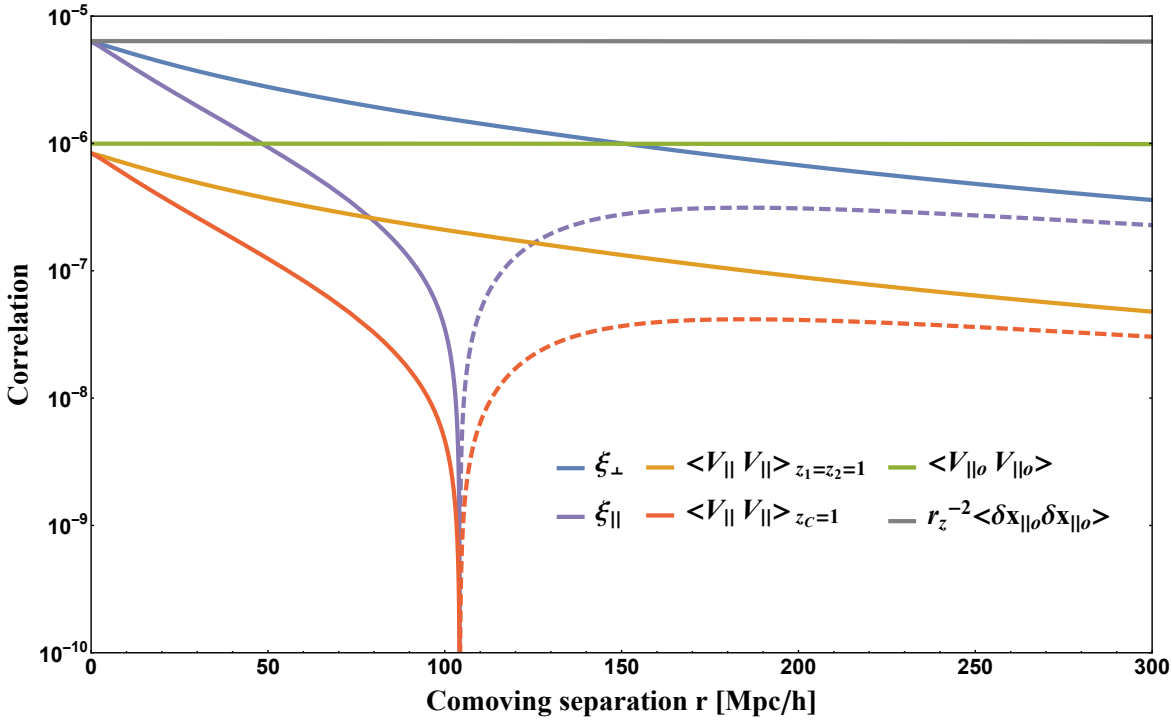

Figure 4.4: The velocity correlation function is decomposed into $\xi_{||}$ and $\xi_\perp$, respectively parallel and perpendicular to the separation between the two points under consideration. The correlation function of the velocities of two galaxies at the same redshift $z_1 = z_2 = 1$ is shown in orange, while that of two galaxies lying on the same line-of-sight with middle point at redshift $z_C = 1$ is shown in red. Dashed lines represent negative values. The correlation functions of the velocities and the spatial shifts at the observer point are shown in green and gray respectively. These are only functions of the angle between the two lines of sight and the relation of this variable with the separation r depends on the redshift considered. Hence they vary as a function of r, but very little over the range in this plot. The value of $\bar{r}_z$ in $\bar{r}_z^2\langle\delta r_o \delta r_o\rangle$ is that at redshift $z = 1$, for consistency with the other functions in the plot. Note that at $r = 0$ the amplitude of $\bar{r}_z^2\langle\delta r_o \delta r_o\rangle$ is not the same as $\xi_{||}$ and $\xi_\perp$, as might appear from the plot. The cut-off choices are $k_{\rm IR} = \mathcal{H}_o$ and $k_{\rm UV} = 10\ h/{\rm Mpc}$.

Fig. 4.1 shows the variances ($r \to 0$) of these contributions as a function of the IR cut-off (top panel) as well as the correlations as functions of r, when $k_{\rm IR} \equiv \mathcal{H}_o$, for two galaxies at the same redshift $z_1 = z_2 = 1$ (bottom panel). One should notice that, while the correlations of the potentials and the time-lapses at the observer are exactly constant, the correlations of ISW and Shapiro time-delay effects vary as a function of scale, though the change is too small to be visible in the range of separations considered, except the correlation of the potential at the sources. Nevertheless, all these correlations are from five to seven orders of magnitude smaller the matter density correlation (compare with fig. 4.3).

The remaining contributions to compute are those of the velocities and the spatial shifts at the observer, which are finite even when the integration is performed from

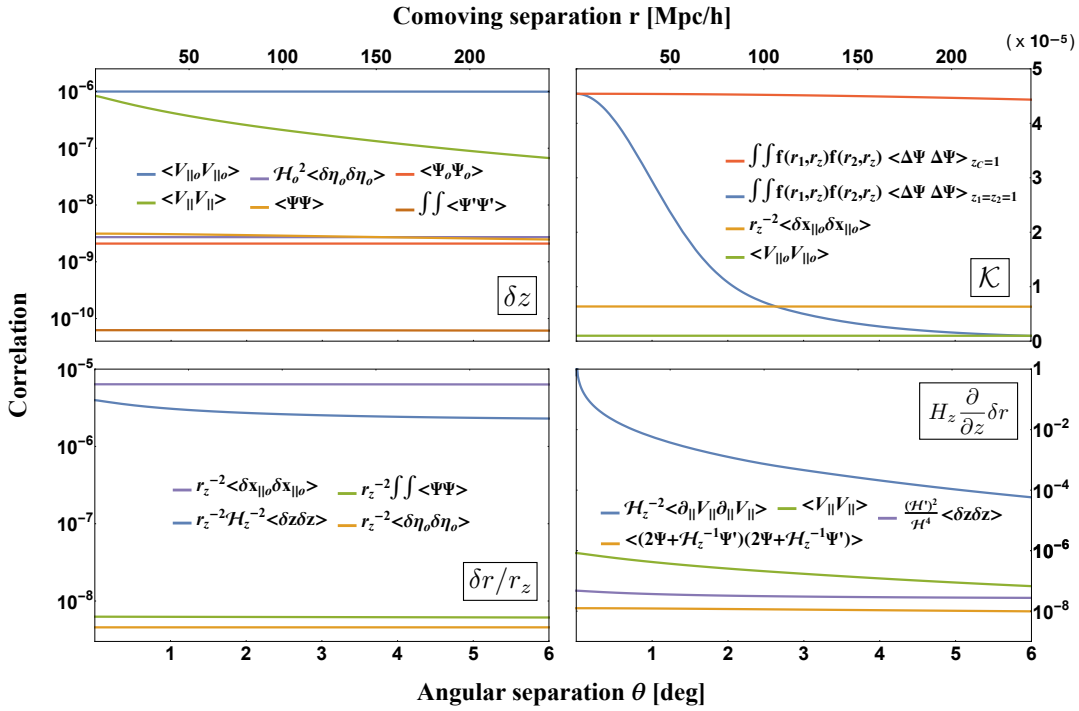

Figure 4.5: Top left panel: auto-correlations of various contributions to $\langle \delta z \delta z \rangle$ as functions of the separation between two galaxies at the same redshift $z_1 = z_2 = 1$. Bottom left panel: auto-correlations of various contributions to $\langle \delta r \delta r \rangle / \bar{r}_z^2$ as functions of the separation between two galaxies at the same redshift $z_1 = z_2 = 1$. Top right panel: The correlation function of the lensing contribution $\int_0^{\bar{r}_z} d\bar{r}\, f(\bar{r}, \bar{r}_z) \Delta\Psi$, where $f(\bar{r}, \bar{r}_z) = (\bar{r}_z - \bar{r}) \frac{\bar{r}}{\bar{r}_z}$, for two galaxies at the same redshift $z_1 = z_2 = 1$ is shown in blue, while that of two galaxies lying on the same line-of-sight with middle point at redshift $z_C = 1$ is shown in red (note that the latter is only a function of the separation r, as in this configuration $\theta = 0$). Auto-correlations of other contributions to the gravitational lensing convergence $\mathcal{K}$ are shown in orange and green. Bottom right panel: auto-correlations of various contributions to $H_z^2 \langle \partial_z \delta r\, \partial_z \delta r \rangle$ as functions of the separation between two galaxies at the same redshift $z_1 = z_2 = 1$. The dominant contribution is given by the Kaiser effect.

$k_{\rm IR} = 0$. By applying the velocity solution $V_\parallel(\eta, \boldsymbol{x}) = D_V(\eta)\, \partial_\parallel \zeta(\boldsymbol{x})$ (see appendix 4.A), the correlation function of the two line-of-sight velocities can be written as

$$\langle V_\parallel(z_1, \hat{n}_1) V_\parallel(z_2, \hat{n}_2) \rangle = \left(\frac{C}{\mathcal{H}_o} \right)^2 D_V(z_1) D_V(z_2) \left\{ \hat{\mathcal{P}}_\parallel \xi_\parallel(r) + \hat{\mathcal{P}}_\perp \xi_\perp(r) \right\}. \tag{4.58}$$

Note that our expression is derived without assuming the distant-observer approximation and it is valid for any two lines of sight. By defining $\hat{\mathcal{P}}_\parallel \equiv \hat{n}_1^i \hat{n}_2^j \hat{r}_i \hat{r}_j$ and $\hat{\mathcal{P}}_\perp \equiv \hat{n}_1^i \hat{n}_2^j (\delta_{ij} - \hat{r}_i \hat{r}_j)$ as in [102], we decomposed the velocity correlation function into

the parallel and perpendicular components with respect to the separation $\boldsymbol{r}$:

$$\xi_{\parallel}(r) \equiv -\mathcal{H}_o^2 \int_{k_{\rm IR}}^{k_{\rm UV}} \frac{dk}{2\pi^2} P_m(k) \frac{j_0'(kr)}{kr}\,, \qquad \xi_{\perp}(r) \equiv -\mathcal{H}_o^2 \int_{k_{\rm IR}}^{k_{\rm UV}} \frac{dk}{2\pi^2} P_m(k) j_0''(kr)\,, \tag{4.59}$$

where $j_0'(x) = \partial_x j_0(x)$ and $j_0''(x) = \partial_x^2 j_0(x)$. Fig. 4.4 shows the behavior of $\xi_{\parallel}$ and $\xi_{\perp}$ with respect to r, as well as the correlations of velocities at the sources (for the two configurations $z_1 = z_2 = 1$ and $z_C = 1$) and at the observer. The latter is only a function of the angle $\theta = \cos^{-1}(\hat{\boldsymbol{n}}_{\boldsymbol{1}} \cdot \hat{\boldsymbol{n}}_{\boldsymbol{2}})$ between the two lines of sight,

$$\langle V_{\parallel o}(\hat{\boldsymbol{n}}_1) V_{\parallel o}(\hat{\boldsymbol{n}}_2)\rangle = \hat{\boldsymbol{n}}_{\boldsymbol{1}} \cdot \hat{\boldsymbol{n}}_{\boldsymbol{2}}\, C^2 D_{Vo}^2 \int_{k_{\rm IR}}^{k_{\rm UV}} \frac{dk}{2\pi^2} \frac{1}{3} P_m(k)\,, \tag{4.60}$$

and therefore it varies very little in the range of r considered, despite not being constant. Note, however, that the relation between the angle θ and the separation r depends on the redshift (the higher is the redshift, the larger is the separation associated to a given angle at the observer) and in fig. 4.4 we take $z = 1$.

The correlation of the spatial shift at the observer is also only a function of the angle between the two lines of sight, given by

$$\langle \delta r_o(\hat{\boldsymbol{n}}_{\boldsymbol{1}}) \delta r_o(\hat{\boldsymbol{n}}_{\boldsymbol{2}})\rangle = \hat{\boldsymbol{n}}_{\boldsymbol{1}} \cdot \hat{\boldsymbol{n}}_{\boldsymbol{2}} \left(C \int_0^{\bar{\eta}_o} d\bar{\eta}\, D_V(\bar{\eta}) \right)^2 \int_{k_{\rm IR}}^{k_{\rm UV}} \frac{dk}{2\pi^2} \frac{1}{3} P_m(k)\,. \tag{4.61}$$

In fig. 4.4 one can see that, when considering two galaxies at redshift $z_1 = z_2 = 1$, the correlation of this effect is higher than that of the velocities at the observer by almost one order of magnitude. Note, additionally, that it can be much higher than the correlation of velocities at the sources if a large separation is considered. Indeed, at $r = 300$ Mpc$/h$, the difference is given by a factor of almost 20.

The spatial shift and the velocity at the observer position are typically ignored in literature, but their contributions are larger than the velocity correlation of two source galaxies. However, note that the spatial shift at the observer cancels at the linear order with the same term in the lensing convergence, such that ignoring this contribution does not cause any systematic error. On the other hand, the contribution of the velocity at the observer (green line in fig. 4.4) must be kept in the calculations, and it is larger than the velocity correlation (orange line in fig. 4.4).

We now have the main ingredients to analyze the correlations of the redshift and the radial distortions. Clearly, one has to compute also cross-correlations among all terms considered so far. Nevertheless, by looking at the auto-correlations of individual contributions to δz and δr one can obtain a clear intuition of the importance of each effect in the correlations $\langle \delta z_1 \delta z_2\rangle$ and $\langle \delta r_1 \delta r_2\rangle / \bar{r}_{z_1} / \bar{r}_{z_2}$. The top left panel of fig. 4.5 shows the auto-correlations of all contributions to δz for two galaxies at the same redshift $z_1 = z_2 = 1$. We immediately see that the correlation of the redshift distortion

$\langle \delta z_1 \delta z_2 \rangle$ is dominated by the Doppler effect of peculiar velocities, including that by the observer velocity, as expected. Indeed, the correlations of local potentials and the time-lapse at the observer are about 2 orders of magnitude smaller than the correlation of velocities at the observer, representing the leading contribution. Compared to the latter the correlation of the ISW effect is even 4 orders of magnitude smaller.

Analogously, the bottom left panel of fig. 4.5 shows the auto-correlations of all contributions to δr for the same configuration ($z_1 = z_2 = 1$). Evidently, the strongest contribution to the correlation of the radial distortions comes from the spatial shift at the observer. However, we again emphasize that the latter is absent in the total expression of the galaxy number density, because the same term appears in the gravitational lensing convergence $\mathcal{K}$ with opposite sign. The correlation of redshift distortions $\langle \delta z_1 \delta z_2 \rangle / \bar{r}_z^2 / \mathcal{H}_z^2$ is smaller than that of the spatial shift at the observer but it contributes with the same order of magnitude ($10^{-6} - 10^{-5}$) to $\langle \delta r_1 \delta r_2 \rangle / \bar{r}_z^2$. So, the correlation of radial distortions, like that of redshift distortions, is dominated by the effect of velocities.

Note, finally, that both the redshift and the radial distortions are not directly observables, they are affected by the long-mode perturbations (see sec. 4.2.3) and their correlations are divergent in the infrared. In other words, the sum of the correlations in eqs. (4.53)–(4.57) and their cross-correlations diverges if the IR cut-off is removed. Such divergence is eliminated when the remaining contributions to the galaxy number density fluctuations are taken into account in the correlation.

We want to emphasize that all the individual components such as δz, δr and so on are gauge-invariant in the Newtonian gauge, but they diverge in the infrared: gauge-invariance is not a sufficient condition for observable quantities. Furthermore, this decomposition of the observable galaxy number density depends on *our gauge choice*, in the sense that while the expressions for δz in the Newtonian gauge or comoving gauge, for instance, are gauge-invariant, their values are different.

Lensing convergence

The next effect to consider in the expression of the galaxy number density is the gravitational lensing convergence. To obtain the correlation function of the lensing convergence it is convenient to first express it as follows:

$$\mathcal{K} = \frac{\delta r_o}{\bar{r}_z} - V_{\parallel o} + 2\,\Psi_o - \Psi + \int_0^{\bar{r}_z} d\bar{r} \left[-2\frac{\bar{r}}{\bar{r}_z}\Psi' - \left(1 - \frac{\bar{r}}{\bar{r}_z}\right)\bar{r}\,\Psi'' + (\bar{r}_z - \bar{r})\frac{\bar{r}}{\bar{r}_z}\Delta\Psi \right], \quad (4.62)$$

where we have used the relation between the angular Laplacian $\hat{\nabla}^2$ and the 3D Laplacian Δ:

$$\Delta = \frac{1}{\bar{r}^2}\hat{\nabla}^2 + \frac{2}{\bar{r}}\frac{\partial}{\partial\bar{r}} + \frac{\partial^2}{\partial\bar{r}^2}\,. \quad (4.63)$$

In this way we can use the Poisson equation ($\Delta\Psi = \frac{3}{2}\mathcal{H}_o^2\Omega_m\delta/a$) and write the correlation function as

$$\begin{aligned}\langle\mathcal{K}(z_1,\hat{\boldsymbol{n}}_1)\mathcal{K}(z_2,\hat{\boldsymbol{n}}_2)\rangle &= \frac{\langle\delta r_o\delta r_o\rangle}{\bar{r}_{z_1}\bar{r}_{z_2}} + \langle V_{\parallel o}(\hat{\boldsymbol{n}}_1)V_{\parallel o}(\hat{\boldsymbol{n}}_2)\rangle + 4\,\langle\Psi_o\Psi_o\rangle + \langle\Psi_1\Psi_2\rangle \\ &+ 4\int_0^{\bar{r}_{z_1}} d\bar{r}_1\int_0^{\bar{r}_{z_2}} d\bar{r}_2\,\frac{\bar{r}_1\bar{r}_2}{\bar{r}_{z_2}\bar{r}_{z_1}}\langle\Psi'(\bar{\eta}_1,\bar{r}_1\,\hat{\boldsymbol{n}}_1)\Psi'(\bar{\eta}_2,\bar{r}_2\,\hat{\boldsymbol{n}}_2)\rangle \\ &+ \int_0^{\bar{r}_{z_1}} d\bar{r}_1\,\frac{(\bar{r}_{z_1}-\bar{r}_1)\bar{r}_1}{\bar{r}_{z_1}}\int_0^{\bar{r}_{z_2}} d\bar{r}_2\,\frac{(\bar{r}_{z_2}-\bar{r}_2)\bar{r}_2}{\bar{r}_{z_2}}\langle\Psi''(\bar{\eta}_1,\bar{r}_1\,\hat{\boldsymbol{n}}_1)\Psi''(\bar{\eta}_2,\bar{r}_2\,\hat{\boldsymbol{n}}_2)\rangle \\ &+ \frac{9}{4}\mathcal{H}_o^4\Omega_m^2\int_0^{\bar{r}_{z_1}} d\bar{r}_1\,g(\bar{r}_1)\int_0^{\bar{r}_{z_2}} d\bar{r}_2\,g(\bar{r}_2)\,\xi_m(|\bar{r}_1\hat{\boldsymbol{n}}_{\boldsymbol{1}}-\bar{r}_2\hat{\boldsymbol{n}}_{\boldsymbol{2}}|) \\ &+ \text{cross-correlations}\,,\end{aligned} \tag{4.64}$$

where we have defined $g(\bar{r}_i) \equiv \frac{(\bar{r}_{z_i}-\bar{r}_i)\bar{r}_i}{\bar{r}_{z_i}}\frac{D(\bar{\eta}_o-\bar{r}_i)}{a(\bar{\eta}_o-\bar{r}_i)}$. While the first two terms have been already discussed, the remaining ones constitute together the convergence of light rays $\int_0^{\bar{r}_z} d\bar{r}\,(\frac{\bar{r}_z-\bar{r}}{\bar{r}_z\bar{r}})\hat{\nabla}^2\Psi$. These terms do not lead to a divergence in the correlation when $k_{\rm IR}\to 0$. Indeed, as confirmed by our analysis in sec. 4.2.3 (see in particular eq. (4.33)), the lensing convergence does not contain the monopole of the long-mode gravitational potential. This is due to the fact that spatial derivatives of the potential are involved in the expression of $\mathcal{K}$, which gives zero when applied to the monopole.

The top right panel in fig. 4.5 shows the auto-correlations of the three contributions to $\mathcal{K}$: the spatial shift at the observer, the velocity at the observer and the non-local convergence. Again, two galaxies at redshift $z_1 = z_2 = 1$ are considered and the correlations are therefore only functions of the separation r between the galaxies. The correlation of the convergences decreases sharply with the separation. This is due to the fact that, when the separation is small, the matter distributions along the two lines of sight (almost parallel for small r), which generate the lensing effects, are more likely to be correlated (if not even the same lenses when $r \approx 0$). In the same figure the auto-correlation of the convergence is also plotted for the configuration in which the two galaxies lie on the same line of sight with the middle point between them being at redshift $z_C = 1$. The reason why in this case the correlation of the convergences decreases much less rapidly with the separation is the following: the distance between the observer and any of the two sources is much bigger than the separation r between the sources, therefore, the matter distribution causing the lensing effects is mostly that lying between the observer and the closer source. As one can see from the figure the contributions from the spatial lapse and the velocity at the observer may have a non negligible effect on the correlation. While the spatial lapse at the observer cancels out in the full expression of the galaxy number density, the velocity at the observer does not and must be taken into account for both theoretical and numerical purposes.

Redshift-space distortion

Finally, in order to obtain the two-point correlation function of the galaxy number density fluctuation in eqs. (4.44) and (4.45), we have to consider the remaining term $H_z \frac{\partial}{\partial z}\delta r$ appearing in the volume distortion. By taking the derivative of the radial distortion with respect to the source redshift, this quantity can be written in terms of the redshift distortion δz as

$$H_z \frac{\partial}{\partial z}\delta r = -\frac{1}{\mathcal{H}_z}\partial_\parallel V_\parallel - V_\parallel + \frac{1}{\mathcal{H}_z}\Psi' + 2\,\Psi - \frac{\mathcal{H}_z'}{\mathcal{H}_z^2}\,\delta z\,. \tag{4.65}$$

The first term represents the so-called redshift-space distortions (RSD), also referred to as the Kaiser effect. The auto-correlation function of this contribution to the galaxy clustering is given by

$$\begin{aligned}\frac{\langle \partial_\parallel V_\parallel(z_1,\hat{\boldsymbol{n}}_1)\partial_\parallel V_\parallel(z_2,\hat{\boldsymbol{n}}_2)\rangle}{\mathcal{H}_{z_1}\mathcal{H}_{z_2}} = \frac{C^2 D_V(z_1) D_V(z_2)}{\mathcal{H}_{z_1}\mathcal{H}_{z_2}} \int_{k_{\rm IR}}^{k_{\rm UV}} \frac{dk}{2\pi^2} k^2 P_m(k) \Bigg\{ j_0''''(kr)\,\mu_1^2\,\mu_2^2 \\ + \left[\frac{j_0''(kr)}{(kr)^2} - \frac{j_0'(kr)}{(kr)^3}\right]\left(1 + 2\,\mu^2 - 3\,\mu_1^2 - 3\,\mu_2^2 - 12\,\mu\,\mu_1\,\mu_2 + 15\,\mu_1^2\,\mu_2^2\right) \\ + \frac{j_0'''(kr)}{kr}\left(\mu_1^2 + \mu_2^2 + 4\,\mu\,\mu_1\,\mu_2 - 6\,\mu_1^2\,\mu_2^2\right)\Bigg\}\,,\end{aligned} \tag{4.66}$$

where we have defined the angles $\mu \equiv \hat{\boldsymbol{n}}_{\boldsymbol{1}} \cdot \hat{\boldsymbol{n}}_{\boldsymbol{2}}$, $\mu_1 \equiv \hat{\boldsymbol{n}}_{\boldsymbol{1}} \cdot \hat{\boldsymbol{r}}$, $\mu_2 \equiv \hat{\boldsymbol{n}}_{\boldsymbol{2}} \cdot \hat{\boldsymbol{r}}$. Fig. 4.3 shows the correlation as a function of the comoving separation r between two galaxies at redshift $z_1 = z_2 = 1$ and between two galaxies on the same line of sight $\hat{\boldsymbol{n}}_{\boldsymbol{1}} = \hat{\boldsymbol{n}}_{\boldsymbol{2}}$ with middle point at redshift $z_C = 1$. In the configuration $z_1 = z_2 = 1$ the correlation of the Kaiser effect has roughly the same amplitude of the matter densities correlation (if $b = 1$ as in the figure). This is the reason why this is the only effect taken into account in the standard galaxy correlation function, as the other effects are at least two orders of magnitude smaller. In the configuration $\hat{\boldsymbol{n}}_{\boldsymbol{1}} = \hat{\boldsymbol{n}}_{\boldsymbol{2}}$ and $z_C = 1$ the correlation of the Kaiser effect is negative for almost all values of r, with a positive maximum at the scale of BAO. The reason why the BAO peak manifests only in the second configuration is that in this case the Kaiser effect of the two galaxies is related to same line of sight and therefore the correlation is sensitive to the clustering caused by the BAO, while in the first configuration the two lines of sight are different and arbitrary. Note that we use "the Kaiser effect" to represent the contribution of the velocity gradient $-\partial_\parallel V_\parallel/\mathcal{H}_z$ only, rather than the sum of the velocity gradient and the density. The complete lack of a correlation between the lines of sight along which the Kaiser effect is evaluated removes the bump due to the BAO, so that the correlation simply decreases monotonically with the separation, independently from the clustering of matter. Clearly, for $r = 0$ the amplitude of the correlation is the same for the two

configurations. However, the correlations are highly oscillatory for values of r smaller than 35 Mpc/h and, therefore, we only plot the functions starting from that separation value. The other terms in eq. (4.65) are much smaller than the Kaiser effect, as one can see from fig. 4.5.

Total two-point correlation function

The total correlation function of the galaxy number density fluctuation δ_g for two galaxies at redshift $z_1 = z_2 = 1$ is shown in fig. 4.6, while that for two galaxies lying on the same line-of-sight with middle point at redshift $z_C = 1$ is shown in fig. 4.7. Note that the pure relativistic contributions, represented by the red lines in both figures, are dominated by the velocity effects. These contributions are roughly the same in the configuration ($z_1 = z_2$) of fig. 4.6 and the configuration ($n_1 = n_2$) of fig. 4.7. From fig. 4.4 we see that the velocity correlation function in the two configurations are of the same order of magnitude, but in the configuration $n_1 = n_2$ the velocity correlation at the source positions becomes negative at around 105 Mpc/h. However, the contribution of the velocity at the observer position, which is positive and greater than that at the source, makes the correlation in the two configurations being roughly the same.

From figs. 4.6–4.7 we readily recognize that on most scales there exists little difference between the full relativistic two-point correlation function $\langle \delta_g \delta_g \rangle$ and the standard correlation function $\xi_{\rm std} = \langle \delta_{\rm std}\, \delta_{\rm std} \rangle$ that takes into account only the matter density and the Kaiser effect ($\delta_{\rm std} \equiv b\, \delta_m - \mathcal{H}_z^{-1} \partial_\parallel V_\parallel$). We further quantify this difference in fig. 4.8 for the configuration $z_1 = z_2 = 1$. Figure 4.8 illustrates the fractional difference of the full relativistic description compared to the standard correlation function, and the orange curve shows the lensing contribution to this difference. More importantly, fig. 4.8 shows that at large separation $r \approx 200$ Mpc/h ($\theta \approx 5\,$deg) the general relativistic effects cause corrections to the standard correlation function at several percent level, comparable or larger than the lensing contribution. Such relativistic correction are mainly due to the velocity contribution $\delta_{\rm vel}$ (see eq. (4.49)), which is in turn dominated by the velocity at the observer position. The latter is often neglected in literature, leading to a systematic misinterpretation of the relativistic corrections. For separations smaller than the BAO scale the relativistic corrections, including lensing, are below the 1% level, so that it can be legit to use the standard expression to analyze upcoming data, provided that the survey precision is not better than 1%. For separations larger than 125 Mpc/h, instead, the lensing and the velocity contributions must be taken into account in the theoretical prediction, otherwise a systematic error of a few percents would affect the analysis. The potential contribution is small and can be neglected on all scales from the numerical point of view (see figs. 4.1 and 4.5), but only once its theoretical importance is understood and under control. Indeed, the potential contribution is necessary for the gauge invariance of the expression and the consistency with the equivalence principle, also indispensable for the convergence of the correlation

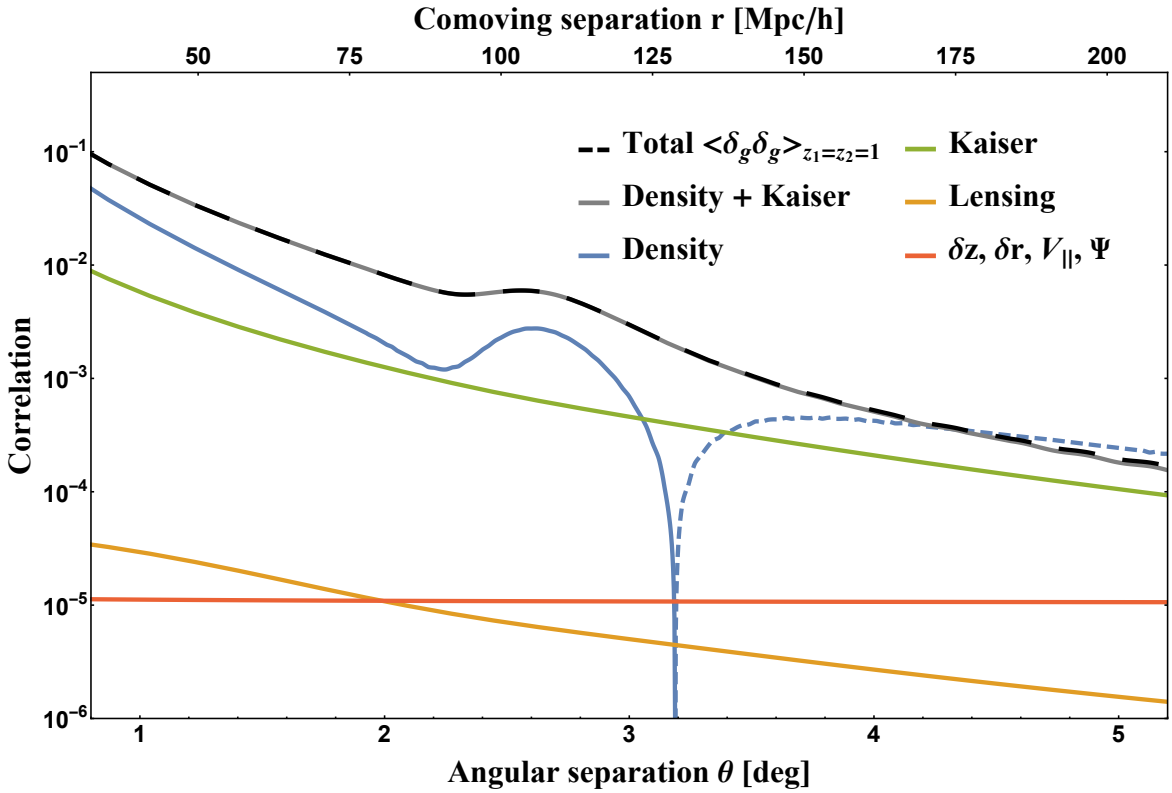

Figure 4.6: The full galaxy two-point correlation function $\langle \delta_g \delta_g \rangle$ for two galaxies at the same redshift $z_1 = z_2 = 1$ is represented by the dashed black line. The gray line represents the standard correlation function that takes into account only the matter density contrast and the Kaiser effect. Other lines represent auto-correlations of various contributions to $\langle \delta_g \delta_g \rangle$: the matter density fluctuation in blue, the Kaiser effect in green, the gravitational lensing convergence in orange and the sum of all other effects in red. The latter is mostly influenced by the velocities effect. The dashed blue line represents negative values of the density correlation function. The value of the galaxy bias factor is set to $b = 2$. The cut-off choices are $k_{\rm IR} = \mathcal{H}_o$ and $k_{\rm UV} = 10\ h/{\rm Mpc}$.

function in the infrared.

4.3.2 Primordial gravitational wave contributions

In this section we investigate the various contributions to the two-point galaxy correlation function considering only tensor perturbations, corresponding to the primordial gravitational waves. In this case the expression of the observer galaxy number density fluctuation is derived in sec. 4.2.3 as

$$\delta_g = (3 - e_z)\,\delta z + 2\,\frac{\delta r}{\bar{r}_z} - 2\,\kappa + H_z \frac{\partial}{\partial z}\delta r\,, \tag{4.67}$$

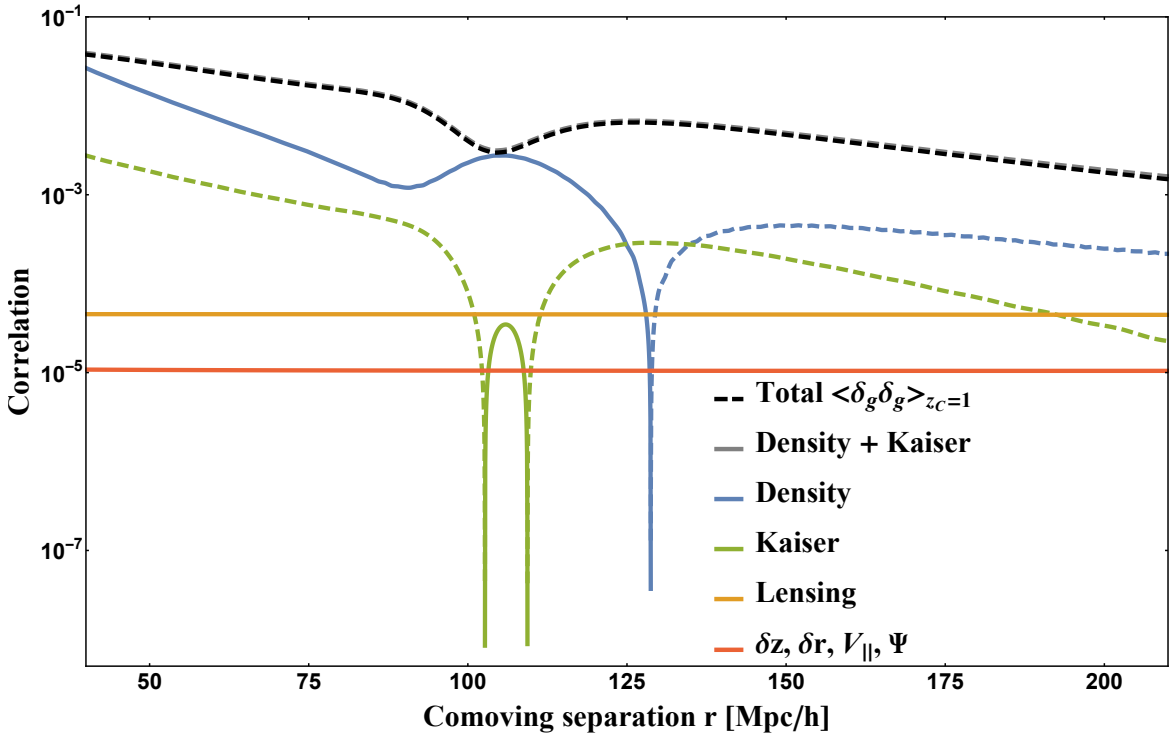

Figure 4.7: The full general relativistic two-point galaxy correlation function $\langle \delta_g \delta_g \rangle$ for two galaxies lying on the same line-of-sight ($\hat{\boldsymbol{n}}_1 = \hat{\boldsymbol{n}}_2$) with middle point at redshift $z_C = 1$ is represented by the black line. The gray line represents the standard correlation function that takes into account only the matter density contrast and the Kaiser effect. Other lines represent auto-correlations of various contributions to $\langle \delta_g \delta_g \rangle$: the matter density fluctuation in blue, the Kaiser effect in green, the gravitational lensing convergence in orange and the sum of all other effects in red. The latter is mostly influenced by the velocities effect. The dashed lines represents negative values of the correlation functions. The value of the galaxy bias factor is set to $b = 2$. The cut-off choices are $k_{\rm IR} = \mathcal{H}_o$ and $k_{\rm UV} = 10\ h/\text{Mpc}$.

where there is no tensor contribution to the matter density fluctuation and the relativistic distortions are given in terms of the projected tensor perturbations $C_\parallel \equiv C_{ij}\hat{n}^i\hat{n}^j$ by

$$
\begin{aligned}
&\delta z = \int_0^{\bar{r}_z} d\bar{r}\, C_\parallel{}' \,, \qquad\qquad \frac{\delta r}{\bar{r}_z} = -\frac{\delta z}{\bar{r}_z \mathcal{H}_z} - \int_0^{\bar{r}_z} \frac{d\bar{r}}{\bar{r}_z} C_\parallel \,, \\
&\kappa = \frac{5}{2} C_{\parallel o} - C_\parallel - 3\int_0^{\bar{r}_z} \frac{d\bar{r}}{\bar{r}} C_\parallel - \int_0^{\bar{r}_z} d\bar{r}\, C_\parallel{}' - \frac{1}{2}\int_0^{\bar{r}_z} d\bar{r} \left(\frac{\bar{r}_z - \bar{r}}{\bar{r}_z \bar{r}}\right) \hat{\nabla}^2 C_\parallel \,, \\
&H_z \frac{\partial}{\partial z}\delta r = -\frac{\mathcal{H}_z'}{\mathcal{H}_z^2}\delta z - \frac{1}{\mathcal{H}_z} C_\parallel{}' - C_\parallel \,.
\end{aligned}
\tag{4.68}
$$

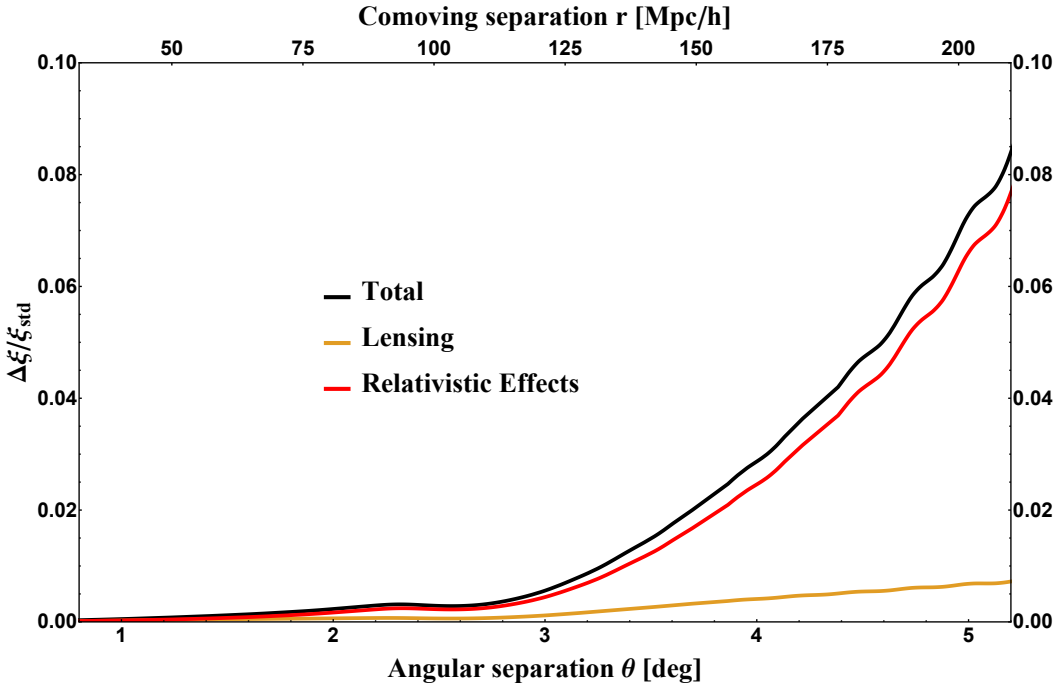

Figure 4.8: The black curve shows the relative difference between the full relativistic galaxy two-point correlation and the standard correlation of density and Kaiser effect only: $(\langle\delta_g\delta_g\rangle - \xi_{\rm std})/\xi_{\rm std}$, where $\xi_{\rm std} \equiv \langle\delta_{\rm std}\,\delta_{\rm std}\rangle$ and $\delta_{\rm std} = b\,\delta_m - \mathcal{H}_z^{-1}\partial_\parallel V_\parallel$. Both $\langle\delta_g\delta_g\rangle$ and $\xi_{\rm std}$ are computed by considering two galaxies at the same redshift $z_1 = z_2 = 1$, so that the relative difference is only a function of the separation between the galaxies. The orange curve shows the contribution from lensing to the relative difference. Specifically, the orange line represents the relative difference between the correlation of lensing, density and Kaiser effect and the standard correlation: $(\xi_{\rm lensing} - \xi_{\rm std})/\xi_{\rm std}$, where $\xi_{\rm lensing} \equiv \langle(\delta_{\rm std} - 2\mathcal{K})(\delta_{\rm std} - 2\mathcal{K})\rangle$. The difference between the black and the orange curves, shown by the red curve, represents the pure relativistic corrections to the standard theoretical predictions : $(\xi_{\rm rel} - \xi_{\rm std})/\xi_{\rm std}$, where $\xi_{\rm rel} = \langle(\delta_{\rm std} + \delta_{\rm vel} + \delta_{\rm pot})(\delta_{\rm std} + \delta_{\rm vel} + \delta_{\rm pot})\rangle$ and $\delta_{\rm vel,\ pot}$ are given in eq. (4.49). In this plot the galaxy bias is $b = 2$ and the cut-off choices are $k_{\rm IR} = \mathcal{H}_o$ and $k_{\rm UV} = 10\ h/{\rm Mpc}$. Note that $\xi_{\rm rel}$ is independent of gauge choice.

Note that the expression of the lensing convergence κ in eq. (4.37) has been manipulated by using the following relations:

$$\hat{\nabla}_i = \bar{r}(\delta^k_i - \hat{n}_i\hat{n}^k)\partial_k = \bar{r}(\partial_i - \hat{n}_i\hat{n}^k\partial_k)\,, \quad \hat{\nabla}^2 = \hat{\nabla}_i\hat{\nabla}^i = \bar{r}^2\Delta - 2\,\bar{r}\,\hat{n}^k\partial_k - \bar{r}^2\,\hat{n}^k\hat{n}^l\partial_k\partial_l\,,$$
$$\hat{n}^k\partial_k = \partial_{\bar{\eta}} + \frac{d}{d\bar{r}}\,. \tag{4.69}$$

In this way, the tensor perturbations C_{ij} appear through the contraction $C_\parallel$ in all terms and in all expressions.

When all contributions in eq. (4.68) are substituted into eq. (4.67), the expression

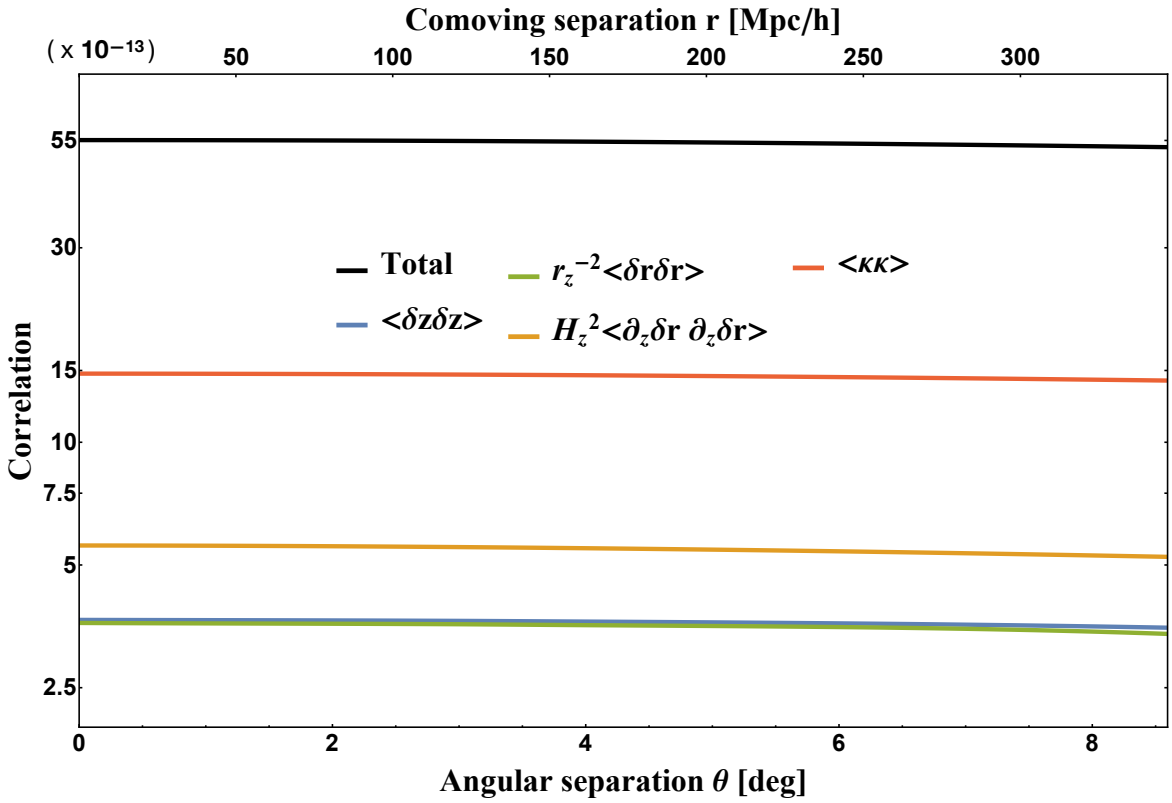

Figure 4.9: Two-point correlations of the relativistic contributions to the galaxy number density due to primordial gravitational waves. The correlations are functions of the separation between two galaxies at the same redshift $z_1 = z_2 = 1$.

of the galaxy number density can be reordered as

$$\begin{aligned}\delta_g = &-5C_{\parallel o} + C_\parallel - \frac{1}{\mathcal{H}_z}C_\parallel{}' + 6\int_0^{\bar{r}_z}\frac{d\bar{r}}{\bar{r}}C_\parallel - 2\int_0^{\bar{r}_z}\frac{d\bar{r}}{\bar{r}_z}C_\parallel \\ &+\left[(3-e_z) + 2 - \frac{2}{\bar{r}_z\mathcal{H}_z} - \frac{\mathcal{H}_z'}{\mathcal{H}_z^2}\right]\int_0^{\bar{r}_z} d\bar{r}\, C_\parallel{}' + \int_0^{\bar{r}_z} d\bar{r}\left(\frac{\bar{r}_z - \bar{r}}{\bar{r}_z\bar{r}}\right)\hat{\nabla}^2 C_\parallel\,,\end{aligned} \tag{4.70}$$

consistently with eqs. (40)–(41) in [107]. Note the presence of the observer term $C_{\parallel o}$, due to the fact that we have set the initial conditions for integrating the geodesic equation by requiring that angular positions match the physical ones measured in the observer rest frame. In other words, such term represents the mismatch between the observer and the FRW coordinate systems, caused by tensor perturbations. As we have discussed in the previous section, considering observer terms in the case of scalar perturbations is important to guarantee the gauge invariance of the expressions,

to ensure the convergence of the correlations in the infrared, and to obtain the correct amplitudes in the numerical evaluations. Despite the fact that there is no gauge ambiguity for tensor perturbations, considering the observer term $C_{\|o}$ is essential for the consistency of the expressions with the equivalence principle. Indeed, as we have demonstrated in sec. 4.2.3, without the observer term the tensor contribution to the galaxy number density would contain the unphysical effects of uniform gravity from long-mode perturbations. Furthermore, it has been already shown in [107] that the observer term $C_{\|o}$ is numerically important for the quadrupole of the observed galaxy number density. If such term is neglected, the tensor contribution to the quadrupole of the galaxy density cannot be estimated correctly.

In order to compute the two-point correlations, we first decompose the tensor perturbations into Fourier modes of two polarization states (labeled by $s = +, \times$) as in eq. (4.38),

$$C_{ij}(\eta, \boldsymbol{k}) = e^{+}_{ij}(\hat{\boldsymbol{k}})\, C^{+}(\eta, \boldsymbol{k}) + e^{\times}_{ij}(\hat{\boldsymbol{k}})\, C^{\times}(\eta, \boldsymbol{k})\,, \tag{4.71}$$

where the polarization tensors $e^{s}_{ij}(\hat{\boldsymbol{k}})$ are transverse, traceless and normalized through $e^{s}_{ij} e^{s'\,ij} = 2\,\delta^{ss'}$. The power spectra of the two polarizations C^{+} and $C^{\times}$ are

$$\langle C_s(\eta_1, \boldsymbol{k}_1)\, C_{s'}(\eta_2, \boldsymbol{k}_2)\rangle = (2\pi)^3 \delta_D(\boldsymbol{k}_1 - \boldsymbol{k}_2)\delta_{ss'}\, \frac{1}{16}\, P_T(k_1, \eta_1, \eta_2)\,, \tag{4.72}$$

where P_T is the total tensor power spectrum $\propto \langle 2C_{ij}\, 2C^{ij}\rangle$. From eqs. (4.71) and (4.72) the two-point correlation of tensor perturbations in terms of the power spectrum is given by

$$\langle C_{ij}(\eta_1, \boldsymbol{k}_1) C_{kl}(\eta_2, \boldsymbol{k}_2)\rangle = (2\pi)^3 \delta_D(\boldsymbol{k}_1 - \boldsymbol{k}_2)\Big[e^{+}_{ij}(\hat{\boldsymbol{k}}_1) e^{+}_{kl}(\hat{\boldsymbol{k}}_1) + e^{\times}_{ij}(\hat{\boldsymbol{k}}_1) e^{\times}_{kl}(\hat{\boldsymbol{k}}_1)\Big]\frac{1}{16} P_T(k_1, \eta_1, \eta_2)\,. \tag{4.73}$$

The tensor power spectrum can be further expressed in terms of the primordial one as

$$P_T(k, \eta_1, \eta_2) = T(k, \eta_1)\, T(k, \eta_2)\, P_{T0}(k)\,, \tag{4.74}$$

where $T(k, \eta)$ is the tensor transfer function and the primordial power spectrum is given by an amplitude A_T and an index n_T as

$$P_{T0}(k) = \frac{2\pi^2}{k^3}\, A_T \left(\frac{k}{k_0}\right)^{n_T}. \tag{4.75}$$

The amplitude can be obtained from that of the scalar modes as $A_T = r\, A_s$, where r is the tensor-to-scalar ratio at the pivot scale k_0 and $A_s = 2 \times 10^{-9}$. The index is also obtained from the tensor-to-scalar ratio as $n_T = -r/8$. Assuming $r = 0.2$ at $k_0 = 0.07$ h/Mpc, we have $A_T = 4 \times 10^{-10}$ and $n_T = -0.025$. As we consider no anisotropic stress

which sources gravitational waves, the tensor modes generated after inflation propagate freely. Thus, in the matter dominated epoch the transfer function is given by

$$T(k,\eta) = 3\frac{j_1(k\eta)}{k\eta}\,. \tag{4.76}$$

This is still a valid approximation in the present epoch of accelerated expansion, and we will use it in the numerical calculations of the correlation functions.

We now study the two-point correlation functions of the tensor contributions. We first write down the analytic expressions of the correlations of each relativistic distortion in eqs. (4.68) for the general case. Then we study the correlations numerically as functions of the comoving separation between the two galaxies, considering only the configuration in which both galaxies are at redshift $z = 1$. In this case, the correlation can be also expressed as a function of the angular separation θ between the two lines of sight. However, the approach we have used to compute the correlation functions of the scalar contributions turns out to be complicated when applied to the tensor perturbations, as in this case the time and space dependence cannot be separated. Therefore, here we derive the correlation functions of the tensor contributions in terms of the angular power spectrum C_l

$$\langle A(z_1,\hat{\boldsymbol{n}}_1)B(z_2,\hat{\boldsymbol{n}}_2)\rangle = \xi_{AB}(z_1,z_2,\theta) = \frac{1}{4\pi}\sum_l (2l+1)C_l^{AB}(z_1,z_2)P_l(\cos\theta)\,, \tag{4.77}$$

where A and B represent any of the relativistic corrections to the galaxy number density, such as δz, $\delta r/\bar{r}_z$, κ, $H_z\partial_z\delta r$, and $P_l(x)$ are the Legendre polynomials.

Note that each term in eq. (4.67) or (4.70) can be written as

$$\begin{aligned} A(z,\hat{\boldsymbol{n}}) &= \int_0^{\bar{r}_z} d\bar{r}\, W_A(z,\bar{r})C_{\parallel}(\bar{\eta},\bar{r}\hat{\boldsymbol{n}}) = \int_0^{\bar{r}_z} d\bar{r}\, W_A(z,\bar{r}) \int \frac{d^3k}{(2\pi)^3} e^{i\bar{r}\boldsymbol{k}\cdot\hat{\boldsymbol{n}}} C_{\parallel}(\bar{\eta},\boldsymbol{k})\,, \\ &\equiv \int \frac{d^3k}{(2\pi)^3} A(z,\hat{\boldsymbol{n}},\boldsymbol{k})\,, \end{aligned} \tag{4.78}$$

where for $A = C_{\parallel}$ then $W_A(z,\bar{r}) = \delta_D(\bar{r}-\bar{r}_z)$, for $A = \delta z$ then $W_A C_{\parallel} = \partial_{\bar{\eta}} C_{\parallel}|_{\bar{\eta}_o-\bar{r}}$ and so on. First, we consider the contribution of a single plane-wave tensor perturbation, propagating along the $\hat{\boldsymbol{z}}$-direction ($\hat{\boldsymbol{k}} \equiv \hat{\boldsymbol{z}}$). Thus, the projection along the line of sight can be written as

$$\hat{n}^i\hat{n}^j C_{ij}(\bar{\eta},\boldsymbol{k}) = \sin^2\theta[\cos 2\phi\, C^+(\bar{\eta},\boldsymbol{k}) + \sin 2\phi\, C^\times(\bar{\eta},\boldsymbol{k})] = \sin^2\theta[e^{i2\phi}C_{+2} + e^{-i2\phi}C_{-2}]\,. \tag{4.79}$$

Note that the helicity states are related to the polarization states as $C_{\pm 2} = \frac{1}{2}(C_+ \mp iC_\times)$, and their power spectra as $\langle C_{+2}C_{+2}\rangle = \langle C_{-2}C_{-2}\rangle = \frac{1}{2}\langle C_+C_+\rangle = \frac{1}{2}\langle C_\times C_\times\rangle$, while $\langle C_{+2}C_{-2}\rangle = 0$. The contribution to $A(z,\hat{\boldsymbol{n}})$ from this perturbation is given by

$$A(z,\hat{\boldsymbol{n}},\boldsymbol{k}) = \int_0^{\bar{r}_z} d\bar{r}\, W_A(z,\bar{r})\, e^{ik\bar{r}\mu}(1-\mu^2)[e^{i2\phi}C_{+2}(\bar{\eta},\boldsymbol{k}) + e^{-i2\phi}C_{-2}(\bar{\eta},\boldsymbol{k})]\,, \tag{4.80}$$

where $\mu = \hat{\boldsymbol{n}} \cdot \hat{\boldsymbol{k}}$. The multipole coefficients of $A(z, \hat{\boldsymbol{n}})$ are then

$$a^A_{lm}(z) = \int d^2\hat{n} Y^*_{lm}(\hat{\boldsymbol{n}}) A(z, \hat{\boldsymbol{n}}) = \int \frac{d^3k}{(2\pi)^3} a^A_{lm}(z, \boldsymbol{k}) \,, \tag{4.81}$$

where the multipole coefficient in Fourier space is

$$\begin{aligned} a^A_{lm}(z, \boldsymbol{k}) &= \int d^2\hat{n} Y^*_{lm}(\hat{\boldsymbol{n}}) A(z, \hat{\boldsymbol{n}}, \boldsymbol{k}) \\ &= \int_0^{\bar{r}_z} d\bar{r}\, W_A(z, \bar{r}) \int d^2\hat{n} Y^*_{lm}(\mu, \phi) e^{ik\bar{r}\mu} (1-\mu^2) \\ &\quad \times \left[e^{i2\phi} C_{+2}(\bar{\eta}, \boldsymbol{k}) + e^{-i2\phi} C_{-2}(\bar{\eta}, \boldsymbol{k}) \right] . \end{aligned} \tag{4.82}$$

By using the identity [107]

$$\int d\Omega\, Y^*_{lm}(1-\mu^2) e^{\pm i2\phi} e^{ix\mu} = -\sqrt{4\pi(2l+1)} \sqrt{\frac{(l+2)!}{(l-2)!}} i^l \frac{j_l(x)}{x^2} \delta_{m\pm 2} \,, \tag{4.83}$$

the latter can be written as

$$\begin{aligned} a^A_{lm}(z, \boldsymbol{k}) &= -i^l \sqrt{4\pi(2l+1)\frac{(l+2)!}{(l-2)!}} \int_0^{\bar{r}_z} d\bar{r}\, W_A(\bar{r}, \bar{r}_z) \\ &\quad \times \left[C_{+2}(\bar{\eta}, \boldsymbol{k}) \delta_{m2} + C_{-2}(\bar{\eta}, \boldsymbol{k}) \delta_{m-2} \right] \frac{j_l(k\bar{r})}{(k\bar{r})^2} \,. \end{aligned} \tag{4.84}$$

We now have all ingredients to compute the angular power spectrum C_l and the two-point correlation functions by using eq. (4.77). We have

$$C^{AB}_l(z_1, z_2) = \frac{1}{2l+1} \sum_m \mathrm{Re}\langle a^{A*}_{lm}(z_1) a^B_{lm}(z_2) \rangle \,, \tag{4.85}$$

where the individual components with $A \equiv B$ are

$$\begin{aligned} C^{\delta z}_l(z_1, z_2) &= \frac{1}{8\pi} \frac{(l+2)!}{(l-2)!} \int dk\, k^2 P_{T0}(k) \int_0^{\bar{r}_{z_1}} d\bar{r}_1 \frac{\partial}{\partial \bar{\eta}_1} T(k, \bar{\eta}_1) \frac{j_l(k\bar{r}_1)}{(k\bar{r}_1)^2} \\ &\quad \times \int_0^{\bar{r}_{z_2}} d\bar{r}_2 \frac{\partial}{\partial \bar{\eta}_2} T(k, \bar{\eta}_2) \frac{j_l(k\bar{r}_2)}{(k\bar{r}_2)^2} \,, \end{aligned} \tag{4.86}$$

$$\begin{aligned} C^{\delta r}_l(z_1, z_2) &= \frac{1}{8\pi} \frac{(l+2)!}{(l-2)!} \int dk\, k^2 P_{T0}(k) \int_0^{\bar{r}_{z_1}} d\bar{r}_1 \left[-\frac{1}{\bar{r}_{z_1} \mathcal{H}_{z_1}} \frac{\partial}{\partial \bar{\eta}_1} - \frac{1}{\bar{r}_{z_1}} \right] T(k, \bar{\eta}_1) \frac{j_l(k\bar{r}_1)}{(k\bar{r}_1)^2} \\ &\quad \times \int_0^{\bar{r}_{z_2}} d\bar{r}_2 \left[-\frac{1}{\bar{r}_{z_2} \mathcal{H}_{z_2}} \frac{\partial}{\partial \bar{\eta}_2} - \frac{1}{\bar{r}_{z_2}} \right] T(k, \bar{\eta}_2) \frac{j_l(k\bar{r}_2)}{(k\bar{r}_2)^2} \,, \end{aligned} \tag{4.87}$$

$$C_l^{\kappa}(z_1,z_2) = \frac{1}{8\pi}\frac{(l+2)!}{(l-2)!}\int dk\, k^2 P_{T0}(k) \\ \times \int_0^{\bar{r}_{z_1}} d\bar{r}_1 \left[\frac{5}{2}\delta_D(\bar{r}_1) - \delta_D(\bar{r}_1-\bar{r}_{z_1}) - \frac{3}{\bar{r}_1} - \frac{\partial}{\partial\bar{\eta}_1} + \frac{l(l+1)}{2}\frac{\bar{r}_{z_1}-\bar{r}_1}{\bar{r}_{z_1}\bar{r}_1}\right] T(k,\bar{\eta}_1)\frac{j_l(k\bar{r}_1)}{(k\bar{r}_1)^2} \\ \times \int_0^{\bar{r}_{z_2}} d\bar{r}_2 \left[\frac{5}{2}\delta_D(\bar{r}_2) - \delta_D(\bar{r}_2-\bar{r}_{z_2}) - \frac{3}{\bar{r}_2} - \frac{\partial}{\partial\bar{\eta}_2} + \frac{l(l+1)}{2}\frac{\bar{r}_{z_2}-\bar{r}_2}{\bar{r}_{z_2}\bar{r}_2}\right] T(k,\bar{\eta}_2)\frac{j_l(k\bar{r}_2)}{(k\bar{r}_2)^2}\,, \tag{4.88}$$

$$C_l^{\partial_z\delta r}(z_1,z_2) = \frac{1}{8\pi}\frac{(l+2)!}{(l-2)!}\int dk\, k^2 P_{T0}(k) \\ \times \int_0^{\bar{r}_{z_1}} d\bar{r}_1 \left[-\frac{\mathcal{H}'_{z_1}}{\mathcal{H}^2_{z_1}}\frac{\partial}{\partial\bar{\eta}_1} - \frac{1}{\mathcal{H}_{z_1}}\delta_D(\bar{r}_1-\bar{r}_{z_1})\frac{\partial}{\partial\bar{\eta}_1} - \delta_D(\bar{r}_1-\bar{r}_{z_1})\right] T(k,\bar{\eta}_1)\frac{j_l(k\bar{r}_1)}{(k\bar{r}_1)^2} \\ \times \int_0^{\bar{r}_{z_2}} d\bar{r}_2 \left[-\frac{\mathcal{H}'_{z_2}}{\mathcal{H}^2_{z_2}}\frac{\partial}{\partial\bar{\eta}_2} - \frac{1}{\mathcal{H}_{z_2}}\delta_D(\bar{r}_2-\bar{r}_{z_2})\frac{\partial}{\partial\bar{\eta}_2} - \delta_D(\bar{r}_2-\bar{r}_{z_2})\right] T(k,\bar{\eta}_2)\frac{j_l(k\bar{r}_2)}{(k\bar{r}_2)^2}\,. \tag{4.89}$$

Note that the time derivatives of the transfer functions are evaluated at $\bar{\eta} = \bar{\eta}_o - \bar{r}$ and we have used the relation $a_{lm}[\hat{\nabla}^2 A] = -l(l+1)a^A_{lm}$ to obtain C_l^{κ}. The angular power spectra for $A \neq B$ are obtained analogously. The total tensor contribution to the angular power spectrum is then given by

$$C_l^{\rm tot}(z_1,z_2) = \frac{1}{8\pi}\frac{(l+2)!}{(l-2)!}\int dk\, k^2 P_{T0}(k) \\ \times \int_0^{\bar{r}_{z_1}} d\bar{r}_1 \Big[(3-e_z)W_{\delta z}(\bar{r}_1) + 2W_{\delta r}(z_1,\bar{r}_1) - 2W_{\kappa}(z_1,\bar{r}_1,l) + W_{\partial_z\delta r}(z_1,\bar{r}_1)\Big] \\ \times T(k,\bar{\eta}_1)\frac{j_l(k\bar{r}_1)}{(k\bar{r}_1)^2} \\ \times \int_0^{\bar{r}_{z_2}} d\bar{r}_2 \Big[(3-e_z)W_{\delta z}(\bar{r}_2) + 2W_{\delta r}(z_2,\bar{r}_2) - 2W_{\kappa}(z_2,\bar{r}_2,l) + W_{\partial_z\delta r}(z_1,\bar{r}_2)\Big] \\ \times T(k,\bar{\eta}_2)\frac{j_l(k\bar{r}_2)}{(k\bar{r}_2)^2}\,, \tag{4.90}$$

where $W_{\delta z}$, $W_{\delta r}$, W_{κ} and $W_{\partial_z\delta r}$ are read off eqs. (4.86)–(4.89). Note that $C_l = 0$ for $l = \{0,1\}$, as for tensor perturbations the only scalar that can be constructed out of C_{ij} is the contraction $\hat{n}^i\hat{n}^j C_{ij}$, whose multipole expansion starts from the quadrupole.

In fig. 4.9 we summarize our numerical results, obtained by considering two galaxies at the same redshift $z_1 = z_2 = 1$. The two-point correlations are therefore functions of the comoving separation r between the two spatial positions or the angular separation θ between the two lines of sight. The plot shows that the total tensor contribution to the two-point galaxy correlation function is of order 10^{-12}, and it varies very little with the separation. Among the relativistic corrections the lensing convergence is the most

important, being four times larger than the contributions from the redshift and the radial distortions. The amplitude of the correlation functions is expected to be small, as primordial gravitational waves decay fast once they enter the horizon. We find, indeed, that the effect of gravitational waves is suppressed by eight or more orders of magnitude with respect to the scalar contributions.

4.4 Summary and Discussion

In this chapter we have studied the two-point galaxy correlation function, both theoretically and numerically, providing the complete general relativistic predictions at linear order that are essential to interpret its measurements. Many groups (e.g. [54, 83, 84, 94, 95, 96, 98, 99, 100, 114]) have already presented the relativistic galaxy two-point correlation function, considering different cosmologies and exploring broad redshift intervals with various configurations of the galaxy pairs. However, this chapter addresses and resolves theoretical issues concerning the expression of the galaxy number density and its two-point correlation function. Following the lead of [84, 101, 102, 105, 107], we have shown that the boundary terms evaluated at the observer position are necessary for the gauge-invariance of the expression, for its consistency with the equivalence principle and for the convergence of the correlation function in the infrared regime.

The galaxy number density is an observable, measured by counting the number of galaxies in the survey volume. As such, its theoretical expression has to be independent from the gauge condition chosen for the computations. We have derived the theoretical expression, starting from a general metric representation with scalar and tensor perturbations, without imposing any gauge choice. In this way, we could explicitly verify the gauge-invariance of our expression and check its validity. It is important to stress that the gauge-invariant expression is obtained by deriving the observed galaxy number density in terms of physical quantities, namely the observed redshift and the angular position on the sky. These quantities are measured in the observer rest frame, which requires the frame change from the FRW coordinates and results in perturbation contributions at the observer position. These boundary terms at the observer position cannot be set zero as it is often done in literature. The perturbations evaluated at the observer position are, indeed, necessary for the gauge-invariance of the expression.

Furthermore, this complete gauge-invariant expression including the boundary terms is needed for the compatibility with the equivalence principle. In sec. 4.2.3 we have demonstrated that our expression satisfies the equivalence principle by showing explicitly that it is unaffected by the uniform gravitational potential and the uniform acceleration generated by long-mode scalar or tensor perturbations, i.e. perturbations with wavelength much larger than the distance between the observer and the source, representing the scale of the system. When considering the two-point galaxy correlation function, the infrared divergences generated by the monopole of the gravitational

potential at the source and integrated along the line of sight are cancelled by the divergent contributions at the observer, providing a finite result (see figures 4.1 and 4.2). If the perturbations at the observer position are set zero by hand, the divergent contributions are not balanced in the two-point correlation function, and one is forced to impose an *arbitrary* infrared cut-off when computing correlations.

One might argue that the perturbation contributions at the observer position are constants and, therefore, taking an ensemble average to correlate them is conceptually incorrect. Furthermore, the real observer only takes spatial average over the sources. Since the ergodic theorem provides a correspondence between the spatial averaging and the theoretical ensemble averaging, one might argue that the ensemble average should not be taken over the perturbations at the observer, as there is no corresponding spatial average [114]. Indeed, we do not have access to measurements taken from different observers in the universe. However, the perturbations at the observer are random fields evaluated at a point, exactly as perturbations at the source. Furthermore, the distinction of the perturbation contributions at the observer position and the rest is a gauge-dependent interpretation. In the conformal Newtonian gauge we adopted for the computation there exist perturbation contributions at the observer position. However, in the comoving gauge, for instance, there are no perturbation contributions at the observer position, but those at the observer position in the conformal Newtonian gauge are instated as the perturbations at the source position. As a consequence, one cannot treat the observer position differently from any other point, when the ensemble average is taken. This approach is the only way that leads to a theoretically consistent result in any gauge conditions.

Adopting the conformal Newtonian gauge, we have performed numerical studies of the individual relativistic contributions to the galaxy two-point correlation function. The contributions to the observed galaxy number density are divided into the redshift distortion δz, the radial distortion δr, the gravitational lensing convergence $\mathcal{K}$, and the Kaiser effect (or the redshift-space distortion). In such decomposition, each contribution is gauge dependent and some of them are IR diverging in the correlation function. However, since we have shown that the sum is gauge invariant and its correlation converges in the infrared, we have imposed an IR cutoff for the purpose of illustration. With this, we have computed the relativistic contributions to the galaxy two-point correlation function, considering two configurations of galaxy pairs: the one in which the two galaxies are at the same redshift $z = 1$ (transverse), and the one in which the two galaxies are along the same line-of-sight with middle point at fixed redshift $z = 1$ (parallel).

Our numerical results reproduce the standard two-point correlation function, which accounts for the density fluctuation and the RSD, in complete agreement with the literature (see fig. 4.3). It is interesting to note that the auto-correlation of the RSD exhibit the BAO feature in the parallel configuration, but not in the transverse one, as for the

latter there is no correlation between the two lines of sight. The standard expression is used to analyze data from current surveys, as the precision of such measurements does not require higher theoretical accuracy. However, for future surveys the sub-percent level of accuracy is demanded by the increasing precision of data, and the theoretical expression must include all the relativistic effects. Our numerical results show that the gravitational lensing convergence represents the most important relativistic effect after the RSD, for small angular separations ($\theta < 2$ deg) in the configuration where both galaxies are at redshift $z = 1$ (see fig. 4.6) and for any comoving separation in the other configuration (see fig. 4.7). The correlations of other relativistic effects are dominated by the effect of peculiar velocities (see fig. 4.5). In particular, the contribution from the velocity at the observer is the most important (see fig. 4.4), but it is often ignored in the literature.

A detailed analysis of the correlation function was performed in [100]. The bottom left panel of fig. 3 in [100] provides the fractional errors due to the individual relativistic contributions to the correlation function in the same format as our fig. 4.8. Compared to the standard calculation $\xi_{\rm std}$ in fig. 4.8, the relativistic contribution is 6% at $r = 200$ Mpc/h, largely due to the velocity contribution. However, we find a factor 10 difference in fig. 3 in [100], where the velocity contribution (blue) is 0.6% at the same separation. Apart from the factor two difference in galaxy bias, the cosmological parameters adopted in [100] and our analysis are fairly identical. However, we note that the calculation of the correlation function in [100] neglects all the contributions at the observer position, and the velocity contribution among those at the observer position is factor 10 larger than the source velocity contribution at $r = 200$ Mpc/h shown in fig. 4.4. We believe that the factor 10 difference in the fractional errors can be attributed to the missing velocity contribution at the observer position. The gravitational potential contribution (green) in [100] appears larger than the velocity contribution (blue), whereas the potential contributions in our calculation are typically three orders of magnitude smaller than the velocity contributions.

As mentioned above, one cannot neglect the boundary terms at the observer in the expression of the observable galaxy number density. While the other perturbations at the observer (the time-lapse and the gravitational potential) are important mostly because they eliminate the unobservable and divergent monopole from the correlation, as their contribution has a very small amplitude compared with the density and RSD, the velocity at the observer contributes to the dipole of the correlation and has a non-negligible effect. Since the correlation of velocities at the observer is almost constant, it is particularly important for large separations, where the correlation of other contributions decreases. Also the spatial shift at the observer δr_o would contribute to the dipole, but it cancels exactly in the theoretical expression. It is important to consider it, however, to correctly predict the correlations of radial distortions, for which it represents the leading contribution, and lensing convergences (fig. 4.5). We

emphasize again that these individual quantities are gauge-dependent, such that the separation of the correlation function into these terms is not unique and ignoring any of these terms would lead to an inconsistent result in a different gauge choice. Indeed, the observable two-point correlation function is only the total one, and the theoretical (gauge-invariant) sum of various (gauge-dependent) contributions has to match it in any gauge. For instance, one can choose the comoving gauge, in which the individual relativistic corrections would contribute differently, but the sum is the same as in the conformal Newtonian gauge. Note, however, that the individual relativistic corrections in the comoving gauge would also diverge differently than in the conformal Newtonian gauge, so that the gauge invariance of the expression is not a sufficient condition.

By computing the total correlation, we have also shown that ignoring relativistic effects on top of the density fluctuation and the RSD would lead to a relative error that can reach the 8% for two galaxies at redshift $z = 1$ separated by 5 deg at the observer (see fig. 4.8). This means that one should use the relativistic expression to interpret future data from upcoming surveys on such large scales. The terms involving the gravitational potential (including Sachs-Wolf and Shapiro time-delay effects) have a negligible contribution to the amplitude, at least 5 orders of magnitude smaller then the (leading) density contribution, and can be ignored. This holds also when the luminosity distance is concerned, as in this case the potential contribution is much smaller than the (leading) velocity one. However, since the terms involving the gravitational potential are cut-off dependent in the infrared, one can neglect them numerically only when their role is understood and theoretically under control. Our work serves also this purpose, providing the correct description of all relativistic effects in the galaxy two-point correlation function.

Finally, we have calculated the correlations of individual relativistic corrections due to the primordial gravitational waves and their total contribution to the two-point galaxy correlation function. Since the galaxy number density is affected by gravitational waves via redshift and volume distortions, the two-point galaxy correlation function can be used as a probe for the primordial gravitational waves predicted by inflation. Unfortunately, tensor modes decay inside the horizon, so that their effect is only important at large scales and high redshifts. Consequently, the tensor contribution to the two-point galaxy correlation function is very small, in particular compared to the scalar contribution that grows in time. In our numerical study we have considered the configuration where both galaxies are at redshift $z = 1$ and the correlation is a function of the angular separation (see fig. 4.9). As expected, our results show that with a tensor-to-scalar ratio of 0.2 the tensor contribution is of order 10^{-12}, which is about eight or more orders of magnitude smaller than the scalar contribution, making it difficult to detect the primordial gravitational waves with galaxy clustering.

We have provided theoretical and numerical studies of the full relativistic two-point galaxy correlation function. A deep understanding of all theoretical subtleties in

the relativistic description of galaxy clustering is essential to interpret the numerous upcoming surveys. Indeed, only the correct theoretical prediction can lead us to the full realization of the cosmological potential of galaxy clustering enabled by precision measurements in future galaxy surveys.

Appendices

4.A ΛCDM solutions for scalar perturbations

At linear order, all Fourier modes grow at the same rate and the time dependence of the scalar perturbations in the conformal Newtonian gauge can be expressed in terms of the growth function D of the linear density fluctuation $\delta(a, \boldsymbol{x}) = D(a)\delta_+(\boldsymbol{x})$ and the curvature perturbation $\zeta(\boldsymbol{x})$ in the comoving gauge. From the conservation of energy and momentum in a ΛCDM universe, one derives the evolution equation for the linear growth function D as

$$\frac{d^2D}{da^2} + (2 - \Omega_m)\frac{3}{2a}\frac{dD}{da} - \frac{3}{2a^2}D = 0\,. \tag{4.91}$$

The analytic solution is well-known:

$$D(a) = a\,{}_2F_1\left[\frac{1}{3}, 1, \frac{11}{6}, -\frac{a^3}{\Omega_m}(1 - \Omega_m)\right], \tag{4.92}$$

where ${}_2F_1$ is the hypergeometric function and $\Omega_m = \Omega_m(a)$ is the matter density parameter.

Using the Einstein equations in the comoving gauge ($\gamma = v = 0\,,\ \varphi \equiv \zeta$), the perturbations can be expressed in terms of the spatial configuration $\delta_+(\boldsymbol{x})$ of the density contrast or the curvature perturbation $\zeta(\boldsymbol{x})$ as [115]

$$\begin{aligned} \zeta(\boldsymbol{x}) &= C\,\Delta^{-1}\,\delta_+(\boldsymbol{x})\,, \\ \beta(a, \boldsymbol{x}) &= \frac{C}{\mathcal{H}\,\Sigma}\,\Delta^{-1}\,\delta_+(\boldsymbol{x}) = \frac{1}{\mathcal{H}\Sigma}\,\zeta(\boldsymbol{x}) \equiv D_\beta(a)\zeta(\boldsymbol{x})\,, \end{aligned} \tag{4.93}$$

where we defined the time-dependent functions

$$D_\beta \equiv \frac{1}{\mathcal{H}\,\Sigma}\,, \qquad \Sigma \equiv 1+\frac{3}{2}\frac{\Omega_m}{f}\,, \qquad f \equiv \frac{d\,\ln D}{d\,\ln a}\,. \tag{4.94}$$

Since ζ is time-independent, C is a constant

$$C \equiv -f\,D\,\mathcal{H}^2\,\Sigma\,, \qquad D(a) \propto \frac{1}{\mathcal{H}^2 f\Sigma}\,, \tag{4.95}$$

and it becomes $C = -\frac{5}{2}\mathcal{H}_o^2\Omega_m$ in the Einstein-de Sitter universe.

The perturbation solutions in the conformal Newtonian gauge with no anisotropic pressure ($\beta = \gamma = 0\,,\ \alpha = -\varphi \equiv \Psi$) are obtained by transforming the solution in the comoving gauge. Given the gauge-transformations in sec. 4.2.1 one obtains $T = \beta$ and $L = 0$. Therefore, the perturbation variables in the conformal Newtonian gauge are related to the comoving gauge variables as

$$\begin{aligned} &\Psi = \frac{1}{a}(a\,\beta)', \qquad \Psi = -\mathcal{H}\beta - \zeta\,, \qquad v = -\beta\,, \\ &\delta\eta_o = -v_o\,, \qquad \delta x^i_o = -\int_0^{\bar\eta_o} d\bar\eta\, v^{,i}\,. \end{aligned} \tag{4.96}$$

These can be further written in terms of the curvature perturbation as

$$\begin{aligned} &\Psi(\eta,\boldsymbol{x}) = D_\Psi(\eta)\zeta(\boldsymbol{x})\,, \qquad v(\eta,\boldsymbol{x}) = -D_V(\eta)\zeta(\boldsymbol{x})\,, \\ &\delta\eta_o = D_{Vo}\,\zeta_o\,, \qquad \delta x^i_o = \left(\zeta^{,i}\right)_o \int_0^{\bar\eta_o} d\bar\eta\, D_V\,, \end{aligned} \tag{4.97}$$

where $D_\Psi = \mathcal{H}D_\beta - 1$ and $D_V = D_\beta$. By combining the above equations, we derive the relations

$$\begin{aligned} &D_\Psi = -\mathcal{H}D_V - D_V'\,, \qquad D_\Psi = -\frac{1}{2}(D_V'+1)\,, \qquad \int_0^{\bar r_z} d\bar r\, D_\Psi = \frac{1}{2}(D_V - D_{Vo} - \bar r_z)\,, \\ &D_V' + 2\,\mathcal{H}D_V - 1 = 0\,, \qquad D_\Psi' = \frac{\mathcal{H}'}{\mathcal{H}}(D_\Psi+1) - 2\,\mathcal{H}(D_\Psi+1) + \mathcal{H}\,. \end{aligned} \tag{4.98}$$

CHAPTER 5

Galaxy Power Spectrum in General Relativity

Preface

In this chapter, which is thoroughly based on the work that will be presented soon in [3], we continue our relativistic study of light-cone observables focusing on the last quantity of our interest: the galaxy power spectrum. By using the complete gauge-invariant expression for the galaxy number density derived in chapters 3 and 4, we present the anisotropic three-dimensional galaxy power spectrum accounting for all relativistic effects for the first time. As for the galaxy correlation function studied in the previous chapter, we demonstrate that, only when all contributions to the observed galaxy number density – the terms evaluated at the observer position, at the source and integrated along the line of sight distance between them – are taken into account, the galaxy power spectrum does not diverge on super-horizon scales. As a consequence, the previous calculations of the galaxy power spectrum that account only for the contributions at the source position are inconsistent with the equivalence principle and indeed exhibit an infrared divergence. This unphysical behavior on large scales vanishes if we consider all the relativistic contributions, so that there are no direct corrections to the measurements of the primordial non-Gaussianity from the relativistic effects in the power spectrum. In this chapter we present a novel approach to compute the power spectrum, which allows to consider all relativistic contributions in the derivation. This is possible only by noting the important difference between the power spectrum commonly derived in theory and what galaxy surveys measure in practice. As we explain, while the theoretical power spectrum is not observable, but is related to the observed power spectrum, there is no ambiguity in its computation. For

this reason, it offers a great opportunity to investigate, at theoretical level, the impact of relativistic effects on large scales, providing the perfect ground to test the validity of our predictions. We finally perform numerical computation of the galaxy power spectrum with focus on the deviations from the standard redshift-space prediction on large scales. Our results indicate that the relativistic effects should be included in future analyses.

Based on:

[3] F. Scaccabarozzi, J. Yoo, S. G. Biern and J. O. Gong,
"*Galaxy Power Spectrum in General Relativity*"
in preparation

Abstract. We present the anisotropic three-dimensional galaxy power spectrum in general relativity. Using a novel approach to computing the power spectrum, we derive the galaxy power spectrum, taking into account all the relativistic contributions of the observed galaxy number density fluctuation. We first demonstrate that the previous calculations of the power spectrum with an infrared divergence are inconsistent with the equivalence principle, and this unphysical behavior on large scales vanishes if we consider all the relativistic contributions. Consequently, there exists no direct corrections to the measurements of the primordial non-Gaussianity from the relativistic effects in the power spectrum. We then numerically compute the galaxy power spectrum with particular emphasis on the deviations from the standard redshift-space prediction on large scales. Our results show that the relativistic effects are indeed not negligible.

5.1 Introduction

The next generation of galaxy surveys [19, 20, 21, 22, 23, 24] is going to explore the large scale structure of the universe with unprecedented precision in their measurements and parameter estimation. By measuring the positions of millions of galaxies, these surveys will probe the distribution of galaxies at high redshifts on very large scales, where the relativistic effects are more important. In order to extract physical information from this map, different observables are computed, such as the galaxy correlation function and the galaxy power spectrum. However, most expressions of the galaxy number density used for the analysis only take into account matter density fluctuations and redshift-space distortions. These standard expressions provide an approximation to what we observe, which is not sufficiently accurate to interpret data from future surveys.

The impact of relativistic effects on the correlation function and the power spectrum has already been investigated by previous works. On the one hand, the galaxy correlation function can be derived directly in terms of observable quantities and its theoretical prediction, including all relativistic effects, has been recently presented in [2, 100, 114]. On the other hand, the galaxy power spectrum has difficulties in its expression, because the Fourier decomposition is non-local in nature. Nevertheless, there have been considerable theoretical efforts to obtain accurate theoretical predictions that accounts for the relativistic effects. First, the significance of the relativistic effects on large scales was investigated in the non-linear matter power spectrum [116, 117, 118]. These studies showed that the relativistic contributions are completely subdominant compared to the density fluctuations, so that Newtonian cosmology is enough to describe large-scale structure formation. However, these studies considered only the clustering of dark matter in the physical coordinate system, not the observable galaxies in the local coordinate system. Taking into account the kinematic Doppler effect in the context of special relativity, Kaiser [48] pioneered the study on the relation between the physical and observational coordinate systems, and presented the anisotropic galaxy power spectrum in the observational coordinates. By extending to general relativity, it was first shown in [70, 71] how to obtain systematically the gauge-invariant expression for the galaxy number density in the observational coordinate system. From that solution, the corresponding galaxy power spectrum was derived and its detection significance was quantified in [71, 83, 84]. However, because of the difficulties associated to the Fourier decomposition, these works ignored the relativistic effects at the observer position and along the line-of-sight direction.

Despite the fact the expression for the galaxy number density accounting for the relativistic effects only at the source position is gauge-invariant, the contributions at source position alone are not the full observable quantity. As a consequence, the galaxy power spectrum obtained in [71, 83, 84] using the incomplete expression diverges on super-horizon scales. In this chapter we show that, when all contributions that are neglected in previous works are taken into account, the expression is in agreement with the equivalence principle (see [2, 84, 101, 105]), and the infrared divergence cancels out. Most importantly, however, we demonstrate that the galaxy power spectrum commonly derived in theory (theoretical power spectrum) by taking a Fourier transformation of the observed galaxy fluctuation does not exactly represents what is observed in galaxy surveys. Indeed, in theory the Fourier transformation is defined on a hypersurface of simultaneity, while galaxy surveys observe the full light-cone within the survey volume. So far, this important distinction between the theoretical and observed galaxy power spectrum has been ignored, leading to confusion in its interpretation.

In this chapter, we first investigate the relation between the theoretical and observed galaxy power spectrum, providing the correct series of steps that allows one to obtain the correct prediction to analyze data. Then we focus on the derivation of the

theoretical power spectrum in general relativity. We present a simple method to compute the galaxy power spectrum from the variance of the density fluctuation, which allows to take into account all the relativistic effects, including those evaluated at the observer and along the line-of-sight direction. With this method, we derive the expression for the three-dimensional anisotropic galaxy power spectrum. As mentioned above, we show that when all terms are taken into account, the theoretical power spectrum is devoid of the infrared divergence claimed in previous works [71, 83, 84]. Furthermore, our numerical results show the correct behavior of the theoretical power spectrum on large scales, where the relativistic effects manifest themselves and cause deviations from the standard prediction given by Kaiser formula.

While a correct description of the relativistic effects is essential to understand the clustering of galaxies on large scales (from the theoretical point of view), in order to obtain the detection significance one has to compute the observed power spectrum. Obviously, a very large survey volume is needed to observe the impact of relativistic effects on the galaxy power spectrum. Here, we do two important steps towards that direction: first of all we clarify what is actually observed and provide the correct interpretation of the galaxy power spectrum commonly computed in theory, second of all we derive the correct theoretical expression considering all relativistic effects for the first time.

The organization of the chapter is as follows. First we introduce the expression for the observed galaxy fluctuation with all required ingredients in secs. 5.2.1 and 5.2.2. Then we discuss the distinction between the observed galaxy power spectrum and the theoretical one in sec. 5.2.3, providing the mathematical relation among the two quantities. We then study the theoretical power spectrum in sec. 5.3, where we derive its analytical expression (sec. 5.3.1) and discuss how the issue concerning the infrared divergence is resolved (sec. 5.3.2). In sec. 5.4 we compute the theoretical power spectrum numerically, first considering the full three-dimensional information but accounting only for the redshift-space distortions and the gravitational lensing (sec. 5.4.1), then accounting for all the relativistic effects but considering only the monopole, quadrupole and hexadecapole contributions (sec. 5.4.2). We conclude with a summary and discussion in sec. 5.5. In appendix 5.B we provide the expressions for the cross power spectra of different contributions to the galaxy fluctuation.

5.2 Preliminaries

In this section we first introduce the perturbation variables needed for the expression of the observed galaxy number density, with the solutions for their time evolution in ΛCDM. Next we present the gauge-invariant expression for the observed galaxy number density fluctuation, which will be referred to as the observed galaxy fluctuation. Finally, we define the "theory" Fourier modes of the observed galaxy fluctuation and

discuss the subtlety associated with them.

5.2.1 Metric convention and ΛCDM solutions for scalar perturbations

We adopt a spatially flat Friedmann-Robertson-Walker (FRW) metric for our theoretical description of the background universe. For an inhomogeneous universe, we consider only linear-order scalar perturbations and pressureless medium (dark matter and baryons on large scales). We choose the conformal Newtonian gauge:

$$ds^2 = -a^2(1+2\Psi)d\eta^2 + a^2(1-2\Psi)dx^2\,, \tag{5.1}$$

where η is the conformal time, x^i are the Cartesian coordinates, $a(\eta)$ is the scale factor and $\Psi(\eta, \boldsymbol{x})$ is the linear-order gravitational potential. In this space-time, the observer moves with time-like four-velocity $u^\mu \equiv a^{-1}(1-\Psi, V^i)$, where the spatial component can be expressed in terms of a scalar perturbation $v(\eta, \boldsymbol{x})$ as $V_i \equiv -\partial_i v$.

The observer identifies the position of a source galaxy by measuring the redshift z and the angular direction $\hat{\boldsymbol{n}}$ of the incoming photons. Given these quantities, the observed source position $x^\mu = (\bar{\eta}_z, \bar{r}_z \hat{n}^i)$ can be computed by using the distance-redshift relation in a homogeneous universe,

$$\bar{r}_z = \bar{\eta}_o - \bar{\eta}_z = \int_0^z \frac{dz'}{H(z')}\,, \tag{5.2}$$

where H is the Hubble parameter and a bar denotes that the coordinates are computed in the background universe at the observer (o) and the source (at redshift z) positions. However, the real position of the source galaxy is different from the one inferred in the background universe, because the photon propagation is affected by the inhomogeneities.

Before introducing the theoretical prediction for the galaxy number density we need the ΛCDM solutions for the scalar perturbations that enter the expression. In a universe with pressureless medium, all Fourier modes at linear order grow at the same rate and the time dependence of the scalar perturbations in the conformal Newtonian gauge can be expressed in terms of the growth function D of the matter density contrast $\delta_m(\eta, \boldsymbol{x}) = D(\eta)/D(\eta_0)\delta(\boldsymbol{x})$, where $\delta(\boldsymbol{x})$ is the spatial configuration at the present time. Using the conservation of energy and momentum in a ΛCDM universe, one can derive the evolution equation for the linear growth function $D(\eta)$

$$\frac{d^2D}{da^2} + (2-\Omega_m)\frac{3}{2a}\frac{dD}{da} - \frac{3}{2a^2}D = 0\,, \tag{5.3}$$

and the solution is

$$D(a) \propto a\,{}_2F_1\left[\frac{1}{3}, 1, \frac{11}{6}, -\frac{a^3}{\Omega_m}(1-\Omega_m)\right], \tag{5.4}$$

where ${}_2F_1$ is the hypergeometric function and $\Omega_m = \Omega_m(a)$ is the matter density parameter. Furthermore, all the perturbations can be expressed in terms of the initial curvature perturbation $\zeta(\boldsymbol{x})$ in the comoving gauge as [115]

$$\Psi(\eta, \boldsymbol{x}) = D_\Psi(\eta)\zeta(\boldsymbol{x})\,, \quad v(\eta, \boldsymbol{x}) = -D_V(\eta)\zeta(\boldsymbol{x})\,, \quad V_i(\eta, \boldsymbol{x}) = D_V(\eta)\partial_i\zeta(\boldsymbol{x})\,, \tag{5.5}$$

where the time-dependent growth functions D_Ψ and D_V are related to D through

$$D_\Psi = \frac{1-\Sigma}{\Sigma}\,, \qquad D_V = \frac{1}{aH\Sigma}\,, \qquad \Sigma \equiv 1 + \frac{3}{2}\frac{\Omega_m}{f}\,, \qquad f \equiv \frac{d\ln D}{d\ln a}\,. \tag{5.6}$$

Furthermore, D_Ψ and D_V satisfy the following equations

$$D_\Psi = \mathcal{H}D_V - 1 = -\mathcal{H}D_V - D_V' = -\frac{1}{2}(D_V' + 1)\,, \qquad \int_0^{\bar{r}_z} d\bar{r}\, D_\Psi = \frac{1}{2}(D_V - D_{Vo} - \bar{r}_z)\,, \tag{5.7}$$

where $\mathcal{H} = aH$ is the conformal Hubble parameter and a prime denotes the derivative with respect to conformal time. Finally, the relation between the spatial configuration $\delta(\boldsymbol{x})$ of the density contrast and the curvature perturbation $\zeta(\boldsymbol{x})$ is given by

$$\zeta(\boldsymbol{x}) = C\Delta^{-1}\delta(\boldsymbol{x})\,. \tag{5.8}$$

Since ζ is time-independent, $C \equiv -\mathcal{H}^2\Sigma f D/D_0$ is a constant, i.e. $D \propto 1/(\mathcal{H}^2\Sigma f)$. As a consequence, one can use the solution $C = -5H_o^2/2$ derived in the simple case of the Einstein-de Sitter universe.

5.2.2 Observed galaxy number density

The observed galaxy number density n_g is obtained by counting the number of galaxies within the observed volume, which is the volume in a homogeneous universe within the observed redshift interval and the observed solid angle. However, in the presence of inhomogeneities in the universe, the observed volume does not correspond to the physical one occupied by the observed galaxies. Such difference contributes to the fluctuation δ_g in the galaxy number density that can be described as $n_g \equiv \bar{n}_g(\bar{\eta}_z)(1+\delta_g)$, where $\bar{n}_g$ is the mean density. Since the galaxy number density is a physical observable, the theoretical expression of δ_g, derived as a function of the observed redshift and angles, is gauge-invariant [70, 71, 103, 104, 84].

We split the expression of the observed galaxy fluctuation into the local contributions evaluated at the source (s) and the observer (o) positions, and the non-local (nl) contributions: $\delta_g(z, \hat{\boldsymbol{n}}) = \delta_s(z, \hat{\boldsymbol{n}}) + \delta_o(z, \hat{\boldsymbol{n}}) + \delta_{nl}(z, \hat{\boldsymbol{n}})$, where we use the term "non-local" to refer to the contributions arising from the line-of-sight integration as opposed to those at the observer or the source positions. Written as a function of the observed

redshift and angles, the expression in the conformal Newtonian gauge is given by

$$\delta_s = b\delta_m - e\mathcal{H}v + \big[4 - h(z)\big](V_\parallel - \Psi) - \frac{1}{\mathcal{H}}(\partial_\parallel V_\parallel - V_\parallel' - \partial_\parallel \Psi - \Psi')\,, \tag{5.9}$$

$$\delta_o = -\left[3 - h(z) + \frac{2}{\bar{r}_z \mathcal{H}_o}\right]\mathcal{H}_o v_o + \big[3 - h(z)\big]\Psi_o + \big[h(z) - 1\big]V_{\parallel o}\,, \tag{5.10}$$

$$\delta_{nl} = \int_0^{\bar{r}_z} d\bar{r}\left[\frac{4}{\bar{r}_z}\Psi + 2\big[h(z) - 3\big]\Psi' - 2\left(\frac{\bar{r}_z - \bar{r}}{\bar{r}_z \bar{r}}\right)\hat{\nabla}^2\Psi\right], \tag{5.11}$$

where b is the galaxy bias, δ_m is the matter density contrast in the comoving gauge, $e \equiv d\ln\bar{n}_g/d\ln(1+z)$ is the evolution bias, $V_\parallel \equiv \hat{n}^i V_i$ is the line-of-sight velocity, $\partial_\parallel \equiv \hat{n}^i\partial_i$ is the derivative along the line of sight, $\hat{\nabla}^2$ is the angular Laplacian, related to the 3D Laplacian $\hat{\nabla}^2 = \bar{r}^2\Delta - 2\bar{r}\,\partial_{\bar{r}} - \bar{r}^2\partial_{\bar{r}}^2$, $\bar{r}$ is the radial coordinate, corresponding to the comoving distance and finally we defined the redshift-dependent function $h(z) \equiv e + \mathcal{H}'/\mathcal{H}^2 + 2/(\bar{r}_z\mathcal{H})$ for compactness.[1]

Using the relations in eqs. (5.5)–(5.8), we can re-arrange the three contributions δ_s, δ_o, δ_{nl} to the observed galaxy fluctuation as

$$\delta_s(z,\hat{\boldsymbol{n}}) = \int \frac{d^3k}{(2\pi)^3} e^{ik\bar{r}_z\mu_k}\left\{bD + \mathcal{A}\,\frac{1}{k^2} + \mathcal{B}\,\frac{i\,\mu_k}{k} + \mathcal{C}\,\mu_k^2\right\}\delta(\boldsymbol{k})\,, \tag{5.12}$$

$$\delta_o(z,\hat{\boldsymbol{n}}) = \int \frac{d^3k}{(2\pi)^3}\left\{\mathcal{D}\frac{1}{k^2} + \mathcal{E}\frac{i\,\mu_k}{k}\right\}\delta(\boldsymbol{k})\,, \tag{5.13}$$

$$\delta_{nl}(z,\hat{\boldsymbol{n}}) = \int \frac{d^3k}{(2\pi)^3}\int_0^{\bar{r}_z} d\bar{r}\, e^{ik\bar{r}\mu_k}\left\{\mathcal{F}(\bar{r})\frac{1}{k^2} + \mathcal{G}(\bar{r})\,\frac{i\,\mu_k}{k} + \mathcal{I}(\bar{r})\,(1-\mu_k^2)\right\}\delta(\boldsymbol{k})\,, \tag{5.14}$$

where $\mu_k \equiv \hat{\boldsymbol{k}}\cdot\hat{\boldsymbol{n}}$ and we defined the following functions of time (or redshift)

$$\mathcal{A} \equiv \left(-2\,[h-3]\mathcal{H}D_V + \frac{2}{\bar{r}_z}D_V - 5 + h\right)C\,, \qquad \mathcal{B} \equiv \big[h-3\big]D_V C\,, \qquad \mathcal{C} \equiv Df\,, \tag{5.15}$$

$$\mathcal{D} \equiv \left([3-h](1-2\mathcal{H}_o D_{Vo}) - \frac{2}{\bar{r}_z}D_{Vo}\right)C\,, \qquad \mathcal{E} \equiv -\big[h-1\big]D_{Vo}C\,, \tag{5.16}$$

$$\mathcal{F}(\bar{r}) \equiv \left(-\frac{4}{\bar{r}_z}D_\Psi(\bar{r}) - 2\big[h-3\big]D_\Psi'(\bar{r})\right)C\,, \quad \mathcal{G}(\bar{r}) \equiv -4\left(\frac{\bar{r}_z - \bar{r}}{\bar{r}_z}\right)D_\Psi(\bar{r})C \equiv \frac{2}{\bar{r}}\mathcal{I}(\bar{r})\,. \tag{5.17}$$

Note that these functions depend on redshift through their dependence on h, $\mathcal{H}$, $\bar{r}_z$, D_V, D and f. Finally, we also used the symmetry in $\boldsymbol{k}$ directions to derive $\hat{\nabla}^2 e^{ik\bar{r}\,\mu_k} = -k\bar{r}\big[2i\mu_k + k\bar{r}(1-\mu_k^2)\big]e^{ik\bar{r}\mu_k}$ in the line-of-sight contribution.

[1] Note that the definition of $h(z)$ here corresponds to $3 - h(z)$ with $h(z)$ defined as in [2], where the evolution bias e is instead called e_z.

As we shall see in sec. 5.3.1, the expressions in eqs. (5.12)–(5.14) are more practical to compute the power spectra of different contributions to the observed galaxy fluctuation. We will derive the galaxy power spectrum as the sum of such contributions and also show that there is no divergence on large scales.

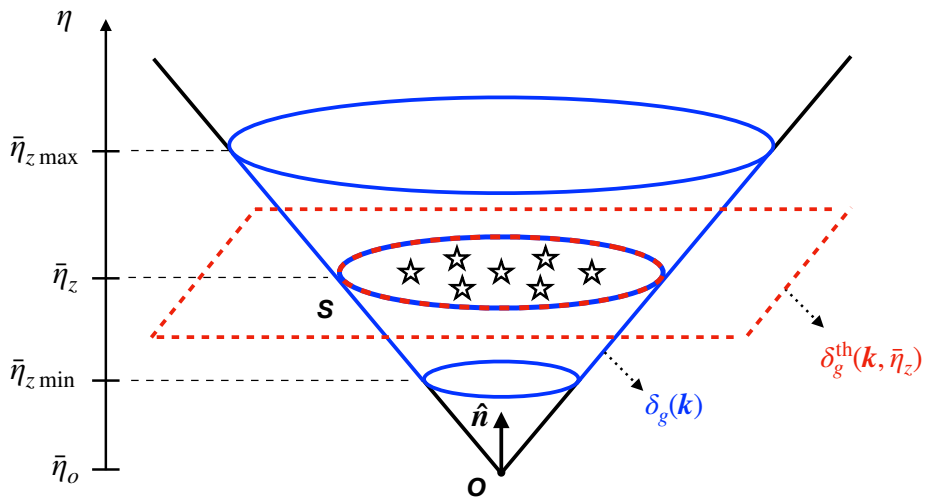

Figure 5.1: Sketch of the observational light-cone volume and the hypersurface of simultaneity. The observer is located at the background time coordinate $\bar{\eta}_o$, and we consider the source field at one (observed) redshift slice z (time coordinate $\bar{\eta}_z$). The (survey) light-cone volume drawn in blue corresponds to the observed hypersurface on which the observed Fourier mode $\delta_g(\boldsymbol{k})$ of $\delta_g(\boldsymbol{x}_{\rm obs})$ is defined. The (spatially infinite) hypersurface of simultaneity at the source redshift drawn in red, in which the theory Fourier modes $\delta_g^{\rm th}(\boldsymbol{k}; \bar{\eta}_z)$ of $\delta_g(\boldsymbol{x}_{\rm obs})$ are defined. Note that the intersection with the light-cone is the only part of the hypersurface of simultaneity to which we have access in observation. We assume that the survey ranges over redshift $z \in [z_{\rm min}, z_{\rm max}]$.

5.2.3 Theory Fourier mode and theory power spectrum

In this section we discuss the relation between the *theory* power spectrum that we compute in sec. 5.3 and the *observed* power spectrum measured in galaxy surveys. As we shall see, the key difference between the two quantities is the hypersurface of simultaneity. The theory power spectrum is defined in a hypersurface of simultaneity shown as red dotted in Figure 5.1, while the observed hypersurface of simultaneity is given by the past light-cone volume within the survey boundary shown as blue solid in Figure 5.1. The observers treat the (survey) light-cone volume as a hypersurface of simultaneity and compute the (observed) power spectrum in this hypersurface. A schematic illustration is presented in Figure 5.1.

In the survey light-cone volume V, the observed Fourier mode $\delta_g(\boldsymbol{k})$ can be obtained by simply taking a Fourier transformation of the observed galaxy fluctuation $\delta_g(\boldsymbol{x}_{\rm obs})$

on V, as though the volume is a hypersurface of simultaneity, as

$$\delta_g(\boldsymbol{k}) \equiv \int_V d^3x_{\rm obs}\ e^{-i\boldsymbol{k}\cdot\boldsymbol{x}_{\rm obs}}\delta_g(\boldsymbol{x}_{\rm obs})\ , \tag{5.18}$$

while the theory Fourier mode $\delta_g^{\rm th}(\boldsymbol{k};\eta_z)$ is defined in a hypersurface set by the observed redshift z as

$$\delta_g(\boldsymbol{x}_{\rm obs}) = \int \frac{d^3k}{(2\pi)^3}\ e^{i\boldsymbol{k}\cdot\boldsymbol{x}_{\rm obs}}\delta_g^{\rm th}(\boldsymbol{k};\bar\eta_z)\ , \tag{5.19}$$

where the observed position on the light cone is in a FRW coordinate

$$\boldsymbol{x}_{\rm obs} \equiv \bar r_z\hat{\boldsymbol{n}}\ . \tag{5.20}$$

The former is literally a Fourier transformation of the field $\delta_g(\boldsymbol{x}_{\rm obs})$ in a volume V, under the assumption that the volume V is a hypersurface of simultaneity, and the observers use this quantity to compute the observed power spectrum. On the other hand, the theory Fourier mode is defined in a hypersurface of simultaneity, regardless of observational accessibility. In general, the theory Fourier mode, such as the matter density $\delta_m(\boldsymbol{k};\eta)$, the peculiar velocity $V_i(\boldsymbol{k};\eta)$ and the gravitational potential $\Psi(\boldsymbol{k};\eta)$, is evolved, according to the solutions of the Einstein equation in sec. 5.2.1, given the initial conditions such as the comoving-gauge curvature perturbation $\zeta(\boldsymbol{k};\eta_i)$ at the initial time η_i. Consequently, these (theory) Fourier modes depend on the hypersurface set by the time coordinate η, as evident in the solutions of the time-dependent growth functions in sec. 5.2.1. In particular, we are interested in the theory Fourier mode $\delta_g^{\rm th}(\boldsymbol{k};\bar\eta_z)$ that is defined in the hypersurface set by the observed redshift z (time coordinate $\bar\eta_z$) and that gives the observed galaxy fluctuation $\delta_g(\boldsymbol{x}_{\rm obs})$ at the intersection $\boldsymbol{x}_{\rm obs}$ of the hypersurface and the survey light-cone volume.

A few more words are in order. First, the hypersurface of our interest is set by the observed redshift z only, independent of the observed angle $\hat{\boldsymbol{n}}$. Second, the fluctuation field $\delta_g(\boldsymbol{x};\bar\eta_z)$ defined in terms of the theory Fourier mode, similar to Eq. (5.19),

$$\delta_g(\boldsymbol{x};\bar\eta_z) = \int \frac{d^3k}{(2\pi)^3}\ e^{i\boldsymbol{k}\cdot\boldsymbol{x}}\delta_g^{\rm th}(\boldsymbol{k};\bar\eta_z) \tag{5.21}$$

is well-defined at all spatial position $\boldsymbol{x}$ in the hypersurface set by the observed redshift z, and it coincides with $\delta_g(\boldsymbol{x}_{\rm obs})$ in eq. (5.19) when $\boldsymbol{x} = \boldsymbol{x}_{\rm obs}$. One subtlety is that since the theoretical description of the observed galaxy fluctuation involves the observed angular position $\hat{\boldsymbol{n}}$, the theory Fourier mode $\delta_g^{\rm th}(\boldsymbol{k};\bar\eta_z)$ and the fluctuation $\delta_g(\boldsymbol{x};\bar\eta_z)$ in the hypersurface are fully specified, only if one observed position $\boldsymbol{x}_{\rm obs}$ within the survey is chosen. The theory Fourier mode is indeed the Fourier transformation of the fluctuation field $\delta_g(\boldsymbol{x};\bar\eta_z)$

$$\delta_g^{\rm th}(\boldsymbol{k};\bar\eta_z) = \int d^3x\ e^{-i\boldsymbol{k}\cdot\boldsymbol{x}}\delta_g(\boldsymbol{x};\bar\eta_z)\ , \tag{5.22}$$

where the spatial integration is over the infinite hypersurface of simultaneity. Last, we will be interested in the power spectrum of the theory Fourier mode (or the theory power spectrum) in the hypersurface. Consequently, the theory power spectrum is *not* a direct observable, but related to the observed power spectrum. More importantly, as we show in section 5.3, it is *more* suitable for theoretical investigations of the observed galaxy fluctuation in Fourier space, independent of the specifications of the survey geometry, which complicates the observed power spectrum.

The observed Fourier mode can be related to the theory Fourier mode as

$$\begin{aligned}\delta_g(\boldsymbol{k}) &\equiv \int_V d^3x_{\rm obs}\, e^{-i\boldsymbol{k}\cdot\boldsymbol{x}_{\rm obs}}\delta_g(\boldsymbol{x}_{\rm obs}) = \int_V d^3x_{\rm obs}\, e^{-i\boldsymbol{k}\cdot\boldsymbol{x}_{\rm obs}} \int \frac{d^3k'}{(2\pi)^3} e^{i\boldsymbol{k}'\cdot\boldsymbol{x}_{\rm obs}}\delta_g^{\rm th}(\boldsymbol{k}';\bar{\eta}_z) \\ &= \int \frac{d^3k'}{(2\pi)^3}\int_V d^3x_{\rm obs}\, e^{i(\boldsymbol{k}'-\boldsymbol{k})\cdot\boldsymbol{x}_{\rm obs}}\delta_g^{\rm th}(\boldsymbol{k}';\bar{\eta}_z)\,.\end{aligned} \tag{5.23}$$

Due to the time-dependence (or the hypersurface), the theory Fourier mode cannot be pulled out of the integration over the light-cone volume V. Only if the survey volume is shallow in redshift depth, it can be pulled out of the integration, and the volume integration can be approximated as a Dirac delta function to yield $\delta_g(\boldsymbol{k}) \approx \delta_g^{\rm th}(\boldsymbol{k};\bar{\eta}_z)$. In general, the observed Fourier mode is a convolution of the theory Fourier mode over multiple hypersurfaces set by the redshift range of the survey and also the survey geometry encoded in the integration range V. The observed power spectrum is then related to the theory power spectrum as

$$\begin{aligned}\langle\delta_g(\boldsymbol{k}_1)\delta_g^*(\boldsymbol{k}_2)\rangle &= \int\frac{d^3k}{(2\pi)^3}\int\frac{d^3k'}{(2\pi)^3}\int_{V_1}d^3x_1\int_{V_2}d^3x_2\, e^{i(\boldsymbol{k}-\boldsymbol{k}_1)\cdot\boldsymbol{x}_1}e^{-i(\boldsymbol{k}'-\boldsymbol{k}_2)\cdot\boldsymbol{x}_2} \\ &\quad\times\langle\delta_g^{\rm th}(\boldsymbol{k};\bar{\eta}_1)\delta_g^{\rm th\,*}(\boldsymbol{k}';\bar{\eta}_2)\rangle \\ &= \int\frac{d^3k}{(2\pi)^3}\int_{V_1}d^3x_1\int_{V_2}d^3x_2\, e^{i\boldsymbol{k}\cdot(\boldsymbol{x}_1-\boldsymbol{x}_2)}e^{-i(\boldsymbol{k}_1\cdot\boldsymbol{x}_1-\boldsymbol{k}_2\cdot\boldsymbol{x}_2)}P_{\rm th}(\boldsymbol{k};\bar{\eta}_1,\bar{\eta}_2)\,,\end{aligned} \tag{5.24}$$

where we used

$$\langle\delta_g^{\rm th}(\boldsymbol{k};\bar{\eta}_1)\delta_g^{\rm th\,*}(\boldsymbol{k}';\bar{\eta}_2)\rangle \equiv (2\pi)^3\delta^D(\boldsymbol{k}-\boldsymbol{k}')P_{\rm th}(\boldsymbol{k},\bar{\eta}_1,\bar{\eta}_2)\,. \tag{5.25}$$

Throughout the chapter, our primary focus is the theory power spectrum in a hypersurface of simultaneity shown as red dotted in Figure 5.1, and we defer the investigation of the observed power spectrum to a future work.

Since the theory Fourier mode is defined in terms of the observed position $\boldsymbol{x}_{\rm obs}$, the theory power spectrum of our interest is also defined in terms of *one* observed position $\boldsymbol{x}_{\rm obs}$, and with eq. (5.19) it can be readily obtained by considering the variance of the observed galaxy fluctuation as

$$\sigma_g^2(\boldsymbol{x}_{\rm obs}) \equiv \langle\delta_g(z,\hat{\boldsymbol{n}})\delta_g^*(z,\hat{\boldsymbol{n}})\rangle = \int\frac{d^3k}{(2\pi)^3}P_{\rm th}(\boldsymbol{k};\bar{\eta}_z)\,. \tag{5.26}$$

Given the expression of the observed galaxy fluctuation in eqs. (5.12)–(5.14), we can compute the variance at a given observed position $\boldsymbol{x}_{\rm obs}$ and simply read off the theory power spectrum defined in the hypersurface set by $\bar{\eta}_z$. As demonstrated in section 5.3, this theory power spectrum is closely related to the theoretical expectations such as the redshift-space distortion, but without the need to make assumptions like the distant observer approximation. Furthermore, since it is defined in terms of one observed point, there is *no* ambiguity involving two points such as the wide angle effect (see [119]).

5.3 Power Spectrum for the Observed Galaxy Number Density

In this section we compute the theory power spectrum of the galaxy fluctuation accounting for all general relativistic effects. We first compute the theory power spectra of the contributions δ_s, δ_o and δ_{nl}, by using the method described in sec. 5.2.3. We then discuss the issue of infrared divergences in the individual contributions, explaining how and why they cancel out in the galaxy power spectrum. The final expression will be used to compute numerically the galaxy power spectrum in sec. 5.4. Since we deal only with the theory power spectrum, from now on we refer to that when saying power spectrum.

5.3.1 Individual contributions to the power spectrum

Following the method described in sec. 5.2.3, the full relativistic galaxy power spectrum $P_g^{\rm th}$ is obtained by computing the variance of the galaxy fluctuation δ_g,

$$\sigma_g^2(\boldsymbol{x}_{\rm obs}) \equiv \langle \delta_g(z,\hat{\boldsymbol{n}})\delta_g^*(z,\hat{\boldsymbol{n}})\rangle = \int \frac{d^3k}{(2\pi)^3} P_g^{\rm th}(z,\boldsymbol{k})\,. \tag{5.27}$$

Since the galaxy fluctuation is given by the sum of the local and non-local contributions as $\delta_g = \delta_s + \delta_o + \delta_{nl}$, the galaxy power spectrum can be written as the sum of their power spectra

$$P_g^{\rm th} \equiv P_s + P_o + P_{nl} + 2\,P_{s\text{-}o} + 2\,P_{s\text{-}nl} + 2\,P_{o\text{-}nl}\,, \tag{5.28}$$

where the individual power spectrum $P_{a\text{-}b}$ is defined as in eq. (5.27) but in terms of $[\langle \delta_a\delta_b^*\rangle + \langle \delta_b\delta_a^*\rangle]/2$ and $P_a \equiv P_{a\text{-}a}$. All the power spectra are evaluated at the obseved redshift z and the wavevector $\boldsymbol{k}$. Note that the splitting of P_g as in eq. (5.28) is gauge-dependent, as it simply follows from the decomposition of δ_g into the local and non-local contributions. However, such decomposition is convenient to compare the complete prediction P_g with the previous work in literature. For example, the power spectrum computed in [71, 83, 84] corresponds to P_s, as we show below.

First we compute the power spectrum P_s of the fluctuation δ_s at the source position and compare it with the result presented in [84, 83]. The variance of δ_s can be directly derived starting from eq. (5.12). We obtain

$$\sigma_s^2(\boldsymbol{x}_{\rm obs}) = \langle \delta_s(z,\hat{\boldsymbol{n}})\delta_s^*(z,\hat{\boldsymbol{n}})\rangle = \int \frac{d^3k}{(2\pi)^3}\Big[\big(b^2D^2 + 2bD\mathcal{C}\mu_k^2 + \mathcal{C}^2\mu_k^4\big) + \big(2bD\mathcal{A} + 2\mathcal{A}\mathcal{C}\mu_k^2 + \mathcal{B}^2\mu_k^2\big)\frac{1}{k^2} + \mathcal{A}^2\frac{1}{k^4}\Big]P_m(k)\,, \tag{5.29}$$

where P_m is the matter power spectrum at redshift zero defined by[2]

$$\langle \delta_m^{\rm th}(\boldsymbol{k};\bar{\eta}_o)\delta_m^{\rm th\,*}(\boldsymbol{k}';\bar{\eta}_o)\rangle \equiv (2\pi)^3\delta^D(\boldsymbol{k}-\boldsymbol{k}')P_m(k)\,.$$

The corresponding power spectrum can now be read off as

$$P_s(z,\boldsymbol{k}) = P_z(z,\boldsymbol{k}) + \Big[\big(2bD\mathcal{A} + 2\mathcal{A}\mathcal{C}\mu_k^2 + \mathcal{B}^2\mu_k^2\big)\frac{1}{k^2} + \mathcal{A}^2\frac{1}{k^4}\Big]P_m(k)\,, \tag{5.30}$$

where we introduced the standard redshift-space power spectrum [48]

$$P_z(z,\boldsymbol{k}) \equiv \big[b^2 + 2bf\mu_k^2 + f^2\mu_k^4\big]D^2P_m(k)\,. \tag{5.31}$$

This result is in agreement with that found in [84, 83]. The contribution at the source to the power spectrum consists of the redshift-space power spectrum P_z and the general relativistic effects, corresponding to the terms in the square brackets that are proportional to $k^{-2}P_m(k)$ and $k^{-4}P_m(k)$. We already notice the advantage of the theory power spectrum: the redshift-space power spectrum is naturally obtained in our theory power spectrum, without adopting the distant observer approximation, which is necessary to obtain the the redshift-space power spectrum in the observed power spectrum, in addition to other approximations such as no z-evolution. Interestingly, since $P_m(k) \propto k^{n_s}$, with the spectral index $n_s \approx 0.96$, these relativistic corrections diverge when k goes to zero. As a result, P_s is infrared-divergent, as already pointed out in [84, 83]. As we will discuss in sec. 5.3.2, such infrared divergence is not physical, as the source contribution P_s alone is not an observable and the equivalence principle is violated in its expression.

Only the expression for the total power spectrum $P_g^{\rm th}$ is consistent with the equivalence principle, because it is related to the observed power spectrum through eq. (5.77). As we have already mentioned, the splitting of $P_g^{\rm th}$ is for convenience and the individual contributions are not by themseleves physical quantities. Nevertheless, considering

[2] The theory Fourier modes $\delta_m^{\rm th}(\boldsymbol{k};\bar{\eta}_z)$ of the matter density fluctuation $\delta_m(z,\hat{\boldsymbol{n}})$ at redshift z are defined as $\delta_m(\boldsymbol{x}_{\rm obs}) = \int \frac{d^3k}{(2\pi)^3}e^{i\boldsymbol{k}\cdot\boldsymbol{x}_{\rm obs}}\delta_m^{\rm th}(\boldsymbol{k};\bar{\eta}_z)$. The quantity $P_m(k)$ corresponds the matter power spectrum computed by Boltzmann codes such as `CLASS` or `CAMB`.

the contributions individually can be useful to understand their importance on different scales for $P_g^{\rm th}$. With the expression for P_s at hand, we now derive the remaining contributions. We expect the remaining expressions to contain terms proportional to $k^{-2}P_m(k)$ and $k^{-4}P_m(k)$ that eventually cancel those in P_s when summed all together. In addition, there can be terms proportional to $P_m(k)$ (non-divergent terms) that would result in a deviation from the prediction P_z of the redshift-space distortions. As we will show, such deviations occur on large scales and they are redshift-dependent. Using the same method applied to obtain P_s, we derive the power spectrum at the observer position and the power spectrum of the non-local contributions:

$$P_o(z,\boldsymbol{k}) = \left[\mathcal{D}^2\frac{1}{k^4} + \mathcal{E}^2\mu_k^2\frac{1}{k^2}\right]P_m(k)\,, \tag{5.32}$$

$$P_{nl}(z,\boldsymbol{k}) = \int_0^{\bar{r}_z} d\bar{r}_1 d\bar{r}_2\, e^{ik\Delta r\mu_k}\left[\mathcal{F}_1\mathcal{F}_2\frac{1}{k^4} + 2\mathcal{F}_1\mathcal{I}_2\frac{1-\mu_k^2}{k^2} + \mathcal{G}_1\mathcal{G}_2\frac{\mu_k^2}{k^2} + \mathcal{I}_1\mathcal{I}_2\big(1-\mu_k^2\big)^2\right]P_m(k)\,, \tag{5.33}$$

where we defined $\int_0^{\bar{r}_z} d\bar{r}_1 d\bar{r}_2 \equiv \int_0^{\bar{r}_z} d\bar{r}_1 \int_0^{\bar{r}_z} d\bar{r}_2$, $\Delta r \equiv \bar{r}_1 - \bar{r}_2$ and $\mathcal{X}_i \equiv \mathcal{X}(\bar{r}_i)$ for $\mathcal{X} \equiv \mathcal{F}, \mathcal{G}, \mathcal{I}$.

The above expressions can be expanded into angular multipoles in terms of the Legendre polynomials $L_\ell(\mu_k)$ as $P(z,\boldsymbol{k}) \equiv \sum_{\ell=0}^{\infty} L_\ell(\mu_k)P_\ell(z,k)$. We obtain

$$\begin{aligned} P_s(z,\boldsymbol{k}) &= P_z(z,\boldsymbol{k}) \\ &\quad + \left\{\mathcal{A}^2 L_0\frac{1}{k^4} + \left[2\left(bD\mathcal{A} + \frac{2}{3}\mathcal{A}\mathcal{C} + \frac{1}{3}\mathcal{B}^2\right)L_0 + \frac{2}{3}(2\mathcal{A}\mathcal{C} + \mathcal{B}^2)L_2\right]\frac{1}{k^2}\right\}P_m(k)\,, \end{aligned} \tag{5.34}$$

$$P_z(z,\boldsymbol{k}) = \left[\left(b^2 + \frac{2}{3}bf + \frac{1}{5}f^2\right)L_0 + \left(\frac{4}{3}bf + \frac{4}{7}f^2\right)L_2 + \frac{8}{35}f^2 L_4\right]D^2 P_m(k)\,. \tag{5.35}$$

$$P_o(z,\boldsymbol{k}) = \left[\mathcal{D}^2 L_0\frac{1}{k^4} + \frac{2}{3}\mathcal{E}^2[L_0 + L_2]\frac{1}{k^2}\right]P_m(k)\,, \tag{5.36}$$

$$\begin{aligned} P_{nl}(z,\boldsymbol{k}) &= \sum_{n=0}^{\infty}(-1)^n(4n+1)L_{2n}\int_0^{\bar{r}_z} d\bar{r}_1 d\bar{r}_2\left[\mathcal{F}_1\mathcal{F}_2\frac{1}{k^4}j_{2n}(\Delta x) - \mathcal{G}_1\mathcal{G}_2\frac{1}{k^2}j_{2n}''(\Delta x)\right. \\ &\left. +2\mathcal{F}_1\mathcal{I}_2\frac{1}{k^2}\big[j_{2n}(\Delta x) + j_{2n}''(\Delta x)\big] + \mathcal{I}_1\mathcal{I}_2\big[j_{2n}(\Delta x) + 2j_{2n}''(\Delta x) + j_{2n}''''(\Delta x)\big]\right]P_m(k)\,, \end{aligned} \tag{5.37}$$

where the Legendre polynomials are functions of μ_k and we defined $\Delta x \equiv k\Delta r$. Furthermore, we used the following relations

$$\begin{aligned} \mu_k^2 &= \frac{2}{3}[L_0(\mu_k) + L_2(\mu_k)]\,, & \mu_k^4 &= \frac{1}{35}[17L_0(\mu_k) + 20L_2(\mu_k) + 8L_4(\mu_k)]\,, \\ e^{iy\mu_k} &= \sum_{\ell=0}^{\infty} i^\ell(2\ell+1)j_\ell(y)L_\ell(\mu_k)\,, & \mu_k^2\, e^{iy\mu_k} &= -\sum_{\ell=0}^{\infty} i^\ell(2\ell+1)j_\ell''(y)L_\ell(\mu_k)\,, \end{aligned} \tag{5.38}$$

where $j_\ell(y)$ are the spherical Bessel functions and $j'_\ell(y) \equiv \partial_y j_\ell(y)$. The cross power spectra $P_{s\text{-}o}$, $P_{s\text{-}nl}$, $P_{o\text{-}nl}$ of δ_s, δ_o and δ_{nl} are derived in the same way and their expressions are presented in appendix 5.B. The redshift-space power spectrum in eq. (5.35) shows the usual decomposition into the monopole, quadrupole and hexadecapole. However, the non-local contribution from the line-of-sight integration gives rise to the contributions at all even multipoles $\ell = 0, 2, 4, 6, 8, \ldots$ (odd multipoles vanish due to the symmetry associated with one line-of-sight direction $\hat{\boldsymbol{n}}$). The results in eqs. (5.34)–(5.37) and (5.78)–(5.80) provide the complete analytical expression for the fully relativistic power spectrum of the observed galaxy fluctuation.

5.3.2 Infrared divergences and cancellation

The gauge invariance and the equivalence principle of general relativity offer a unique way to test the validity of the theoretical predictions for the observed galaxy fluctuation δ_g and its (theoretical) power spectrum. It was shown [2, 72] that the expression of the galaxy fluctuation in eqs. (5.9)–(5.11) is gauge-invariant and compatible with the equivalence principle. In particular, by isolating the contributions from a uniform gravitational field in the perturbations, it was shown that the expression is devoid of the corresponding terms. Besides confirming the derivations of [72], it was shown that the expression does not exhibit any infrared divergence on super horizon-scales, as demonstrated in [101, 106].

The equivalence principle states that a gravitational field is equivalent to the corresponding acceleration of the reference system. It implies that the laws of physics in a reference frame that is in free fall are the same as in the complete absence of gravity. This means that a uniform gravitational field has no effect on observations. In the case of our interest, where the source and the observer are on the past light-cone separated by the (comoving) distance $\bar{r}_z$, any perturbation with wavelength larger than $\bar{r}_z$ behaves like a uniform gravitational field. We refer to such modes as long-mode perturbations, which should not affect any observable. Indeed, these modes produce unphysical infrared divergences and it is important to check that their contributions cancel out in the expressions. In this section, we revisit these issues in the power spectrum.

Following the argumentation of [2], to focus on the effects of long-mode perturbations we introduce an infrared cut-off scale $k_{\rm IR}$ set by $k_{\rm IR}\bar{r}_z \ll 1$. We then split the gravitational potential into long and short modes with respect to $k_{\rm IR}$ as

$$\Psi(\eta, \bar{r}\hat{\boldsymbol{n}}) \equiv \Psi_{\rm long} + \Psi_{\rm short} = \int_0^{k_{\rm IR}} \frac{d^3k}{(2\pi)^3} e^{i\boldsymbol{k}\cdot\bar{r}\hat{\boldsymbol{n}}} \Psi(\boldsymbol{k};\eta) + \int_{k_{\rm IR}}^{\infty} \frac{d^3k}{(2\pi)^3} e^{i\boldsymbol{k}\cdot\bar{r}\hat{\boldsymbol{n}}} \Psi(\boldsymbol{k};\eta)\,. \quad (5.39)$$

By expanding the exponential in terms of $k_{\rm IR}\bar{r}$, the long-mode potential can be written

as

$$\Psi_{\rm long} = \Psi_o + \bar{r}\,\Psi_1 + \sum_{n\geq 2}\frac{(\bar{r})^n}{n!}\Psi_n\,, \tag{5.40}$$

where

$$\Psi_o \equiv \int_0^{k_{\rm IR}}\frac{d^3k}{(2\pi)^3}\Psi(\eta,\boldsymbol{k})\,, \quad \Psi_1 \equiv \hat{n}^i\big[\partial_i\Psi\big]_o \equiv \hat{n}^i\int_0^{k_{\rm IR}}\frac{d^3k}{(2\pi)^3}\,(ik_i)\Psi(\eta,\boldsymbol{k})\,, \quad \Psi_n \equiv \partial_\parallel^n\Psi\big|_{\bar{r}=0}\,. \tag{5.41}$$

This simple expansion shows that the gravitational potential between the observer and source positions contains both Ψ_o and Ψ_1, corresponding to the uniform gravity modes, and these two contributions are called the uniform gravitational potential and the uniform gravitational force respectively. According to the equivalence principle, the contributions of Ψ_o and Ψ_1 are indistinguishable from the free-fall. Consequently, Ψ_o and Ψ_1 should have no effect on physical observables measured by this observer.

It was shown [2] that the gauge-invariant expression of the galaxy fluctuation δ_g does not contain Ψ_o and Ψ_1, as the terms proportional to such long modes cancel each other when all local (δ_s, δ_o) and non-local contributions (δ_{nl}) are put together. The point is that the resulting power spectrum has no infrared divergences, contrary to what was found in previous works (see [84, 83]). In order to see how the long-mode contributions lead to infrared divergences in the power spectrum, we look at the variances σ_o^2 and σ_1^2 of Ψ_o and Ψ_1 respectively,

$$\sigma_o^2 = \langle\Psi_o\Psi_o\rangle \propto \int_0^{k_{\rm IR}}\frac{d^3k}{(2\pi)^3}\frac{1}{k^4}P_m(k)\,, \qquad \sigma_1^2 = \langle\Psi_1\Psi_1\rangle \propto \int_0^{k_{\rm IR}}\frac{d^3k}{(2\pi)^3}\mu_k^2\frac{1}{k^2}P_m(k)\,, \tag{5.42}$$

Considering that the contribution to the power spectrum are given by the quantities integrated over Fourier space, we immediately see that the long modes yield the divergent terms $k^{-2}P_m(k)$ and $k^{-4}P_m(k)$.

The scale dependence of the general relativistic contributions implies that the super-horizon modes play a significant role. While the terms leading to infrared divergences vanish in the galaxy fluctuation, other effects (represented by non-divergent terms) can manifest on large scales. This means that the standard redshift-space power spectrum may not be accurate enough to describe the behavior of the galaxy power spectrum on large scales. In other words, the total power spectrum (including all contributions) does not exhibit any infrared divergence on super horizon-scales, but it can contain features that appear on large scales and are not taken into account by the standard calculation.

While the redshift-space power spectrum is not divergent for $k \to 0$, considering only the contribution δ_s (in which Ψ_o and Ψ_1 do not cancel out) yields an expression that is inconsistent with the equivalence principle (despite being gauge-invariant). Now we isolate the divergent part in the power spectrum P_s at the source position that is

eventually cancelled when the total power spectrum is computed. On large very scales the source power spectrum is indeed given by

$$P^{s}_{k\to 0}(z,\boldsymbol{k}) = \left[\mathcal{A}^2 L_0 \frac{1}{k^4} + 2\left(bD\mathcal{A} + \frac{2}{3}\mathcal{A}\mathcal{C} + \frac{1}{3}\mathcal{B}^2\right) L_0 \frac{1}{k^2} + \frac{2}{3}(2\mathcal{A}\mathcal{C} + \mathcal{B}^2) L_2 \frac{1}{k^2}\right] P_m(k)\,. \quad (5.43)$$

As explained above, this diverging contribution is unphysical. In the same spirit, we compute the divergent parts in the power spectrum P_o at the observer position and the power spectrum P_{nl} of the contributions integrated along the line of sight:

$$P^{o}_{k\to 0}(z,\boldsymbol{k}) = \left[\mathcal{D}^2 L_0 \frac{1}{k^4} + \frac{2}{3}\mathcal{E}^2[L_0 + L_2]\frac{1}{k^2}\right] P_m(k)\,, \quad (5.44)$$

$$P^{nl}_{k\to 0}(z,\boldsymbol{k}) = \int_0^{\bar{r}_z} d\bar{r}_1 d\bar{r}_2 \left\{\mathcal{F}_1\mathcal{F}_2\left[\left(1 - \frac{1}{6}\Delta x^2\right)L_0 - \frac{1}{3}\Delta x^2 L_2\right]\frac{1}{k^4} + \frac{4}{3}\mathcal{F}_1\mathcal{I}_2\big[L_0 - L_2\big]\frac{1}{k^2} + \frac{1}{3}\mathcal{G}_1\mathcal{G}_2\big[L_0 + 2L_2\big]\frac{1}{k^2}\right\} P_m(k)\,. \quad (5.45)$$

The cross power spectra of δ_s, δ_o and δ_{nl} are given by the eqs. (5.81)–(5.83) in appendix 5.B. In order to obtain the divergent contributions to the power spectra in eqs. (5.37) and (5.78)–(5.80) we expanded the Bessel functions around zero up to the order required to have terms scaling as $k^{-4}P_m(k)$ and $k^{-2}P_m(k)$ in the power spectra.

The sum of these divergent contributions given by eqs. (5.43)–(5.45) and (5.81)–(5.83) vanishes. As a result, the total power spectrum has no infrared divergence, in agreement with the equivalence principle. Note that, according to the multipole expansion, the divergent contributions only appear in the monopoles and the quadrupoles of the power spectra, i.e. the quantities proportional to L_0 and L_2. The reason is that, at linear order in the perturbations, the uniform gravity modes Ψ_o and Ψ_1 only contribute to the multipoles with $\ell \leq 2$, because the highest power of μ_k in their correlations is μ_k^2 (see eq. (5.42)). In other words, the sum of the monopoles and the quadrupoles in eqs. (5.43)–(5.45) and (5.81)–(5.83) are both zero independently, as one can check using eqs. (5.15)–(5.17) and the relations in eq. (5.7).

Since the divergent contributions do not manifest in the total power spectrum, we can write down "IR-safe" power spectra by simply subtracting the divergent parts, eqs. (5.43)–(5.45) and (5.81)–(5.83), from the respective power spectra in eqs. (5.34)–(5.37) and (5.78)–(5.80). The IR-safe power spectra are given by the following expressions

and eqs. (5.84)–(5.86),

$$P^{s}_{\text{IR-safe}}(z,\boldsymbol{k}) = P_s(z,\boldsymbol{k}) - P^{s}_{k\to0}(z,\boldsymbol{k}) = P_z(z,\boldsymbol{k})\,, \tag{5.46}$$

$$P^{o}_{\text{IR-safe}}(z,\boldsymbol{k}) = P_o(z,\boldsymbol{k}) - P^{o}_{k\to0}(z,\boldsymbol{k}) = 0\,, \tag{5.47}$$

$$\begin{aligned}
&P^{nl}_{\text{IR-safe}}(z,\boldsymbol{k}) = P_{nl}(z,\boldsymbol{k}) - P^{nl}_{k\to0}(z,\boldsymbol{k}) \\
&= \int_0^{\bar{r}_z} d\bar{r}_1 d\bar{r}_2 \Bigg\{ \sum_{n=2}^{\infty}(-1)^n(4n+1)L_{2n}\Bigg[\mathcal{F}_1\mathcal{F}_2\frac{j_{2n}(\Delta x)}{k^4} + 2\mathcal{F}_1\mathcal{I}_2\frac{\big[j_{2n}(\Delta x) + j''_{2n}(\Delta x)\big]}{k^2} \\
&- \mathcal{G}_1\mathcal{G}_2\frac{j''_{2n}(\Delta x)}{k^2}\Bigg] + \mathcal{I}_1\mathcal{I}_2\sum_{n=0}^{\infty}(-1)^n(4n+1)L_{2n}\big[j_{2n}(\Delta x) + 2j''_{2n}(\Delta x) + j''''_{2n}(\Delta x)\big] \\
&+ \mathcal{F}_1\mathcal{F}_2\Bigg[L_0\bigg(j_0(\Delta x) - 1 + \frac{1}{6}\Delta x^2\bigg) + L_2\bigg(-5j_2(\Delta x) + \frac{1}{3}\Delta x^2\bigg)\Bigg]\frac{1}{k^4} \\
&+ 2\mathcal{F}_1\mathcal{I}_2\Bigg[L_0\bigg(j_0(\Delta x) + j''_0(\Delta x) - \frac{2}{3}\bigg) + L_2\bigg(-5j_2(\Delta x) - 5j''_2(\Delta x) + \frac{2}{3}\bigg)\Bigg]\frac{1}{k^2} \\
&- \mathcal{G}_1\mathcal{G}_2\Bigg[L_0\bigg(j''_0(\Delta x) + \frac{1}{3}\bigg) + L_2\bigg(5j''_2(\Delta x) - \frac{2}{3}\bigg)\Bigg]\frac{1}{k^2}\Bigg\}P_m(k)\,.
\end{aligned} \tag{5.48}$$

These quantities can be computed numerically at any scale, as they do not diverge for small k values. Naturally the IR-safe contributions do not have a direct physical meaning when considered individually, but their expressions are useful because the sum corresponds to the total power spectrum and they do not contain unphysical effects that would eventually cancel.

5.4 Numerical Computation of the Power Spectrum

In this section we numerically compute the theoretical galaxy power spectrum. Since the full relativistic three-dimensional power spectrum is very complicated, we first compute the redshift-space distortion and the gravitational lensing contributions to the power spectrum, ignoring other relativistic contributions, as they represent the dominant components. Next we compute the monopole, quadrupole and hexadecapole of the galaxy power spectrum including all the general relativistic effects.

For numerical calculations we assume a flat ΛCDM universe with matter density $\Omega_m = 0.3038$, baryon density $\Omega_b = 0.0462$, dark energy density $\Omega_\Lambda = 0.65$, scalar amplitude $A_s = 2.1\times10^{-9}$ at the pivot scale $k_0 = 0.05\,\text{Mpc}^{-1}$, spectral index $n_s = 0.96$, Hubble parameter $h = 0.70$ and bias factor $b = 1$. Furthermore, we assume no magnification bias and the evolution bias is set to $e = 3$ at any redshift. In short, we treat galaxies as non-relativistic matter for illustration.

5.4.1 Redshift-space distortion and gravitational lensing

We consider the main contributions to the galaxy number density: the matter density, the redshift-space distortion and the gravitational lensing. Compared to the full general relativistic expression we neglect the contributions from the gravitational potential and the velocity. In this way, we can easily compute the three-dimensional power spectrum and present a result that very well approximates the total power spectrum on most scales. The expression for the galaxy fluctuation in this case is given by

$$\delta_{zL}(z,\hat{\boldsymbol{n}}) = \delta_z + \delta_L\,, \tag{5.49}$$

where the standard redshift-space galaxy fluctuation is

$$\delta_z(z,\hat{\boldsymbol{n}}) = b\delta_m - \frac{1}{\mathcal{H}}\partial_\parallel V_\parallel = \int \frac{d^3k}{(2\pi)^3} e^{ik\bar{r}_z\mu_k}\left[b + f\mu_k^2\right] D\delta(\boldsymbol{k})\,, \tag{5.50}$$

and the gravitational lensing contribution is

$$\begin{aligned}\delta_L(z,\hat{\boldsymbol{n}}) &= -2\int_0^{\bar{r}_z} d\bar{r}\left(\frac{\bar{r}_z-\bar{r}}{\bar{r}_z\bar{r}}\right)\hat{\nabla}^2\Psi \\ &= -2\int \frac{d^3k}{(2\pi)^3}\int_0^{\bar{r}_z} d\bar{r}\, e^{ik\bar{r}\mu_k}\left(\frac{\bar{r}_z-\bar{r}}{\bar{r}_z}\right)\left[2\frac{i\,\mu_k}{k} + \bar{r}\left(1-\mu_k^2\right)\right] D_\Psi(\bar{r}) C\delta(\boldsymbol{k})\,.\end{aligned} \tag{5.51}$$

We want to compute the three-dimensional power spectrum of δ_{zL}. This can be written as

$$P_{zL}(z,\boldsymbol{k}) = P_z + P_L + 2\,P_{z\text{-}L}\,, \tag{5.52}$$

where the first term is the redshift-space power spectrum,

$$P_z(z,\boldsymbol{k}) = \left[\left(b^2 + \frac{2}{3}bf + \frac{1}{5}f^2\right)L_0 + \left(\frac{4}{3}bf + \frac{4}{7}f^2\right)L_2 + \frac{8}{35}f^2 L_4\right] D^2 P_m(k)\,, \tag{5.53}$$

the second term is the IR-safe lensing power spectrum obtained from $\langle\delta_L(z,\hat{\boldsymbol{n}})\delta_L^*(z,\hat{\boldsymbol{n}})\rangle$,

$$\begin{aligned}P_L(z,\boldsymbol{k}) = \int_0^{\bar{r}_z} d\bar{r}_1 d\bar{r}_2 \Bigg\{ &\mathcal{I}_1\mathcal{I}_2 \sum_{n=0}^{\infty}(-1)^n(4n+1)L_{2n}\left[j_{2n}(\Delta x) + 2j_{2n}''(\Delta x) + j_{2n}''''(\Delta x)\right] \\ &+ \mathcal{G}_1\mathcal{G}_2 \sum_{n=2}^{\infty}(-1)^{n+1}(4n+1)L_{2n}\, j_{2n}''(\Delta x)\frac{1}{k^2} \\ &- \mathcal{G}_1\mathcal{G}_2\left[L_0\left(j_0''(\Delta x) + \frac{1}{3}\right) + L_2\left(5j_2''(\Delta x) - \frac{2}{3}\right)\right]\frac{1}{k^2}\Bigg\} P_m(k)\,,\end{aligned} \tag{5.54}$$

and the last term is the cross power spectrum obtained from $\langle \delta_K(z,\hat{\boldsymbol{n}})\delta_L^*(z,\hat{\boldsymbol{n}})\rangle$,

$$P_{zL}(z,\boldsymbol{k}) = \int_0^{\bar{r}_z} d\bar{r}\ \sum_{n=0}^{\infty}(-1)^n(4n+1)L_{2n}\Bigg[\mathcal{C}\mathcal{G}(\bar{r})\frac{1}{k}j''_{2n}(\Delta x_z) - bD\mathcal{G}(\bar{r})\frac{1}{k}j'_{2n}(\Delta x_z) \\ +bD\mathcal{I}(\bar{r})\big[j_{2n}(\Delta x_z) + j''_{2n}(\Delta x_z)\big] - \mathcal{C}\mathcal{I}(\bar{r})[j''_{2n}(\Delta x_z) + j''''_{2n}(\Delta x_z)]\Bigg]P_m(k)\,. \tag{5.55}$$

where we defined $\Delta x_z \equiv k\Delta r_z$. Note that eqs. (5.54) and (5.55) can be obtained from eqs. (5.48) and (5.79) by setting $\mathcal{A} \equiv \mathcal{B} \equiv \mathcal{F} \equiv 0$, as the contributions proportional to these functions do not appear in δ_{zL}. Note that the lensing power spectrum is divergent and, therefore, one has to subtract the divergent part if interested in the behavior on large scales. For this reason, we subtracted the divergent contributions in the monopole and the quadrupole of eq. (5.54). To simplify the numerical computations of eqs. (5.54)–(5.55) one can use the relation

$$j'_n(y) = \frac{1}{2n+1}\big[nj_{n-1}(y) - (n+1)j_{n+1}(y)\big]\,, \tag{5.56}$$

and avoid computing the derivatives at every step in the integration and the sum.

5.4.2 Full relativistic contributions

We now take into account the complete gauge-invariant expression of the galaxy number density in eqs. (5.9)–(5.11). We expand the three-dimensional power spectrum in the Legendre polynomials. The multipole power spectra $P_\ell(z,k)$ can be calculated numerically including all the relativistic effects. In the next three subsections we compute the total monopole ($\ell = 0$), quadrupole ($\ell = 2$) and hexadecapole ($\ell = 4$), accounting for all the individual contributions at the source, at the observer and integrated along the line of sight. We only consider these multipoles because they can be compared one-to-one with the monopole, quadrupole and hexadecapole of the standard redshift-space power spectrum, which is given by the sum of only these three multipoles without the general relativistic effects. Note that the odd multipoles vanish due to symmetry. We plot our results at three different redshift values: $z = \{0.5, 1, 2\}$, in order to show the redshift dependence of the relativistic effects. We investigate the behavior of the power spectra on large scales, where the deviation from the standard redshift-space power spectrum is largest.

Monopole

The monopole (angle-averaged) power spectrum is obtained by integrating the three-dimensional power spectrum over the angle $\hat{\boldsymbol{k}}$, or by taking the derivative of the variance

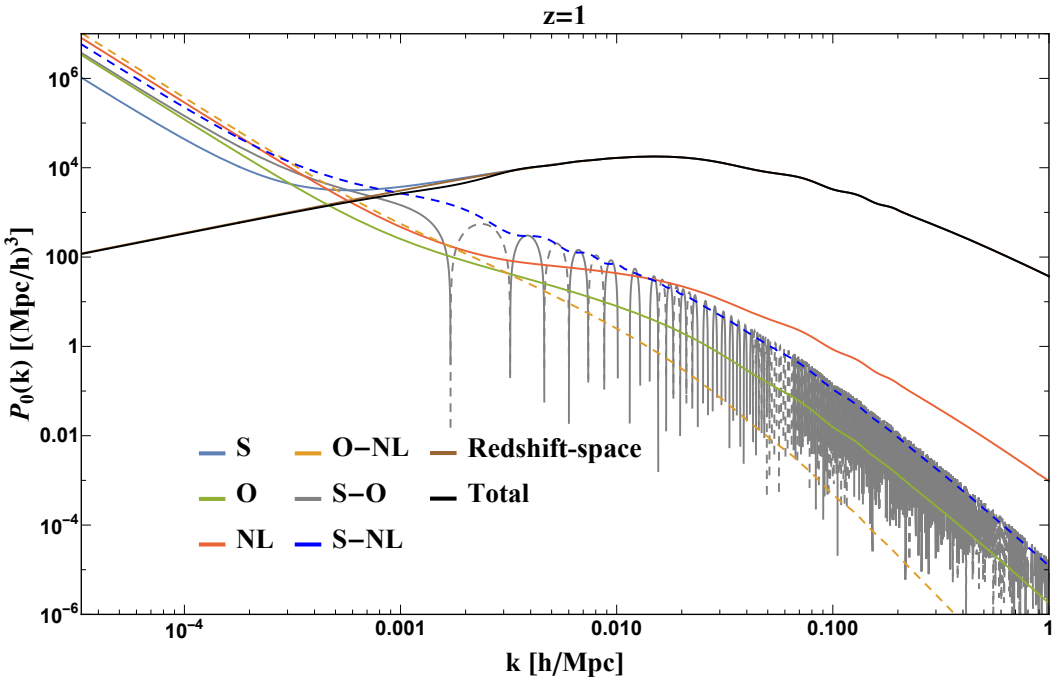

Figure 5.2: Monopole power spectrum at redshift $z = 1$ as a function of k. The colored lines represent the individual contributions, while the black line represent the total power spectrum. Dashed lines represent negative values. Note the diverging trend of the individual contributions to the monopole power spectrum on large scales, while the total power spectrum remains finite on all scales.

of the galaxy fluctuation, as

$$P_0(z,k) = \int \frac{d\mu_k}{2} P(z,\boldsymbol{k}) = \frac{2\pi^2}{k^2}\frac{\partial}{\partial k}\sigma^2(z,k)\,. \tag{5.57}$$

Note that the above equalities hold for each contributions. For instance, the monopole of the power spectrum P_s at the source is given by $P_0^s = \int \frac{d\mu_k}{2} P_s = \frac{2\pi^2}{k^2}\frac{\partial}{\partial k}\sigma_s^2$. Therefore, by integrating eqs. (5.34)–(5.37) and (5.78)–(5.80) over the angles, we obtain the individual contributions to the monopole power spectrum as

$$P_0^s(z,k) = P_0^z(z,k) + P_m(k)\left\{\left[\frac{\mathcal{B}^2}{3} + 2D\left(b+\frac{f}{3}\right)\mathcal{A}\right]\frac{1}{k^2} + \mathcal{A}^2\frac{1}{k^4}\right\}, \tag{5.58}$$

$$P_0^o(z,k) = \left[\mathcal{D}^2\frac{1}{k^4} + \frac{1}{3}\mathcal{E}^2\frac{1}{k^2}\right]P_m(k)\,, \tag{5.59}$$

$$P_0^{nl}(z,k) = \int_0^{\bar{r}_z} d\bar{r}_1\, d\bar{r}_2 \left[\mathcal{F}_1\mathcal{F}_2\frac{j_0(\Delta x)}{k^2} + 4\mathcal{F}_1\mathcal{I}_2\frac{j_1(\Delta x)}{\Delta x} + \mathcal{G}_1\mathcal{G}_2\left(j_0(\Delta x) - 2\frac{j_1(\Delta x)}{\Delta x}\right)\right.$$
$$\left. - 8\mathcal{I}_1\mathcal{I}_2\left(\frac{j_0(\Delta x)}{\Delta x^2} - 3\frac{j_1(\Delta x)}{\Delta x^3}\right)\right]\frac{1}{k^2}P_m(k)\,, \tag{5.60}$$

where $P_0^z(z,k) = \left(b^2 + \frac{2}{3}bf + \frac{1}{5}f^2\right)D^2P_m(k)$ is the redshift-space monopole power spectrum. Finally, the cross power spectra are given by the coefficients of L_0 in eqs. (5.78)–(5.80). Indeed, also the above expressions can be obtained by taking the coefficients of L_0 in the three-dimensional power spectra derived in sec. 5.3.1, specifically eqs. (5.34)–(5.37).

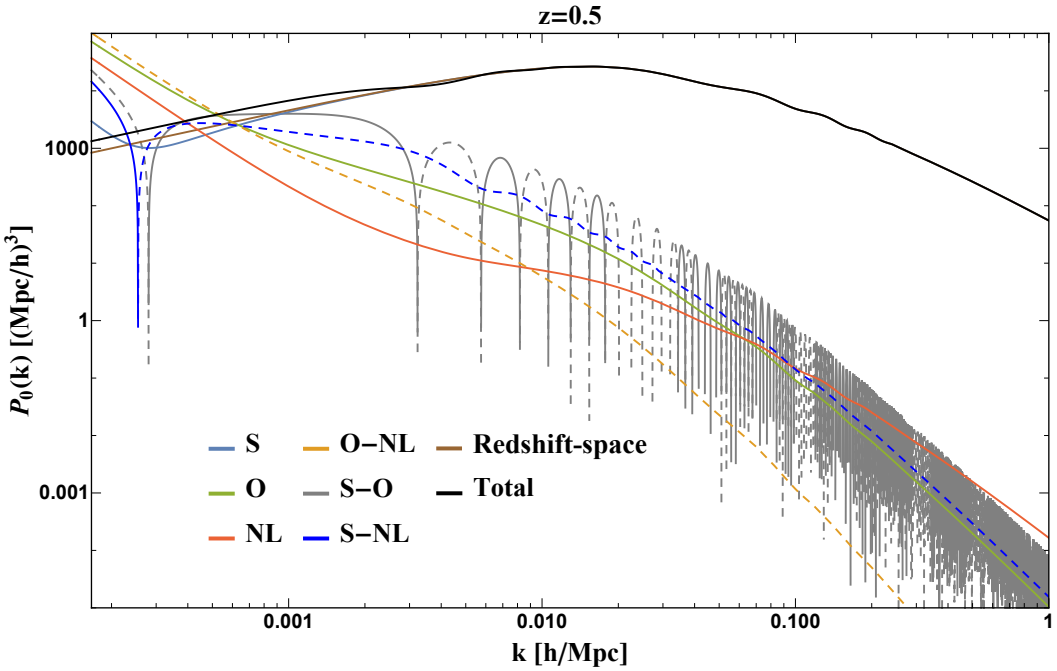

Figure 5.3: Same as fig. 5.2 but at redshift $z = 0.5$.

On large scales, the individual contributions to the monopole power spectrum P_0 (except the redshift-space monopole P_0^z) diverge, because of terms proportional to $k^{-2}P_m(k)$ and $k^{-4}P_m(k)$. For instance, the light blue line in fig. 5.2 represents the monopole power spectrum of the contribution at the source at redshift $z = 1$, whose expression is given by eq. (5.58). In the plot one can see how the behavior of P_0^s (light blue line) deviates from the standard redshift-space prediction (represented by the brown line overlapping with the black one but visible at $k \sim 0.001\ h/\text{Mpc}$) as $k \lesssim 0.005\ h/\text{Mpc}$ and then goes to infinity as $k \to 0$, in agreement with what found in [83, 84]. The infrared divergence in P_0^s is a consequence of the violation of the equivalence principle in the incomplete expression, as discussed in sec. 5.3.2. Indeed, the contribution P_0^s itself is not an observable quantity and the divergence is canceled when the remaining contributions are taken into account to compute the total monopole power spectrum.

In order to see how the divergent parts in the individual local and non-local contributions cancel each other in the total monopole power spectrum, it is useful to write

down the expressions of the power spectra when $k \to 0$. We obtain

$$P^{s}_{0\,k\to 0}(z,k) = P_m(k)\left\{\mathcal{A}^2\frac{1}{k^4} + \left[\frac{\mathcal{B}^2}{3} + 2D\left(b+\frac{f}{3}\right)\mathcal{A}\right]\frac{1}{k^2}\right\}, \tag{5.61}$$

$$P^{o}_{0\,k\to 0}(z,k) = \left[\mathcal{D}^2\frac{1}{k^4} + \frac{1}{3}\mathcal{E}^2\frac{1}{k^2}\right]P_m(k)\,, \tag{5.62}$$

$$P^{nl}_{0\,k\to 0}(z,k) = \int_0^{\bar{r}_z} d\bar{r}_1 d\bar{r}_2\left[\mathcal{F}_1\mathcal{F}_2\frac{1}{k^4} + \frac{1}{3}\left(\mathcal{G}_1\mathcal{G}_2 - \frac{1}{2}\Delta r^2\mathcal{F}_1\mathcal{F}_2 + 4\mathcal{F}_1\mathcal{I}_2\right)\frac{1}{k^2}\right]P_m(k)\,, \tag{5.63}$$

and the cross power spectra are given by the coefficients of L_0 in eqs. (5.81)–(5.83). To isolate the divergent parts in the power spectra we expanded around zero the Bessel functions in the expressions of the monopole contributions obtained above, up to the order required to have terms scaling as $k^{-2}P_m(k)$ and $k^{-4}P_m(k)$.

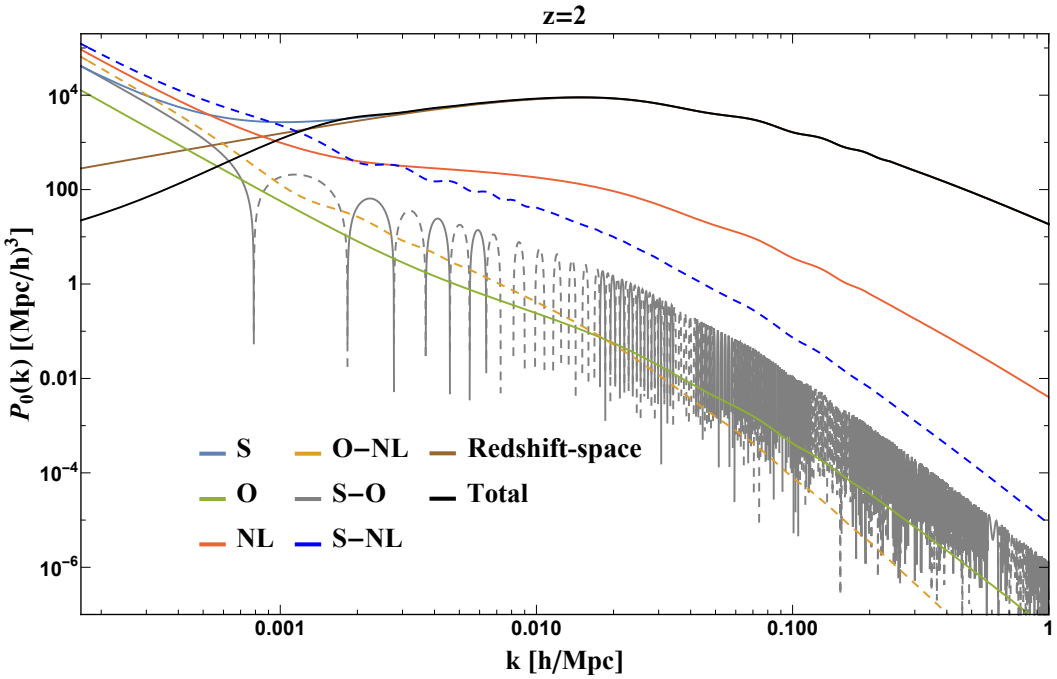

Figure 5.4: Same as fig. 5.2 but at redshift $z = 2$.

As one can verify by using eqs. (5.15)–(5.17) and the relations between different growth functions in eq. (5.7), the sum of eqs. (5.61)–(5.63) and the coefficients of L_0 in eqs. (5.81)–(5.83) is zero, as the divergent terms cancel each other. In particular, both the coefficients of $k^{-2}P_m(k)$ and $k^{-4}P_m(k)$ are zero. We can therefore define IR-safe power spectra by simply taking away the divergent terms from each contribution. We

obtain

$$P^{s}_{0\,\text{IR-safe}}(z,k) = P^{s}_{0}(z,k) - P^{s}_{0\,k\to 0}(z,k) = P^{z}_{0}(z,k)\,, \tag{5.64}$$

$$P^{o}_{0\,\text{IR-safe}}(z,k) = P^{o}_{0}(z,k) - P^{o}_{0\,k\to 0}(z,k) = 0\,, \tag{5.65}$$

$$\begin{aligned} P^{nl}_{0\,\text{IR-safe}}(z,k) &= P^{nl}_{0}(z,k) - P^{nl}_{0\,k\to 0}(z,k) \\ &= P_m(k)\int_0^{\bar{r}_z} d\bar{r}_1 d\bar{r}_2 \left[\mathcal{F}_1\mathcal{F}_2\frac{1}{k^4}\left(j_0(\Delta x) - 1 + \frac{1}{6}\Delta x^2\right) + 4\mathcal{F}_1\mathcal{I}_2\frac{1}{k^2}\left(\frac{j_1(\Delta x)}{\Delta x} - \frac{1}{3}\right)\right. \end{aligned} \tag{5.66}$$

$$\left. + \mathcal{G}_1\mathcal{G}_2\frac{1}{k^2}\left(j_0(\Delta x) - 2\frac{j_1(\Delta x)}{\Delta x} - \frac{1}{3}\right) - 8\mathcal{I}_1\mathcal{I}_2\left(\frac{j_0(\Delta x)}{\Delta x^2} - 3\frac{j_1(\Delta x)}{\Delta x^3}\right)\right], \tag{5.67}$$

and the expressions of the cross power spectra are given by the coefficients of L_0 in eqs. (5.84)–(5.86).

In figs. 5.2, 5.3 and 5.4 we show the results of our numerical computations of the monopole power spectrum at redshift $z = 1$, 0.5 and 2 respectively. From these figures one can see that, while the individual contributions diverge in the infrared, the total power spectrum does not. Furthermore, the relativistic effects produce features in the power spectrum for $k < k_{\text{eq}}$, where k_{eq} corresponds to the scale of matter-radiation equality (at which we have the turn-over in the standard redshift-space power spectrum). These features consist of oscillations as well as changes in the amplitude. The behavior of the oscillations depends on the redshift, as different contributions can be more or less important in the total power spectrum according to the distance of the sources. For example, at redshift $z = 0.5$ we observe more oscillations than at $z = 1$ and 2 because the source-observer contribution, which oscillates fast due to the Doppler effect, is the largest after the source power spectrum, almost on all scales. At redshift $z = 2$, instead, the oscillations are slower but the change in amplitude is larger, as in this case the dominant contributions (after the source one) are the non-local density contrast and its cross correlation with the source density contrast. This is due to the fact that the integrated effects, such as the lensing convergence, become more important at higher redshift, and they smear out the oscillations due to the Doppler effect.

In the top plot of fig. 5.5 we compare the total relativistic monopole power spectrum with the redshift-space monopole power spectrum at redshift $z = 0.5$, 1, 2. The redshift-space power spectrum represents the standard theoretical prediction that is used to analyze the data from galaxy surveys. However, the plot shows that the total relativistic monopole power spectrum deviates from the redshift-space one on large scales (for $k \lesssim k_{\text{eq}}$), for all redshift values considered. As we will see in the next subsections, this occurs also for higher multipoles.

We analyze further the difference between our relativistic prediction and the redshift-space one in the bottom plot of fig. 5.5. The plot shows that the fractional difference reaches the percent level on scales larger than $k = 0.02\ h/\text{Mpc}$. We can therefore infer

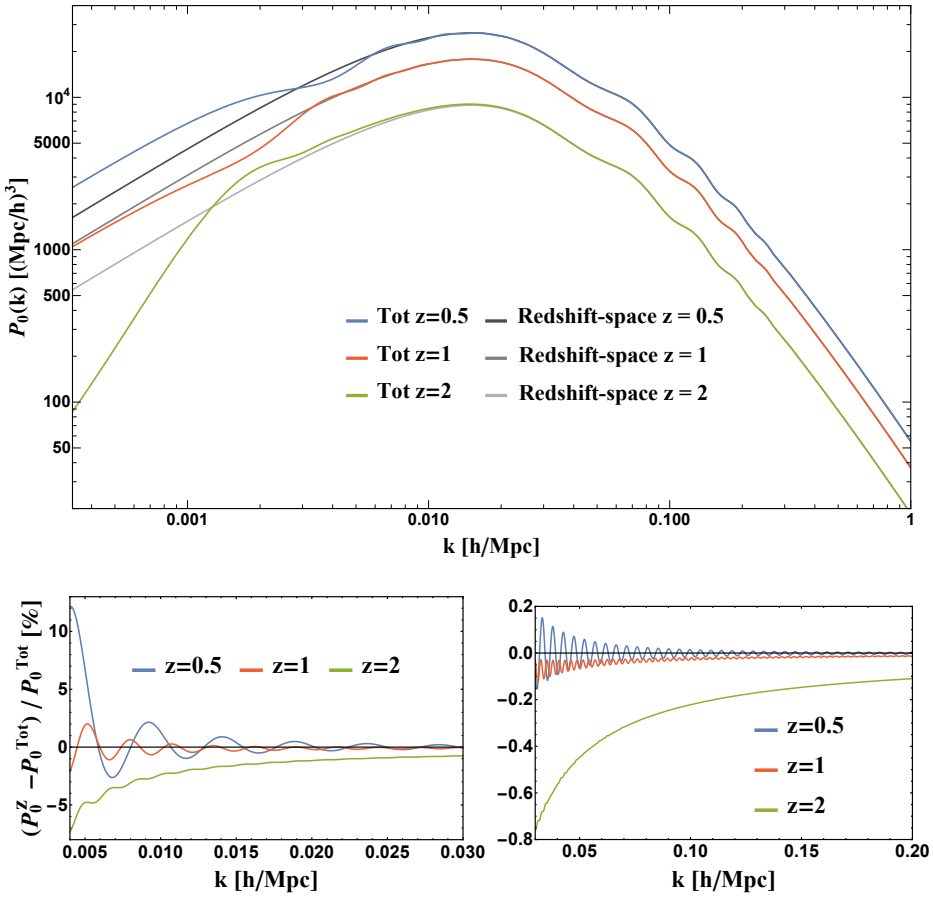

Figure 5.5: *Top plot:* Comparison between the full relativistic and the redshift-space monopole power spectrum at redshift $z = \{0.5, 1, 2\}$ as a function of k. *Bottom plots:* Fractional difference between the full relativistic and the redshift-space monopole power spectrum at redshift $z = 0.5$, 1, 2 as a function of k. The numerical calculations are performed assuming a flat ΛCDM universe with $\Omega_m = 0.3$ and the bias factor is set to unity ($b = 1$).

that the relativistic effects, and in particular the contributions at the observer and integrated along the line of sight, are not negligible. Indeed, not only the observer and non-local contributions cancel the infrared divergence in the source power spectrum, but also they involve (non-divergent) terms that change the amplitude on large scales.

Quadrupole

As for the monopole power spectrum, we proceed to compute the quadrupole power spectrum. The individual contributions to the quadrupole power spectrum can be obtained from the coefficients of $L_2(\mu_k)$ in the expressions for the three-dimensional

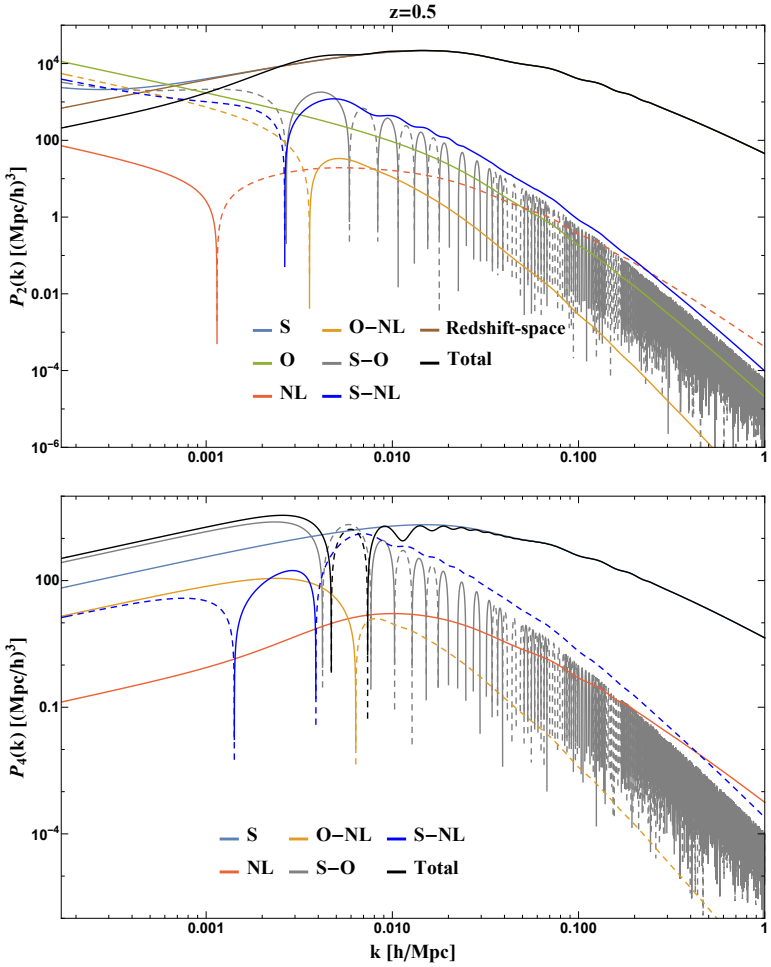

Figure 5.6: Quadrupole (top plot) and Hexadecapole (bottom plot) power spectrum at redshift $z = 0.5$ as a function of k. The colored lines represent the individual contributions, while the black line represent the total power spectrum. Dashed lines represent negative values.

power spectra in sec. 5.3.1 and appendix 5.B. We obtain

$$P_2^s(z,k) = P_2^z(z,k) + \left(\frac{4}{3}\mathcal{A}\mathcal{C} + \frac{2}{3}\mathcal{B}^2\right)\frac{1}{k^2}P_m(k)\,, \qquad P_2^o(z,k) = \frac{2}{3}\mathcal{E}^2\frac{1}{k^2}P_m(k)\,, \tag{5.68}$$

$$P_2^{nl}(z,k) = -5\int_0^{\bar{r}_z} d\bar{r}_1 d\bar{r}_2 \Big[\mathcal{F}_1\mathcal{F}_2\frac{1}{k^4}j_2(\Delta x) + 2\mathcal{F}_1\mathcal{I}_2\frac{1}{k^2}\big[j_2(\Delta x) + j_2''(\Delta x)\big] - \mathcal{G}_1\mathcal{G}_2\frac{1}{k^2}j_2''(\Delta x) + \mathcal{I}_1\mathcal{I}_2\big[j_2(\Delta x) + 2j_2''(\Delta x) + j_2''''(\Delta x)\big]\Big]P_m(k)\,, \tag{5.69}$$

where $P_2^z(z,k) = (4/3bf + 4/7f^2)D^2P_m(k)$. The cross power spectra are given by the coefficients of L_2 in eqs. (5.78)–(5.80).

On large scales, the individual contributions to the quadrupole diverge, because of terms proportional to $k^{-2}P_m(k)$. The behavior of the power spectra when $k \to 0$ is given by

$$P^s_{2\,k\to 0}(z,k) = \left(\frac{4}{3}\mathcal{A}\mathcal{C} + \frac{2}{3}\mathcal{B}^2\right)\frac{1}{k^2}P_m(k)\,, \qquad P^o_{2\,k\to 0}(z,k) = \frac{2}{3}\mathcal{E}^2\frac{1}{k^2}P_m(k)\,, \tag{5.70}$$

$$P^{nl}_{2\,k\to 0}(z,k) = -\frac{1}{3}\int_0^{\bar{r}_z} d\bar{r}_1 d\bar{r}_2 \left[\mathcal{F}_1\mathcal{F}_2\frac{x^2}{k^4} + 4\mathcal{F}_1\mathcal{I}_2\frac{1}{k^2} - 2\mathcal{G}_1\mathcal{G}_2\frac{1}{k^2}\right]P_m(k)\,, \tag{5.71}$$

and the coefficients of L_2 in eqs. (5.81)–(5.83). Note that we expanded around zero the Bessel functions in the expressions of the quadrupole contributions, up to the order required to have terms scaling as $k^{-2}P_m(k)$.

As for the monopole, the divergent terms cancel out in the total quadrupole power spectrum. In other words, the sum of eqs. (5.70)–(5.71) and the coefficients of L_2 in eqs. (5.81)–(5.83) vanishes. We can therefore define IR-safe power spectra by simply taking away the divergent terms. Again we obtain that the IR-safe source power spectrum corresponds to the redshift-space quadrupole, $P^s_{2\,\text{IR-safe}}(z,k) = P^z_2(z,k)$, and the contribution at the observer vanishes, $P^o_{2\,\text{IR-safe}}(z,k) = 0$. On the other hand, the non-local contribution is given by

$$P^{nl}_{2\,\text{IR-safe}}(z,k) = -5\int_0^{\bar{r}_z} d\bar{r}_1 d\bar{r}_2 \left[\mathcal{F}_1\mathcal{F}_2\frac{1}{k^4}\left(j_2(\Delta x) - \frac{1}{15}\Delta x^2\right) + 2\mathcal{F}_1\mathcal{I}_2\frac{1}{k^2}\left(j_2(\Delta x)\right.\right.$$
$$\left.\left. + j_2''(\Delta x) - \frac{2}{15}\right) - \mathcal{G}_1\mathcal{G}_2\frac{1}{k^2}\left(j_2''(\Delta x) - \frac{2}{15}\right) + \mathcal{I}_1\mathcal{I}_2\big[j_2(\Delta x) + 2j_2''(\Delta x) + j_2''''(\Delta x)\big]\right]P_m(k)\,, \tag{5.72}$$

and the IR-safe cross power spectra are given by the coefficients of L_2 in eqs. (5.84)–(5.86).

In the top panels of figs. 5.6, 5.7 and 5.8 we show the results of our numerical computations of the quadrupole power spectrum at redshift $z = 0.5$, 1, and 2 respectively. As for the monopole, while the individual contributions diverge as k goes to zero, the total quadrupole power spectrum does not. Instead, the relativistic effects produce features in the power spectrum for $k < k_{\text{eq}}$, with a redshift-dependent behavior. At redshift $z = 0.5$ the quadrupole power spectrum deviates from the redshift-space prediction with some oscillations between $k \approx 0.001\ h/\text{Mpc}$ and $k \approx 0.01\ h/\text{Mpc}$. Then it decreases monotonically for $k \lesssim 0.001\ h/\text{Mpc}$, but with smaller amplitude than the redshift-space prediction. Also at redshift $z = 1$ and $z = 2$ the quadrupole power spectrum shows some oscillations between $k \approx 0.001\ h/\text{Mpc}$ and $k \approx 0.01\ h/\text{Mpc}$, but then it becomes negative for $k \lesssim 0.001\ h/\text{Mpc}$. If we look at the fractional difference between the full relativistic and the redshift-space quadrupole power spectrum in the top plots of fig. 5.9, we observe that it reaches the percent level on scales larger than $k = 0.015\ h/\text{Mpc}$ for all redshifts considered. This strengthens the conclusion we made

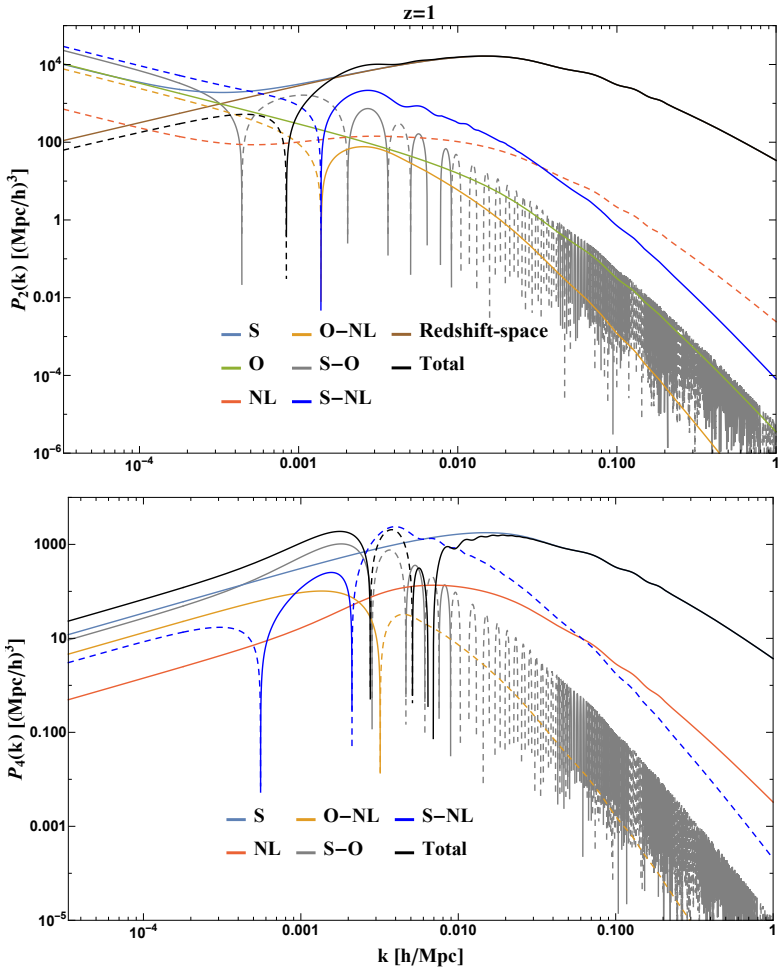

Figure 5.7: Same as fig. 5.6 but at redshift $z = 1$.

after analyzing the monopole power spectrum: the relativistic effects must be taken into account in the theoretical prediction when looking at large scales (for $k \lesssim k_{\rm eq}$).

Hexadecapole

The individual contributions to the hexadecapole power spectrum can be obtained from the coefficients of $L_4(\mu_k)$ in the expressions of the three-dimensional power spectra in sec. 5.3.1 and appendix 5.B. We obtain that the contribution at the source corresponds to the redshift-space power spectrum, $P_4^s(z,k) = P_4^z(z,k) = 8/35 f^2 D^2 P_m(k)$, and the contribution at the observer vanishes, $P_4^o(z,k) = 0$. The non-local contribution is

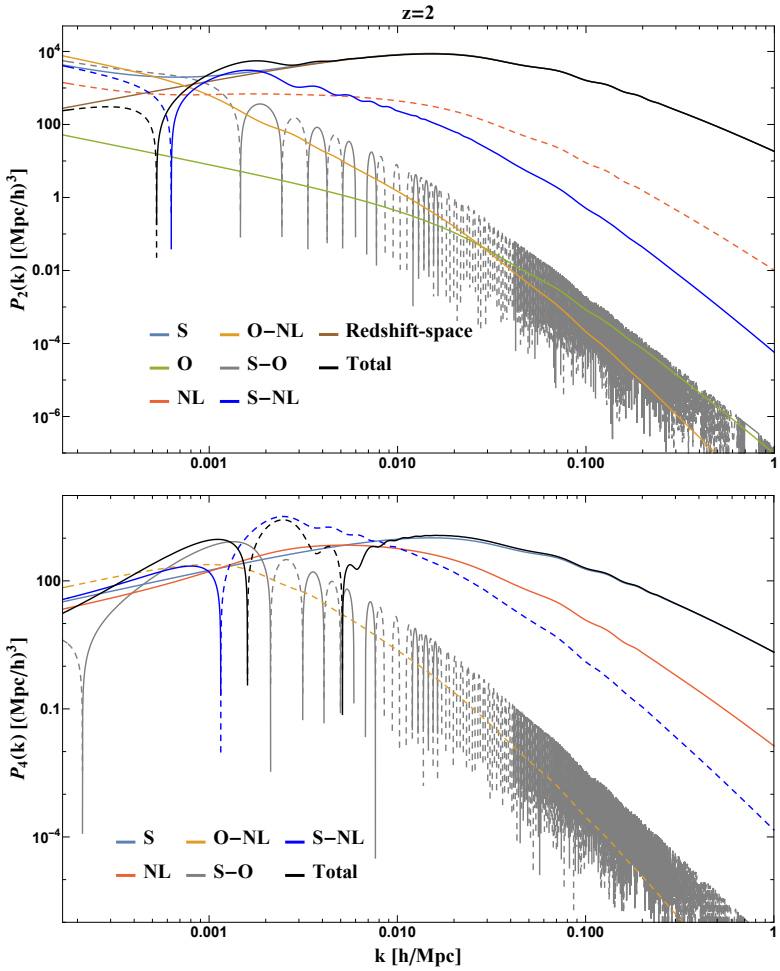

Figure 5.8: Same as fig. 5.6 but at redshift $z = 2$.

instead given by

$$P_4^{nl}(z,k) = 9\int_0^{\bar{r}_z} d\bar{r}_1 d\bar{r}_2 \Bigg[\mathcal{F}_1\mathcal{F}_2\frac{j_4(\Delta x)}{k^4} + 2\mathcal{F}_1\mathcal{I}_2\frac{\big[j_4(\Delta x) + j_4''(\Delta x)\big]}{k^2} - \mathcal{G}_1\mathcal{G}_2\frac{j_4''(\Delta x)}{k^2} + \mathcal{I}_1\mathcal{I}_2\big[j_4(\Delta x) + 2j_4''(\Delta x) + j_4''''(\Delta x)\big]\Bigg]P_m(k)\,. \tag{5.73}$$

Finally, the cross power spectra are given by the coefficients of L_4 in eqs. (5.78)–(5.80).

The individual contributions to the hexadecapole power spectrum do not diverge, as well as those of higher mulitpoles. In the bottom panels of figs. 5.6, 5.7 and 5.8 we show the results of our numerical computations of the quadrupole power spectrum at redshift $z = 0.5$, 1, and 2 respectively. We analyze the difference between our full relativistic

prediction and the redshift-space one in the bottom plots of fig. 5.9. Compared to the monopole and quadrupole, in this case we observe an even larger difference with respect to the standard redshift-space prediction. Furthermore, the deviations from the redshift-space power spectrum appear on smaller scales. The fractional difference reaches the percent level already at $k \approx 0.05\, h/\mathrm{Mpc}$ and $z = 0.5$. Finally, the oscillations starts on smaller scales than for the monopole and quadrupole, they are faster and with larger amplitude.

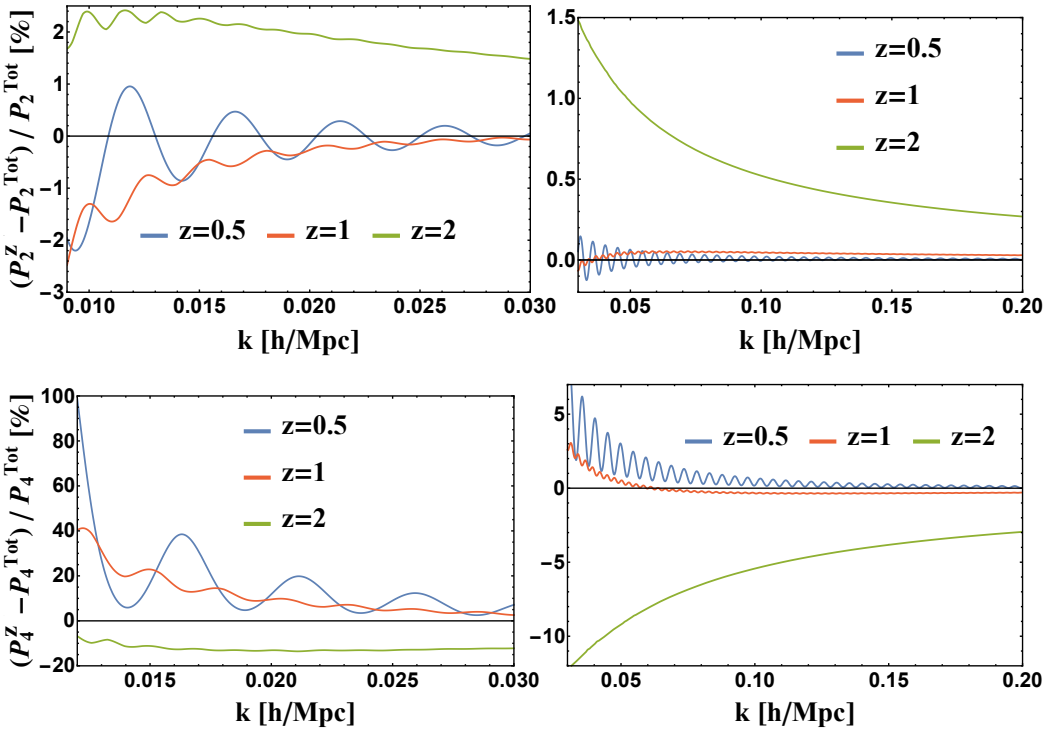

Figure 5.9: Fractional difference between the full relativistic and the redshift-space quadrupole (top panels) and hexadecapole (bottom panels) power spectrum at redshift $z = \{0.5, 1, 2\}$. The numerical calculations are performed assuming a flat ΛCDM universe with $\Omega_m = 0.3$ and the bias factor is set to unity ($b = 1$).

5.5 Conclusions

In this chapter we have studied the galaxy power spectrum in general relativity, clarifying the important difference between the power spectrum commonly derived in theory and what galaxy surveys measure in practice. As we have explained in sec. 5.2.3, on the one hand, the theoretical power spectrum is obtained by taking a Fourier transformation of the observed galaxy fluctuation on the hypersurface of simultaneity at the

source time coordinate. On the other hand, the observed power spectrum is obtained by taking a Fourier transformation of the observed galaxy fluctuation on the light-cone hypersurface. While the theoretical power spectrum is not observable, because we do not observe spatial hypersurfaces but the past light-cone, there is no ambiguity in its computation. For this reason, it offers a great opportunity to investigate, at theoretical level, the effects of general relativity on large scales, providing the perfect ground to test the validity of our theoretical predictions. Even though observations are restricted to a limited range of scales, the expression for the theoretical power spectrum can be used to derived the observed power spectrum, as we show in appendix 5.B.

After discussing the subtleties in its definition, we have derived the theoretical galaxy power spectrum in general relativity, accounting for all the contributions to the observed galaxy number density fluctuation for the first time. The complete gauge-invariant expression of the observed galaxy number density fluctuation δ_g consists of local terms evaluated at the source (δ_s) and at the observer (δ_o) and non-local terms (δ_{nl}) integrated along the line-of-sight distance between source and observer [70, 71, 84]. After decomposing the expression into these three contributions in sec. 5.2.2, we have derived their power spectra by using a new and simple method. As described in sec. 5.2.3, instead of computing the power spectrum directly from the Fourier modes, we have made use of the duality between the variance of δ_g and its power spectrum. In this way, we have been able to easily take into account all contributions and to compute their individual power spectra in sec. 5.3.1, demonstrating their importance in order to obtain a correct theoretical prediction.

In the past there have been considerable theoretical efforts to derive the galaxy power spectrum in general relativity. The current state of the art is given by the results presented in [84, 71, 83]. However, these studies considered only the contribution at the source (δ_s) to the observed galaxy fluctuation. Indeed, it was commonly believed that δ_s contributes dominantly to the power spectrum. The reason is that δ_{nl} is only important for the pure transverse modes, while δ_o consists only of uniform gravity modes that have no physical effects. Furthermore, when the power spectrum is derived directly from the Fourier modes of the density fluctuation, taking into account δ_o and δ_{nl} is mathematically obstructed. While it is true that δ_s contributes dominantly mostly on all scales, the other contributions are comparable on very large scales, where the power spectrum of δ_s diverges (see for instance fig. 5.2). In addition, the uniform gravity modes not only affect δ_o but also δ_s and δ_{nl} (see also [2]). As a consequence, as discussed in sec. 5.3.2, the power spectra of δ_s, δ_o and δ_{nl} are all divergent on very large scales. Here we have explicitly confirmed that the divergent behavior near the horizon scale, obtained previously by considering only the local contributions to the galaxy number density fluctuation evaluated at the source, is the result of the uniform gravity modes and is inconsistent with the equivalence principle. Moreover, we have demonstrated that this divergent behavior is precisely cancelled when the other

contributions to the galaxy fluctuation are taken into account (see again fig. 5.2).

By considering the complete gauge-invariant expression of δ_g, which is consistent with the equivalence principle and devoid of infrared divergence, we have derived the correct theoretical expression for the galaxy power spectrum. Our results show the correct behavior of the theoretical power spectrum on large scales, where the relativistic effects manifest themselves and cause deviations from the standard prediction given by redshift-space formula. Indeed, by computing numerically the monopole, quadrupole and hexadecapole of the power spectrum, we have shown the presence of oscillations on scales comparable or larger than the scale $k_{\rm eq}$ of matter-radiation equality. The behavior of these features depends on the redshift (see for instance fig. 5.5), first of all, because the redshift sets the unique scale of the system defining which modes are relevant and, second of all, because different contributions can be more or less important according to the distance of the sources. We find that, for the multipoles that we analyzed, the fractional difference with the redshift-space prediction reaches the percent level on scales larger than $k_{\rm eq}$.

To conclude, we have shown that the relativistic effects do not yield the divergent feature in the galaxy power spectrum. In particular, the contributions to the observed galaxy fluctuation at the observer and integrated along the line of sight are not negligible and must be taken into account for obtaining a correct theoretical prediction. Our results can be used in the future to obtain the observed power spectrum, considering a specific galaxy survey, and quantify the impact of the relativistic effects on the measurements performed on large scales.

Appendices

5.A Observed power spectrum vs. theory power spectrum

In this appendix we extend the discussion of sec. 5.2.3 and present the relation between the theory power spectrum and the observed power spectrum.

Starting from eq. (5.24), we assume for simplicity that $\delta_g \equiv \delta_m$, as our argument is independent of such approximation and all derivations can be easily generalized to the complete expression. In this case, we can then factorize the time dependence of the galaxy fluctuation as $\delta_g(\bar{\eta}_z, \boldsymbol{k}) = D(\bar{\eta}_z)\delta(\boldsymbol{k})$, so that $P_{\rm th}(\boldsymbol{k}, \bar{\eta}_1, \bar{\eta}_2) = P_{\rm th}(\boldsymbol{k})D(\bar{\eta}_1)D(\bar{\eta}_2)$. Then we have

$$\langle \delta_g(\boldsymbol{k}_1)\delta_g^*(\boldsymbol{k}_2)\rangle = \int \frac{d^3k}{(2\pi)^3} F(\boldsymbol{k}, \boldsymbol{k}_1)F^*(\boldsymbol{k}, \boldsymbol{k}_2)P_{\rm th}(\boldsymbol{k})\,, \tag{5.74}$$

where the kernel $F(\boldsymbol{k}, \boldsymbol{k}')$ is defined as

$$\begin{aligned} F(\boldsymbol{k}, \boldsymbol{k}') &\equiv \int_V d^3x_{\rm obs}\, e^{i(\boldsymbol{k}-\boldsymbol{k}')\cdot\boldsymbol{x}} D(\bar{\eta}_z) \\ &= \int_{r_{\rm min}}^{r_{\rm max}} d\bar{r}_z\, \bar{r}_z^2\, D(\bar{\eta}_o - \bar{r}_z) \int_0^{\theta_{\rm max}} d\theta\, \sin\theta \int_0^{2\pi} d\varphi\, e^{i\bar{r}_z(\boldsymbol{k}-\boldsymbol{k}')\cdot\hat{\boldsymbol{n}}}\,. \end{aligned} \tag{5.75}$$

Note that $D(\bar{\eta}_z)$ cannot be pulled out, because when we integrate over the survey volume we also integrate over a time interval. The quantities $r_{\rm min}$, $r_{\rm max}$ and $\theta_{\rm max}$ define the survey volume with center at distance $\bar{r}_z = (r_{\rm min} + r_{\rm max})/2$ from the observer and opening angle $2\theta_{\rm max}$. This relation is simplified if one takes $\boldsymbol{k}_1 = \boldsymbol{k}_2 = \boldsymbol{k}$:

$$\langle \delta_g(\boldsymbol{k})\delta_g^*(\boldsymbol{k})\rangle = \int \frac{d^3k'}{(2\pi)^3} P_{\rm th}(\boldsymbol{k}')|F(\boldsymbol{k}', \boldsymbol{k})|^2\,. \tag{5.76}$$

For an idealized case, where the survey volume is infinite, eq. (5.74) is equal to $\langle \delta_g(\boldsymbol{k}_1)\delta_g^*(\boldsymbol{k}_2)\rangle = (2\pi)^3\delta^D(\boldsymbol{k}_1-\boldsymbol{k}_2)P(\boldsymbol{k}_1)$. However, with a finite survey volume, the Dirac delta is $(2\pi)^3\delta^D(0) = \int_V d^3x = V$ and we derive the observed power spectrum

$$P_{\rm obs}(\boldsymbol{k}) = \frac{1}{V}\int \frac{d^3k'}{(2\pi)^3} P_{\rm th}(\boldsymbol{k}')|F(\boldsymbol{k}',\boldsymbol{k})|^2\,. \tag{5.77}$$

In conclusion, one can use the theory power spectrum to obtain the observed counterpart using eq. (5.77) by convolving with the survey geometry.

5.B Cross power spectra

In this appendix we provide the expressions for the cross power spectra of the contributions δ_s, δ_o, δ_{nl} to the observed galaxy fluctuation δ_g in eqs. (5.9)–(5.11). We present the full expressions for the cross power spectra $P_{s\text{-}o}$, $P_{s\text{-}nl}$ and $P_{o\text{-}nl}$, expanding them into angular multipoles with respect to the angle $\hat{\boldsymbol{k}}$. Since the power spectra are real, their expressions are only given by the sums of even multipoles, and the odd multipoles vanish, because they are proportional to the imaginary number in the expression $e^{iy\mu_k} = \sum_{\ell=0}^{\infty} i^\ell(2\ell+1)j_\ell(y)L_\ell(\mu_k)$. As discusses in sec. 5.3.2, the infrared divergence occurs only in the monopole and quadrupole contributions in the individual power spectra. However, the divergent parts cancel out when all the monopole and quadrupole power spectra are summed. Therefore, after isolating the divergent parts, we present the expressions for the IR-safe cross power spectra.

The cross power spectra of the contributions δ_s, δ_o, δ_{nl} to the density fluctuation δ_g are obtained from the variances $\langle\delta_s\delta_o^*\rangle$, $\langle\delta_s\delta_{nl}^*\rangle$, $\langle\delta_o\delta_{nl}^*\rangle$ by using the method described in sec. 5.3.1. We obtain

$$\begin{aligned}\frac{P_{s\text{-}o}(z,\boldsymbol{k})}{P_m(k)} = \sum_{n=0}^{\infty}(-1)^n(4n+1)L_{2n}\Bigg[&\mathcal{A}\mathcal{D}\frac{1}{k^4}j_{2n}(k\bar{r}_z) + \big[\mathcal{B}\mathcal{D}-\mathcal{A}\mathcal{E}\big]\frac{1}{k^3}j'_{2n}(k\bar{r}_z)\\ &+ bD\mathcal{D}\frac{1}{k^2}j_{2n}(k\bar{r}_z) - \big[\mathcal{B}\mathcal{E}+\mathcal{C}\mathcal{D}\big]\frac{1}{k^2}j''_{2n}(k\bar{r}_z) + bD\mathcal{E}\frac{1}{k}j'_{2n}(k\bar{r}_z) + \mathcal{C}\mathcal{E}\frac{1}{k}j'''_{2n}(k\bar{r}_z)\Bigg],\end{aligned} \tag{5.78}$$

$$\begin{aligned}\frac{P_{s\text{-}nl}(z,\boldsymbol{k})}{P_m(k)} = \sum_{n=0}^{\infty}(-1)^n(4n+1)L_{2n}\int_0^{\bar{r}_z}d\bar{r}\Bigg[&\mathcal{F}\frac{j_{2n}(\Delta x_z)}{k^2}\left(\frac{\mathcal{A}}{k^2}+bD\right) + \big[\mathcal{B}\mathcal{F}-\mathcal{A}\mathcal{G}\big]\frac{j'_{2n}(\Delta x_z)}{k^3}\\ &+ \mathcal{A}\mathcal{I}\frac{j_{2n}(\Delta x_z)+j''_{2n}(\Delta x_z)}{k^2} - \big[\mathcal{C}\mathcal{F}+\mathcal{B}\mathcal{G}\big]\frac{j''_{2n}(\Delta x_z)}{k^2} + \mathcal{C}\mathcal{G}\frac{j'''_{2n}(\Delta x_z)}{k} - bD\mathcal{G}\frac{j'_{2n}(\Delta x_z)}{k}\\ &+ \mathcal{B}\mathcal{I}\frac{j'_{2n}(\Delta x_z)+j'''_{2n}(\Delta x_z)}{k} + bD\mathcal{I}\big[j_{2n}(\Delta x_z)+j''_{2n}(\Delta x_z)\big] - \mathcal{C}\mathcal{I}\big[j''_{2n}(\Delta x_z)+j''''_{2n}(\Delta x_z)\big]\Bigg],\end{aligned} \tag{5.79}$$

$$\frac{P_{o\text{-}nl}(z,\boldsymbol{k})}{P_m(k)} = \sum_{n=0}^{\infty}(-1)^n(4n+1)L_{2n}\int_0^{\bar{r}_z} d\bar{r}\left[\mathcal{D}\mathcal{F}\frac{1}{k^4}j_{2n}(k\bar{r}) - \left[\mathcal{E}\mathcal{F}-\mathcal{D}\mathcal{G}\right]\frac{1}{k^3}j'_{2n}(k\bar{r})\right.$$
$$\left. -\mathcal{E}\mathcal{G}\frac{1}{k^2}j''_{2n}(k\bar{r}) + \mathcal{D}\mathcal{I}\frac{1}{k^2}\left[j_{2n}(k\bar{r}) + j''_{2n}(k\bar{r})\right] - \mathcal{E}\mathcal{I}\frac{1}{k}\left[j'_{2n}(k\bar{r}) + j'''_{2n}(k\bar{r})\right]\right], \tag{5.80}$$

where the Legendre polynomials are functions of μ_k and we defined $\Delta r_z \equiv \bar{r}_z - \bar{r}$ and $\Delta x_z \equiv k\Delta r_z$ for compactness. Note that the imaginary parts (corresponding to odd multipoles) correctly vanish.

We now isolate the divergent terms in the above cross power spectra:

$$P^{s\text{-}o}_{k\to 0}(z,\boldsymbol{k}) = \left\{\mathcal{A}\mathcal{D}\frac{1}{k^4}\left[\left(1-\frac{1}{6}k^2\bar{r}_z^2\right)L_0 - \frac{1}{3}k^2\bar{r}_z^2L_2\right] + bD\mathcal{D}\frac{1}{k^2}L_0\right.$$
$$\left. -\frac{1}{3}\left[\bar{r}_z\mathcal{B}\mathcal{D} - \bar{r}_z\mathcal{A}\mathcal{E} - \mathcal{B}\mathcal{E} - \mathcal{C}\mathcal{D}\right]\frac{1}{k^2}\left[L_0+2L_2\right]\right\}P_m(k)\,, \tag{5.81}$$

$$P^{s\text{-}nl}_{k\to 0}(z,\boldsymbol{k}) = \int_0^{\bar{r}_z} d\bar{r}\left\{\mathcal{A}\mathcal{F}\frac{1}{k^4}\left[\left(1-\frac{1}{6}\Delta x_z^2\right)L_0 - \frac{1}{3}\Delta x_z^2L_2\right] + \frac{2}{3}\mathcal{A}\mathcal{I}\frac{1}{k^2}\left[L_0-L_2\right]\right.$$
$$\left. -\frac{1}{3}\left[\Delta r_z(\mathcal{B}\mathcal{F}-\mathcal{A}\mathcal{G}) - \mathcal{C}\mathcal{F} - \mathcal{B}\mathcal{G}\right]\frac{1}{k^2}\left[L_0+2L_2\right] + bD\mathcal{F}L_0\right\}P_m(k)\,, \tag{5.82}$$

$$P^{o\text{-}nl}_{k\to 0}(z,\boldsymbol{k}) = \int_0^{\bar{r}_z} d\bar{r}\left\{\mathcal{D}\mathcal{F}\frac{1}{k^4}\left[\left(1-\frac{1}{6}k^2\bar{r}^2\right)L_0 - \frac{1}{3}k^2\bar{r}^2L_2\right] + \frac{2}{3}\mathcal{D}\mathcal{I}\frac{1}{k^2}\left[L_0-L_2\right]\right.$$
$$\left. +\frac{1}{3}\left[\bar{r}\mathcal{E}\mathcal{F} - \bar{r}\mathcal{D}\mathcal{G} + \mathcal{E}\mathcal{G}\right]\frac{1}{k^2}\left[L_0+2L_2\right]\right\}P_m(k)\,. \tag{5.83}$$

Note that the divergent contributions, given by the terms proportional to $k^{-2}P_m$ and $k^{-4}P_m$, only appear in the monopoles and the quadrupoles of the cross power spectra.

The IR-safe cross power spectra, in which the divergent terms are removed as

defined in sec. 5.3.2, are then given by

$$
\begin{aligned}
P^{s\text{-}o}_{\text{IR-safe}}(z,\boldsymbol{k}) &= P_{s\text{-}o}(z,\boldsymbol{k}) - P^{s\text{-}o}_{k\to 0}(z,\boldsymbol{k}) = \Bigg\{ \sum_{n=2}^{\infty}(-1)^n(4n+1)L_{2n}\Bigg[\mathcal{A}\mathcal{D}\frac{j_{2n}(k\bar{r}_z)}{k^4} + bD\mathcal{D}\frac{j_{2n}(k\bar{r}_z)}{k^2} \\
&+ \big[\mathcal{B}\mathcal{D}-\mathcal{A}\mathcal{E}\big]\frac{j'_{2n}(k\bar{r}_z)}{k^3} - \big[\mathcal{B}\mathcal{E}+\mathcal{C}\mathcal{D}\big]\frac{j''_{2n}(k\bar{r}_z)}{k^2}\Bigg] + \sum_{n=0}^{\infty}(-1)^n(4n+1)L_{2n}\mathcal{E}\Bigg[bD\frac{j'_{2n}(k\bar{r}_z)}{k} + \mathcal{C}\frac{j'''_{2n}(k\bar{r}_z)}{k}\Bigg] \\
&+ \mathcal{A}\mathcal{D}\frac{1}{k^4}\Bigg[L_0\bigg(j_0(k\bar{r}_z) - 1 + \frac{1}{6}k^2\bar{r}_z^2\bigg) - L_2\bigg(5j_2(k\bar{r}_z) - \frac{1}{3}k^2\bar{r}_z^2\bigg)\Bigg] + bD\mathcal{D}\frac{1}{k^2}\Bigg[L_0\bigg(j_0(k\bar{r}_z) - 1\bigg) \\
&- 5L_2 j_2(k\bar{r}_z)\Bigg] + \big[\mathcal{B}\mathcal{D}-\mathcal{A}\mathcal{E}\big]\frac{1}{k^3}\Bigg[L_0\bigg(j'_0(k\bar{r}_z) + \frac{1}{3}k\bar{r}_z\bigg) - L_2\bigg(5j'_2(k\bar{r}_z) - \frac{2}{3}k\bar{r}_z\bigg)\Bigg] \\
&- \big[\mathcal{B}\mathcal{E}+\mathcal{C}\mathcal{D}\big]\frac{1}{k^2}\Bigg[L_0\bigg(j''_0(k\bar{r}_z) + \frac{1}{3}\bigg) - L_2\bigg(5j''_2(k\bar{r}_z) - \frac{2}{3}\bigg)\Bigg]\Bigg\}P_m(k)\,,
\end{aligned}
\tag{5.84}
$$

$$
\begin{aligned}
P^{s\text{-}nl}_{\text{IR-safe}}(z,\boldsymbol{k}) &= P_{s\text{-}nl}(z,\boldsymbol{k}) - P^{s\text{-}nl}_{k\to 0}(z,\boldsymbol{k}) = P_m(k)\int_0^{\bar{r}_z} d\bar{r}\,\Bigg\{ \sum_{n=2}^{\infty}(-1)^n(4n+1)L_{2n}\Bigg[\mathcal{A}\mathcal{F}\frac{j_{2n}(\Delta x_z)}{k^4} \\
&+ \big[\mathcal{B}\mathcal{F}-\mathcal{A}\mathcal{G}\big]\frac{j'_{2n}(\Delta x_z)}{k^3} + bD\mathcal{F}\frac{j_{2n}(\Delta x_z)}{k^2} + \mathcal{A}\mathcal{I}\frac{j_{2n}(\Delta x_z)+j''_{2n}(\Delta x_z)}{k^2} - \big[\mathcal{C}\mathcal{F}+\mathcal{B}\mathcal{G}\big]\frac{j''_{2n}(\Delta x_z)}{k^2}\Bigg] \\
&+ \sum_{n=0}^{\infty}(-1)^n(4n+1)L_{2n}\Bigg[\mathcal{B}\mathcal{I}\frac{j'_{2n}(\Delta x_z)+j'''_{2n}(\Delta x_z)}{k} - bD\mathcal{G}\frac{1}{k}j'_{2n}(\Delta x_z) + bD\mathcal{I}\big[j_{2n}(\Delta x_z)+j''_{2n}(\Delta x_z)\big] \\
&- \mathcal{C}\mathcal{I}[j''_{2n}(\Delta x_z)+j''''_{2n}(\Delta x_z)] + \mathcal{C}\mathcal{G}\frac{1}{k}j'''_{2n}(\Delta x_z)\Bigg] + \mathcal{A}\mathcal{F}\frac{1}{k^4}\Bigg[L_0\bigg(j_0(\Delta x_z) - 1 + \frac{1}{6}\Delta x_z^2\bigg) \\
&- L_2\bigg(5j_2(\Delta x_z) - \frac{1}{3}\Delta x_z^2\bigg)\Bigg] + \big[\mathcal{B}\mathcal{F}-\mathcal{A}\mathcal{G}\big]\frac{1}{k^3}\Bigg[L_0\bigg(j'_0(\Delta x_z) + \frac{1}{3}\Delta x_z\bigg) - L_2\bigg(5j'_2(\Delta x_z) - \frac{2}{3}\Delta x_z\bigg)\Bigg] \\
&+ bD\mathcal{F}\frac{1}{k^2}\Bigg[L_0\bigg(j_0(\Delta x_z) - 1\bigg) - 5L_2 j_2(\Delta x_z)\Bigg] + \mathcal{A}\mathcal{I}\frac{1}{k^2}\Bigg[L_0\bigg(\big[j_0(\Delta x_z)+j''_0(\Delta x_z)\big] - \frac{2}{3}\bigg) \\
&- L_2\bigg(5\big[j_2(\Delta x_z)+j''_2(\Delta x_z)\big] - \frac{2}{3}\bigg)\Bigg] - \big[\mathcal{C}\mathcal{F}+\mathcal{B}\mathcal{G}\big]\frac{1}{k^2}\Bigg[L_0\bigg(j''_0(\Delta x_z) + \frac{1}{3}\bigg) - L_2\bigg(5j''_2(\Delta x_z) - \frac{2}{3}\bigg)\Bigg]\Bigg\}\,,
\end{aligned}
\tag{5.85}
$$

$$P^{o\text{-}nl}_{\text{IR-safe}}(z,\boldsymbol{k}) = P_{o\text{-}nl}(z,\boldsymbol{k}) - P^{o\text{-}nl}_{k\to 0}(z,\boldsymbol{k}) = P_m(k)\int_0^{\bar{r}_z} d\bar{r}\left\{\sum_{n=2}^{\infty}(-1)^n(4n+1)L_{2n}\Bigg[\mathcal{D}\mathcal{F}\frac{1}{k^4}j_{2n}(k\bar{r})\right.$$
$$-\big[\mathcal{E}\mathcal{F}-\mathcal{D}\mathcal{G}\big]\frac{1}{k^3}j'_{2n}(k\bar{r}) - \mathcal{E}\mathcal{G}\frac{1}{k^2}j''_{2n}(k\bar{r}) + \mathcal{D}\mathcal{I}\frac{1}{k^2}\big[j_{2n}(k\bar{r}) + j''_{2n}(k\bar{r})\big]\Bigg] - \mathcal{E}\mathcal{G}\frac{1}{k^2}\Bigg[L_0\Bigg(j''_0(k\bar{r}) + \frac{1}{3}\Bigg)$$
$$- L_2\Bigg(5j''_2(k\bar{r}) - \frac{2}{3}\Bigg)\Bigg] - \mathcal{E}\mathcal{I}\frac{1}{k}\sum_{n=0}^{\infty}(-1)^n(4n+1)L_{2n}\big[j'_{2n}(k\bar{r}) + j'''_{2n}(k\bar{r})\big] + \mathcal{D}\mathcal{F}\frac{1}{k^4}\Bigg[L_0\Bigg(j_0(k\bar{r}) - 1$$
$$+ \frac{1}{6}k^2\bar{r}^2\Bigg) - L_2\Bigg(5j_2(k\bar{r}) - \frac{1}{3}k^2\bar{r}^2\Bigg)\Bigg] - \big[\mathcal{E}\mathcal{F}-\mathcal{D}\mathcal{G}\big]\frac{1}{k^3}\Bigg[L_0\Bigg(j'_0(k\bar{r}) + \frac{1}{3}k\bar{r}\Bigg) - L_2\Bigg(5j'_2(k\bar{r}) - \frac{2}{3}k\bar{r}\Bigg)\Bigg]$$
$$\left. + \mathcal{D}\mathcal{I}\frac{1}{k^2}\Bigg[L_0\Bigg(\big[j_0(k\bar{r}) + j''_0(k\bar{r})\big] - \frac{2}{3}\Bigg) - L_2\Bigg(5\big[j_2(k\bar{r}) + j''_2(k\bar{r})\big] - \frac{2}{3}\Bigg)\Bigg]\right\}. \tag{5.86}$$

Note that the derivatives of the Bessel functions can be converted using eq. (5.56).

The expressions for the monopole, quadrupole and hexadecapole cross power spectra, their divergent parts and their IR-safe versions can be read off the above expressions by taking the coefficients of L_0, L_2 and L_4 respectively.

CHAPTER 6

Summary and conclusions

In this thesis we investigated the impact of general relativistic effects on large scale structure (LSS) observables. In particular we have studied various theoretical aspects and analyzed different issues involved in the general relativistic description of the galaxy number density, the galaxy correlation function and the galaxy power spectrum. Theoretical predictions in general relativity for these observables are of great importance considering the huge amount of high precision data coming from future surveys. Indeed, we need accurate expressions for the data analysis in order to interpret correctly the physical information in the measurements. The standard expressions used so far, which account only for the galaxy fluctuation with the bias factor and the redshift-space distortions, provide a very good approximation of what is observed but they may be not accurate enough to match the precision that will be achieved by future surveys. If we want to put tighter constraints on cosmological parameter and study the behavior of gravity on very large scales, we need to account for all relativistic effects in the observed galaxy number density. This thesis contributes to the efforts done in recent years to achieve a complete description of LSS observables in general relativity. In this final chapter we summarize our results. We will discuss again how we resolved the theoretical issues involved in the relativistic description of the galaxy correlation function and the galaxy power spectrum. We will summarize our numerical results obtained by using expressions that are gauge-invariant and consistent with the equivalence principle, and, as such, free from the theoretical issues often plaguing the theoretical predictions presented in literature. We will then discuss the implications of our findings for future observations and we will indicate research directions to follow in order to complement our achievements.

The relativistic description of galaxy clustering presented in this thesis is based on

linear perturbation theory. The latter is able to describe a significant range of scales and most of the history of the universe but it eventually breaks down as perturbations grow under the effect of gravity, so that we cannot trust the linear predictions on scales smaller than about 0.1 Mpc^{-1}. While linear perturbation theory is valid on the large scales of our interest, where the general relativistic effects manifest themselves, it is not the only approach available to describe light-cone observations. In chapter 3 we studied the geodesic light-cone (GLC) formalism, an approach alternative to perturbation theory that allows analytic expressions for light-cone observables, providing a new non-perturbative way to compute the effects of inhomogeneities in our universe. In particular, we proved the gauge invariance of the expressions derived in the GLC formalism for the observed redshift, the luminosity distance and the physical area and volume of the observed sources. As we discussed already in sec. 2.2.2, the gauge invariance of general relativity offers a powerful way to test the validity of theoretical predictions. Indeed, the expressions for observable quantities must not depend on our choice of coordinates, whatever the approach used for their derivations. By studying the gauge invariance in the GLC formalism, we were able to point out the presence of terms that were missing in the expressions presented in the literature. These terms originate from perturbations evaluated at the observer position. It is often argued that they can be set to zero, because the perturbations at the observer position are not observable by themselves. However, as we demonstrated, if these effects are neglected, the resulting expressions are gauge dependent, as they cannot be written as functions of the observed redshift and angles measured in the observer rest frame, which represent the truly and unprocessed observable quantities. The perturbations at the observer position are indeed a consequence of the frame change from the FRW coordinates to the observer's coordinates. Furthermore, while it is true that the perturbations at the observer are not observable, they contribute to the total expression like any other terms, so that the same (incorrect) argument would apply also to terms evaluated at the source position or integrated along the line of sight. The importance of considering all terms in the theoretical predictions, including those evaluated at the observer position, represents one of the main points of this thesis. As we showed also in chapters 4 and 5, this is the only way to obtain expressions that are gauge invariant, consistent with the equivalence principle and free from infrared divergences.

In chapter 4 we presented our study of two-point galaxy correlation function, considering the linear-order scalar and tensor perturbation contributions and the wide-angle effects. First, we demonstrated that the complete theoretical expression for the observed galaxy fluctuation, which accounts for the perturbations at the observer position, is devoid of any long-mode contributions from scalar and tensor perturbations and it lacks the infrared divergences in agreement with the equivalence principle. The idea is that perturbations with wavelength larger than the comoving distance between source and observer (called long-mode perturbations in this thesis) should not affect

any light-cone observables because they can only be responsible for uniform gravity modes, and the equivalence principle implies that observations are not sensitive to the presence of a uniform gravitational field. After identifying the terms associated with the long-mode contributions, we showed that they cancel out in the complete expression for the observed galaxy fluctuation. Indeed, all perturbations contain a long-mode contribution. As a result, it is important to take into account all together the perturbations evaluated at the observer and the source positions as well as the perturbations integrated along the line of sight. If the terms at the observer are set to zero, as it is often done in literature, the long-mode contributions of the perturbations at the source and integrated along the line of sight are not cancelled. As we showed, this results in unphysical infrared divergencies in the galaxy correlation function. This problem is usually circumvented by imposing an arbitrary infrared cut-off when computing correlations. In this thesis, instead, we presented a natural and simple solution to the problem. Then, using the complete expression for the observed galaxy fluctuation, we numerically computed the galaxy two-point correlation function and studied the impact of various relativistic effects in the conformal Newtonian gauge. We found that some terms at the observer position dominate over the other relativistic effects such as the source velocity, the gravitational potential at the source, the integrated Sachs-Wolf effect, the Shapiro time-delay and the lensing convergence. Compared to the standard theoretical predictions that consider only the density fluctuation with the bias factor and redshift-space distortions, the general relativistic effects introduce a few percent-level systematic errors beyond the scale of the baryonic acoustic oscillation: we found a 2% relative error at 150 Mpc/h and redshift one. This means that one should use the relativistic expression to interpret future data from upcoming surveys on such large scales.

Finally, in chapter 5, we presented our study of the anisotropic three-dimensional galaxy power spectrum in general relativity. As for the correlation function in chapter 4, we demonstrated that the previous calculations of the galaxy power spectrum with an infrared divergence are inconsistent with the equivalence principle, and this unphysical behavior on large scales vanishes if we consider all the relativistic contributions to the observed galaxy fluctuation. Indeed, the previous studies only considered the perturbations at the source position and calculated the power spectrum from their Fourier modes. In this thesis, instead of computing the power spectrum directly from the Fourier modes of the observed galaxy fluctuation δ_g, we have made use of the duality between the variance of δ_g and its power spectrum. In this way, we have been able to easily take into account also the contributions from the perturbations at the observer position and integrated along the line of sight. We then demonstrated that, while the power spectra of these individual contributions are all infrared-divergent, the total galaxy power spectrum given by their sum is not. Most importantly, however, we clarified the the important difference between the power spectrum commonly

derived in theory and what galaxy surveys really measure. In theory the power spectrum is obtained by taking a Fourier transformation of the observed galaxy fluctuation on the hypersurface of simultaneity at the source time coordinate. In observations, instead, the power spectrum is obtained by taking a Fourier transformation of the observed galaxy fluctuation on the light-cone hypersurface. As a consequence, the power spectrum derived in theory is not observable, because we do not observe spatial hypersurfaces but the past light-cone. Nevertheless, as we explained, the observed power spectrum can be obtained from the theoretical one by convolving with the survey geometry, with no ambiguity in the computations. In this thesis we focused on the theoretical power spectrum, presenting its complete relativistic expression for the first time in literature. With this we performed numerical computations to show the behavior on large scales, where the relativistic effects cause deviations from the standard prediction given by the redshift-space power spectrum. Our results pointed out the presence of redshift-dependent oscillations on scales comparable or larger than the scale of matter-radiation equality, leading to a percent-level fractional difference with the standard prediction.

A deep understanding of all theoretical subtleties in the relativistic description of galaxy clustering is essential to interpret the numerous upcoming surveys. Indeed, only the correct theoretical predictions can lead us to the full realization of the potential information contained in galaxy clustering and offered by precision measurements in future galaxy surveys. The work summarized in this thesis anticipates the implications of general relativity for future observations. However, in order to investigate the detectability and estimate the impact of general relativistic effects in specific LSS measurements, Fisher forecasts need to be performed. For this purpose our study of the two-point galaxy correlation function offers expressions that can be directly used in the analysis and represent the prediction of general relativity. Then, if the experimental precision allows it, our prediction can be used to test general relativity and ΛCDM against different theories of gravity and cosmological models. Regarding the galaxy power spectrum we made important steps forward by providing a complete theoretical description for this observable. However, more work is required in the future to obtain the observed power spectrum considering specific galaxy surveys. As for the galaxy correlation function, this will allow to quantify the impact of the relativistic effects on the measurements performed on large scales. Other research directions to follow in order to complement our achievements definitely involve better formulations of the galaxy bias and pushing the computations to higher order in perturbation theory. Indeed, while it is true that a scale-independent linear bias is fairly justified on large scales, the precision goal of future parameter estimations demand to study the bias issue in parallel with the relativistic effects. Likewise, the non-linearities in the gravitational evolution of the perturbations that we did not consider, because they are subdominant on very large scales, affect the measurements on most scales where the

desired accuracy cannot be achieved with linear perturbation theory.

Bibliography

[1] F. Scaccabarozzi and J. Yoo, JCAP **1706** (2017) no.06, 007 doi:10.1088/1475-7516/2017/06/007 [arXiv:1703.08552 [gr-qc]].

[2] F. Scaccabarozzi, J. Yoo and S. G. Biern, JCAP **1810** (2018) no.10, 024 doi:10.1088/1475-7516/2018/10/024 [arXiv:1807.09796 [astro-ph.CO]].

[3] F. Scaccabarozzi, J. Yoo, S. G. Biern and J. O. Gong

[4] J. Yoo and F. Scaccabarozzi, JCAP **1609** (2016) no.09, 046 doi:10.1088/1475-7516/2016/09/046 [arXiv:1606.08453 [astro-ph.CO]].

[5] E. Mitsou, F. Scaccabarozzi and G. Fanizza, Class. Quant. Grav. **35** (2018) no.10, 107002 doi:10.1088/1361-6382/aab06b [arXiv:1712.05675 [gr-qc]].

[6] E. Mitsou, J. Yoo, R. Durrer, F. Scaccabarozzi and V. Tansella, arXiv:1905.01293 [astro-ph.CO].

[7] A. Friedmann, Z. Phys. **21** (1924) 326 [Gen. Rel. Grav. **31** (1999) 2001]. doi:10.1007/BF01328280

[8] G. Lemaitre, Mon. Not. Roy. Astron. Soc. **91** (1931) 483.

[9] H. P. Robertson, Astrophys. J. **82** (1935) 284. doi:10.1086/143681

[10] H. P. Robertson, Astrophys. J. **83** (1935) 187. doi:10.1086/143716

[11] H. P. Robertson, Astrophys. J. **83** (1936) 257. doi:10.1086/143726

[12] A. G. Walker, Proceedings of the London Mathematical Society, s2-42(1):90.127, 1937. doi:10.1112/plms/s2-42.1.90

[13] E. Hubble, Proc. Nat. Acad. Sci. **15** (1929) 168. doi:10.1073/pnas.15.3.168

[14] A. A. Penzias and R. W. Wilson, Astrophys. J. **142** (1965) 419. doi:10.1086/148307

[15] A. G. Riess *et al.* [Supernova Search Team], Astron. J. **116** (1998) 1009 doi:10.1086/300499 [astro-ph/9805201].

[16] S. Perlmutter *et al.* [Supernova Cosmology Project Collaboration], Astrophys. J. **517** (1999) 565 doi:10.1086/307221 [astro-ph/9812133].

[17] B. P. Schmidt *et al.* [Supernova Search Team], Astrophys. J. **507** (1998) 46 doi:10.1086/306308 [astro-ph/9805200].

[18] A. H. Guth, Phys. Rev. D **23** (1981) 347 [Adv. Ser. Astrophys. Cosmol. **3** (1987) 139]. doi:10.1103/PhysRevD.23.347

[19] R. Laureijs *et al.* [EUCLID Collaboration], arXiv:1110.3193 [astro-ph.CO].

[20] L. Amendola *et al.*, Living Rev. Rel. **21** (2018) no.1, 2 doi:10.1007/s41114-017-0010-3 [arXiv:1606.00180 [astro-ph.CO]].

[21] A. Abate *et al.* [LSST Dark Energy Science Collaboration], arXiv:1211.0310 [astro-ph.CO].

[22] P. A. Abell *et al.* [LSST Science and LSST Project Collaborations], arXiv:0912.0201 [astro-ph.IM].

[23] A. Aghamousa *et al.* [DESI Collaboration], arXiv:1611.00036 [astro-ph.IM].

[24] C. L. Carilli and S. Rawlings, New Astron. Rev. **48** (2004) 979 doi:10.1016/j.newar.2004.09.001

[25] C. L. Bennett *et al.* [WMAP Collaboration], Astrophys. J. Suppl. **208** (2013) 20 doi:10.1088/0067-0049/208/2/20 [arXiv:1212.5225 [astro-ph.CO]].

[26] D. Blas, J. Lesgourgues and T. Tram, JCAP **1107** (2011) 034 doi:10.1088/1475-7516/2011/07/034 [arXiv:1104.2933 [astro-ph.CO]].

[27] A. Lewis, A. Challinor and A. Lasenby, Astrophys. J. **538** (2000) 473 doi:10.1086/309179 [astro-ph/9911177].

[28] F. Bernardeau, S. Colombi, E. Gaztanaga and R. Scoccimarro, Phys. Rept. **367** (2002) 1 doi:10.1016/S0370-1573(02)00135-7 [astro-ph/0112551].

[29] F. R. Bouchet, astro-ph/9603013.

[30] E. Bertschinger, astro-ph/9503125.

[31] T. Baldauf, E. Schaan and M. Zaldarriaga, JCAP **1603** (2016) no.03, 017 doi:10.1088/1475-7516/2016/03/017 [arXiv:1505.07098 [astro-ph.CO]].

[32] J. Ehlers and T. Buchert, Gen. Rel. Grav. **29** (1997) 733 doi:10.1023/A:1018885922682 [astro-ph/9609036].

[33] T. Matsubara, Phys. Rev. D **92** (2015) no.2, 023534 doi:10.1103/PhysRevD.92.023534 [arXiv:1505.01481 [astro-ph.CO]].

[34] B. Jain and E. Bertschinger, Astrophys. J. **431** (1994) 495 doi:10.1086/174502 [astro-ph/9311070].

[35] N. Makino, M. Sasaki and Y. Suto, Phys. Rev. D 46:585?602, 1992 doi:10.1103/PhysRevD.46.585.

[36] R. Scoccimarro and J. Frieman, Astrophys. J. Suppl. **105** (1996) 37 doi:10.1086/192306 [astro-ph/9509047].

[37] T. Buchert, Mon. Not. Roy. Astron. Soc. **267** (1994) 811 doi:10.1093/mnras/267.4.811 [astro-ph/9309055].

[38] C. Rampf, JCAP **1212** (2012) 004 doi:10.1088/1475-7516/2012/12/004 [arXiv:1205.5274 [astro-ph.CO]].

[39] D. Baumann, A. Nicolis, L. Senatore and M. Zaldarriaga, JCAP **1207** (2012) 051 doi:10.1088/1475-7516/2012/07/051 [arXiv:1004.2488 [astro-ph.CO]].

[40] J. J. M. Carrasco, M. P. Hertzberg and L. Senatore, JHEP **1209** (2012) 082 doi:10.1007/JHEP09(2012)082 [arXiv:1206.2926 [astro-ph.CO]].

[41] B. Bose, K. Koyama, M. Lewandowski, F. Vernizzi and H. A. Winther, JCAP **1804** (2018) no.04, 063 doi:10.1088/1475-7516/2018/04/063 [arXiv:1802.01566 [astro-ph.CO]].

[42] J. A. Fillmore and P. Goldreich, Astrophys. J., vol. 281, p. 1?8, 1984 doi:10.1086/162070.

[43] J. E. Gunn and J. R. Gott, III, Astrophys. J. **176** (1972) 1. doi:10.1086/151605

[44] Y. B. Zeldovich, Astron. Astrophys. **5** (1970) 84.

[45] W. H. Press and P. Schechter, Astrophys. J. **187** (1974) 425. doi:10.1086/152650

[46] J. R. Bond, S. Cole, G. Efstathiou and N. Kaiser, Astrophys. J. **379** (1991) 440. doi:10.1086/170520

[47] V. Desjacques, D. Jeong and F. Schmidt, Phys. Rept. **733** (2018) 1 doi:10.1016/j.physrep.2017.12.002 [arXiv:1611.09787 [astro-ph.CO]].

[48] N. Kaiser, Mon. Not. Roy. Astron. Soc. **227** (1987).

[49] L. Amendola *et al.* [Euclid Theory Working Group], Living Rev. Rel. **16** (2013) 6

[50] Z. Ivezic *et al.* [LSST Collaboration], arXiv:0805.2366 [astro-ph].

[51] G. J. Hill *et al.*, ASP Conf. Ser. **399** (2008) 115

[52] J. Yoo and V. Desjacques, Phys. Rev. D **88** (2013) no.2, 023502

[53] J. Yoo, Phys. Rev. D **82** (2010) 083508

[54] A. Raccanelli, F. Montanari, D. Bertacca, O. Doré and R. Durrer, JCAP **1605** (2016) no.05, 009

[55] J. M. Bardeen, Phys. Rev. D **22** (1980) 1882

[56] M. Gasperini, G. Marozzi, F. Nugier and G. Veneziano, JCAP **1107** (2011) 008

[57] Temple. 1938. New Systems of Normal Co-ordinates for Relativistic Optics, Royal Society of London Proceedings Series A 168 (Oct.,) 122-148.

[58] J. Kristian, R. K. Sachs. 1966. Observations in Cosmology, Astrophysical Journal, vol. 143, p.379.

[59] P. T. Saunders, Observations in homogeneous model universes, Month. Not. R. Astron. Soc. 141 (1968) 427.

[60] P. T. Saunders, Observations in some simple cosmological models with shear, Month. Not. R. Astron. Soc. 142 (1969) 213.

[61] I. Ben-Dayan, M. Gasperini, G. Marozzi, F. Nugier and G. Veneziano, JCAP **1204** (2012) 036

[62] I. Ben-Dayan, G. Marozzi, F. Nugier and G. Veneziano, JCAP **1211** (2012) 045

[63] I. Ben-Dayan, M. Gasperini, G. Marozzi, F. Nugier and G. Veneziano, JCAP **1306** (2013) 002

[64] G. Fanizza, M. Gasperini, G. Marozzi and G. Veneziano, JCAP **1311** (2013) 019

[65] P. Fleury, F. Nugier and G. Fanizza, JCAP **1606** (2016) no.06, 008

[66] J. Yoo and F. Scaccabarozzi, JCAP **1609** (2016) no.09, 046

[67] G. Marozzi, Class. Quant. Grav. **32** (2015) no.4, 045004 Corrigendum: [Class. Quant. Grav. **32** (2015) 179501]

[68] E. Di Dio, R. Durrer, G. Marozzi and F. Montanari, JCAP **1412** (2014) 017 Erratum: [JCAP **1506** (2015) no.06, E01]

[69] G. Fanizza, M. Gasperini, G. Marozzi and G. Veneziano, JCAP **1508** (2015) no.08, 020

[70] J. Yoo, A. L. Fitzpatrick and M. Zaldarriaga, Phys. Rev. D **80** (2009) 083514

[71] J. Yoo, Phys. Rev. D **82** (2010) 083508

[72] J. Yoo, Class. Quant. Grav. **31** (2014) 234001

[73] G. Fanizza and F. Nugier, JCAP **1502** (2015) no.02, 002

[74] I. Ben-Dayan, M. Gasperini, G. Marozzi, F. Nugier and G. Veneziano, Phys. Rev. Lett. **110** (2013) no.2, 021301

[75] F. Nugier, arXiv:1508.07464 [astro-ph.CO].

[76] D. Jeong, F. Schmidt and C. M. Hirata, Phys. Rev. D **85** (2012) 023504

[77] S. G. Biern and J. Yoo, JCAP **1704** (2017) no.04, 045

[78] P. Fleury, C. Clarkson and R. Maartens, arXiv:1612.03726 [astro-ph.CO].

[79] I. Ben-Dayan, R. Durrer, G. Marozzi and D. J. Schwarz, Phys. Rev. Lett. **112**, 221301 (2014)

[80] T. Okumura, T. Matsubara, D. J. Eisenstein, I. Kayo, C. Hikage, A. S. Szalay and D. P. Schneider, Astrophys. J. **676** (2008) 889 doi:10.1086/528951 [arXiv:0711.3640 [astro-ph]].

[81] V. Tansella, arXiv:1804.05826 [astro-ph.CO].

[82] D. Baumann, D. Green and M. Zaldarriaga, JCAP **1711** (2017) no.11, 007 doi:10.1088/1475-7516/2017/11/007 [arXiv:1703.00894 [astro-ph.CO]].

[83] J. Yoo, N. Hamaus, U. Seljak and M. Zaldarriaga, Phys. Rev. D **86** (2012) 063514 doi:10.1103/PhysRevD.86.063514 [arXiv:1206.5809 [astro-ph.CO]].

[84] D. Jeong, F. Schmidt and C. M. Hirata, Phys. Rev. D **85** (2012) 023504 doi:10.1103/PhysRevD.85.023504 [arXiv:1107.5427 [astro-ph.CO]].

[85] J. Yoo and V. Desjacques, Phys. Rev. D **88** (2013) 023502 doi:10.1103/PhysRevD.88.023502 [arXiv:1301.4501 [astro-ph.CO]].

[86] A. Raccanelli, L. Samushia and W. J. Percival, Mon. Not. Roy. Astron. Soc. **409** (2010) 1525 doi:10.1111/j.1365-2966.2010.17388.x [arXiv:1006.1652 [astro-ph.CO]].

[87] I. Szapudi, Astrophys. J. **614** (2004) 51 doi:10.1086/423168 [astro-ph/0404477].

[88] A. S. Szalay, T. Matsubara and S. D. Landy, Astrophys. J. **498** (1998) L1 doi:10.1086/311293 [astro-ph/9712007].

[89] P. Papai and I. Szapudi, Mon. Not. Roy. Astron. Soc. **389** (2008) 292 doi:10.1111/j.1365-2966.2008.13572.x [arXiv:0802.2940 [astro-ph]].

[90] Z. Slepian and D. J. Eisenstein, arXiv:1510.04809 [astro-ph.CO].

[91] L. Samushia, W. J. Percival and A. Raccanelli, Mon. Not. Roy. Astron. Soc. **420** (2012) 2102 doi:10.1111/j.1365-2966.2011.20169.x [arXiv:1102.1014 [astro-ph.CO]].

[92] J. Yoo and U. Seljak, Mon. Not. Roy. Astron. Soc. **447** (2015) no.2, 1789 doi:10.1093/mnras/stu2491 [arXiv:1308.1093 [astro-ph.CO]].

[93] D. Bertacca, R. Maartens, A. Raccanelli and C. Clarkson, JCAP **1210** (2012) 025 doi:10.1088/1475-7516/2012/10/025 [arXiv:1205.5221 [astro-ph.CO]].

[94] A. Raccanelli, D. Bertacca, O. Doré and R. Maartens, JCAP **1408** (2014) 022 doi:10.1088/1475-7516/2014/08/022 [arXiv:1306.6646 [astro-ph.CO]].

[95] A. Raccanelli, D. Bertacca, R. Maartens, C. Clarkson and O. Doré, Gen. Rel. Grav. **48** (2016) no.7, 84 doi:10.1007/s10714-016-2076-8 [arXiv:1311.6813 [astro-ph.CO]].

[96] L. Hui, E. Gaztanaga and M. LoVerde, Phys. Rev. D **77** (2008) 063526 doi:10.1103/PhysRevD.77.063526 [arXiv:0710.4191 [astro-ph]].

[97] J Yoo and J. Miralda-Escudé, Phys. Rev. D **82** (2010) 043527 doi:10.1103/PhysRevD.82.043527 [arXiv:0901.0708 [astro-ph.CO]].

[98] L. Hui, E. Gaztanaga and M. LoVerde, Phys. Rev. D **76** (2007) 103502 doi:10.1103/PhysRevD.76.103502 [arXiv:0706.1071 [astro-ph]].

[99] M. LoVerde, L. Hui and E. Gaztanaga, Phys. Rev. D **77** (2008) 023512 doi:10.1103/PhysRevD.77.023512 [arXiv:0708.0031 [astro-ph]].

[100] V. Tansella, C. Bonvin, R. Durrer, B. Ghosh and E. Sellentin, JCAP **1803** (2018) no.03, 019 doi:10.1088/1475-7516/2018/03/019 [arXiv:1708.00492 [astro-ph.CO]].

[101] S. G. Biern and J. Yoo, JCAP **1704** (2017) no.04, 045 doi:10.1088/1475-7516/2017/04/045 [arXiv:1606.01910 [astro-ph.CO]].

[102] S. G. Biern and J. Yoo, JCAP **1709** (2017) no.09, 026 doi:10.1088/1475-7516/2017/09/026 [arXiv:1704.07380 [astro-ph.CO]].

[103] C. Bonvin and R. Durrer, Phys. Rev. D **84** (2011) 063505 doi:10.1103/PhysRevD.84.063505 [arXiv:1105.5280 [astro-ph.CO]].

[104] A. Challinor and A. Lewis, Phys. Rev. D **84** (2011) 043516 doi:10.1103/PhysRevD.84.043516 [arXiv:1105.5292 [astro-ph.CO]].

[105] F. Schmidt and D. Jeong, Phys. Rev. D **86** (2012) 083527 doi:10.1103/PhysRevD.86.083527 [arXiv:1204.3625 [astro-ph.CO]].

[106] J. Yoo and J.-O. Gong, Phys. Let. B **754** (2016) 94 doi:10.1016/j.physletb.2016.01.021 [arXiv:1509.08466 [astro-ph.CO]].

[107] D. Jeong and F. Schmidt, Phys. Rev. D **86** (2012) 083512 doi:10.1103/PhysRevD.86.083512 [arXiv:1205.1512 [astro-ph.CO]].

[108] F. Schmidt and D. Jeong, Phys. Rev. D **86** (2012) 083513 doi:10.1103/PhysRevD.86.083513 [arXiv:1205.1514 [astro-ph.CO]].

[109] J. Yoo and M. Zaldarriaga, Phys. Rev. D **90** (2014) no.2, 023513 doi:10.1103/PhysRevD.90.023513 [arXiv:1406.4140 [astro-ph.CO]].

[110] D. Bertacca, R. Maartens and C. Clarkson, JCAP **1409** (2014) no.09, 037 doi:10.1088/1475-7516/2014/09/037 [arXiv:1405.4403 [astro-ph.CO]].

[111] D. Bertacca, R. Maartens and C. Clarkson, JCAP **1411** (2014) no.11, 013 doi:10.1088/1475-7516/2014/11/013 [arXiv:1406.0319 [astro-ph.CO]].

[112] E. Di Dio, R. Durrer, G. Marozzi and F. Montanari, JCAP **1601** (2016) 016 doi:10.1088/1475-7516/2016/01/016 [arXiv:1510.04202 [astro-ph.CO]].

[113] F. Scaccabarozzi and J. Yoo, JCAP **1706** (2017) no.06, 007 doi:10.1088/1475-7516/2017/06/007 [arXiv:1703.08552 [gr-qc]].

[114] V. Tansella, G. Jelic-Cizmek, C. Bonvin and R. Durrer, JCAP **1810** (2018) no.10, 032 doi:10.1088/1475-7516/2018/10/032 [arXiv:1806.11090 [astro-ph.CO]].

[115] J. Yoo and J. O. Gong, JCAP **1607** (2016) no.07, 017 doi:10.1088/1475-7516/2016/07/017 [arXiv:1602.06300 [gr-qc]].

[116] J. c. Hwang, H. Noh, D. Jeong, J. O. Gong and S. G. Biern, JCAP **1505** (2015) no.05, 055 doi:10.1088/1475-7516/2015/05/055 [arXiv:1408.4656 [astro-ph.CO]].

[117] D. Jeong, J. O. Gong, H. Noh and J. c. Hwang, Astrophys. J. **727** (2011) 22 doi:10.1088/0004-637X/727/1/22 [arXiv:1010.3489 [astro-ph.CO]].

[118] J. c. Hwang, D. Jeong and H. Noh, Mon. Not. Roy. Astron. Soc. **459** (2016) no.1, 1124 doi:10.1093/mnras/stw621 [arXiv:1509.07534 [astro-ph.CO]].

[119] J. Yoo and U. Seljak, Mon. Not. Roy. Astron. Soc. **447** (2015) no.2, 1789 doi:10.1093/mnras/stu2491 [arXiv:1308.1093 [astro-ph.CO]].